THE STUDY OF THE REACTION OF CARBON MONOXIDE WITH *Pseudomonas putida* CYTOCHROME P450cam

by

SIMON PIERS ALBON
B.Sc. (Majors), University of British Columbia, 1979

A THESIS SUBMITTED IN PARTIAL FULFILLMENT OF
THE REQUIREMENTS FOR THE DEGREE OF
MASTER OF SCIENCE

in

THE FACULTY OF GRADUATE STUDIES
(Department of Chemistry)

We accept this thesis as conforming to
the required standard

THE UNIVERSITY OF BRITISH COLUMBIA
SEPTEMBER 1983

© Simon Albon 1983

In presenting this thesis in partial fulfilment of the requirements for an advanced degree at the University of British Columbia, I agree that the Library shall make it freely available for reference and study. I further agree that permission for extensive copying of this thesis for scholarly purposes may be granted by the head of my department or by his or her representatives. It is understood that copying or publication of this thesis for financial gain shall not be allowed without my written permission.

Department of Chemistry

The University of British Columbia
2075 Wesbrook Place
Vancouver, Canada
V6T 1W5

Date Oct. 20, 1983

Abstract

Interest remains very high in the class of thiolate-bound heme-containing monooxygenase enzymes called the cytochromes P450. These enzymes generally activate molecular dioxygen for selective hydroxylation of organic substrates, such as saturated hydrocarbons (RH), in accordance with Reaction (1).

$$RH + O_2 + 2e^- + 2H^+ \longrightarrow ROH + H_2O \qquad (1)$$

Development of protein-free model catalysts that mimic P450 reactivity are of great industrial importance and require, in part, an understanding of the reactivity of the native hemoprotein towards small gas molecules such as carbon monoxide (CO) and dioxygen (O_2).

The work in this thesis describes the reaction of carbon monoxide with the ferrous state of substrate-bound, native and protohemin-reconstituted *Pseudomonas putida* cytochrome P450cam (Reaction (2)).

$$Fe(II)P450cam + CO \underset{k_{off}}{\overset{k_{on}}{\rightleftharpoons}} Fe(II)P450cam\text{-}CO, Kco = \frac{k_{on}}{k_{off}} \qquad (2)$$

A method is described for the growth of *P. putida*, strain PpG 786, and the subsequent isolation and purification of native cytochrome P450cam and associated electron transport proteins, putidaredoxin and putidaredoxin reductase; only purified cytochrome P450cam and putidaredoxin were successfully obtained by this method. The native enzyme has been reconstituted with protohemin by a method general for the insertion of hemins modified in the 2- and 4- positions. Meso-, deutero-, diacetyldeutero-, and dibromodeuterohemins were synthesized

but were not used for reconstituting the native cytochrome. Spectral analyses were performed on the substituted hemins, the native cytochrome and related electron transport proteins and the protohemin-reconstituted enzyme; the data agreed well with literature values.

Kinetic constants for the forward CO-association and reverse dissociation reactions (k_{on} and k_{off}, respectively; see Reaction (2)) were determined by flash photolysis; experiments were run under conditions in which the CO ligand was in substantial excess and all systems showed pseudo first-order dependence on hemoprotein concentration. The flash photolysis unit described below was tested and developed with the myoglobin-CO system and then used to study the substrate-bound native and protohemin-reconstituted P450cam-CO systems. The second-order rate constants for CO-binding to ferrous myoglobin and native substrate-bound P450cam were in excellent agreement with published values and reconstitution of the native P450cam enzyme had little effect on the k_{on} value for CO-binding. The first-order rate constants for the CO-dissociation reaction were determined also from the flash photolysis studies but were considered unreliable when compared with published literature data. A k_{off} value for the native P450cam system, in good agreement with the literature, was calculated from the equilibrium constant, Kco, derived by spectrophotometric analysis of Reaction (2); Kco values in reasonable agreement with literature data were obtained but indicated an interesting dependence on the concentration of

the dithionite reducing agent. This thesis begins with an extensive literature review on the subject and ends with some general conclusions on this work and some recommendations for future work.

TABLE OF CONTENTS

		Page
ABSTRACT		ii
TABLE OF CONTENTS		v
LIST OF TABLES		xii
LIST OF FIGURES		xv
LIST OF ABBREVIATIONS		xxi
ACKNOWLEDGEMENTS		xxviii
CHAPTER I	INTRODUCTION	1
CHAPTER II	LITERATURE REVIEW	12
II.1	Historical Overview	13
II.2	Biological Importance of the P450 Cytochromes	21
II.3	Structure	35
II.4	Mechanism of Action	45
II.5	The Interaction of Carbon Monoxide with Cytochrome P450	62
CHAPTER III	EXPERIMENTAL PROCEDURES	88
III.1	Synthesis of Substituted Hemins from Protohemin Chloride	89
III.1.1	General Information	89
III.1.2	Materials	91
III.1.3	Spectrophotometric Analysis of Pyridine Hemochromes	93
III.1.4	Synthesis of Deuterohemin	95
III.1.5	Synthesis of Mesohemin	101
III.1.6	Synthesis of Diacetyldeuterohemin	108
III.1.7	Synthesis of Dibromodeuterohemin	112

Page

III.2 Growth of *Pseudomonas putida*, strain PpG 786 118

III.2.1 General Information 118

III.2.2 Materials 120

III.2.3 Organism 121

III.2.4 Media 122

III.2.4.1 Minimal Agar 122

III.2.4.2 Starter Media 123

III.2.4.3 Large Scale Media 123

III.2.5 Growth Procedure 125

III.3 Isolation and Purification of Cytochrome P450cam and Related Bacterial Monooxygenase Components . . 132

III.3.1 General Information 132

III.3.1.1 Materials 132

III.3.1.2 Buffers 134

III.3.1.3 Column Chromatography . . 135

III.3.2 Isolation of Cytochrome P450cam and Related Bacterial Monooxygenase Components 140

III.3.2.1 Cell-Free Extract 140

III.3.2.2 Isolation Procedure . . . 140

III.3.2.3 Ammonium Salt Fractionation 142

III.3.3 Purification of Cytochrome P450cam and Related Bacterial Monooxygenase Components 144

III.3.3.1 Purification Procedure . . 144

Page

III.3.4 Spectral Analysis of Cytochrome P450cam and Related Bacterial Monooxygenase Components 147

III.3.4.1 Concentration Determinations 149

III.3.4.2 Purity Assay 150

III.4 Preparation of Protohemin-reconstituted Cytochrome P450cam 151

III.4.1 General Information 151

III.4.1.1 Materials 151

III.4.2 Extraction of the Heme Group from Native Cytochrome P450cam . . . 152

III.4.2.1 Extraction Procedure 152

III.4.2.2 Analysis of Heme Prosthetic Group 153

III.4.3 Reconstitution of Apocytochrome P450cam 155

III.4.3.1 Reconstitution Procedure . . 155

III.4.4 Purification of Protohemin-reconstituted Cytochrome P450cam . . 157

III.4.4.1 DE-52 Anion Exchange Chromatography 157

III.4.4.2 Removal of P420 Impurities . 157

III.4.4.3 Procedure for Removal of P420 Impurities 160

III.4.4.4 Preparation of Apomyoglobin . 161

III.5 Kinetic Study of the Reaction of Carbon Monoxide with the Ferrous Cytochrome P450cam and Myoglobin Proteins by Flash Photolysis 163

III.5.1 The Flash Photolysis Apparatus . . . 163

Page

III.5.1.1 Monitoring Light Source 165

III.5.1.2 Flash and Sample Compartment 165

III.5.1.3 Flashing Light Source . . 168

III.5.1.4 Detector and Recording System 171

III.5.1.5 Operation of the Flash Photolysis Apparatus . . . 173

III.5.2 The Flash Photolysis Experiment . . 174

III.5.2.1 General Information . . . 174

III.5.2.2 Procedure 179

III.5.3 Preliminary Experiments 181

III.5.3.1 Selection of Filtering System 181

III.5.3.2 Light Pulse Characteristics 183

III.5.3.3 Calibration Check 187

III.5.3.4 Extent of Photodecomposition 188

III.5.3.5 Kinetic Study of CO-Binding to Ferrous Myoglobin . . . 190

III.6 Spectrophotometric Determination of the Equilibrium Constant for the Reaction of Carbon Monoxide with Ferrous Cytochrome P450cam 192

III.6.1 General Information 192

III.6.2 Materials 192

III.6.3 Procedure 194

CHAPTER IV RESULTS AND DISCUSSION 196

IV.1 Growth of *P. putida*, strain PpG 786 197

IV.2 Properties of Cytochrome P450cam and Related Monooxygenase Components 207

Page

IV.2.1 Putidaredoxin Reductase 207

IV.2.1.1 Spectral Analysis 207

IV.2.2 Putidaredoxin 212

IV.2.2.1 Spectral Analysis 212

IV.2.2.2 Purity 212

IV.2.2.3 Stability 215

IV.2.3 Cytochrome P450cam 216

IV.2.3.1 Spectral Analysis of Substrate-Bound P450cam . . 216

IV.2.3.2 Spectral Analysis of Substrate-Free P450cam . . . 219

IV.2.3.3 Purity 224

IV.2.3.4 Stability 225

IV.2.4 Myoglobin 230

IV.2.4.1 Spectral Analysis 230

IV.3 Reconstitution of Cytochrome P450cam with Hemin Chloride 233

IV.3.1 Apocytochrome P450cam 233

IV.3.2 Pyridine Hemochrome of Extracted Heme 237

IV.3.3 Reconstitution of Cytochrome P450cam 238

IV.3.4 Purity of Reconstituted Cytochrome P450cam 246

IV.3.5 Stability of Reconstituted Cytochrome P450cam 246

IV.4 Study of the Reaction of CO with the Ferrous State of Myoglobin and the P450cam Systems by Flash Photolysis . . . 247

Page

IV.4.1 Treatment of Data 247

IV.4.2 Study of the Reaction of CO with the Ferrous State of Myoglobin by Flash Photolysis . . . 249

IV.4.3 Study of the Reaction of CO with the Ferrous State of Native, Substrate-bound Cytochrome P450cam by Flash Photolysis 263

IV.4.4 Study of the Reaction of CO with the Ferrous State of Protohemin-reconstituted, Substrate-bound Cytochrome P450cam by Flash Photolysis 277

IV.5 Spectrophotometric Determination of the Equilibrium Constant for the Reaction of CO with the Ferrous State of Native, Substrate-bound Cytochrome P450cam 291

IV.5.1 Treatment of Data 291

IV.5.2 CO-Binding to Native Cytochrome P450cam 293

CHAPTER V GENERAL CONCLUSIONS AND SOME RECOMMENDATIONS FOR FUTURE WORK 308

REFERENCES 314

APPENDIX 326

APPENDIX I Flash Photolysis Unit Operating Instructions 327

APPENDIX II Derivation of the Rate Law for the Interaction of Carbon Monoxide with Simple Hemoproteins 340

APPENDIX III Raw Data for the Preliminary Determination of the Extent of Photodecomposition of Fully Carbonylated Myoglobin and Cytochrome P450cam 345

APPENDIX IV Raw Data for the Flash Photolysis Studies of the Reaction of CO with the Ferrous State of Myoglobin and the P450cam Systems 348

		Page
APPENDIX IVa	Kinetic Run 2 for the Myoglobin-CO System	349
APPENDIX IVa	Kinetic Run 3 for the Native P450cam-CO System	353
APPENDIX IVc	Kinetic Run 2 for the Protohemin-reconstituted P450cam-CO System . . .	357
APPENDIX V	Raw Data for the Spectrophotometric Determination of the Equilibrium Constant for the Reaction of CO with the Ferrous State of Native Cytochrome P450cam	361
APPENDIX Va	Equilibrium Runs 1, 2 and 4	362
APPENDIX Vb	Equilibrium Runs 5 and 6	363

LIST OF TABLES

Table		Page
II.1	Equilibrium Data for Reversible CO-binding to Cytochrome P450	71
II.2	Kinetic Data for Reversible CO-binding to Cytochrome P450	72
II.3	Data for Binding of CO and O_2 to the Ferrous States of Substrate-bound P450cam, and Myoglobin	86
III.1	Absorbance Data for the Pyridine Hemochromes Derived from Proto- and Deuterohemin	99
III.2	Absorbance Data for the Pyridine Hemochrome Derived from Mesohemin	106
III.3	Absorbance Data for the Pyridine Hemochrome Derived from Diacetyl-deuterohemin	110
III.4	Absorbance Data for the Pyridine Hemochrome Derived from Dibromo-deuterohemin	116
III.5	Volumes of Buffers Utilized during Protein Isolation and Purification	137
III.6	Quantities of Reagents for Protein Isolation and Purification	138
III.7	Saturation Levels and Quantities of $(NH_4)_2 SO_4$ Required for the Precipitation of Cytochrome P450cam and Related Protein Components	143
III.8	Yields of Cytochrome P450cam and Related Protein Components	146
III.9	Absorbance Data for the Pyridine Hemochrome Derived from Heme Extracted from Cytochrome P450cam	154
III.10	Most Effective Filter Combinations for the Flash Photolysis Study of Ferrous Myoglobin and Cytochrome P450cam with CO .	184

Table		Page
IV.1	Absorbance Data for Putidaredoxin reductase and Substrate-free Cytochrome P450cam	209
IV.2	Absorbance Data for Putidaredoxin	214
IV.3	Absorbance Data for Substrate-bound Cytochrome P450cam	218
IV.4	Absorbance Data for Substrate-free Cytochrome P450cam	223
IV.5	Absorbance Data for the Various forms of Myoglobin	232
IV.6	Absorbance Data for Substrate-bound Reconstituted Cytochrome P450cam	244
IV.6.1	Kinetic Data from Kinetic Run 2 for the Reaction of CO with Ferrous Myoglobin at 20°C.	251
IV.7	Kinetic Data from Kinetic Run 1 for the Reaction of CO with Ferrous Myoglobin at 20°C.	252
IV.8	Kinetic Data from Kinetic Run 3 for the Reaction of CO with Ferrous Myoglobin at 20°C.	253
IV.9	Kinetic Constants obtained for the Reaction of CO with Ferrous Myoglobin at 20°C.	261
IV.10	Kinetic Data from Kinetic Run 3 for the Reaction of CO with the Ferrous State of Native Substrate-bound, Cytochrome P450cam at 20°C.	265
IV.11	Kinetic Data from Kinetic Run 1 for the Reaction of CO with the Ferrous State of Native Substrate-bound, Cytochrome P450cam at 20°C.	266
IV.12	Kinetic Data from Kinetic Run 2 for the Reaction of CO with the Ferrous State of Native Substrate-bound, Cytochrome P450cam at 20°C.	267

Table		Page
IV.13	Kinetic Constants obtained for the Reaction of CO with the Ferrous State of Native Substrate-bound Cytochrome P450cam at 20°C.	276
IV.14	Kinetic Data from Kinetic Run 2 for the Reaction of CO with the Ferrous, Substrate-bound State of Protohemin-reconstituted Cytochrome P450cam at 20°C.	279
IV.15	Kinetic Data from Kinetic Run 1 for the Reaction of CO with the Ferrous, Substrate-bound State of Protohemin-reconstituted Cytochrome P450cam at 20°C.	280
IV.16	Kinetic Data from Kinetic Run 3 for the Reaction of CO with the Ferrous, Substrate-bound State of Protohemin-reconstituted Cytochrome P450cam at 20°C.	281
IV.17	Kinetic Constants obtained for the Reaction of CO with the Ferrous, Substrate-bound State of Protohemin-reconstituted Cytochrome P450cam at 20°C.	289

LIST OF FIGURES

Figure		Page
I.1	The structure of the heme unit.	4
I.2	Some oxygen chemistry	6
I.3	Various substituted hemins	9
II.1	The first reported spectrum of the carbon monoxide complex of reduced liver microsomal cytochrome P450	13
II.2	Photochemical action spectrum for the light reversal of the CO-inhibited C-21 hydroxylation of 17α-hydroxy-progesterone	15
II.3	The first reported spectral changes that occurred upon addition of substrate to microsomal P450	17
II.4	Some reaction pathways catalysed by cytochrome P450	23
II.5	Proposed classes of cytochrome P450 . . .	24
II.6	The cytochrome P450-mediated activation of phenanthrene	30
II.7	Structure of one of the four possible isomers of N-(2-oxoethyl) protoporphyrin IX isolated from acetylene-treated liver microsomes	31
II.8	Postulated mechanism of the auto-catalytic alkylation of the prosthetic heme of cytochrome P450 during attempted metabolism of acetylenes	33
II.9	Heme environments of Myoglobin, Hemoglobin and Peroxidase	43
II.10	Proposed reaction cycle of cytochrome P450	46

Figure		Page
II.11	Absorption spectra of the various states of cytochrome P450cam	48
II.12	Optical spectra of carbonylated and oxygenated ferrous cytochrome P450cam . . .	50
II.13	General features of a flash photolysis apparatus	68
III.1	Absorption spectrum of the deuterohemin pyridine hemochrome	100
III.2	Absorption spectrum of protoporphyrin IX in formic acid	103
III.3	Absorption spectrum of mesoporphyrin IX in formic acid	103
III.4	Absorption spectrum of the mesohemin pyridine hemochrome	107
III.5	Absorption spectrum of the diacetyl-deuterohemin pyridine hemochrome	111
III.6	Absorption spectrum of the dibromo-deuterohemin pyridine hemochrome	117
III.7	OD660nm and pH profiles for bacterial growth in the L-broth medium	128
III.8	OD660nm and pH profiles for bacterial growth in the first set of 500mL shake-flask media	129
III.9	OD660nm and pH profiles for bacterial growth in the second set of 500 mL shake-flask media	130
III.10	OD660nm and pH profiles for bacterial growth in the 14L fermentor media	131
III.11	Flow chart for the isolation and purification of cytochrome P450cam and related bacterial monooxygenase components from *P putida*, strain ^{P}PG786	133

Figure		Page
III.12	A schematic diagram of the Sephadex G-100 columns	136
III.13	The cell-tonometer	138
III.14	A schematic drawing of the DE-52 column constructed from a 50mL disposable syringe	158
III.15	Block diagram of the flash photolysis apparatus	164
III.16	Structural details of the flash and sample compartment of the flash photolysis unit	166
III.17	Schematic diagram of the cylindrical water-bath	169
III.18	Complete working circuit of the Analog Rate converter	172
III.19	Schematic diagram of the rectangular water-bath	176
III.20	Data acquisition sheets utilized for the collection of kinetic data	178
III.21	Absorption spectra of the ferrous and ferrous-CO states of myoglobin and cytochrome P450cam along with the broadband cutoff and narrowline interference filters most suited for the flash photolysis experiments	182
III.22	Time-based characteristics of the flash output from a typical photographic flashgun	186
III.23	Pulse characteristics of the flash output from the Braun flashgun	186
III.24	Graph of optical density measured on the Cary spectrophotometer *vs* voltage on the flash unit	189

Figure		Page
III.25	Spectra of the kinetic intermediates formed by the photodecomposition of the ferrous-CO complexes of myoglobin and cytochrome P450cam	191
III.26	Data acquisition sheets utilized for the collection of equilibrium data	193
IV.1	Growth of *P. putida* strain PpG786, at the 1.0L shake-flask during early growth experiments	199
IV.2	Growth of *P. putida*, strain PpG786, at the 14L fermentor stage during early growth experiments	199
IV.3	Growth characteristics of *P. putida*, strain PpG786, over extended lengths of time in shake-flask media	200
IV.4	Absorption spectra of putidaredoxin reductase	208
IV.5	Reference spectra of purified putida-redoxin reductase	211
IV.6	Absorption spectra of various states of putidaredoxin	213
IV.7	Absorption spectra of various states of substrate-bound cytochrome P450cam . . .	217
IV.8	Absorption spectra of the ferric state of substrate-bound and substrate-free cytochrome P450cam	220
IV.9	Absorption spectra of various states of substrate-free cytochrome P450cam	222
IV.10	Absorption spectra of cytochrome P450cam purified in the presence of 20-50 mM potassium ions and in the absence of substrate	226
IV.11	Various spectra of partially dimerized substrate-bound cytochrome P450cam	228

Figure		Page
IV.12	Absorption spectra of various states of myoglobin	231
IV 13	Absorption spectra of apocytochrome P450cam	234
IV.14	Absorption spectra of various states of the protohemin - apocytochrome solution	239
IV.15	Absorption spectra of various states of protohemin in aqueous phosphate buffer	239
IV.16	Absorption spectra of the cysteine-incubated protohemin-apocytochrome solution	242
IV.17	Absorption spectra of various states of the reconstituted cytochrome P450cam following DE-52 anion exchange chromatography	242
IV.18	Absorption spectra of various states of the substrate-bound protohemin-reconstituted cytochrome P450cam	243
IV.19	Representative data from Kinetic Run 2 for the reaction of CO with the ferrous state of myoglobin	250
IV.20	Variation in the slope of the ln(A-Ae) *vs.* time plots with changes in CO concentration for Kinetic Run 2 of the myoglobin system	256
IV.21	Plots of $t_{\frac{1}{2}}$ *vs.* k_{obs}^{-1} data from kinetic Runs 1, 2 and 3 for the myoglobin-CO system	258
IV.22	Plots of k_{obs} *vs.* CO concentration data from kinetic Runs 1, 2 and 3 for the myoglobin -CO system	259
IV.23	Graph of the fluctuation in protein concentration during kinetic Runs 1, 2 and 3 for the myoglobin -CO system . .	260

Figure		Page
IV.24	Representative data from kinetic Run 3 for the reaction of CO with the ferrous substrate-bound state of native cytochrome P450cam	264
IV.25	Variation in the slope of the ln(A-Ae) *vs.* time plots with changes in CO concentration for kinetic Run 3 of the native P450cam-CO system	269
IV.26	Plots of $t_{\frac{1}{2}}$ *vs.* the analog-derived k_{obs}^{-1} values for kinetic Runs 1, 2 and 3 for the native P450cam-CO system . .	271
IV.27	Plots of $t_{\frac{1}{2}}$ *vs.* the computer-derived k_{obs}^{-1} values for kinetic Runs 1, 2 and 3 for the native P450cam-CO system . .	272
IV.28	Plots of k_{obs} *vs.* CO concentration data for kinetic Runs 1, 2 and 3 for the substrate-bound native P450cam-CO system . .	274
IV.29	Graph of the fluctuations in protein concentration throughout kinetic Runs 1, 2 and 3 for the native P450cam-CO system . .	275
IV.30	Representative data from kinetic Run 2 for the reaction of CO with the ferrous substrate-bound state of protohemin-reconstituted cytochrome P450cam	278
IV.31	Variation of the slope of the ln(A-Ae) *vs.* time plots with CO concentration for kinetic Run 2 of the protohemin-reconstituted P450cam-CO system	283
IV.32	Plots of $t_{\frac{1}{2}}$ *vs.* the analog-derived k_{obs}^{-1} data for kinetic Runs 1, 2 and 3 for the protohemin-reconstituted P450cam-CO system	285
IV.33	Plots of $t_{\frac{1}{2}}$ *vs.* the computer-derived k_{obs}^{-1} data for kinetic Runs 1, 2 and 3 for the protohemin-reconstituted P450cam system	286
IV.34	Plots of k_{obs} *vs.* CO concentration data for kinetic Runs 1, 2 and 3 for the substrate-bound protohemin-reconstituted P450cam-CO system	287

Figure		Page
IV.35	Graph of the fluctuations in protein concentration during kinetic Runs 1, 2 and 3 for the substrate-bound protohemin-reconstituted P450cam-CO system	288
IV.36	Spectral changes observed for Equilibrium Run 3 by the addition of CO to the ferrous substrate-bound state of native cytochrome P450cam	294
IV.37	Raw data obtained for Equilibrium Run 3 . .	296
IV.38	Plots of log $\frac{A-Ao}{A_\infty-A}$ *vs.* log[CO] for Equilibrium Runs 1-4	297
IV.39	Decomposition of dithionite in phosphate buffer	300
IV.40	Decomposition of dithionite in the presence of ferrous cytochrome P450cam	301
IV.41	Decomposition of dithionite in the presence of fully carbonylated ferrous P450cam enzyme	302
IV.42	Absorbance changes observed at 445nm of the partially carbonylated P450cam system following disappearance of the dithionite peak	303
IV.43	Spectral changes observed for Equilibrium Run 5	305
IV.44	Plots of log $\frac{A-Ao}{A_\infty-A}$ *vs.* log[CO] for Equilibrium Runs 5 and 6	306

LIST OF ABBREVIATIONS

The following list of abbreviations and common names, many of which are commonly adopted in chemical research literature, will be employed in this thesis.

A	absorbance
Å	angstrom(s)
Ao	observed absorbance at the start of an experiment
Ae	observed absorbance when equilibrium has been established
A_∞	observed absorbance when a reaction has been completed
amp	ampere(s)
Asn	asparagine
atm	atmosphere(s)
Br	bromo, -Br
buffer P	50mM phosphate buffer, pH 7.0
buffer P-100	50mM phosphate buffer, pH 7.0, 50mM KCl
buffer T	50mM Tris buffer, pH 7.3
buffer T-50	50mM Tris buffer, pH 7.3, 50mM KCl
buffer T-100	50mM Tris buffer, pH 7.3, 100mM KCl
buffer T-600	50mM Tris buffer, pH 7.3, 600mM KCl
βME	β-mercaptoethanol
^oC	degrees centigrade
cam or camphor	D-(+)-camphor (2-bornanone)
Cat	catalase
C-H	carbon-hydrogen bond
cm	centimetre(s)

CO	carbon monoxide
Cys	cysteine
D.C.	direct current
DE-52	anion exchange resin
deuterohemin	deuteroporphyrinatoiron(III)
diacetyldeuterohemin	diacetyldeuteroporphyrinatoiron(III)
dibromodeuterohemin	dibromodeuteroporphyrinatoiron(III)
DMF	N,N-dimethylformamide
DNase	deoxyribonuclease I
DTT	dithiothrietol
ENDOR	electron nuclear double resonance
EPR	electron paramagnetic resonance
ESR	electron spin resonance
g	gram
Gly	glycine
h	hour or Planck's constant
ΔH^{o}	standard enthalpy change for the reaction
ΔH^{*}	enthalpy of activation
H_2	hydrogen gas
H_2O_2	hydrogen peroxide
Hb	hemoglobin
HCl	hydrochloric acid (gas or solution)
heme	iron(II) porphyrin(s)
heme unit	protoporphyrinatoiron(II) complex
hemin	iron(III) porphyrin(s)
hemoprotein	biological heme-containing protein
His	histidine
HRP	horse-radish peroxidase

K	equilibrium constant
k	kinetic rate constant
Kco	equilibrium constant for carbon monoxide binding
Ko_2	equilibrium constant for dioxygen binding
k_{on}	kinetic rate constant for CO-association to myoglobin or cytochrome P450cam
k_{off}	kinetic rate constant for the dissociation of CO from ligand-bound myoglobin or cytochrome P450cam
k_{obs}	pseudo first-order rate constant
L	litre
ln	natural logarithm
log	common logarithm
Lys	lysine
M	molarity
max	maximum
Mb	myoglobin
MCD	magnetic circular dichroism
mesohemin	mesoporphyrinatoiron(III)
methmyoglobin	ferrous (Fe(II)) state of myoglobin
metmyoglobin	ferric (Fe(III)) state of myoglobin
mg	milligram(s)
min	minute(s) or minimum
mL	millilitre(s)
mm	millimetre(s)
mM	millimolar
msec	millisecond(s)
myoglobin-CO	carbon monoxide complex of methmyoglobin

NADH	reduced nicotinamide adenine dinucleotide
NAD^+	oxidized nicotinamide adenine dinucleotide
NADPH	reduced nicotinamide adenine dinucleotide phosphate
$NADP^+$	oxidized nicotinamide adenine dinucleotide phosphate
nm	nanometre(s)
NMR	nuclear magnetic resonance
O_2	dioxygen
OD660nm	optical density at 660nm
$P_{\frac{1}{2}}$	pressure at which 50% of the system is converted
$P_{\frac{1}{2}}^{CO}$	pressure at which 50% of the system is carbonylated
$P_{\frac{1}{2}}^{O}2$	pressure at which 50% of the system is oxygenated
P420	degraded form of cytochrome P450
P450	cytochrome P450
P450cam	*Pseudomonas putida* cytochrome P450cam
P450Fe(II) or Fe(II)P450	ferrous state of cytochrome P450
P450camFe(II) or Fe(II)P450cam	ferrous state of *Pseudomonas putida* cytochrome P450cam
P450-CO, P450Fe(II)-CO or Fe(II)P450-CO	carbonylated cytochrome P450
P450cam-CO or Fe(II)P450cam-CO	carbonylated *Pseudomonas putida* cytochrome P450cam
PA	phosphate-ammonium
pH	$-\log [H^+]$
pI	isoelectric point
protohemin	protoporphyrinatoiron(III)

RNase	ribonuclease I
rpm	revolutions per minute
RR	resonance Raman
RS^-	mecaptide or thiolate anion
S or sec.	second(s)
S	spin state
ΔS^o	standard entropy change for the reaction
ΔS^*	entropy of activation
Ser	serine
T	temperature
t	time
$t_{\frac{1}{2}}$	half-life
Thr	threonine
TLC	thin layer chromatography
Tris	tris(hydroxymethyl)aminomethane
Trizma base	tris(hydroxymethyl)aminomethane free base
Tyr	tyrosine
UV	ultraviolet
V	voltage
W	watt(s)
Y	fraction of product formed during a particular experiment
ε_{mM}	millimolar extinction coefficient
λ	wavelength
μ	micro
ν	frequency
Π	bonding where electron density is on either side of the internuclear plane

σ	bonding where electron density is maximum on an internuclear axis
100xsalts	stock solution of essentials salts required for bacterial growth
[ ]	square brackets denote molar concentration
v/v	volume per volume
v/w	volume per weight
%	percentage
≃	approximately equals to
>	greater than
<	less than

ACKNOWLEDGEMENTS

I wish to thank Professors David Dolphin and Brian R. James for their guidance and encouragement throughout the course of this work, particularly for their many valuable comments (and patience) during the preparation of this thesis.

I also would like to acknowledge Diana Colnett for her expert artistry and my wife, Andrea, whose constant support helped me keep my sanity during the writing of this thesis. Finally, I must thank Annette Hiom (who deserves the Purple Heart) and Judy Munz for their expertise in typing this thesis.

CHAPTER I

INTRODUCTION

I Introduction

Throughout the evolution of living organisms Nature has devised complex and intricate physiological systems capable of sustaining life. The chemistry of these systems is frequently controlled by enzymes, which are highly specialized protein molecules capable of catalysing the biochemical reactions necessary to support functioning cells. The catalytic center, or active site, of many of these enzyme systems requires only their three dimensional structure as proteins for enzymatic activity; however, others utilize, in addition, non-protein cofactors for catalytic functioning. These cofactors, which are known as coenzymes, often take the form of metal ions or complex organic molecules, and sometimes both are required. Scientists from all disciplines have long been fascinated by the remarkable chemistry produced at these biocatalytic centers, which far exceed their man-made counterparts in reaction specificity, catalytic efficiency and capacity to operate under mild conditions. As a result, a great deal of research has been directed towards understanding the particular biological and structural properties which allow for enzymatic functioning, as well as mimicking the catalytic properties for the purpose of designing efficient model and industrial catalysts.

One class of biocatalysts which has been under increasingly intensive investigation for the past two decades is the cytochromes P450 (P450).[1-5] The active site of this

group of enzymes is an iron atom centered at the core of the complex organic protoporphyrin IX nucleus (Figure I.1). This non-protein moiety, known as the heme unit, is utilized extensively in Nature where small changes in the heme environment, as provided by the protein, can dramatically alter the catalytic process that occurs at the iron center.[6] One particular reaction catalysed by the cytochromes P450 can be generalized in Reaction I.1, where R is a saturated hydrocarbon molecule.

$$RH + O_2 + NADH + H^+ \longrightarrow ROH + H_2O + NAD^+ \quad (I.1)$$

The unique environment of the heme unit in these enzyme systems allows for direct metal-mediated activation of molecular dioxygen (O_2) for the selective insertion of one oxygen atom into substrates. As shown in Reaction I.1, the active oxidizing agent is typically capable of oxidizing unactivated C-H bonds to the corresponding alcohols. For this particular function the cytochromes P450 are collectively known as oxygenases, which are a class of biocatalysts that incorporate one or two atoms from O_2 into a substrate; the P450 cytochromes are therefore monooxygenases. Dioxygen is also activated by heme-containing oxidases whose catalytic function closely resembles that of the oxygenases but both atoms of O_2 are converted to water or hydrogen peroxide (H_2O_2) *via* what are frequently dehydrogenation reactions.

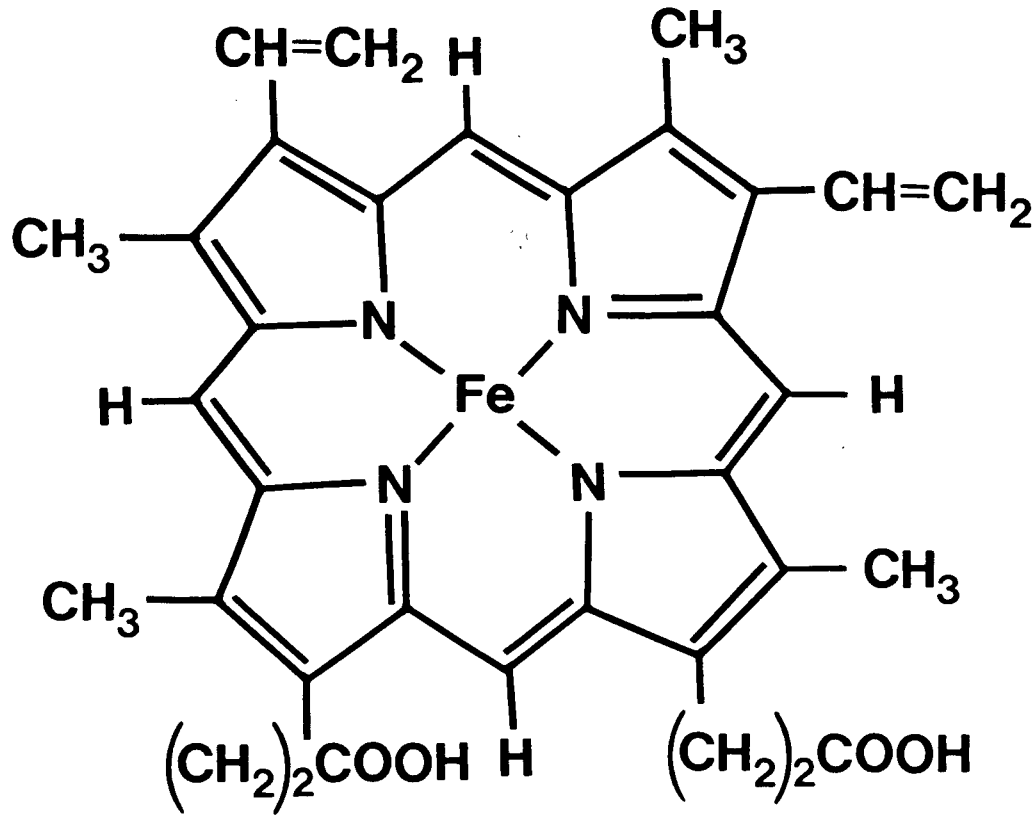
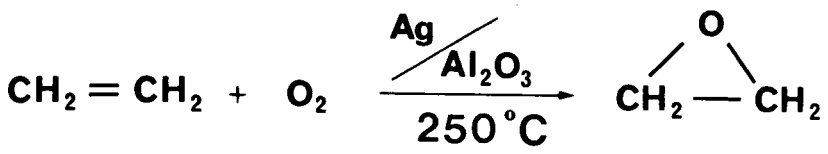


Figure I.1 The structure of the heme unit

The activation of molecular dioxygen by metal complexes for the oxidation of organic compounds is of great industrial importance and is used extensively today.[7] The best known example of a metal-mediated transfer of an oxygen atom to an organic substance is the commercially important gas-phase oxidation of ethylene to ethylene oxide using a silver catalyst (Reaction I.2).



(I.2)

As well, the oxidation of organic substrates by transition-metal salts has been used widely in the petrochemical industry for many years.[7] A substantial drawback to many of the metal-catalysed oxidation processes is that the reactions are frequently non-selective because they proceed *via* free-radical pathways that are often initiated by the metal ion. That is, the chemical fate of O_2, activated through metal-coordination in these processes, is difficult to control because of the variety of pathways open for O_2 reactions after activation (Figure I.2). Therefore, the search for metal catalysts to promote more selective oxidations, especially using O_2, is a prime goal that has immense potential on an industrial scale and is thus an important research area.[8] The ultimate aim would be to mimic the O_2-activation ability of the cytochromes P450.

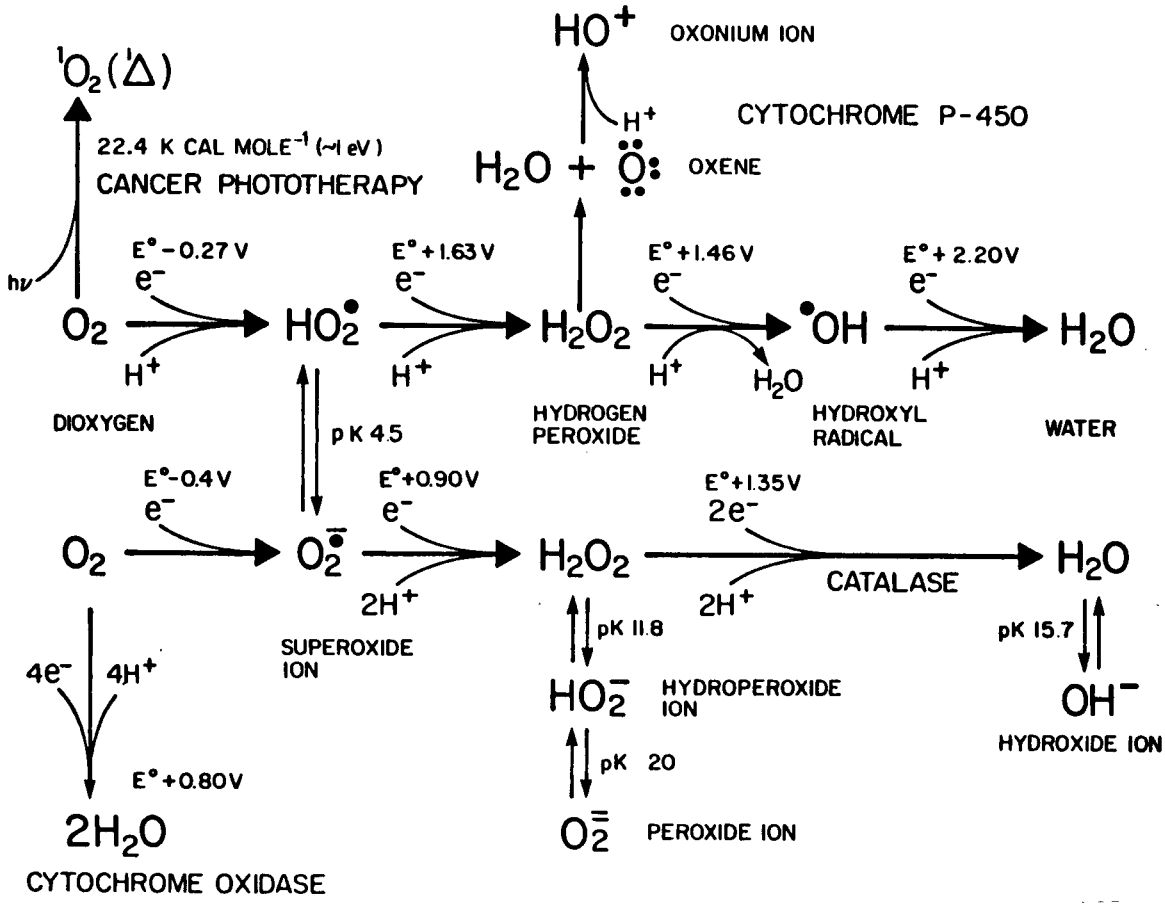
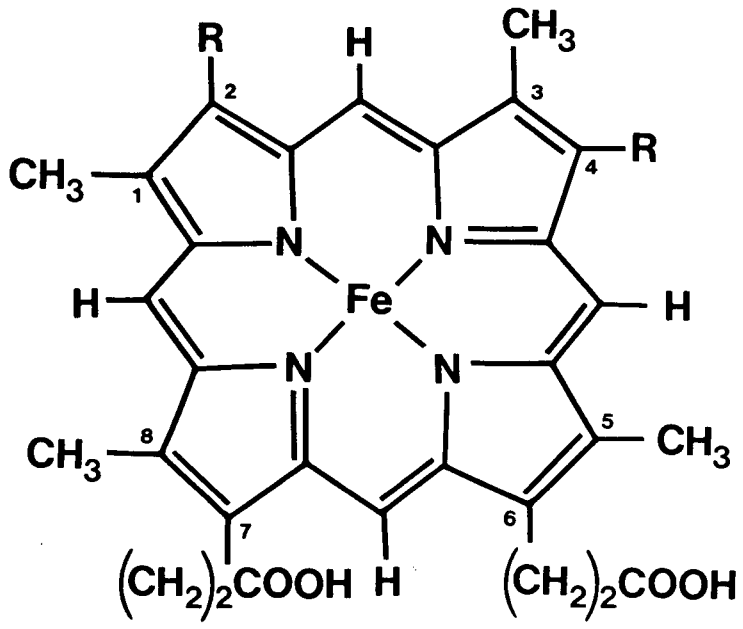


Figure I.2 Some oxygen chemistry. Potentials in the top half of the figure are at pH 0.0 while the bottom half are at pH 7.0 ; Ref. 106.

The use of metalloporphyrins as catalysts for selective O_2 activation is an attractive idea because of their use as selective catalytic centers in many biological systems. Comparison of the cytochrome P450 monooxygenases with various other heme-containing proteins such as myoglobin (Mb) and hemoglobin (Hb) (reversible O_2 binding), cytochrome *c* oxidase (the terminal enzyme in the respiratory redox chain that reduces O_2 to H_2O), and the enzymes catalase (Cat) and horseradish peroxidase (HRP) (catalytic decomposition of H_2O_2) indicates the diversity of selective O_2-related chemistry that can take place at the (iron) metalloporphyrin center.[6] People have long sought for simpler protein-free coordination complexes, such as metalloporphyrins, that might mimic the properties of the natural systems, for example, in terms of O_2-carrying ability and for activation of O_2 for subsequent reactivity as in the oxygenases and oxidases. With regard to model catalysts mimicking cytochrome P450 oxygenations, simple metalloporphyrins have been shown to catalyze the autoxidation (which refers to oxidation with dioxygen) of olefins such as cyclohexene.[9] The catalyses however, are thought to proceed *via* olefin activation rather than O_2 activation. Furthermore, since no reports have appeared to date on the oxidation of substrates using metalloporphyrins under conditions at which dioxygen complexes are known to exist, substrate rather than O_2 activation is thought to be a common feature of these reactions. It is evident, therefore, that

although metalloporphyrins remain as attractive catalysts *via* such substrate activation, they appear to have limited ability for O_2 activation.[9] The apparent differences in catalytic function of the natural P450 systems and the model catalysts are difficult to assess and are the subject of extensive reviews.[7,8] Clearly, a more thorough understanding of the factors affecting the interaction of O_2 with the natural enzymes as well as the model systems is required for a better appreciation of the nature of the metal-O_2 interaction and the role of the protein. These structure-function relationships are vital for the production of metalloporphyrin catalysts that closely mimic monooxygenase activity.

Recently, reduced bacterial cytochrome P450, containing proto-, meso-, deutero-, dibromodeutero-, and diacetyldeuteroporphyrinatoiron (II) (heme) centers, (Figure I.3) has been shown to bind O_2 reversibly as well as carbon monoxide (CO).[10] The reconstituted systems, which were all shown to catalyze Reaction I.1, provide an excellent opportunity to further assess the factors affecting the catalytic properties of the metalloporphyrins that activate O_2. Kinetic and thermodynamic studies on the reaction of small gas molecules (i.e. O_2 and CO) with these natural protein systems, although relatively complex,[8] may provide some conclusions regarding the nature of the metal-gas interaction as well as the role of the protein in cytochrome P450-mediated oxidations. This will, in turn,



R = $-CH_2-CH_3$ Mesoporphyrinatoiron (III)

$-H$ Deuteroporphyrinatoiron (III)

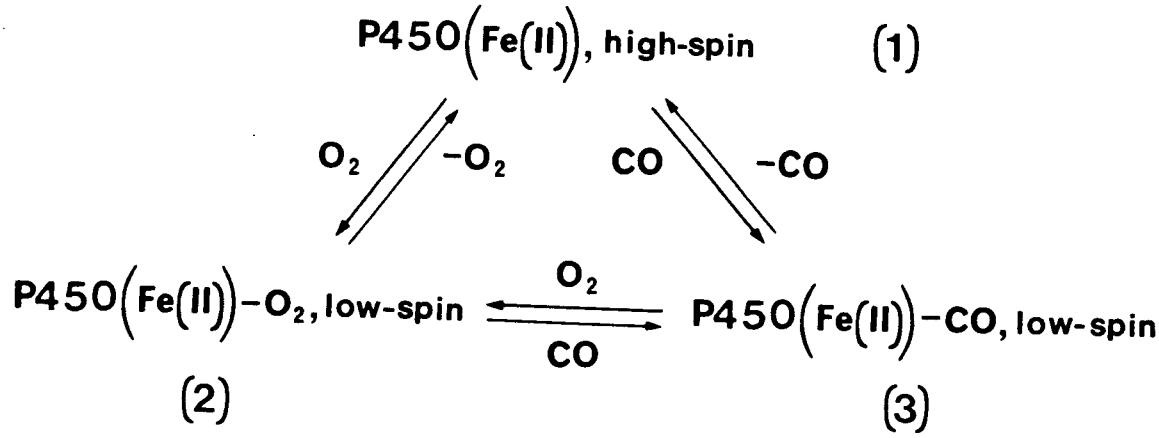
$-C(=O)-CH_3$ Diacetyldeuteroporphyrinatoiron (III)

$-Br$ Dibromodeuteroporphyrinatoiron (III)

Figure I.3 Various substituted hemins.

provide a better understanding of the structure-function relationships required for more selective O_2-activation by simple (protein-free) metalloporphyrin catalysts.

The main object of the work described in this thesis was therefore, to set up a flash photolysis apparatus for the systematic kinetic analysis of conversions such as 1 ⟶ 2 and 1 ⟶ 3 for native and the heme-reconstituted *Pseudomonas putida* P450cam (P450cam) systems (Scheme I.1).



Scheme I.1

Only the conversion of 1 ⟶ 3 (i.e. the carbonylation reactions) is considered here. Synthesis and purification of the meso-, deutero-, diacetyldeutero-, and dibromodeutero-porphyrinatoiron (III) (hemin) macrocycles are outlined. Procedures for growth of *P. putida* and isolation and purification of cytochrome P450cam are detailed along with a general method for reconstitution of native P450cam with modified hemin derivatives. Spectral data for these systems are discussed. The flash photolysis apparatus used for kinetic analyses will be described, together with results from carbonylation

of myoglobin, and native and protohemin-reconstituted cytochrome P450cam. The equilibrium binding constant for the carbonylation of native P450cam, Kco (i.e. for conversion 1 ⟶ 3), is determined and the results discussed. The thesis begins with a literature review examining areas of interest including some historical, biochemical, structural, and mechanistic data followed by a survey of the work reported on the interaction of CO with all classes of cytochromes P450. This thesis finishes with some general conclusions regarding this work and recommendations for future studies.

CHAPTER II

LITERATURE REVIEW

II.1 Historical Overview

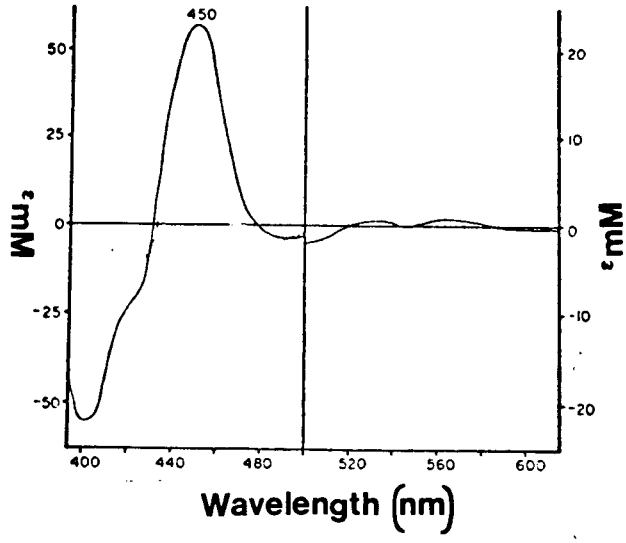


Figure II.1 The first report on the spectral properties of the carbon monoxide complex of reduced liver microsomal cytochrome P450. The solid line curve represents the difference spectrum observed after sodium dithionite reduction in the presence of CO ; Ref. 11.

The presence of a carbon monoxide-binding pigment in liver microsomes was originally reported by Klingenberg[11] in 1958, although this observation was made earlier by G. R. Williams.[12] In these experiments a prominent absorbance band maximum near 450nm in the difference absorbance spectrum was observed when the suspension of microsomes was reduced with sodium dithionite ($Na_2S_2O_4$) in the presence of carbon monoxide (Figure II.1).

Since the CO complexes of the hemoproteins known at that time had Soret maxima at considerably shorter wavelengths (≃420nm), and since the CO difference spectrum of the reduced liver microsomes showed only the peak at 450nm, there was no immediate clue as to the chemical nature of this newly discovered pigment. In 1964, Omura and Sato[13,14] established the hemoprotein nature of the CO-binding pigment. Characterization as a hemoprotein was actually determined from a purified degradation product exhibiting a reduced CO-absorption peak at 420nm. Omura and Sato termed the CO-binding pigments as cytochromes P450 and P420 according to the position of the Soret absorption maximum of the reduced-CO complexes.

Concurrent with these spectroscopic experiments, evidence was accumulating[15] for the presence in liver microsomes of an enzyme system that catalysed the general Reaction II.1.

$$NADPH + H^+ + {}^{18}O_2 + RH \longrightarrow NADP^+ + H_2{}^{18}O + R^{18}OH \quad (II.1)$$

This type of reaction was designated a mixed function oxidation by Mason,[16] a monoxygenation by Hayaishi,[17] and a hydroxylation by Massart and Vercauteren.[17a] The role of cytochrome P450 in the general Reaction II.1 was first shown with adrenal cortex microsomes in 1963 by utilizing evidence indicating that the microsomal fraction known to catalyse the C21-hydroxylation of steroids was inhibited

by carbon monoxide.[18] Taking advantage of the observed light reversibility of the carbonylated ferrous hemoprotein complex (at 450nm) and using a Warburg apparatus,[19] Estabrook and co-workers were able to produce the photochemical action spectrum of the active monoxygenase enzyme present in adrenal cortex microsomes[20] (Figure II.2). Since the photochemical action spectrum showed the same intense absorption peak at 450nm as indicated in the reduced -CO difference spectrum of the liver microsomes, cytochrome P450 was proven to be

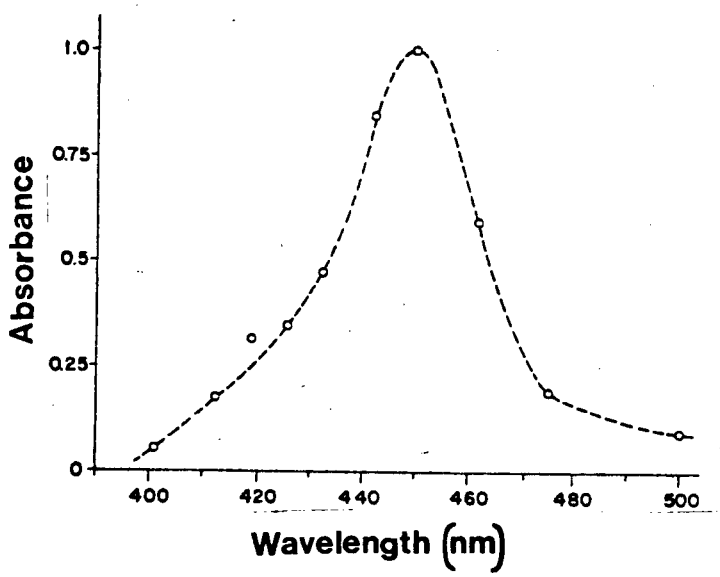
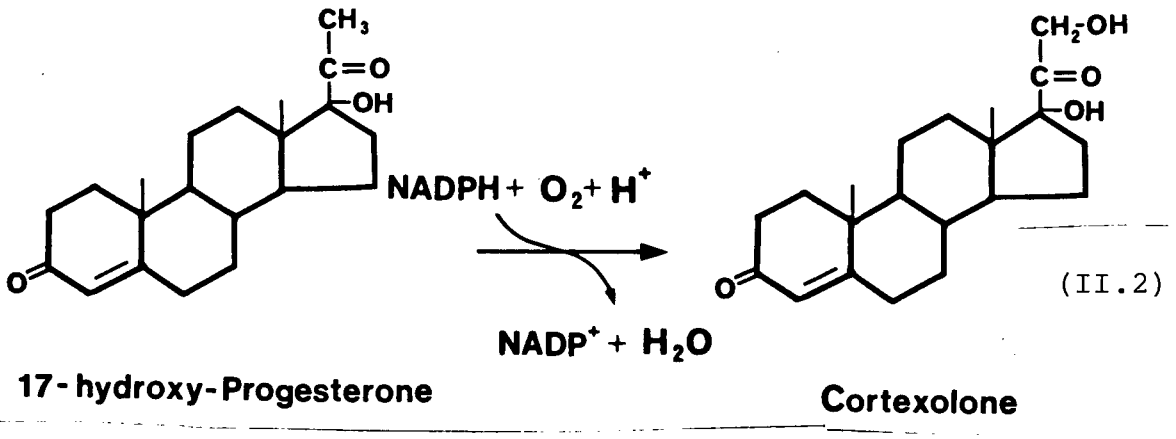


Figure II.2 Photochemical action spectrum for the light reversal of the CO-inhibited C-21 hydroxylation of 17∝-hydroxy-progesterone; Ref.20.

the terminal oxygenase functioning in the C21-hydroxylation of a 17α-hydroxyprogesterone (Reaction II.2).



(II.2)

17-hydroxy-Progesterone

Cortexolone

Today, cytochrome P450 is established to be the terminal oxygenase involved in the monooxygenation of a great variety of foreign, as well as endogenous, lipid soluble compounds.[21,36]

During the mid 1960's, following recognition that cytochrome P450 functioned in a variety of hydroxylation reactions, experiments were carried out to evaluate the molecular events associated with substrate interaction with this hemoprotein. The first successful experiments were performed by Narasimhulu *et al.*[22] who reported a major spectral change in the difference spectrum when 17-hydroxyprogesterone was added to a suspension of adrenal cortex microsomes containing cytochrome P450 (Figure II.3). Subsequent to this observation a wide variety of exogenous and endogenous substrates were examined and the spectral changes characterized.[23]

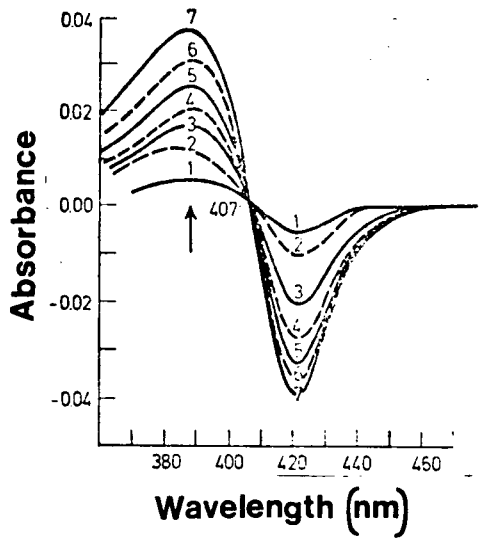
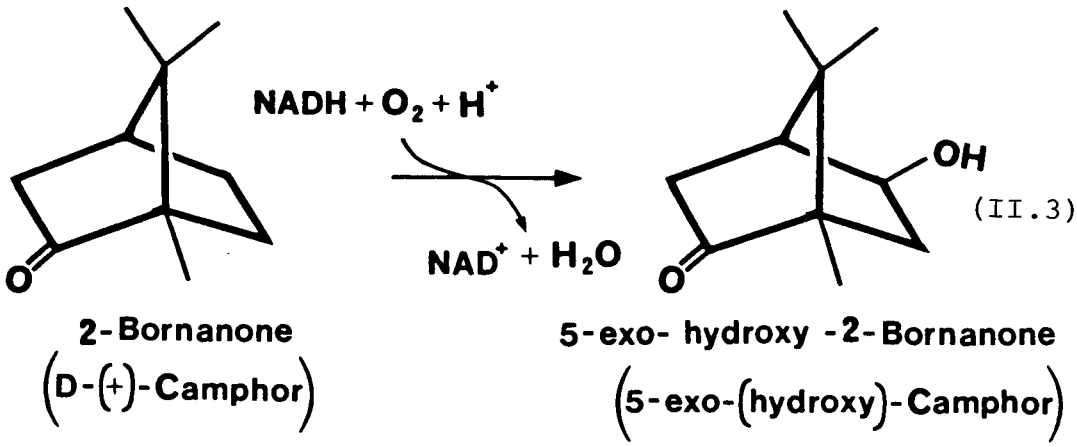


Figure II.3 The first substrate-induced difference spectrum resulting from the addition of increasing amounts of 17-hydroxy-progesterone (up to 10mM) to adrenal cortex microsomes in the absence of reducing agents. The spectrum indicates the magnitude of the spectral change at 420nm (trace 7 represents the maximum depth of the trough) and 388nm (trace 7 represents the maximum height of the peak) with increasing steroid concentration; Ref.22

The spectral changes were interpreted as representing the formation of a high-spin complex between the substrate and the ferric state of the enzyme.[23] Along with these studies, enzyme induction experiments indicated a complex *in vivo* behavior of the drug-metabolizing cytochrome P450 enzymes in liver microsomes.[24] It was postulated that administration of various substrates not only induced the biosynthesis of the enzyme,[24] but also induced specific forms of the enzyme depending on the particular substrate.[25] With improved chromatographic techniques, the isolation and identification of distinct species of cytochrome P450[26] has supported the hypothesis that different classes of inducing agents stimulate

the synthesis of distinct forms of this heme protein.[27]

Since the initial discovery of the enzyme, detailed *in vitro* characterization has been hampered because of the difficulty in obtaining purified, enzymatically active cytochrome P450 samples from mammalian tissues. Attempts to solubilize and purify the microsomal proteins led only to the modified inactive form of the hemoprotein designated as cytochrome P420.[13,14] The mammalian sources of the cytochrome were found to be closely associated with the lipid membrane,[28] and degradation readily occurred upon isolation. A major breakthrough by Gunsalus and co-workers[29] occurred in 1968 during an intensive search for the genetic basis of metabolic diversity among the vast range of bacterial strains found in soil and water. The cytochrome P450 monooxygenase enzyme was isolated from *Pseudomonas putida*, strain PpG 1, known to be involved in the stereospecific oxidation of the bicyclic monoterpene, 2-bornanone (D-(+)-camphor) (Reaction II.3).[30]



(II.3)

Unlike its mammalian counterparts, the enzyme was soluble and readily purified, as were the associated electron transfer proteins required for camphor monooxygenase activity; a flavoprotein designated a NADH-putidaredoxin reductase and an iron-sulphur protein, putidaredoxin.[31] The monooxygenase component was termed cytochrome P450cam (P450cam)[29] since it was isolated from bacteria utilizing camphor as the sole carbon and energy source.

The discovery of this bacterial monooxygenase system has greatly advanced the understanding of the mechanism of cytochrome P450 catalytic action, as well as the biological function of these enzymes. Since the initial identification of an oxygenated form of cytochrome P450cam by Ishimura,[32] the chemical, physical, and biological properties of the individual steps of the catalytic cycle have been probed in detail by Gunsalus[30] and Peterson.[33] The results from these studies confirmed the original hypothesis of Estabrook *et al.*[34] concerning the catalytic cycle of microsomal cytochrome P450. Today, the purified bacterial enzyme is accepted as a definite prototype or biological model representing the entire class of P450 cytochromes. Further refinements of earlier procedures[33d,35,36] for large scale bacterial growth employing a readily autolytic mutant, *Pseudomonas putida*, strain PpG 786, and improved purification techniques, have led to the isolation of crystalline forms of the bacterial enzyme.[37] Detailed studies of the crystalline cytochrome P450cam have produced unambiguous assignment of

much of the structural and spectroscopic properties of the heme active site throughout the catalytic cycle, as well as provided a homogenous source of the protein for sequence and X-ray diffraction analysis.[38] These results have been partially confirmed with the isolation of highly purified, catalytically active liver microsomal cytochrome P450.[39,40] Recently, with the isolation and characterization of a synthetic complex in 1981 by Groves *et al.*[41] analogous to the illusive "activated oxygen complex" produced by the P450 cytochromes, several questions regarding the catalytic cycle have been answered. Thus, the combined efforts of research from all disciplines have promoted an understanding of the catalytic and biological role to such an extent that recently a competent description of the enzymatic mechanism has been possible.[42] Today,[43] major research efforts are directed to explaining the structure-function relationships of the P450 cytochromes and related redox coupling proteins, the *in vivo* induction characteristics of the enzyme in mammalian tissues, the involvement of mammalian P450 cytochromes in chemical carcinogenesis, and modelling P450 oxidations[9] with simpler protein-free catalysts for production of efficient and selective synthetic catalysts. Completion of a three-dimensional model of the bacterial enzyme will verify, as well as complement, much of the present knowledge of the entire class of P450 cytochromes, and will direct research efforts in the future.

II.2 Biological Importance of the P450 Cytochromes

The role of cytochrome P450 in biological systems is the activation of molecular dioxygen for the oxidative biotransformation of substrates. Each of these enzymes is associated with an electron transport system as the terminal electron acceptor which catalyses the reductive cleavage of molecular dioxygen (O_2) with the concomitant transfer of one oxygen atom to the substrate; the other oxygen atom is reduced to water. This specific reactivity has labelled the P450 cytochromes as mixed function oxidase,[16] monooxygenase,[17] or hydroxylase[17] enzyme systems.

The number of substrates that are modified by the cytochrome P450 monooxygenases include a diversified and ever-expanding number of compounds.[44,45] These encompass such materials as steroids,[46] bile acids,[47] fatty acids,[48] approximately 200 different drugs,[25] cyclic and straight-chain hydrocarbons (from saturated to acetylenic species), terpenes, amines, alcohols, phenols, thiophenes, pesticides, food preservatives and additives, and carcinogens.[43-45,49] Although the primary reaction involves incorporation of one oxygen atom into these substrates, the observable consequences of the oxygen atom transfer depends on the precise nature of the substrate. In general,[50,51] the established intermediate outcome of the catalysed oxygen atom transfer is: (a) formation of a hydroxylated derivative by insertion into the bond between a hydrogen and a carbon atom; (b) formation

of an epoxide by addition across a carbon-carbon double bond; or (c) formation of a dipolar oxide by combination with the free electron pair of the heteroatom. These primary reactions often yield unstable intermediates which undergo secondary transformations to yield the final experimentally observed products. Some typical examples of these reaction pathways are given in Figure II.4. Observations have also indicated that the same substrate may further undergo several of the same transformations, or be subjected to a cross section of the possible reactions.[47,52] The proportion between the different alternative reactions is again dependent on the nature of the substrate. The important result of these reactions, however, is the production of a more polar metabolite that can be efficiently utilized by the cell. In cells of lower organisms, these polar intermediates are susceptible to degradative enzymes for rapid access to carbon and energy,[30] while in mammalian cells the by-products can be directed along the physiological biosynthetic pathways or solubilized and excreted.[52]

The significance of these particular biochemical monooxygenation reactions to living organisms is exemplified by the existence of P450 cytochromes in most living organisms. These monooxygenases have been observed in such diverse sources as insects,[56] bacteria[57,58] green plants,[59] fungi,[60] yeasts,[61] fish, birds, amphibians, and mammals.[62] Within the mammalian systems cytochrome P450 is localized

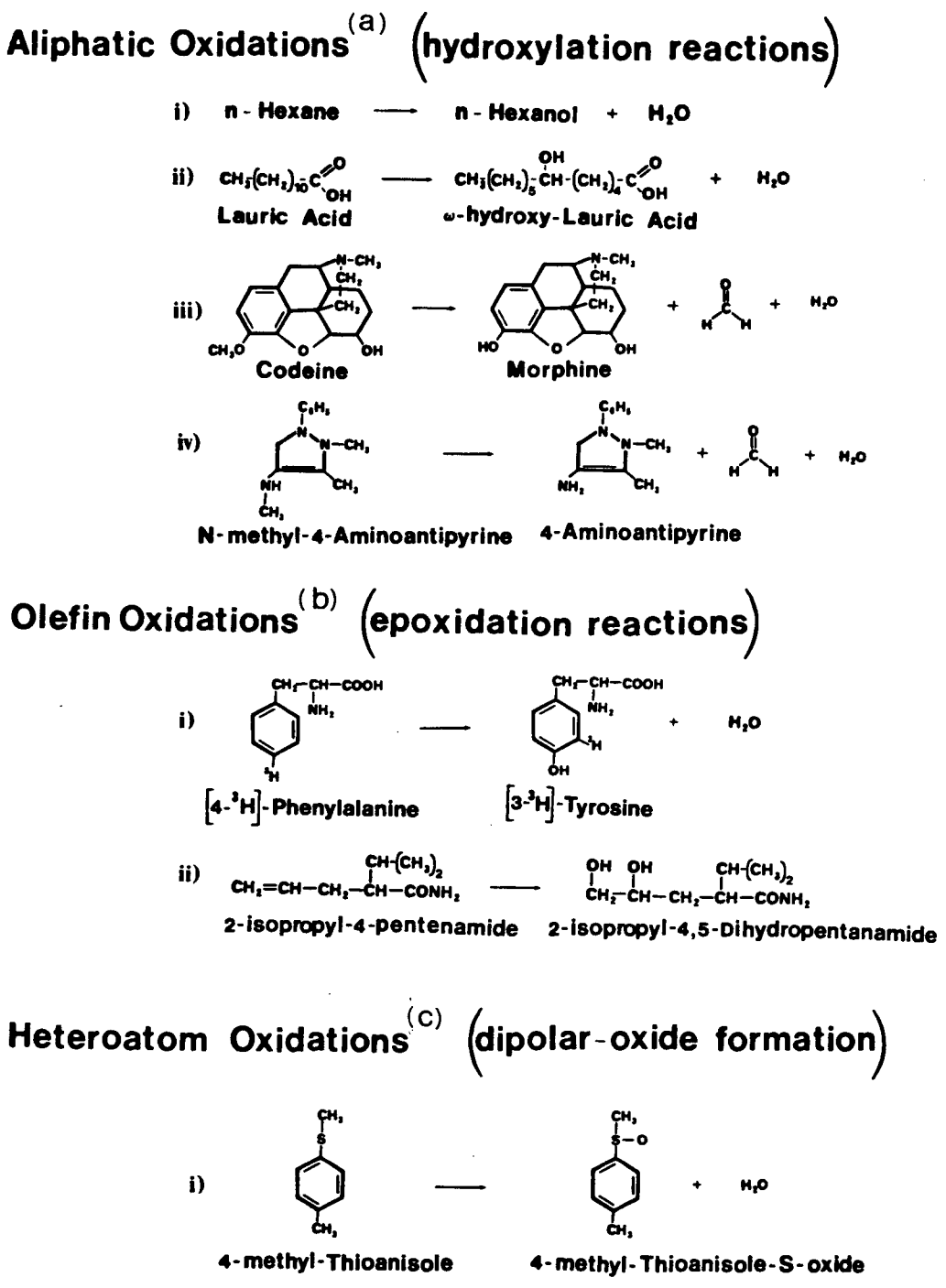


Figure II.4 Some reaction pathways catalysed by cytochrome P450 in the presence of NADH, O_2 and H^+ ions. Note (a) Ref. 53; (b), i) Ref.7 and ii) Ref.54; and (c), Ref.55.

in the endoplasmic reticulum, the mitochondria of the lungs, liver, intestinal mucosa, kidney, pituitary glands, and the steroidogenic organs; adrenal cortex, testes, placenta, and the ovaries.[62] As well, there are three general classes of the P450 cytochromes recognized to catalyse the dioxygen cleavage reaction.[53] These systems are characterized according to source of the enzyme, the nature of the primary electron donors of the electron transport chain, the structural organization required for catalytic activity (Figure II.5) and according to the specific need of the cell where it is found.

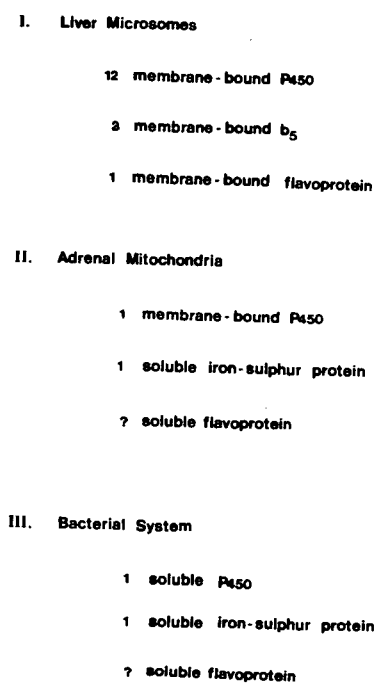


Figure II.5 Proposed classes of cytochrome P450 based on the relationship of the hemoprotein to membrane structure and other electron transfer components required for the overall monooxygenation reaction; Ref.53.

The first class of enzyme systems (the "liver microsomal type") is characterized by cytochrome P450 associated with the endoplasmic reticulum of the liver. The cytochrome P450 monooxygenases in this class exist in a non-equivalent relationship with a second hemoprotein, cytochrome b_5, and at least one flavoprotein dehydrogenase (either NADPH cytochrome c reductase or NADH cytochrome b_5 reductase).[63] The reactivity of this system is intricately involved with the membrane to which it is bound but the function of the membrane in directing the spatial relationships between the electron transport components is, as yet, unknown. A phospholipid component (phospholidyl choline) is also required for enzymatic activity[64] and appears to play some role in mediating the flow of electrons to cytochrome P450 from the flavoproteins.

The liver microsomal cytochrome P450 monooxygenases dominate the hepatic metabolism of endogenous and xenobiotic lipophilic substances.[43-45,49] Characteristic of this enzyme system, and distinguishing it from those of the steroidogenic animal tissues and of microorganisms to be described below, is its virtual lack of substrate specificity;[25] the entire range of compounds mentioned previously can serve as substrates for the liver monooxygenase system. The ability to utilize such a wide range of compounds is manifested in the existence of several different forms of the enzyme in hepatic tissues,[26] each exhibiting slightly different but

overlapping substrate selectivities. These cytochrome P450 isoenzymes are characterized by small but significant changes in the Soret maximum of the reduced CO complexes, distinct molecular weights, and varying catalytic activities.[27,65] Thus, the hepatic organs can produce several types of functional cytochrome P450, which exhibit somewhat different properties and which collectively produce a metabolic apparatus capable of dealing with the great variety of compounds to which these tissues are exposed. Rationale for a metabolic system containing several isoenzymes with a certain degree of specificity instead of one completely unspecific enzyme is speculative;[66] however, with increasing specificity the affinity of an enzyme towards its substrate also increases and high affinity would be required to efficiently remove low levels of toxic compounds from the body. These properties of liver microsomal cytochrome P450 serve as a focal point for present day investigations.[43]

Another important characteristic of the liver microsomal P450 cytochromes concerns the regulation of the isoenzymes in hepatic tissues. The effectiveness of this multienzyme system is optimized through differential induction of the P450 isoenzymes by specific substrates.[25,67] That is, particular substrates can induce the production of forms of the isoenzymes specific for the removal of those particular substrates. As well, the particular isoenzyme can be induced to represent as much as 15-20% of the total membrane-bound

protein in these tissues.[53] Therefore, this metabolic apparatus not only utilizes several different P450 cytochromes but the individual isoenzymes are selectively mobilized depending on the substrate. In this way, it is more economical for the cell to rapidly build up large concentrations of selected isoenzymes which can effectively metabolize a particular substrate than continuously synthesize large amounts of a less efficient enzyme. The versatility of this enzyme system indicates that its primary function is the protection of the host. Recently, Nubert[68] has suggested that this metabolic apparatus may in fact be analogous to a mammalian immune system in producing a different isoenzyme to deal with each substrate. These properties of the liver microsomal cytochrome P450 serve again as a focal point of research today.[43]

The second class of the P450 cytochromes is characterized by a membrane-bound association with the mitochondrial fractions of the steroidogenic tissues[62] (see Figure II.5). It is distinguishable from the first class, by the presence of an $Fe_2S_2CyS_4$ iron-sulphur protein (adrenodoxin) instead of cytochrome b_5 or the phospholipid, as the mediator of electron transport between the flavoprotein dehydrogenase (NADPH-adrenodoxin reductase), and cytochrome P450.[69] Generally, the cytochrome exists in a 1:1 stoichiometric relationship with the iron-sulphur protein.[70] In the

steroidogenic organs, cytochrome P450 is specifically involved in the biosynthesis of messenger and regulatory hormones,[46] the degradation of fatty acids,[47] and the biosynthesis and metabolism of bile acids.[48] Although this enzyme system has not been studied as extensively as the liver microsomal type, it is known to exist in smaller concentrations within the steroidogenic organs (compared with hepatic systems) and exhibit very high substrate specificity.[49] Recently, multiple forms of cytochrome P450-dependent mixed function oxidase systems have been isolated from bovine adrenocortical microsomes,[71] which suggests the same kind of enzyme regulation may be present in the steroidogenic organs as found in liver microsomes. In the steroidogenic organs, high substrate specificity is required for strict control of the physiological pathways found in these tissues.

The final class of cytochrome P450 monooxygenases originates as a bacterial source from *Pseudomonas putida*,[29] although the enzyme system has been isolated from other species of bacteria[30,57,58] (see Figure II.5). Like the cytochrome systems in the mitochondria, the bacterial cytochrome P450 exists in a 1:1 stoichiometric relationship with an $Fe_2S_2Cys_4$ iron-sulphur protein (putidaredoxin). This system also utilizes a flavoprotein which can either be of the NADH or NADPH mediated type (putidaredoxin reductase).[21] The great advantage of this system is that all components are readily soluble and easily purified proteins which do

not require membrane association for catalytic activity. In the microbe, high turnover rates with rapid access to carbon and energy require high substrate specificity for competitive advantages.[30]

Comparison of the broad phylogenetic separation of these three classes of P450 cytochromes indicates that these enzymes are a basic metabolic tool required by most organisms for survival. Recently, however, it has become evident that the action of the P450 cytochromes on a number of different classes of substrates creates reactive metabolites that exhibit fatal effects on the cell.[43] Two specific groups of substrates that have undergone extensive investigation lately are the polycyclic aromatic hydrocarbons[72] and the insecticides.[73] Each of these groups of substrates manifest their metabolic toxicity *via* different mechanisms but will serve as examples of how the action of the P450 cytochromes can exhibit harmful effects to the cell.

Figure II.6 shows the cytochrome P450-mediated metabolic activation of phenanthrene.[72] Initial action of the cytochrome on the substrate produces an arene oxide by addition of an oxygen atom to a carbon-carbon double band. Opening of the epoxide functionality is catalysed by a specific epoxide hydrase enzyme giving the corresponding dihydrodiol. At this point the metabolite, which may not be polar enough to be efficiently removed from the cell, is further epoxidated by cytochrome P450 at the non-aromatic double bond forming the diol epoxide. Subsequent covalent interaction of the

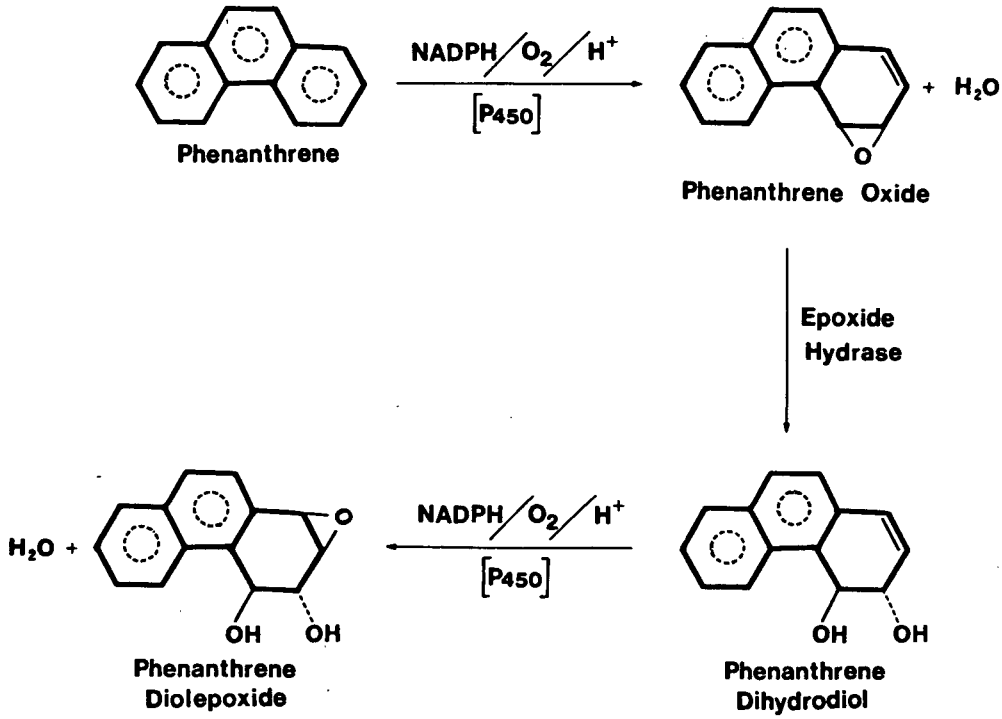


Figure II.6 The cytochrome P450 - mediated activation of phenanthrene ; Ref.72.

highly reactive electrophilic diol epoxide with critical targets in DNA is assumed to be an essential event in the initiation of carcinogenesis.[74] Therefore, the interaction of the P450 cytochromes with initially unactivated molecules (phenanthrene) can produce highly reactive metabolites (diol epoxides) which can be detrimental to cell survival.

The insecticides on the other hand, exhibit their toxic effects by direct interaction of the cytochrome P450-activated substrate with the prosthetic heme moiety of the enzyme.[73] During the catalytic transfer of activated oxygen to the monosubstituted acetylene functionality, which characterize some classes of insecticide substrates, cytochrome P450 is destroyed by alkylation of the heme

group. *In vivo* inactivation of the enzyme in hepatic tissues is accompanied by the accumulation of an abnormal "green pigment".[75] Isolation and purification of this green pigment from animals treated with thirteen different acetylenic insecticides has unequivocally confirmed that in each case a 1:1 covalent N-alkylation of the protoporphyrin IX skeleton of prosthetic heme leads to inactivation of the enzyme and formation of the abnormal hepatic pigment.[73] With the recent isolation and identification of four isomeric N-(2-oxoethyl)protoporphyrin IX N-derivatives (Figure II.7) from rats treated with acetylene gas, the

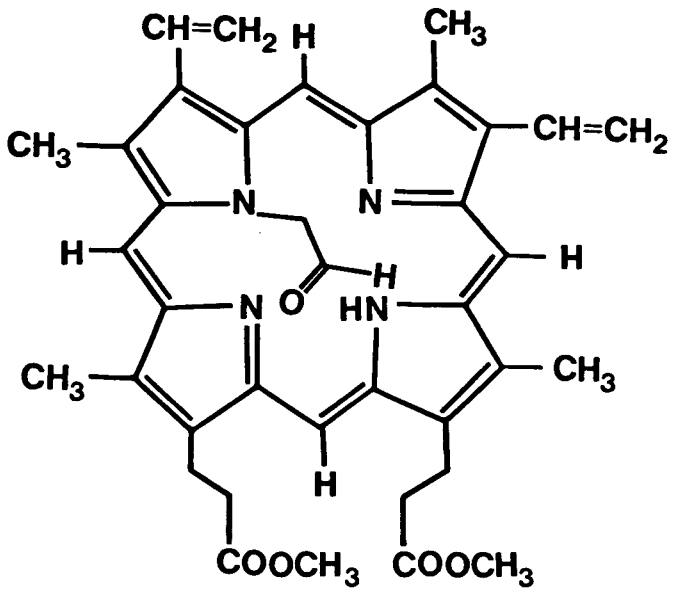


Figure II.7 Structure of one of the four possible isomers of N-(2-oxoethyl) protoporphyrin IX isolated from acetylene-treated liver microsomes; Ref.76.

mechanism of the cytochrome P450 self-deactivation has been speculated upon[76] (Figure II.8). Catalytic oxygen transfer to the acetylene π-bond produces a transient species which can partition into two pathways, one leading to N-alkylation of the prosthetic heme moiety and the other to formation of acetylenic group metabolites.[77] Comparison of the *in vivo* abnormal hepatic porphyrins with those prepared synthetically[78,79] not only verified that the prosthetic heme of the cytochrome P450 was exclusively N-alkylated but has permitted the assignment of the preferred N-alkylated isomer formed in the hepatic tissues. The important point, however, is that N-alkylation of the prosthetic heme renders the enzyme inactive to further enzymatic cycles. This, in turn, causes the accumulation of toxic concentrations of the parent molecule and its metabolites and eventual necrosis of the cell. Thus, the P450 cytochromes can participate in their own self-inactivation and again create conditions which are hazardous to cell survival. The self inactivation of cytochrome P450 is also known to be mediated by several other groups of substrates which are all characterized by unsaturated carbon-carbon bonds.[80]

In summary, following this examination of the complex biological features exhibited by the P450 cytochromes, the role they play seems to be two-fold. Firstly, these enzymes are extremely important in the oxidative biosynthesis and

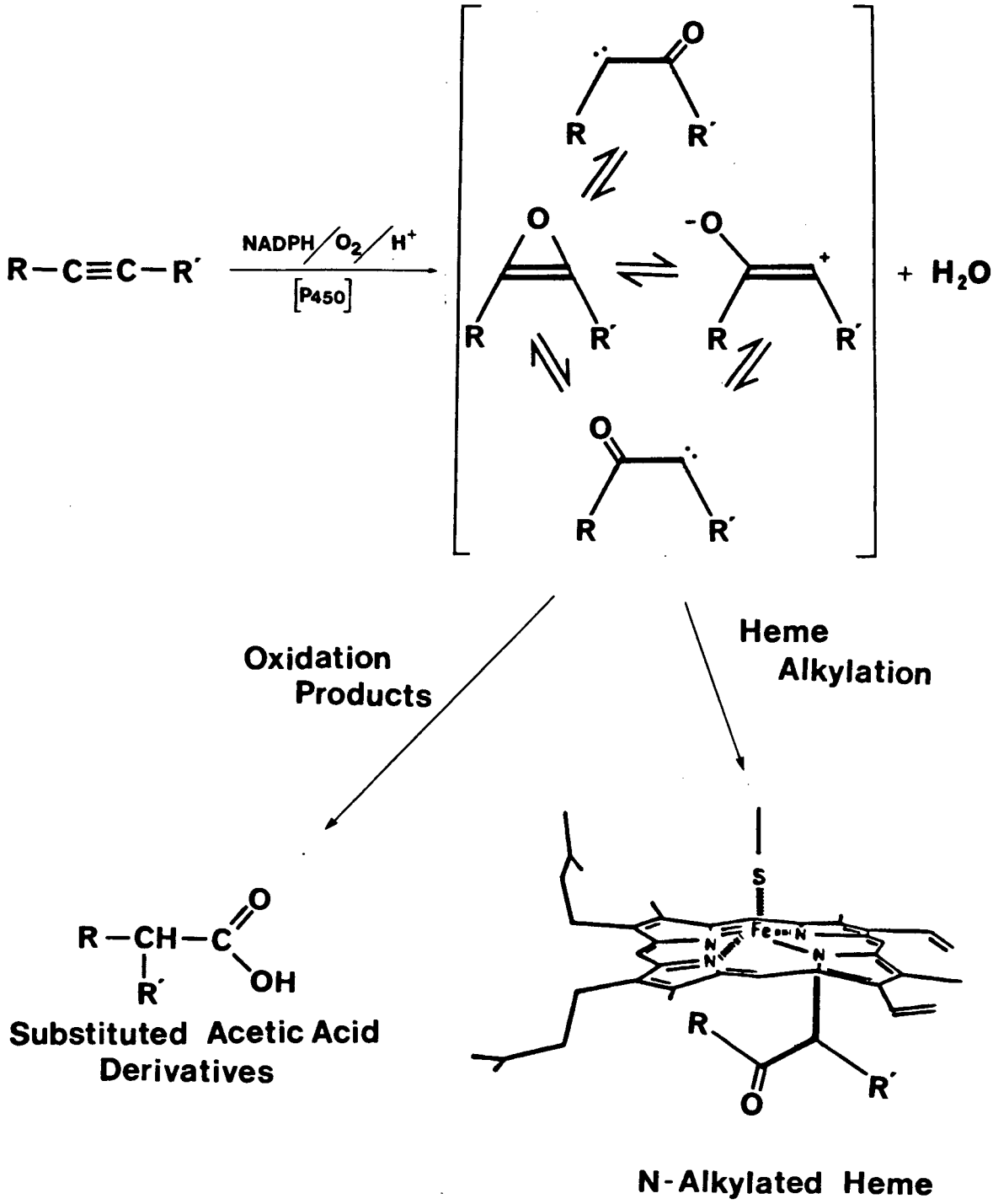


Figure II.8 Postulated mechanism of the autocatalytic alkylation of the prosthetic heme of cytochrome P450 during attempted metabolism of acetylenes where R and R' represent hydrogens or alkyl substituents; Ref.77.

metabolism of a large number of endogenous and exogenous substrates. Therefore, they are concerned, not only with regulation and control of the cell but also protecting the host from the destructive effects of xenobiotics through various detoxification reactions. In this sense, cytochrome P450 is an essential cellular component. In contrast, however, cytochrome P450 can be the causitive agent in cellular transformations, causing malignancies and eventual death to the host. In this sense, cytochrome P450 exists as a destructive force within the cell.

II.3 Structure

The majority of knowledge concerning the structure of the P450 cytochromes has been determined from the solution and crystalline states of bacterial cytochrome P450cam. The water-soluble and membrane-free characteristics of this enzyme system allow for chemical and physical characterization much more readily than with the membrane bound species. The features of cytochrome P450cam have been investigated and reviewed extensively[33a,38,81,82] and are used in this structural overview as a point of reference. The structural properties to be described are applicable to all classes of P450 cytochromes.

The P450 cytochromes are hemoproteins composed of a single polypeptide chain and a single molecule of iron protoporphyrin IX as the prosthetic group[13,14] (Figure I.1). Because of the intracellular localization and their function in oxidation-reduction reactions, the general name "cytochrome" has been given to these enzymes.[83] The suffix P450, as mentioned earlier, was derived from the unusual Soret absorption peak at 450nm of the carbon monoxide derivative of the reduced (i.e. Fe(II))hemoprotein.[13,14] Since the porphyrin skeleton of the heme prosthetic group is attached to the protein via acid labile non-covalent linkages, these enzymes are considered a member of the cytochrome *b* group. Recently the primary structure of cytochrome P450cam has been deduced from the sequence of proteolytic[84] and CNBr[85]

peptide fragments. The peptide chain contains 412 amino acid residues of which approximately half are non-polar. The remaining polar groups are divided equally between ionized and neutral functions; eight cysteine residues[85] and relatively few aromatic amino acids were observed (i.e ≃10 tyrosine; ≃4 tryptophan).[86] This is not surprising since aromatic molecules are readily oxidized by the P450 cytochromes. These findings are generally consistent with the original amino acid analysis reported by Dus *et al.*[87] Sequencing of the amino and carboxy terminal peptides[88] suggests that all of the cysteine residues are located in the interior of the polypeptide chain. Specifically in the cytochrome P450cam polypeptide, there are no cysteine residues at least 40 residues in from the NH_2-terminal end, and no cysteine residues at least 38 residues in from the COOH-terminal portion. This has since been confirmed by the recent completion of the primary structure of cytochrome P450cam.[85] The NH_2-terminal amino acid sequence of rabbit liver cytochrome P450 also indicates that the cysteine residues are located toward the central portion of the peptide.[89] The possible reasons for the apparent localization of the cysteine residues are under investigation.[88] Molecular weights of the enzymes range from 47,000 Daltons in the bacterial strain[88] to 55,000 Daltons in membrane bound isolations.[26] Predictions of secondary structure for the cytochrome P450cam system[38,85] indicate slightly less than

half of the protein form α-helical domains including half of the cysteine residues. The remainder of the residues are divided between β-pleated, β-turn, and random coil protein structures. The three-dimensional shape of the bacterial enzyme has been described as a "donut with a tail".[90]

In order to understand the unique catalytic properties of the P450 cytochromes, the immediate environment of the heme prosthetic group must be established throughout the reaction cycle. More specifically, the axial ligands provided by the polypeptide which allow for the particular reactivity of the enzyme must be determined. The question of axial ligands of cytochrome P450 has received considerable attention because of the unusual spectral changes that occur on substrate binding and on complexation of the ferrous enzyme with carbon monoxide. Information gathered to date strongly indicates a covalently bound thiolate or sulphydryl anion (RS^-) as the axial ligand (of the heme-iron) in the P450 cytochromes that is contributed via one of the cysteine residues of the polypeptide. The first clue to the nature of this axial ligand was derived from electron paramagnetic resonance (EPR) experiments. In 1968 Miyake *et al.*[91] demonstrated that the native "ferric resting enzyme" was predominantly a low-spin ($S=\frac{1}{2}$) hemoprotein, while Jefcoate and Gaylor,[92] and Blumberg and Peisch[93] subsequently showed that the EPR spectra of low-spin cytochrome P450 were similar to

those obtained from the addition of mercaptoethanol or other alkyl mercaptides to ferric hemoglobin or ferric myoglobin. Following these initial experiments, the absorption spectrum of the unusual red-shifted Soret band of the carbonylated cytochrome P450 species was duplicated with simple iron (II) porphyrins having a mercaptide ion ligated *trans* to the CO.[94-96] The model studies of Chang and Dolphin[94] were not only able to mimic the spectral properties of the ferric and ferrous states of the enzyme but were also able to reproduce the low energy Soret band at ≈450nm of the reduced -CO complex. In addition, these model complexes showed a second high energy band at ≈360nm, thought originally to be indicative of the dithionite reducing agent. This high energy band was subsequently observed in the enzyme itself.[97] As well, the spectral properties of the ferric, ferrous, and ferrous-O_2 P450 complexes were modelled but were subsequently shown to be derived from a bisthiolate iron (III) species which had not been detected in the previous P450 model studies.[98] Spectra which exhibit such split-Soret bands are now known as "hyper-spectra" and are characteristic of iron porphyrins coordinated by ligands of high electron density.[97] Direct evidence for the coordination of the mercaptide ion has recently been elucidated from resonance Raman (RR) spectroscopy of the ferric enzyme substrate complex labelled with heavy and light isotopes of iron and sulphur.[38] Furthermore, measurement of the changes in proton concentration during the binding of

dioxygen, carbon monoxide, and for the exchange of dioxygen by carbon monoxide at ferrous cytochrome P450cam,[99] have indicated that the heme-iron mercaptide linkage is retained throughout the entire reaction cycle. The existence of the axial mercaptide ligand is manifested in extremely low reduction potentials exhibited in both substrate-free (-270mV) and substrate-bound (-170mV) cytochrome P450cam.[30] A large electron rich sulphur anion is able to readily donate density onto the iron atom to produce an easily oxidizable metal center. Comparison with other heme-protein systems exemplifies this point. Some ferridoxins, which contain direct iron-sulphur linkages, are characterized by extremely low reduction potentials (-400mV), while higher potentials are found for the peroxidases(-130mV) and more convincingly for the myoglobin system (+46mV).[100] Both of these species are known to contain a nitrogen bound histidine residue as an axial ligand.

Even though the above evidence has seemingly assigned a mercaptide ion as the axial ligand in the P450 cytochromes this suggestion has been challenged by information obtained from another heme-protein system, Chloroperoxidase, which exhibits many of the unique spectral characteristics of bacterial and microsomal P450 cytochromes.[101]

Chloroperoxidase is a glycohemoprotein of M.W. 42,000 which is found in the extracellular fluid of the growth medium of the mould *Calderiomyces fumago*.[102] The reaction

catalysed by this protein is the activation of halogen ions for insertion into alkyl residues (Reaction II.4).

$$RH + Cl^- + H_2O_2 \longrightarrow RCl + H_2O + OH^- \quad (II.4)$$

Extensive probing of the active site of chloroperoxidase has shown that this enzyme exhibits many similar physiochemical properties of the P450 cytochromes.[33] The interesting feature of this system is, however, that in all oxidation states the polypeptide contains no free sulphydryl groups; yet the reduced carbon monoxide derivative exhibits the same hyperspectra with a low energy Soret absorption at 443nm.[103] These facts have produced skepticism about the characterization of the thiolate anion as an axial ligand of the heme-iron in the P450 cytochromes.

The nature of the sixth ligand of the heme-iron in the ferric state of the enzyme has also been extensively investigated and, as yet, remains ambiguous.[82] Since the substrate-free resting enzyme has a low-spin configuration, comparison with other low-spin hemoproteins supports the assignment of a second axial ligand. Though the nature of this ligand remains obscure, nitrogen, sulphur, and oxygen based ligands, including water and hydroxide have each been considered;[82] a water ligand has been implicated in order to explain the effect of ferric heme on the nuclear magnetic resonance (NMR) relaxation rate of H_2O protons, and the observed exchange of the ligand protons between the coordination sphere of the

cation and the bulk solution. A proton exchange mechanism mediated through a heme-iron ligand has since been proposed and subsequently confirmed by an electron nuclear double resonance (ENDOR) investigation.[82] The loss of the observed spectral characteristics in the presence of substrate suggests that the native substrate-free, low-spin ferric enzyme has a rapidly exchanging water molecule as the sixth axial ligand. Aside from H_2O, the alcohols of tyrosine (Tyr), serine (Ser), or threonine (Thr), the distal amino of lysine (Lys), the thiol of cystein (Cys) and the terminal amides of glutamine (Gln) and asparagine (Asn) have been considered as potential candidates.[82] Measurements are not consistent with the N-1 proton of histidine (His). The deoxy-ferrous substrate-free and substrate-bound enzyme states contain no sixth axial ligand.[38]

The structural properties of the heme pocket are also of interest since the activated oxygen species produced by cytochrome P450 is capable of oxidizing any of the known amino acids. Analysis of the amino acid composition originally published by Dus *et al.*[87] shows that 37% of the polypeptide is made up of residues containing completely unactivated alkyl side chains (i.e. alanine, valine, leucine, isoleucine, proline, and glycine), while 19% of the polypeptide contains residues that are more susceptible to oxidation (i.e. Tyr, phenylalanine, His, tryptophane). Since the enzyme produces an extremely powerful oxidizing agent it would be logical to assume

then, that the heme pocket must be composed of largely those amino acids most resistant to oxidation, such as the aliphatic species mentioned above. Also, it would be plausible to suggest that of these resistant amino acids, those with the least bulky side chains should be utilized in the heme pocket. In this way, any potentially harmful interactions between the amino acids and the active oxidizing species would be minimized. A heme pocket constructed, essentially, of the aliphatic amino acids is consistent with the kinetic data for substrate binding in cytochrome P450.[100] This information indicates a strong hydrophobic interaction between the enzyme and the substrate. At $4^{o}C$, the forward rate constant for camphor binding in cytochrome P450cam is 4.1×10^{6} M^{-1} S^{-1} while the reverse rate constant is 6.0 S^{-1}. The heme pocket described above is in general agreement with the rather hydrophobic heme environments of the peroxidase, myoglobin, and hemoglobin systems (Figure II.9).

It is of interest to note that the β-chain of the hemoglobin molecule contains a cysteine residue adjacent to the axially co-ordinated histidine moiety which readily binds to the iron atom on mild denaturing of the protein.[104] This then, may provide a possible phylogenetic link between these enzymes.

Although the preceding hypotheses cannot be proven until the crystallographic structure of cytochrome P450 is

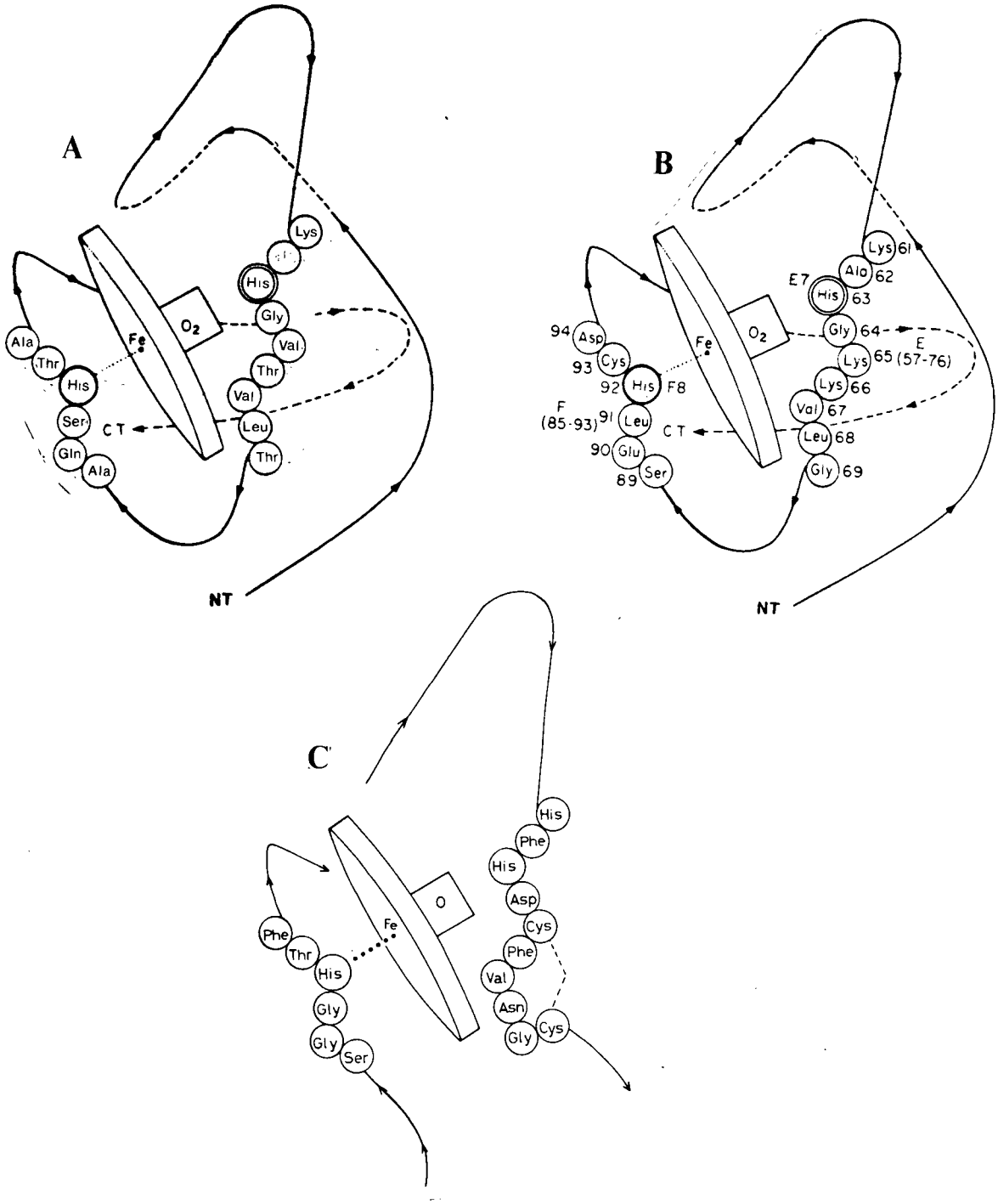


Figure II.9 Heme environments of myoglobin (A), hemoglobin (B), and peroxidase(C); Ref.104.

complete, it can be said that the heme pocket must be manipulated in the enzyme to provide an environment in which the possible side reactions are avoided. Some suggestions put forth[104] include the formation of a cavity around the activated species so that contact with the amino acids in the heme pocket is unlikely, and, possibly steric compression of the substrate against the reactive oxidizing unit allowing only reaction with the substrate to take place. The actual mode of interaction, however, can only be elucidated by extensive study in the future.

II.4 Mechanism of Action

Limiting the discussion to the mechanism of oxidation of unactivated C-H bonds, the overall reaction catalysed by cytochrome P450 can be generalized by Reaction I.1. The postulated catalytic sequence is a six step process involving the transfer of high energy electrons from NADH/NADPH to cytochrome P450 with the concomitant two electron reduction of molecular oxygen to yield the oxidized substrate and water (Figure II.10). The mechanism by which this process takes place has been an intriguing problem and although a large majority of the reaction pathway has been elucidated, a detailed description of the total catalytic pathway still remains obscure. The catalytic cycle to be described was originally proposed by Estabrook[34] and is valid for all classes of cytochrome P450.

Many spectroscopic techniques, including electronic absorption, EPR, Mössbauer, RR, NMR, magnetic circular dichroism(MCD), and ENDOR, have been utilized to probe the active site at each step in the catalytic sequence.[33a,38,81,82] Only brief reference to a few of these techniques will be given here.

The first step in the catalytic pathway (Figure II.10; conversion 1 ⟶ 2) is the reversible binding of substrate by the low-spin ferric cytochrome P450 (resting enzyme) which produces a high-spin substrate complex.[105] Formation of these substrate complexes is generally manifested in

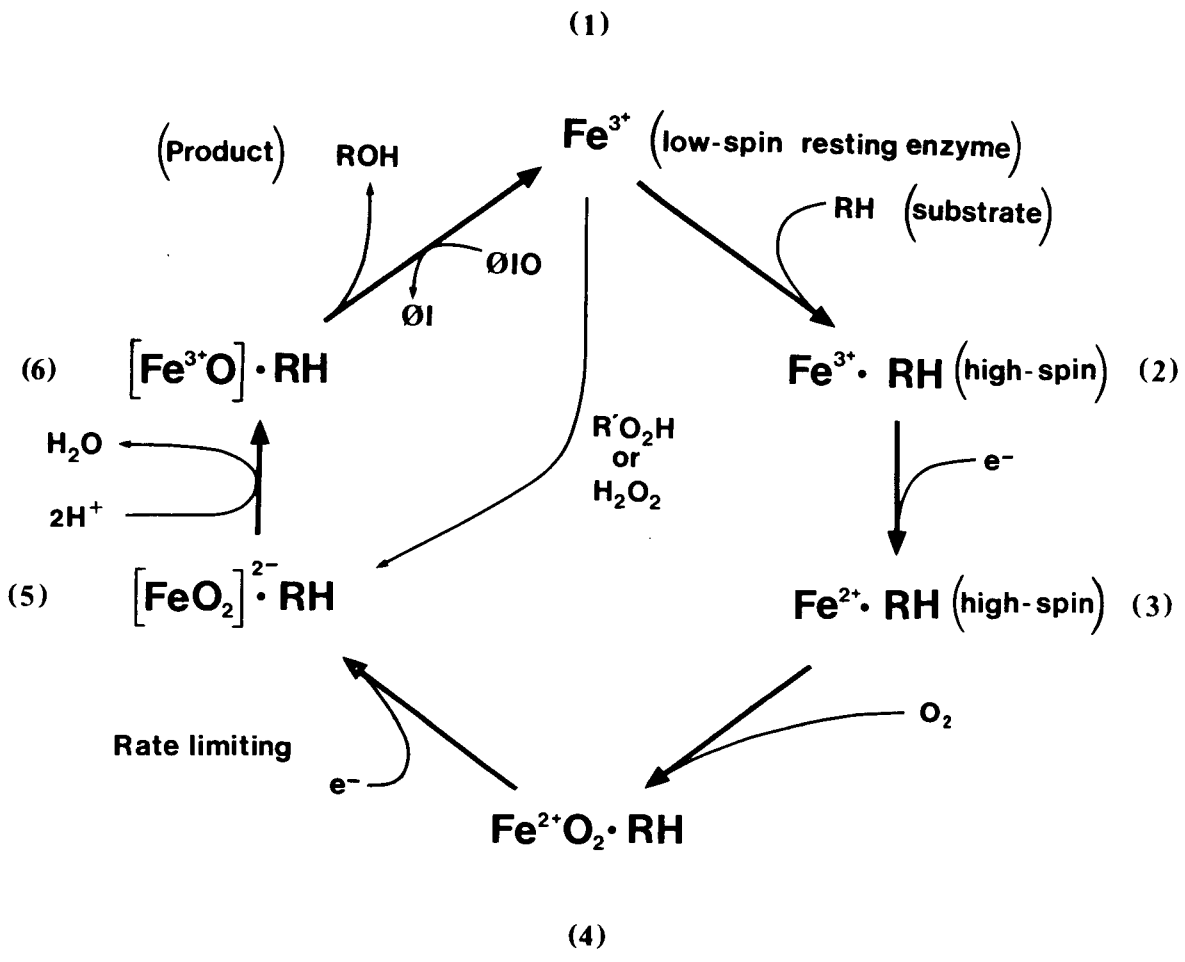


Figure II.10 Proposed reaction cycle of cytochrome P450

dramatic changes in the absorbance spectrum of the ferric form of the hemoprotein, regardless of source. For example, the Soret region of *P. putida* cytochrome P450cam has an intense band at 418nm for the substrate-free complex which shifts to 391nm on the addition of camphor (Figure II.11). Distinct spectral changes are also observed in the 500-600nm region. The spectral changes observed during binding of substrate to the P450 cytochromes are paralleled by spin changes at the paramagnetic iron center. EPR and Mössbauer signals characteristic of a low-spin iron heme ($S=\frac{1}{2}$) are observed in the substrate-free complex, while signals indicating a high-spin iron species (S=5/2) are observed on the binding of substrate.[38] Other changes include an increase in the reduction potential of the enzyme[100] from -270 to -170mV, as well as an increase in the isoelectric point (pI) of the enzyme (4.55 to 4.67).[87] Proton NMR and ENDOR studies suggest the loss of an axially coordinated oxygen or nitrogen based ligand (most likely a water molecule), and an increase in the distance between the solvent protons and the paramagnetic iron centre.[82] From these data, the interaction of the resting enzyme with the substrate for bacterial P450cam has been speculated upon.[107] Initially, the thiolate and water-bound iron atom is found in the plane of the porphyrin as the low-spin species. The prosthetic group is surrounded by the heme pocket existing as a rather exposed hydrophobic area of the

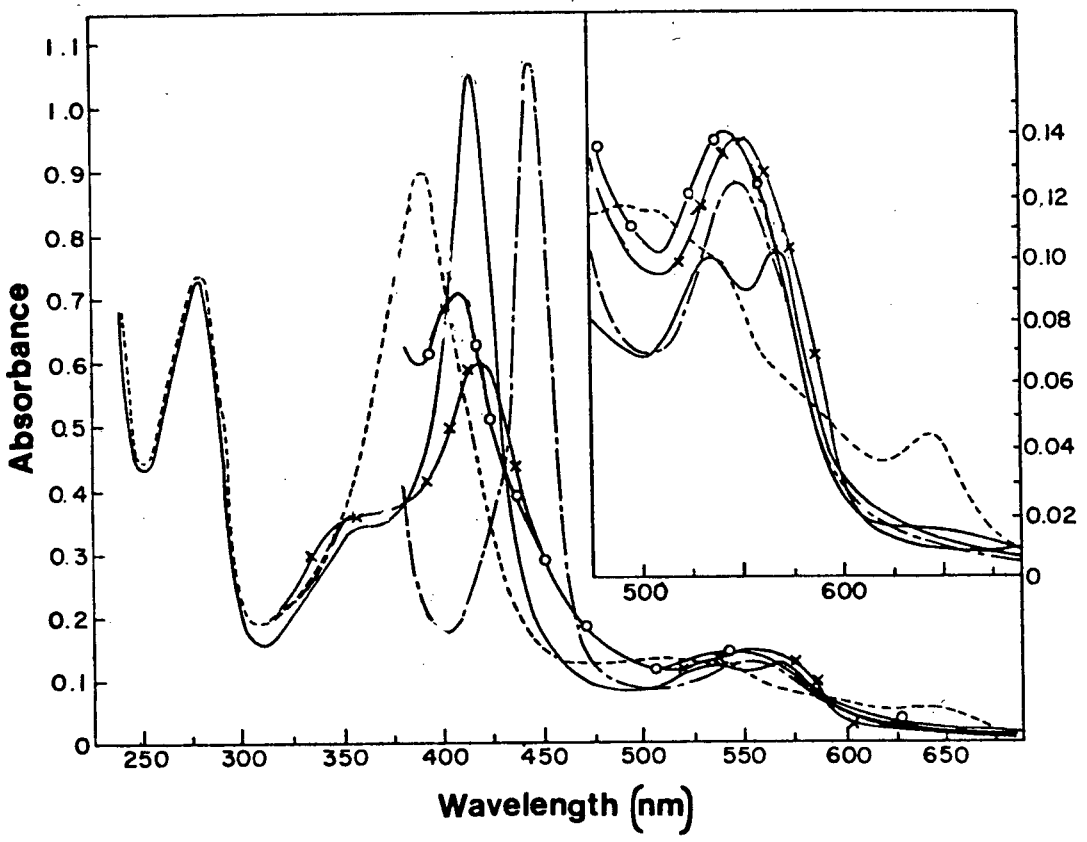


Figure II.11 Absorption spectra of the various states of cytochrome P450cam ; substrate-free (———), substrate-bound (----), ferrous substrate-bound (—o—o—), ferrous -O_2 substrate-bound (–x–x–) and ferrous -CO (— - — - —); Ref.100.

enzyme. Removal of the hydrophobic hydrocarbon camphor substrate from the aqueous environment into the open non-polar pocket provides the driving force for the binding of substrate, which produces conformational changes involving the polypeptide. The iron atom is, in turn, pulled out of the plane of the porphyrin with the loss of the aquo ligand creating the high-spin ferric cytochrome P450. The heme pocket subsequently constricts around the substrate and reduces exposure to the bulk solvent. Hydrogen bonding,[104] steric compression[104] and more recently, thiohemiketal bond formation[108] have been thought to constrain the substrate molecule in close proximity to the active site. Substrate binding is a reversible process and is not the rate-limiting step in the catalytic pathway.

The change in redox potential on substrate binding (i.e. -270 to -170mV) allows for the second step of the cycle to proceed (Figure II.10; conversion 2 ⟶ 3). This step involves the rapid one electron reduction, *via* an iron-sulphur protein (-240mV) to the high-spin ferrous state (S=2). Reduction of the ferric complex is again manifested in marked changes in both the Soret and visible regions of the absorption spectrum; reduction of camphor-bound cytochrome P450cam causes a red shift of the Soret band at 391nm to 409nm and formation of a distinct visible band at 540nm (Figure II.11).

The third step in the mechanistic pathway (Figure II.10; conversion 3 ⟶ 4) is the reversible binding of dioxygen to

the high-spin ferrous substrate complex with formation of a low-spin oxygenated substrate complex. The binding of dioxygen is accompanied by the appearance of a new spectral species characterized by a distinct "hyper-spectrum" exhibiting a Soret absorption at 418nm and a higher energy transition at 350nm (Figure II.11). Substitution of the dioxygen molecule by carbon monoxide at this point gives the characteristic cytochrome P450 absorption spectrum from which the enzyme was named (Figure II.11). Figure II.12 shows the distinct "hyper-spectra" of oxy-and carboxy-P450cam. EPR studies of oxycytochrome P450 indicate that

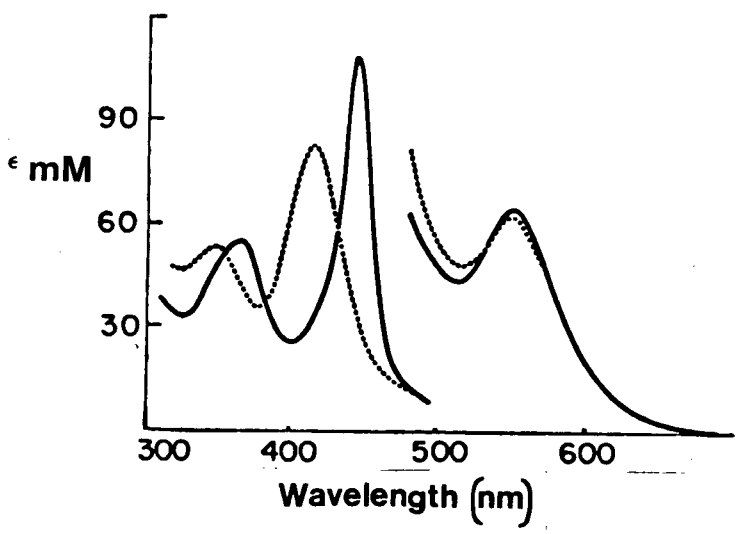


Figure II.12 Optical spectra of carbonylated (——) and oxygenated (-----) ferrous cytochrome P450cam; Ref.42.

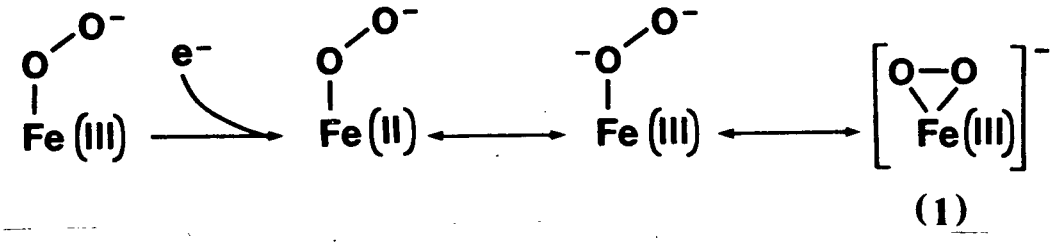
the complex is a low-spin species which is comparable with dioxygen complexes of other hemoproteins[109] such as myoglobin and hemoglobin. However, in contrast to oxymyoglobin and oxyhemoglobin, the oxygenated P450 species are characterized by marked instability at ambient temperatures (e.g. at 22°C and pH 7.0, $t_{\frac{1}{2}} \simeq 1$ min). The P450-autooxidation process is thought to proceed *via* a proton-assisted displacement of superoxide as HO_2 with regeneration of the corresponding ferric (resting) state.[10] The instability of oxycytochrome P450 is attributed to the high electron density of the thiolate ligand being transmitted to the coordinated oxygen molecule. Mössbauer spectroscopy[110] has demonstrated that the iron of the overall diamagnetic oxy-P450 complex closely resembles that of ferric iron, and thus the oxygenated intermediate can be considered to have a superoxide-ferric iron charge distribution. Oxycytochrome P450 complexes have been subsequently stabilized at lower temperatures and by reconstituting the native enzyme with several different heme derivatives[10] (e.g. at 0°C and pH 7.0 the iron (II) dioxygen form of diacetyldeuteroheme reconstituted cytochrome P450 has a half-life of 450 minutes). Generally up to this stage of dioxygen addition in the enzymatic cycle, the rates, the nature of the axial ligation, and the electronic configurations around the heme are reasonably well understood.

The next, and rate limiting step, in the enzymatic reaction (Figure II.10; conversion 4 ⟶ 5) is a further

one-electron reduction of oxycytochrome P450. This step induces the cleavage of bound dioxygen to produce an "activated oxygen" complex that is typically capable of oxidizing unactivated C-H bonds. As yet, little is known or understood about this second reduction step as well as the subsequent steps leading to the oxygenation of the substrate. However, from information accumulated to date on the native P450cam system, other hemoproteins, and chemical model studies, the completion of the catalytic cycle is thought to occur as indicated in the final three steps of Figure II.10.

The ability to shunt the enzymatic cycle (Figure II.10; conversion 1 ⟶ 5) using organic peroxides[111] as well as hydrogen peroxide itself,[112] and still obtain the stereospecific oxidation products without an external electron donor, suggested that the initial reduction product of the oxygenated enzyme (Figure II.10; conversion 4 ⟶ 5) was a heme-iron coordinated peroxide complex. Subsequent model studies[113,114] showed that this intermediate may in fact be the high-spin ferric η^2-peroxide complex (1) shown in Scheme II.1.

The mononuclear peroxo complex (1) was produced both synthetically[113] and electrochemically[114] but unfortunately did not exhibit any of the oxidizing powers of the native enzyme presumably due to the absence in the model systems of the axial thiolate ligand.[114] Other

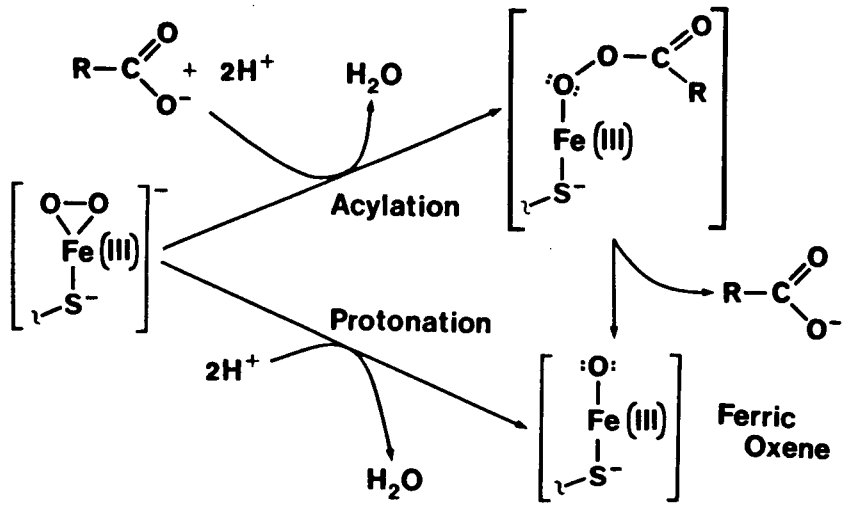


(1)

Scheme II.1

probable structures for the reduced oxy-P450 complex have been proposed all of which invoke a similar peroxide-like intermediate.[115] Although the intermediacy of this species is only speculative, the proposed peroxy complex represents a plausible precusor that has all the electron equivalents needed for methylene carbon hydroxylation, water production, and regeneration of the ferric P450 resting enzyme.

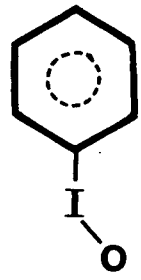
Assuming then that the peroxy complex (1) represents the electronic configuration at the heme centre immediately after the reduction of oxycytochrome P450, production of the "activated oxygen complex" (Figure II.10; conversion 5 ⟶ 6) is speculated to occur *via* cleavage of the peroxy O-O bond. Presently, the evidence is in favour of heterolytic O-O bond cleavage before substrate oxidation. The mechanism of the heterolytic cleavage reaction as depicted in Scheme II.2 is



(2)

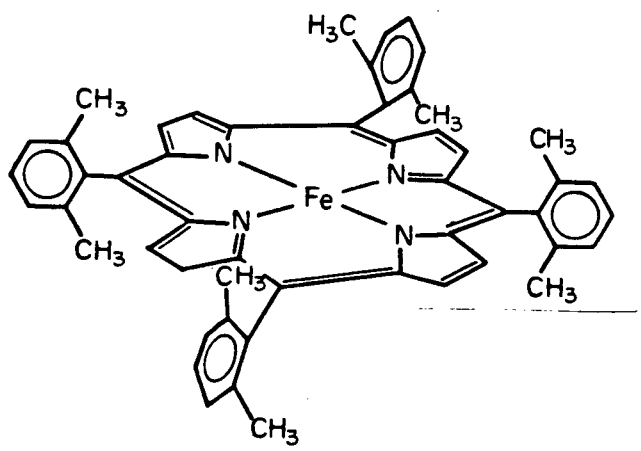
Scheme II.2

thought to proceed either by double protonation with loss of water, or by nucleophilic attack of the bound peroxide at a carboxylate residue of an amino acid side chain (producing a transient acyl peroxide) followed by O-O bond cleavage and elimination of carboxylate.[115] Irregardless of the precise mechanism of O-O bond cleavage, one of the oxygen atoms leaves at the oxidation level of water while the other is thought to remain coordinated to the heme-iron. This species, formally a ferric oxene (oxygen atom) complex (2), is speculated as the powerful oxidizing agent utilized by the P450 cytochromes. Support for such a monooxy-iron species was derived from the fact that iodosylbenzene (3), a single oxygen atom donor, can be used to effect the oxygen atom transfer in a manner similar to that of the fully reconstituted enzyme systems (Figure II.10; conversion 1 ⟶ 6).[116] Peracids have been



(3)

used as well to produce the same results with the native enzyme.[111] The ability of iodosylbenzene to replace both NADPH and dioxygen in the enzymatic cycle of liver microsomal P450 was first observed by Ullrich *et al.*[117] and has subsequently been modelled by Groves *et al.*[41,118] using ferric porphyrins in the presence of iodosylbenzene. More recently, Groves *et al.*[41] have followed up these findings showing that ferric tetra-mesityl porphyrin (4), when treated with a peracid, yields a monoxy-iron porphyrin derivative analogous to the postulated oxene complex utilized



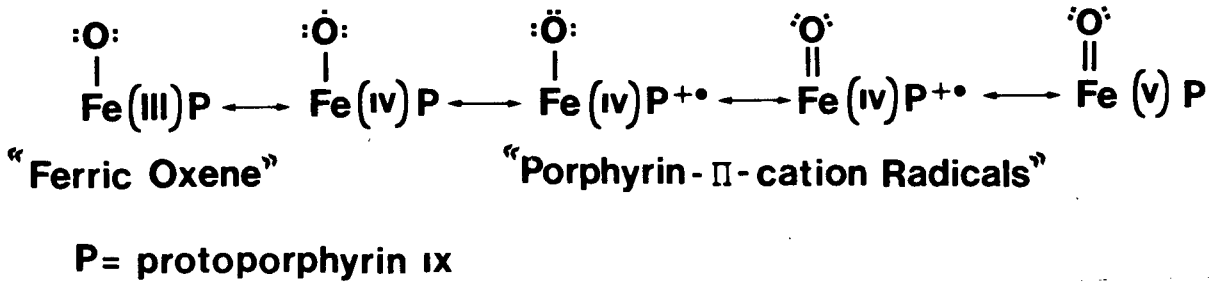
(4)

by the native P450 enzymes. A monoxy-ruthenium analog has been recently produced also.[119] Support for the monoxygenated oxidizing agent of the P450 cytochromes is further substantiated by comparing this "activated oxygen" species with the enzymes catalase (Cat) and horseradish peroxidase (HRP) in their highest, enzymatically active, oxidation states known as compounds I.[120] Compounds I of both catalase (Cat I) and horseradish peroxidase (HRP I) are generated when the resting ferric heme proteins undergo a two electron, hydrogen peroxide-mediated, oxidation. These enzyme systems along with the P450 cytochromes are thought to invoke the same monooxy-iron intermediate in their respective enzymatic cycles. Labelled oxygen[121] and more recently ENDOR[122] studies of HRPI have shown that the complex contains an oxo ligand bound to the heme-iron, which is analogous to the ferric oxene complex postulated as the active oxidizing agent of the P450 cytochromes.

Although formulated as a ferric-oxene species, the exact nature of the oxenoid complex is not clear. If an oxene complex, the observed reactivity of these species could be expected to parallel that of the analogous carbene species.[123] That is, the oxygen atom should insert directly into C-H bonds and across olefinic double bonds without loss of stereochemistry. It has been determined, however, that cytochrome P450-mediated oxidations do not function *via* such direct insertion and that the pure ferric-oxene analogy is

not correct.[118]

Other possible formulations can be arrived at from the various resonance structures of the oxene complex as shown in Scheme II.3.



Scheme II.3

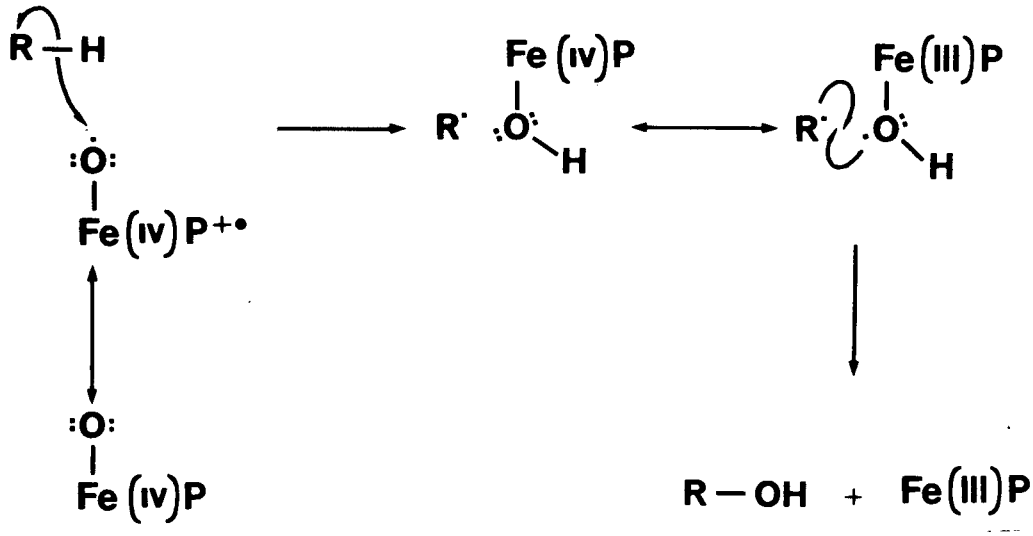
Extensive characterization of the oxo-iron tetramesityl porphyrin complex isolated by Groves *et al.*[41] has shown that the most likely structure for the "activated oxygen" complex is the oxo-iron (IV)-porphyrin π-cation radical (Scheme II.3); however, depending on the axial ligand the intermediate can also exist as the Fe(V) complex. The recent characterization of an oxoporphinatochromium (V) complex[124] provides indirect evidence that an oxo-iron (V) intermediate may be involved in the P450 enzymatic cycle, while Ullrich *et al.*[125] have suggested the Fe^{IV} - Ö· structure for the activated intermediate. Although the "activated oxygen" complex is probably a resonance mixture of the

structures listed in Scheme II.3, support for the Fe(IV)-porphyrin π-cation radical intermediate is provided by extensive investigations of the active enzymatic intermediates of HRPI and Cat I.[120,126] As well, catalase can catalyse the N-demethylation of small substrates,[127] a reaction characteristic of the P450 cytochromes, thus suggesting the existence of a common iron-oxo π-cation radical intermediate within these enzyme systems. The reason that Cat and HRP do not actively catalyse P450-like oxidations is thought to be due to the extremely small heme-pocket surrounding the heme group in these enzymes.

The role of the thiolate ligand thus far, in conversions 4 ⟶ 6 (Figure II.10) of the catalytic cycle is also unclear and speculative at best. It has been suggested that the thiolate aids in splitting the peroxide bond by weakening the O-O bond through charge repulsion in the neighbourhood of the electron-rich iron atom.[106] Comparison of the auto-oxidation rates of oxy-P450[10] with oxy-Mb suggests that the increase in electron density provided by the thiolate ligand versus imidazole may enhance the facility of the O-O bond cleavage reaction.[10,109] Ullrich *et al.*[125] on the other hand, suggests that the thiolate ligand is only required for the stabilization of the oxenoid complex for the transfer to organic substrates and not in the actual production of the "activated oxygen" complex. It may be noted here

that thiolate is not a required ligand for the Cat I and HRP I systems which involve axial phenoxide and imidazole, respectively.[120] Since little definitive information is known, the thiolate is generally thought of as providing an extremely electron rich ion atom which both destabilizes the peroxy intermediate and stabilizes the electrophilic characteristics of the oxenoid complex. The precise role of the thiolate awaits further study.

The final step in the catalytic cycle (Figure II.10; conversion 6 ⟶ 1) is the oxidation of the organic substrate by the active "oxenoid" oxidizing agent. Studies with both cytochromes P450 and model systems suggest that hydrocarbon oxidation proceeds via the intermediacy of a substrate radical;[42,111,118a,128] the isotope effects and regio-and stereoselectivity of P450 oxidations all argue for the substrate radical intermediate. The hydrophobic nature of the binding site has also been used to argue for anuncharged (radical) substrate intermediate[42,106] as has the interpretation of the microsomal metabolism of the insecticide Dieldrin.[129] The formation and hydroxylation of such a substrate free radical is thought to occur as outlined in Scheme II.4. Abstraction of a hydrogen atom from substrate (R-H) by the active oxidizing agent of P450 produces the substrate radical and an iron (IV) porphyrin complexed by hydroxide. Subsequent transfer of an iron-bound hydroxyl radical to the substrate radical generates the oxidized substrate and the resting enzyme (Fe(III))



Scheme II.4

ready for another catalytic cycle. Elimination of the polar metabolite from the non-polar heme pocket provides the driving force for the release of the oxidized substrate. Here again, these speculations on the details of this oxidative step in the catalytic cycle of the P450 cytochromes require more experimental support.

It is interesting to note that in many areas of oxygen chemistry, Nature has used iron porphyrins for the transport, storage, and utilization of dioxygen and its reduced derivatives.[42,106] In fact, the intermediacy of both the oxene and hydroxyl radical in the catalytic cycle of P450 oxidations, which are stabilized by coordination to an iron porphyrin, has completed the picture for the oxygen chemistry outlined in Figure I.2. Each of the possible oxygen

intermediates shown there has been utilized by Nature and is stabilized in each case by the use of a heme protein.[106] Therefore, in summary, cytochrome P450 has been considered as Nature's equivalent to Fenton's reagent[106] where the highly reactive hydroxyl radicals and oxenes are controlled by their interaction with the hemoprotein.

II.5 The Interaction of Carbon Monoxide with Cytochrome P450

The interaction of small gas molecules, such as CO and O_2, with metalloporphyrin species has intrigued scientists of all disciplines ever since such species were recognized as being the catalytic centers in numerous naturally occurring biological systems. The most common examples of metalloporphyrin containing proteins are the O_2 carriers, myoglobin and hemoglobin,[109] although various oxidases (i.e. cytochrome oxidase)[130] and oxygenases (i.e. P450 cytochromes)[33a] have also been studied extensively. All of these biosystems utilize the ferric-iron porphyrin moiety (the heme unit) as their prosthetic group which in the ferrous state characteristically binds O_2 and forms stable complexes with CO; in each case the O_2 or CO molecule binds as an axial ligand to the iron atom of the heme moiety. An important property of the oxy-(O_2 complex) and the carbon monoxy-(CO complex) iron bonds is that they can be broken by irradiation with visible light. The ability of visible light to dissociate, in particular, the carbon monoxide complexes of these natural hemoproteins has been recognized for years. Early experiments with mixtures of oxy and carbon monoxy Hb (Haldane and Smith, 1896) showed that exposure to solar light of a mixture of oxy- and carbon monoxy-complexes produced a marked decrease in the amount of the CO- derivative and an increase in the O_2 form.[131] As well, the ability of white light to reverse the carbon

monoxide inhibition of the steroid C21 hydroxylation of 17-hydroxyprogesterone led to the initial discovery of the function of the P450 cytochromes in mammalian systems (Section II.1).[21a] To date, photodissociation with a high quantum yield has been shown to be a general characteristic of all carbon monoxy-hemoprotein complexes and that the protein-free CO-heme complex itself is photodissociated with a quantum yield of one.[109] The oxy-derivatives of these hemoproteins are also photodissociable;[109] however, the quantum yield is much lower by a factor of ≈30 than for the corresponding CO complexes. The photolability of these hemoprotein complexes, particularly in the case of the CO complexes, is of great practical importance because it represents the basis for kinetic measurements by the flash photolysis method. Indeed, the first special method for studying fast reactions by the flash photolysis method was introduced by Gibson[132] in the mid 1950's for the study of myoglobin and hemoglobin with CO. Information gathered from kinetic experiments such as these, together with data obtained from static equilibrium studies, although difficult to interpret, can be used to draw conclusions on the structure-function relationships in these hemoproteins as well as on the mechanism of the interaction of gasses such as CO with the various hemoproteins.[109] This section will be concerned, therefore, with the method of flash photolysis as applied to the interaction of the P450 cytochromes with CO. A brief description of the theoretical

and practical aspects of the flash photolysis method will be given followed by a compilation of kinetic information gathered to date from this as well as other kinetic methods (e.g. stopped flow). Some conclusions are drawn. Equilibrium binding studies will be included where necessary, and information gathered on the P450 system will be compared with relevant data from the Mb and Hb systems, as well as from models for cytochrome P450.

The interaction of proteins containing a single heme per molecule, such as the P450 or Mb systems, with CO can be represented by Reaction II.5. Where Fe(II) is the ferrous

$$\text{Fe(II)} + \text{CO} \underset{k_{off}}{\overset{k_{on}}{\rightleftharpoons}} \text{Fe(II)-CO}, \quad Kco = \frac{k_{on}}{k_{off}} \qquad \text{(II.5)}$$

hemoprotein, Kco is the equilibrium constant, k_{on} is the association rate constant, and k_{off} is the dissociation rate constant. For these simple protein systems, the formation of the CO-complexes corresponds to a second-order reaction, while the dissociation of the CO from the ligand-bound complex to a first-order process.[30,109] Since these reactions are usually carried out under conditions where the CO ligand is in great excess, i.e. pseudo first-order in hemoprotein, the combination of CO and hemoprotein can be expressed by rate equation II.6 (see Appendix II).

$$k_{obs} = k_{on}[CO] + k_{off} \qquad (II.6)$$

The use of different CO concentrations allows for the direct measurement of the association rate constant, k_{on} and the dissociation rate constant, k_{off}. However, in practice, the value of k_{off} derived by extrapolation, is subject to greater error than the value of k_{on}, and should be checked against the value calculated from the static equilibrium measurement of Kco = k_{on}/k_{off}, or obtained directly *via* a different kinetic method such as stopped-flow. The kinetics of the reaction of CO with hemoglobin, which contains four heme units per molecule, are much more complex.[109]

The reaction of the simple hemoproteins (e.g. P450 and Mb) with CO are "rapid" with half-lives of <1 second at "ordinary" temperatures and concentrations, and require the use of special monitoring methods. These special techniques[109] include flow methods (continuous- or stopped-flow), relaxation methods (particularly temperature-jump), or flash photolysis methods. Although only the flash photolysis method will be described here, consistent data have been obtained by all three methods for the Mb-CO system; only the flash and stopped-flow methods have been used for the cytochrome P450-CO system

Flash photolysis can be considered an extreme relaxation method in which a perturbation is applied suddenly to a pre-mixed system in equilibrium. The perturbation is "violent" so that the equilibrium is greatly displaced. This contrasts with other relaxation methods such as temperature-jump[109] where the system is perturbed from equilibrium by only a small amount. The extreme disturbance utilized in the flash photolysis method is produced by sudden irradiation of the system with a very intense burst of light energy. Up to 10^5 joules of energy may be absorbed in a few hundred microseconds or more typically several hundred joules in a few microseconds. This absorbed light energy causes both electronic excitation and chemical reaction and produces relatively high concentrations of the excited or reactive species. This makes it possible to identify and study these intermediates by measuring their characteristic absorption spectra and by following the kinetics of the excited molecules in the time following the flash. This method can be applied equally well in the gas phase or in solution.

Application of the flash photolysis method to the kinetic study of hemoproteins with ligands as exemplified by Reaction II.5 has become routine since the pioneering work of Gibson.[132] In particular, the reaction of the P450 cytochrome[10,13,21a,30,33c,94c,133] and the myoglobin system[109,132] with CO has received much attention. When these ligand-bound hemoprotein solutions are exposed to an intense light pulse of an electronic flash,

dissociation of the ligand occurs (the reverse of Reaction II.5) : Fe(II)-CO $\xrightarrow{h\nu}$ Fe(II) + CO. At the end of the flash, the system returns to equilibrium in the dark, and the recombination reaction Fe(II) + CO $\xrightarrow{k_{on}}$ Fe(II)-CO can be followed (the forward of Reaction II.5). As mentioned previously, this allows for the measurement of the rate constants indicated in Reaction II.5. The photodissociation and subsequent rebinding can be observed optically since the Soret absorption maxima of the CO-bound and free ferrous hemoproteins are easily distinguishable: P450-CO, 445 nm; P450, 408 nm (see Figure II.11); Mb-CO, 423 nm; Mb, 434 nm (see Figure III.20a). Therefore, upon photodissociation the absorption changes to that of the CO-free protein, and as the CO rebinds the absorption returns to the original value (CO-bound) with a time dependence that provides information about the binding kinetics. The absorption can be monitored with a light beam centered at the Soret peak of either the CO- or CO-free complex, and thus, changes in concentrations can be monitored spectrophotometrically. Low levels of monitoring light are used to avoid disturbing the reaction kinetics. It should be noted that in these studies the only effect of the light pulse is to promote the dissociation of the ligand, with no other direct or indirect photochemical effects. That is, the axial linkage to the heme moiety, *via* the thiolate ligand in the P450 cytochrome and the imidazole in the myoglobin system, is unaffected by the

flash. Using a flash photolysis set-up capable of precisely monitoring the absorbance change of the heme solution at the very moment when the CO is flashed off, P450 model studies[94c] have shown that the CO-dissociated spectrum is identical to the unliganded spectrum. This substantiates the postulate that the CO-dissociated complex of the model and the P450 enzyme systems is indeed pentacoordinate. As originally deduced,[132] the kinetics of the reaction of hemoproteins with CO are independent of the amount of light energy and of the fraction of complex photodissociated.

The flash photolysis machines used for the study of the CO reactions follow the general features of that described by Gibson[132] and Porter[134] and are illustrated in Figure II.13. The solution to be examined is placed

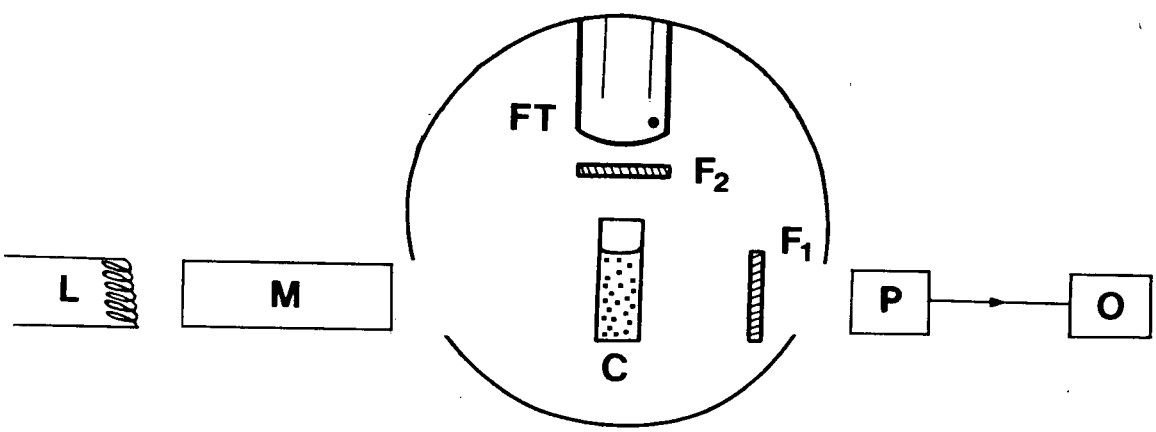


Figure II.13 General features of a flash photolysis apparatus; Ref.132. Consult text for details.

in cell (C) through which the monochromatic observation light beam is passed from light source (L) on its way to the photomultiplier (P). This monitoring light is rendered approximately monochromatic by passing through a monochromator (M), and a narrow-line interference filter at (F_1). The output of the photomultiplier is recorded with oscilloscope (O). The photodecomposition of the compound in the cell is initiated by a brief but brilliant flash of light produced by the flash tube (FT), at right angles to the monitoring beam. The flash light is appropriately filtered as well, (F_2), to insure that it does not interfere with the monitoring beam. The "dead time" of the flash photolysis apparatus, which is the time elapsed between initiation of reaction and the first useful observation, depends on the characteristics of the light pulse and on the efficiency of screening of the stray light from the flash. Overall dead times from a few milliseconds to fractions of milliseconds can be obtained. High energy flashes have been used but the high quantum yield for the dissociation of the carbon monoxide derivatives permits the use of low energy flashes, and even commerical flash lamps used for photography can be successfully employed.[109]

For the homogeneous *Pseudomonas putida* cytochrome P450cam enzyme, the experimental findings indicate that the interaction of carbon monoxide can be expressed according to Reaction II.5. The interaction of CO with the microsomal P450 species, on the other hand, appears

to present a much more complex situation. Tables II.1 and II.2 represent the complete collection of published equilibrium and kinetic data for the binding of CO to the P450 cytochromes. Data are compiled for the bacterial P450cam system (both substrate-free and bound), the microsomal P450 enzymes, some P450 model complexes, and for the myoglobin system. These data will be analysed and compared to present a description of the equilibrium and kinetic behavior of the P450 cytochromes in their reaction with CO; no detailed interpretation of the data in terms of structure-function relationships will be attempted but, whenever possible, correlation of equilibrium and kinetic behavior with structural features will be emphasized. Comprehensive interpretations of structure-function relationships can be found elsewhere.[8,109,135]

Comparison of the equilibrium constants (Kco) for CO-binding to cytochrome P450 shows that within the experimental limits of pH (7.0-7.5) and temperature (4-24^{o}C) the values are very consistent; they range from $1.3 \times 10^{5} M^{-1}$ at 24^{o}C for substrate-bound P450cam[99] to $22 \times 10^{5} M^{-1}$ at 4^{o}C for substrate-free P450cam,[33c] with the microsomal species being of intermediate value.[133b] Analysis of the Kco values for the P450cam enzymes indicates that the interaction with CO is affected by the camphor substrate. Peterson and Griffin[33c] report an almost 10-fold increase in the equilibrium binding constant at 4^{o}C in the absence of the substrate

Table II.1

Equilibrium Data for Reversible CO-binding to Cytochrome P450

Source	pH	T(^{o}C)	Kco(M^{-1})	ΔH^{o} (Kcal mol^{-1})	ΔS^{o} (cal mol^{-1} deg^{-1})	Ref.
P450cam (substrate-free)	7.4	4	2.2×10^{6}			33c
	7.0	24	1.7×10^{5}			10
P450cam (substrate-bound)	7.4	4	2.6×10^{5}			33c
	7.5	12	2.6×10^{5}	-12	-17	10
	7.0	20	6.6×10^{5}			133a
	7.0	24	1.3×10^{5}			99
Liver Microsomal P450	7-7.5	4	$3\text{-}7 \times 10^{5}$	0		13, 133b,c
	7.4-7.5	20	$0.7\text{-}1 \times 10^{6}$	0		133,b,d
P450 models		23	1.1×10^{4}	-16	-35	94c
Mb[a]	7.0	20	2.9×10^{7}	-12.6	-7.4	109

a) Enthalpy and entropy values quoted for myoglobin were calculated from activation parameters (ΔH^{*} and ΔS^{*}) for CO-on and off reactions as in Ref. 10.

Table II.2

Kinetic Data for Reversible CO-Binding to Cytochrome P450

Source	Method (a)	pH	T°C	k_{on} (M^{-1} S^{-1})	k_{off} (S^{-1})	Ea(on) (Kcal mol^{-1}) (c)	Ref.
P450cam (substrate-free)	SF	7.4	4	5.1×10^6	2.3(b)		33c
	FP		5	2.7×10^6	1.2(b)	8.9	30
			15	4.7×10^6		$\Delta H^* = 8.3$	
			25	8.4×10^6		$\Delta S^* = 1.9$	
P450cam (substrate-bound)	SF	7.4	4	3.8×10^4			33c
	SF	7.0	20	3.6×10^5	2.8		133a
	SF	7.0	24	2.2×10^5	1.7		10
	FP		5	8×10^4		8.9	30
			15	1.3×10^5		$\Delta H^* = 8.3$	
			25	2.3×10^5		$\Delta S^* = -6.0$	
	FP	7.3	12	3.5×10^4		8.0 ±0.4 $\Delta H^* = 7.4$ $\Delta S^* = -11$	133e
Mb		7.0	20	5×10^5	0.02	7.1 $\Delta H^* = 6.5$ $\Delta S^* = -10$	109 156
		7.0	25	3.8×10^5		4.7 $\Delta H^* = 4.1$ $\Delta S^* = -19.4$	
P450 Model			23	1.1×10^5	18		94c
Microsomal P450	FP	7.4	4	3.4×10^5	0.068		133h
	SF	7.5	4	4.5×10^5	0.63	8.3 $\Delta H^* = 7.8$ $\Delta S^* = -4.2$	133b

a) SF and FP refer to the kinetic methods of stopped-flow and flash photolysis respectively.

Notes for Table II.2 continued

b) Calculated values of k_{off} from the expression $Kco = \frac{k_{on}}{k_{off}}$ (see Reaction II.5).

c) Ea (on) refers to the activation energy measured for binding of CO to the various hemoprotein systems. Activation parameters (ΔH^* and ΔS^*) for the "on" reaction are shown in brackets underneath the Ea (on) values. Enthalpy and entropy of activation was calculated from $\Delta H^*(on) = Ea(on) - RT$ and $k_{on} = \frac{kT}{h} e^{-\frac{\Delta H^*}{RT}} e^{\frac{\Delta S^*}{R}}$ respectively. ΔH^* values have units of Kcal mol^{-1} while ΔS^* values are in cal mol^{-1} deg^{-1}; Ref.167.

($22 \times 10^5 M^{-1}$ *vs.* $2.6 \times 10^5 M^{-1}$). However, Dolphin and James *et al.*[10] report that at higher temperatures (24°C) the binding constant for substrate-free P450cam ($1.7 \times 10^5 M^{-1}$) approaches those for the substrate-bound enzyme (Kco = $1.3\text{-}6.6 \times 10^5 M^{-1}$).[10,99,133a] Since only two Kco values for substrate-free P450cam have been published to date, further studies are needed. The apparent lower affinity of substrate-bound P450cam for CO has been rationalized in terms of steric effects of the camphor molecule in the vicinity of the heme moiety;[33c] binding of the camphor close to the heme group is considered to restrict access of the CO molecule to the heme-iron and have a destabilizing effect on the heme-CO complex. The effect of the camphor substrate on the rate constants, to be discussed shortly, substantiates this rationalization. Analysis of the equilibrium binding constants for microsomal cytochrome P450 shows a slight increase in CO affinity as compared to the substrate-bound bacterial enzyme; these values approach those of substrate-free P450cam (Kco(microsomal P450) $\simeq 10^6 M^{-1}$; Kco(substrate-free P450cam) = $2.2 \times 10^6 M^{-1}$)), but whether or not the increased CO-affinity is due to a similar substrate-effect for the microsomal systems is not known. The observed differences in CO-affinity between the microsomal and bacterial P450 enzymes have not been interpreted because of the complex make-up of the microsomal systems (see Section II.2). Kinetic studies on the reaction of CO with

the microsomal enzyme exemplify these complex characteristics, and this information will be discussed shortly.

Comparison of the P450 cytochromes with mercaptide-heme model complexes[94c] and the myoglobin system[109] indicates the CO-affinities of the cytochromes are intermediate between the model complexes and that of myoglobin. In the case of the protein-free P450 models, CO is bound 10-100 times weaker than in the enzyme, whereas for myoglobin, carbon monoxide is bound up to 220 times tighter than in cytochrome P450 (see Table II.1). Lower CO-affinity for the P450 model complexes compared to the enzyme has been attributed to loss of stability provided by interaction of the CO-heme complex with the protein,[94c] for example, *via* hydrogen bonding with protein residues. These interactions are called cis-effects[109] and are used to assess the effect of the protein on ligand binding. The higher affinity for CO observed for the Mb system is thought to indicate the differences in proximal-ligand coordination in the two hemoproteins; imidazole in Mb, and thiolate in P450 cytochromes. The axial(RS^-) thiolate anion, coordinated to the heme moiety in the P450 systems, is thought to produce an electron-rich iron atom which in turn produces a general lowering of ligand affinity through σ-repulsions.[133a] Since imidazole coordination in the Mb system does not delocalize electron density onto the iron atom of the heme group so effectively, the same lowering of ligand affinities is not observed. The

effects of axial coordination on the reactivity of hemoproteins with ligands are called trans effects,[109] and again can be used to assess the effect of the protein on ligand binding.

Measurement of the equilibrium CO-binding constants for the P450 cytochromes as a function of temperature has provided only a single set of these thermodynamic parameters for substrate-bound P450cam system and no values for the corresponding substrate-free enzyme. Very limited data[133b] have been cited also for the microsomal P450 systems. Clearly, more thermodynamic data are needed to further understand the reaction of the P450 cytochromes with CO, as well as for comparison with other hemoprotein and P450 model systems.

Analysis of the thermodynamic data outlined in Table II.1 shows that the enthalpy change of CO-binding for the substrate-bound P450cam system[10] (ΔH^{o} = -12.0 Kcal mol^{-1}) is comparable to that of the myoglobin system[10] (ΔH^{o} = -12.6 Kcal mol^{-1}) and somewhat lower than that of the protein-free P450 model complex [94c] (ΔH^{o} = -16 Kcal mol^{-1}). The smaller enthalpy changes for the protein complexes is thought to be due to a weakly coordinated ligand[94c] from the bulk solvent or the protein which compensates slightly for the heat of reaction. Comparison of these ΔH^{o} values with the literature report that no enthalpy change was observed for the liver microsomal P450[133b] system is therefore surprising, and implies that in the microsomal enzymes an endogenous or exogenous ligand

could be strongly coordinated at the sixth site of the reduced P450 which compensates fully for the heat of reaction.

Limited entropy data for CO-binding (Table II.1) indicate that the binding is unfavourable. The negative ΔS^{o} values are attributed mainly to loss of translational and rotational freedom of the CO molecule on coordination.[8] Comparison of these systems shows that the differences in CO-affinity as determined by Kco values (i.e. Mb>P450cam >P450 models) result to a considerable extent from increasingly less favourable entropy terms. Explanations[8,10,109] based on cis and trans effects of the protein, as well as steric effects due to the presence of camphor in the P450 system, have been used to assess the different CO-affinities; however, these effects are subtle and difficult to assess precisely. The kinetic constants also reflect the observed trend in entropy changes (see below). Entropy data for microsomal P450 are needed for comparison with the bacterial enzyme as well as myoglobin and P450 model complexes.

Analysis of the kinetic data listed in Table II.2 shows that much attention has been directed to the determination of the CO-association rate constant, k_{on}, as defined in Reaction II.5. The determination of the CO-dissociation rate constant, k_{off}, has received less effort. The experimental conditions (i.e. pH and temperature ranges) utilized are almost identical to those quoted for Kco

evaluations, and rate constant determinations were obtained *via* both flash photolysis and stopped-flow techniques. Comparison of the substrate-free and substrate-bound P450cam systems shows that the interaction of CO is affected by the substrate camphor. Peterson and Griffin[33c] report second-order reaction rate constants for the reaction of the camphor-free and camphor ferrous cytochrome, of 5.1 x $10^{6}M^{-1}S^{-1}$ and 3.8 x $10^{4}M^{-1}S^{-1}$ respectively. Comparison of the k_{on} values for P450cam in the absence and the presence of substrate over the quoted experimental conditions indicates a general rate enhancement for the substrate-free complex : k_{on} (substrate-free) ≃ 2.0-9.0 x $10^{6}M^{-1}S^{-1}$; k_{on} (substrate-bound) ≃ 3.0-36 x $10^{4}M^{-1}S^{-1}$. The data are reflected in the higher Kco values for the substrate-free systems and camphor binding by the ferrous cytochrome is thought to reduce the accessibility of the heme-iron to the CO.[10,33c] For the substrate-free complex, both flash photolysis[30] and stopped-flow[33c] techniques gave consistent k_{on} values and measurement of k_{on} with temperature[30] yielded an activation energy, Ea, of 8.9 Kcal mol^{-1}. Values of k_{off} for the substrate-free system have not been measured directly although Peterson and Griffin,[33c] for example, have reported a calculated value of 2.3 S^{-1}. Using the Kco value (2.2 x $10^{6}M^{-1}$) at 4°C for the substrate-free complex [33c] and the k_{on} value (2.7 x $10^{6}M^{-1}$ S^{-1}) obtained by Gunsalus *et al.*[30] by flash photolysis at 5°C, a k_{off} value of 1.2 S^{-1} was calculated. The

two values of such calculated k_{off} data are reasonably consistent (Table II.2); however, direct measurement of k_{off} values for substrate-free P450cam are needed for comparison as well as activation parameters.

The kinetic data for the substrate-bound P450cam, although quite extensive, are not as consistent as for the substrate-free enzyme. Under the experimental conditions utilized (i.e. pH and temperature), the k_{on} values range from 3.5-36 x $10^4 M^{-1} S^{-1}$ with the faster rates occurring generally at higher temperatures. Inconsistencies arise however, when comparing stopped-flow measurements of Peterson and Griffin[33e] at 4°C (k_{on} = 3.8 x 10^4 M^{-1} S^{-1}) with flash photolysis measurement at 5°C by Gunsalus *et al.*[30] (k_{on} = 8 x 10^4 M^{-1} S^{-1}). Also, comparison of the flash photolysis measurements by Bonfils *et al.*[133e] at 12°C (k_{on} = 3.5 x 10^4 M^{-1} S^{-1}) and Gunsalus *et al.*[30] at 15°C (k_{on} = 13 x $10^4 M^{-1} S^{-1}$) show a factor of 4 difference between the two values. These inconsistencies, along with a 10-fold change in the CO-association rate constant over the quoted temperature range (which is not observed for the substrate-free enzyme), indicate that further measurement of k_{on} values are required to assess these observations. The activation energy for the association of CO with substrate-bound P450cam has been measured in the flash photolysis experiments of Gunsalus *et al.*[30] (Ea = 8.9 Kcal mol^{-1}) and Bonfils *et al.*[133e] (Ea = 8.0 $\pm$ 0.4 Kcal mol^{-1}). These activation

energies agree well with that obtained by Gunsalus *et al.*[30] (Ea = 8.9 Kcal mol^{-1}) for the substrate-free enzyme. Comparison of the calculated activation parameters for the association reaction (see Table II.2) indicate that CO-binding to the substrate-free enzyme is accompanied by a more favourable entropy term (ΔS^* = 1.9 cal mol^{-1} deg^{-1}) where as CO-binding in the presence of substrate is less favoured (ΔS^* = -6 - -11 cal in the smaller k_{on} values which, in turn, have been attributed to the restricted access to the CO-binding site in the enzyme in the presence of substrate.[33c] The measured k_{off} values for the dissociation of CO from substrate-bound P450cam (2.8 and 1.7 S^{-1})[10,133a] are similar to those calculated for the substrate-free enzyme and imply that the overall affinity of the P450cam systems for CO (i.e. Kco) is governed primarily by the k_{on} values as reflected by the absence or presence of the camphor substrate. The measured k_{off} values are also consistent with the k_{on} values calculated from the expression, $Kco = \frac{k_{on}}{k_{off}}$ (see Reaction II.5). The value of k_{off} = 1.7 S^{-1} measured by stopped-flow techniques,[10] along with the Kco = 1.3 x $10^5 M^{-1}$ reported from the same laboratory,[133a] provides a calculated k_{on} = 2.2 x 10^5 M^{-1} S^{-1} at 24°C, which is consistent with the CO-association rates reported at higher termeratures by Gunsalus *et al.*[30] The activation energy for the dissociation of CO from substrate-bound P450cam has not been measured.

Comparison of measured values of Kco with those calculated from the ratio of the "on" and "off" kinetic constants (see Reaction II.5) is afforded by only a single set of data.[133a] Using the k_{on} (3.6×10^5 M^{-1} S^{-1}) and k_{off} values (2.8 S^{-1}) values at 20°C,[133a] the calculated value of Kco = 1.3×10^5 M^{-1} may be compared with the measured value of 6.6×10^5 M^{-1}.[133a] To determine more definitively the level of agreement between Kco values measured in static experiments, and those calculated from the ratio of k_{on} and k_{off} values for the P450cam system, requires further study.

The kinetics of CO binding to microsomal cytochrome P450 apparently cannot be described accurately by Reaction II.5. Kinetic data have been reported in several short papers[133b,c,f,g] and in general the rate constants do not agree. The discrepancy is not surprising because of the varied conditions of the experiments and the different animal species from which the microsomes were isolated. However, with the exception of the flash photolysis study of Debey *et al.*,[133c] the time course of CO-binding was reported to consist of a single kinetic process as described for the bacterial enzyme. Indeed, the kinetic constants listed in Table II.2 for the microsomal P450, obtained from early experiments,[133b,h] are comparable to those of the P450cam systems, which is surprising in view of the heterogeneity of microsomal P450 (see Section II.2). More recently, liver microsomal P450 has been shown to react heterogenously with CO, exhibiting at least three species distinguished by their second-order rate constants for CO-

binding.[133d] This kinetic heterogeneity of microsomal P450 is thought to lie either in the molecular structure of the hemoprotein itself, or perhaps in an asymmetric placement of the cytochromes within the membranes.[133d] The activation energy for the "on" reaction has been measured by Debey *et al.*[133b] for microsomal P450 (Ea = 8.3 Kcal mol^{-1}) and, along with the calculated activation parameters, appears to be similar to that for the bacterial enzyme in the presence of substrate.

Comparison of the P450cam systems with the corresponding kinetic data for CO-binding to myoglobin and the P450 model complexes (see Table II.2) indicates that the major differences lie in the CO off-rates. The CO on-rates for myoglobin ($5.0 \times 10^5 M^{-1} S^{-1}$ at 20°C,[109] and $3.8 \times 10^5 M^{-1} S^{-1}$) at 25°C[156] are intermediate between the k_{on} values for P450cam in the presence and absence of substrate, while the CO on-rate for the P450 model complexes ($k_{on} = 1.1 \times 10^5 M^{-1} S^{-1}$ at 23°C) compares well with $k_{on} = 1.3 \times 10^5 M^{-1} S^{-1}$ reported by Gunsalus *et al.*[30] at 15°C for the camphor-bound system. In contrast, the CO off-rate constant for myoglobin is up to 140 times smaller than the k_{off} values for the P450cam system and is approximately 900 times smaller than that for the corresponding P450 model complex; the overall affinity for CO is governed by the CO off-rates. The differences in the CO off-rates is thought to indicate the effects of an electron-rich heme, provided by the proximal thiolate ligand in both the

P450cam and P450 model systems (Trans Effects).[133a] Increased σ-density due to the trans thiolate ligand is thought to result in the increase in CO off-rates through σ-repulsion, the CO molecule being unable to accept this excess electron density.[8] The major difference between the P450cam systems and the model system again lies in the CO off-rate. The smaller k_{off} of CO-P450cam is attributed to the protein, which imparts some stabilizing effect upon the CO-complex.[94c] The activation energy for binding CO to myoglobin (Ea = 4.7-7.1 Kcal mol^{-1}) is somewhat lower than the energy barrier surmounted by the CO molecule to bind to P450cam (Ea ≃8.5 Kcal mol^{-1}) but analysis of the activation parameters for myoglobin and substrate-bound P450cam shows that, although the ΔH* values are more favourable for myoglobin, the ΔS* values indicate CO-binding is less favourable and that the overall transition state is probably very similar in both proteins. This is reflected in the reasonably similar k_{on} values for CO-binding to both Mb and P450cam. Activation parameters for substrate-free P450cam indicate more favourable CO-binding than in myoglobin due primarily to a more favourable ΔS* term; this is again reflected in the k_{on} values.

The interpretation of structure-function relationships, based on equilibrium and kinetic data such as described above for the interaction of CO with cytochrome P450, is difficult because of the many different factors influencing the interaction.[8,109] As mentioned earlier, one structural factor,

which influences the interaction of CO with both the P450 enzymes and the myoglobins, is proximal ligation provided by the protein (Trans Effects). The important groups are the iron-binding thiolate ligand in the P450 systems and the more familiar imidazole ligand in the globins. Kinetic and equilibrium data for these hemoproteins do provide, however, information about the strength of CO-hemoprotein interaction which depends, in turn, on the nature and on the bond strength of this proximal ligation. The nature of the heme-iron - CO bond in these complexes has been described in detail[8] as a combination of σ donation from the CO molecule and d-π backbonding from the heme-iron to the CO. The effects of the thiolate ligand on spectral as well as kinetic and equilibrium behavior of the P450cam system, based on these σ and π effects, have been outlined previously and reported in the literature.[133a] The effect of porphyrin σ- and π- electron density on the interaction of CO with hemoproteins can be investigated using hemoproteins reconstituted with hemes differing in the side chains in positions 2 and 4 (i.e. meso-, deutero-, proto-, diacetyl-deutero-, and dibromodeuteroporphyrinatoiron species; (see Figure I.3). Changes in σ-electron density at the iron center are reflected in the basicity of these heme groups, as measured by pK_3;[8] strongly basic porphyrins (large pK_3 values) increase σ-density at the iron center. Such studies are therefore directed at explaining different ligand affinities in various hemoproteins with the changes

in electron density at the level of the iron atom resulting from changes in electronic structure of the heme group and proximal ligation to the iron. The net effect in the hemoprotein will depend on the balance between these factors, as well as on the control that the protein exerts on the porphyrin through interaction with the proximal linkage. The effect on σ-electron density on the interaction of CO, as well as O_2, with cytochrome P450 has been investigated recently using heme-substituted P450cam systems.[10] Native P450cam was reconstituted with meso-, deutero-, proto-, diacetyldeutero- and dibromodeuteroporphyrinatoiron species and the equilibrium binding constants for the reaction with CO and O_2 were measured. Table II.3 lists pK_3 values for each porphyrin as well as $P_{\frac{1}{2}}^{CO}$ and corresponding Kco values for each of the reconstituted P450cam systems. Corresponding data for myoglobin have not been reported. $P_{\frac{1}{2}}^{O_2}$ and K_{O_2} values for reconstituted P450cam and myoglobin systems are also included for comparison. Equilibrium binding data for the P450cam systems are for the substrate-bound enzymes only.

Analysis of the data presented in Table II.3 indicates that binding of CO to substrate-bound P450cam is enhanced with more basic porphyrins (i.e. meso ≈ deutero > proto > diacetyl deutero > dibromodeutero).[10] That is, the higher pk_3 values indicate increasing σ-electron density at the central iron atom which in turn strengthens the CO-hemoprotein interaction.[8] Such correlations are indicated for some cobalt and manganese

Table II.3

Data(a) for Binding of CO and O_2 to the Ferrous States of Substrate-bound P450cam[10] and Myoglobin[109]

Porphyrin System	pK_3	Kco (P450cam) (M^{-1})	K_{O_2} (P450cam) (M^{-1})	K_{O_2} (Mb) (M^{-1})
Meso	5.8	1.7×10^5 (4.3)		1.5×10^6 (0.38)
Deutero	5.5	1.8×10^5 (4.0)	2.7×10^5 (2)	2.6×10^6 (0.21)
Proto	4.8	1.3×10^5 (5.5)	2.2×10^5 (2.5)	1.1×10^6 (0.52)
Diacetyl-deutero	3.3	5.3×10^4 (13.8)	2.7×10^4 (20)	5.5×10^5 (1.0)
Dibromo-deutero	3.0	4.6×10^4 (16.1)	2.5×10^4 (22)	5.0×10^5 (1.1)

a) $P_{\frac{1}{2}}$ (mm Hg) values are in brackets.

Kco values calculated assuming 1 mm CO = 1.36×10^{-6}M;

K_{O_2} values calculated assuming 1mm O_2 = 1.82×10^{-6}; Ref.109.

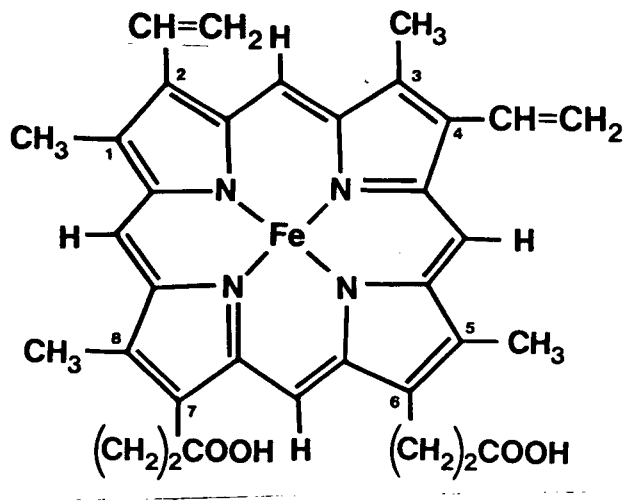
porphyrin systems, but the effects are small and the interplay of σ and π effect is subtle.[8] Comparison with the corresponding O_2-binding data for substrate-bound P450 systems and myoglobin shows the same correlation of stronger binding with lower porphyrin basicity. This indicates that similar electronic factors are probably operative for both CO- and O_2- binding.[10] It is worth noting that the most basic meso systems binds CO somewhat less strongly than the deutero system and this trend is also found with O_2-binding to reconstituted P450cam and myoglobin systems. Again explanations based on σ and π effects at the heme center have been offered but the trend is poorly understood.[8] More detailed interpretation of the equilibrium constants for the reaction with CO requires evaluation of the enthalpy and entropy contributions by studies at different temperatures. These data, along with a complete set of kinetic constants and activation energies for the reaction of CO with the reconstituted P450cam system in the presence and absence of the camphor substrate, are needed to further evaluate the structure-function relationships manifested by cytochrome P450. In short, since no kinetic data have been published on these reconstituted P450cam systems to date, an excellent opportunity presents itself to study further the interaction of carbon monoxide with this enzyme system.

CHAPTER III

EXPERIMENTAL PROCEDURES

III.1 Synthesis of Substituted Hemins Derived from Protohemin Chloride [(chloro)protoporphyrinatoiron (III)]

III.1.1 General Information



(1)

Protohemin (1) is the prosthetic group of hemoglobin, myoglobin, many peroxidases, catalase, cytochrome P450 and many other proteins. It is thus the most widely occurring porphyrin derivative found in Nature. Syntheses of porphyrins and hemins derived from those found in animal material invariably involve protohemin as the starting material. Indeed, the syntheses of deutero-, meso-, diacetyldeutero-, and dibromodeuterohemin (see Figure I.3) to be described presently involve protohemin as the starting material. In each case, the corresponding hemin derivative is obtained through modification of the vinyl groups in the 2 and 4

positions of the porphyrin periphery of protohemin (1) : for deuterohemin the vinyl groups are replaced by hydrogen; for mesohemin the vinyl groups are converted to ethyl groups, for diacetydeuterohemin the vinyl groups are exchanged for acetyl groups; and for dibromodeuterhemin the vinyl groups are replaced by bromogroups (-Br). The preparation of these substituted hemins involves either direct conversion of the vinyl groups or replacement of them by direct substitution on the porphyrin ring. The synthetic methods to be described have been used for many years as standard procedures for modification of the porphyrin periphery at the 2 and 4 positions of protohemin. As well, each of the substituted hemins have been fully characterized[136] in terms of their physical properties. Therefore, although the same standard preparative methods are used to synthesize the four modified hemins, characterization was limited to spectrophotometric analysis in the visible region (400-700nm) of the pyridine hemochrome complex of each hemin (see Section III.1.3). Absolute absorption peak maxima (λ_{max}) and millimolar extinction coefficient (ε_{mM}) data obtained experimentally were compared with data reported in the literature. These data are listed following the preparative method of each hemin. In all cases, λ_{max} and ε_{mM} values obtained experimentally were in excellent agreement with the literature. Thin layer chromatography (TLC) on silica gel and polyamide was also used to assess the purity of each hemin.

III.1.2 Materials

Reagents were obtained as follows : from Allied Chemical Canada Ltd., glacial acetic acid: from American Scientific and Chemical Co., concentrated ammonium hydroxide (NH_4OH), ferrous chloride, ferrous sulphate, concentrated hydrochloric acid (HCl), potassium hydroxide (KOH), pyridine, and sodium hydroxide (NaOH); from Caledon Laboratories Ltd., benzene; from Eastman Kodak Co., acetone, chloroform, N,N'-dimethyl formamide (DMF), methanol, and propionic acid; from Fisher Scientific Co., acetic anhydride, bromine, hydrobromic acid (48%), resorcinol, sodium dithionite ($Na_2S_2O_4$) anhydrous sodium sulphate and anhydrous stannic chloride ($SnCl_4$); from Mallinckrodt, anhydrous diethyl-ether, and sodium tartrate AR; from MCB, ammonium acetate, formic acid (88%) and palladium oxide ($PdO \times H_2O$); and from Sigma Chemical Co., protoporphyrinatoiron (III) (protohemin). All solvents were used directly without further purification.

Hydrogen gas (H_2) and gaseous hydrochloric acid were obtained from Matheson of Canada Ltd. and were used without further purification.

Purified argon, obtained from Canadian Liquid Air Ltd., was further purified by passing it through a copper catalyst (Fisher) heated to 50°C to remove trace oxygen and then through two drying tubes containing fresh phosphorous pentoxide (M.C.B.), and sodium hydroxide pellets with Indicating Drierite (Fisher).

Analytical thin layer chromatography (TLC) was performed on silica gel (Precoated Eastman Chromatogram sheets) and polyamide (Polygram Polyamide-6, 0.1 mm) available from the Eastman Kodak Co., and Brinkman, respectively.

III.1.3 Spectrophotometric Analysis of Pyridine Hemochromes

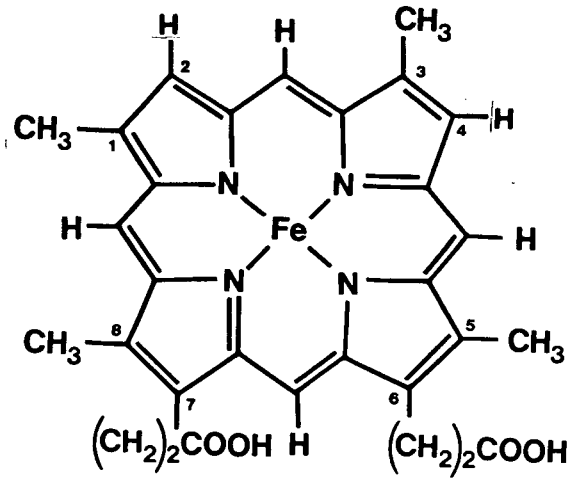
Ultraviolet and visible absorption spectra were recorded on a Cary 17D spectrophotometer at room temperature (23±2°C). Quartz cells (Hellma) of pathlength 0.1 and 1 cm were used.

As mentioned in Section III.1.1, the substituted hemin derivatives were characterized as the pyridine hemochrome species.[137a] The hemochromes are complexes formed by the coordination of two molecules of a base to a ferrous porphyrin (heme); the heme molecule is coordinated by two pyridine molecules in the pyridine hemochrome complexes. The hemochromes produce sharp and characteristic three-banded visible absorption spectra consisting of a strong Soret absorption peak at ≈400nm and two weaker absorption maxima (i.e. the α and β bands) between 500 and 600nm. The position and intensity of these bands are extremely sensitive to changes in the porphyrin skeleton, such as peripheral modifications at the 2-,4-vinyl groups of protohemin, as well as to the purity of the hemin sample. Therefore, the samples of deutero-, meso-, diacetyldeutero-, and dibromodeuterohemin synthesized from protohemin were identified readily by this method.

In practice, the pyridine hemochrome spectra were measured in aqueous alkaline pyridine solutions after reduction with solid sodium dithionite ($Na_2S_2O_4$), according to the method of Paul *et al.*[138] The hemochrome was prepared by mixing 2.0mL of 0.1mM NaOH, 0.5mL pyridine and 25μL of a

pyridine-heme solution made up by dissolving ≃ 1mg of hemin in 1mL of pyridine. The final hemin concentrations in the reaction mixtures were ≃ 1 x 10^{-5}M, whereas the final concentrations of NaOH and pyridine were 0.079 N and 2.2M respectively; such conditions have been found satisfactory for the production of the pyridine hemochrome species.[137a] The reaction components were transferred to a 1cm quartz cell (maximum volume, 3mL), degassed by purging the solutions with argon, and finally, reduced by the addition of ≃ 1mg of $Na_2S_2O_4$. Hemochrome formation was almost instantaneous as indicated by the rapid color change of the solution; on reduction the solution changed from brown to red. The cell was immediately stoppered and the visible absorption spectrum obtained. All hemochrome spectra were run against a matched 1cm quartz reference cell containing the pyridine-NaOH solvent and $Na_2S_2O_4$. Cells containing only the pyridine-NaOH solvent system and $Na_2S_2O_4$ were used to determine the baseline absorption before the hemochrome spectra were obtained. If a particularly concentrated solution of the hemochrome was prepared, 0.1cm quartz cells were used to measure the strong Soret absorption maxima. The millimolar extinction coefficients were determined by direct spectroscopic measurement and compared to literature data.

III.1.4 Deuterohemin (2)



(2)

Crude deuterohemin was prepared from protohemin by the resorcinol melt procedure described by Dinello and Chang.[136a] Five grams of protohemin (dark blue crystals) and fifteen grams of resorcinol (flaky white solid) were mixed together and placed in a 250mL round-bottom flask. The flask was kept under an air condenser in an oil-bath at 140° - 150°C. The mixture becomes liquid at ≈110°C (i.e. the melting point of resorcinol) but the solution does not reflux as a liquid. Instead, the resorcinol crystallizes on the walls of the flask and eventually, the white solid falls back into the solution. The progress of the reaction was monitored spectrophotometrically by withdrawing an aliquot of the reaction mixture and preparing the pyridine hemochrome species (see Section III.1.3). The

visible absorption spectrum was then compared with that of the protohemin pyridine hemochrome (Table III.1). Completion of the reaction was determined by the disappearance of the protohemin pyridine hemochrome spectrum. The reaction was complete after 45 min. After cooling to room temperature, the black tar-like mass was triturated with diethyl-ether and the solid collected by suction filtration with a fine sintered-glass funnel. The solid was washed further with diethyl-ether until the filtrate was clear, and then air dried. The yield of the crude brown deuterohemin was quantitative. Prior to further use in the preparation of diacetyldeutero- (Section III.1.6) and dibromodeuterohemins (see Section III.1.7), the crude deuterohemin was stored in the dark at $\simeq 0^{\circ}C$. Purified deuterohemin, on the other hand, was obtained in high yields following the method developed by Dinello and Chang.[136a]

Six hundred milligrams of the crude deuterohemin were dissolved in minimal pyridine ($\simeq$ 2mL) and applied to a silica-gel thick layer plate (Analtech Inc. 2mm thick). The plate was dried using a stream of warm air from a heat gun. The dry preloaded silica gel was scraped off the plate and thoroughly powdered. Meanwhile, 90g of polyamide powder (Machery and Nagel, 0.07mm available from Brinkman) was slurried in benzene-methanol-formic acid (BMF) 110:30:1 (v/v/v) and poured into a column 2.5cm in diameter and 90cm high. The column was packed and equilibrated with at least 500mL

solvent at a flow-rate of 6-9mL/min using N_2 pressure. Higher than normal flow-rates of about 1mL/min reduces the amount of esterification during column elution that take place due to the presence of methanol and an acid catalyst (i.e. formic acid).[153a] A layer of solvent 5-10cm was left over the top of the column. The silica gel loaded with crude deuterohemin was poured directly on top of the column using a powder funnel (100mm diameter) equipped with an extended shaft (≃ 20cm). If the shaft of the funnel was held just above the upper solvent level on the column and, if a sufficient layer of solvent (≃ 10cm) was left over the column bed, the top of the polyamide bed was undisturbed and the loaded silica gel settled evenly. The funnel was rinsed thoroughly with eluting solvent. The liquid level was brought to the top of the column and the column was eluted at 6-9mL/min with BMF (110:30:1).

The crude deuterohemin separated into two bands. The first, which was eluted from polyamide before deuterohemin, was present as a small pink band that was collected and discarded. The second band, which contained deuterohemin, eluted more slowly as a major dark brown band.

The fractions corresponding to deuterohemin from the above column chromatography were taken to dryness and dissolved in 1.5mL pyridine. Chloroform (3mL) was added and the solution was filtered through a pipette containing glass wool into a 50mL round-bottom flask. The glass wool

was washed with two 1.35mL portions of pyridine-chloroform 35:100. The pyridine-chloroform solution of deuterohemin was then heated to boiling and 35mL boiling acetic acid were added. Concentrated HCl (0.35mL) was added and the solution again heated to boiling. Deuterohemin chloride((chloro) deuteroporphyrinatoiron (III)) was recovered by suction filtration after standing overnight to complete crystallization. The yield of crystalline deuterohemin (dark blue crystals) from 600mg of crude material was 250mg or 42% from protohemin. The crystalline hemin showed a single spot on TLC on silica gel (BMF 110:30:1) and polyamide (BMF 110:30:1 and methanol-acetic acid 100:2). Table III.1 lists absorbance data for the pyridine hemochrome of deuterohemin as well as proto-hemin, while Figure III.1 shows the absolute absorption spectrum of the deuterohemin pyridine hemochrome.

Table III.1

Absorbance Data for the Pyridine Hemochromes Derived from Proto- and Deuterohemin.

Heme	λ_{max}(nm) ε_{mM}	Soret Band	β_{max}	α_{max}
Proto-[a]	λ	418,5	526	557
	ε	191.4	17.5	34.4
Deutero-[a]	λ	405.5	514	544
	ε	134.6	18.3	26.4
Deutero-[b]	λ	406	514	544
	ε	135	18.8	25

a) Published λ_{max} and ε_{mM} values for the proto- and deuterohemin pyridine hemochromes; Ref.136a.

b) Experimentally determined λ_{max} and ε_{mM} values for the deuterohemin pyridine hemochrome.

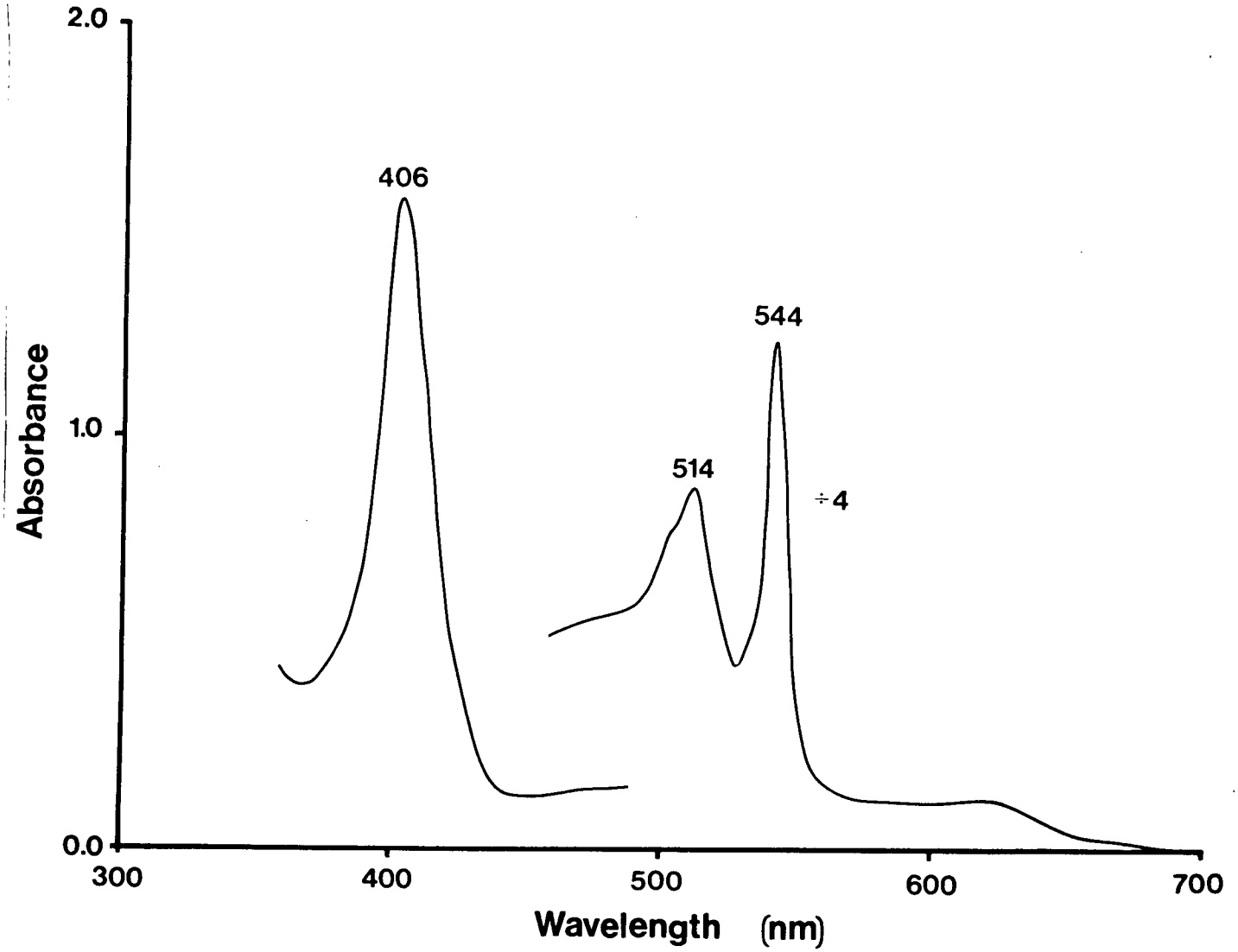
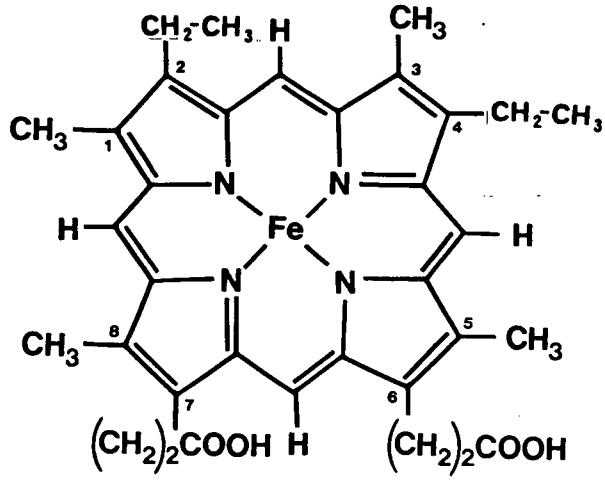


Figure III.1 Absorption spectrum of the deuterohemin pyridine hemochrome.

III.1.5 Mesohemin (3)



(3)

Crude mesohemin was prepared by metallation of mesoporphyrin free acid by the method of Adler *et al.*[139] Mesoporphyrin free acid was synthesized from protohemin by the method described by Caughey *et al.*[136b] The method involved the simultaneous reduction of the vinyl sidechains to ethyl groups with hydrogen gas (H_2), and removal of iron through the action of formic acid. Palladium oxide (PdO) was used as the reducing catalyst. Ferrous protohemin was initially formed by the reduction of Fe(III) to Fe(II). Since Fe(II) has a larger ionic radius, 0.74Å, compared with that of Fe(III), 0.64Å, Fe(II) was more readily dissociated from the porphyrin macrocycle, and thus protoporphyrin IX was obtained initially. The final mesoporphyrin IX

was obtained by catalytic hydrogenation of the vinyl groups of protoporphyrin IX.

Protohemin (2.0g) was suspended in formic acid (90%; 165mL) containing palladium oxide (500mg) in a 250mL two-necked round-bottom flask fitted with a reflux condenser and a fine glass frit for purging the solution with hydrogen gas. The mixture was maintained at 94-98^{o}C for 1h while the H_2 gas was passed through the mixture. The progress of the reaction was again followed spectrophotometrically by withdrawing an aliquot of the reaction mixture and then diluting with formic acid. The visible absorption spectrum was then compared with that of protoporphyrin IX (Figures III.2 and III.3). Completion of the reaction was determined by the disappearance of the protoporphyrin IX spectrum. The palladium oxide was filtered off using a sintered glass funnel of fine porosity, and was washed with formic acid. The filtrate was then poured into 30% ammonium acetate solution (600mL) with efficient stirring. After being allowed to stand for 45min, the precipitate was collected by centrifugation at 10,000rpm using a Servall RC2 refrigerated centrifuge equipped with an SS-34 rotorhead and washed repeatedly with deionized water. The precipitate was taken up in 2% aqueous ammonia solution (140mL) to give a brown solution. The disodium salt of mesohemin was "salted out" with 30% sodium tartrate solution (20mL). The precipitate was collected by centrifugation and, if the supernatant remained brown, the above procedure was repeated.

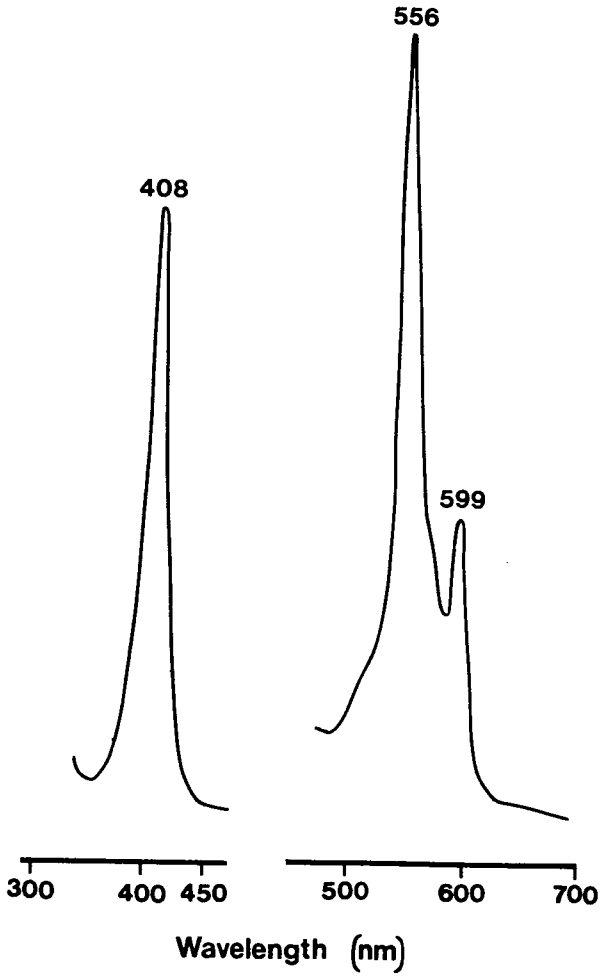


Figure III.2 Absorption spectrum of protoporphryin IX in formic acid.

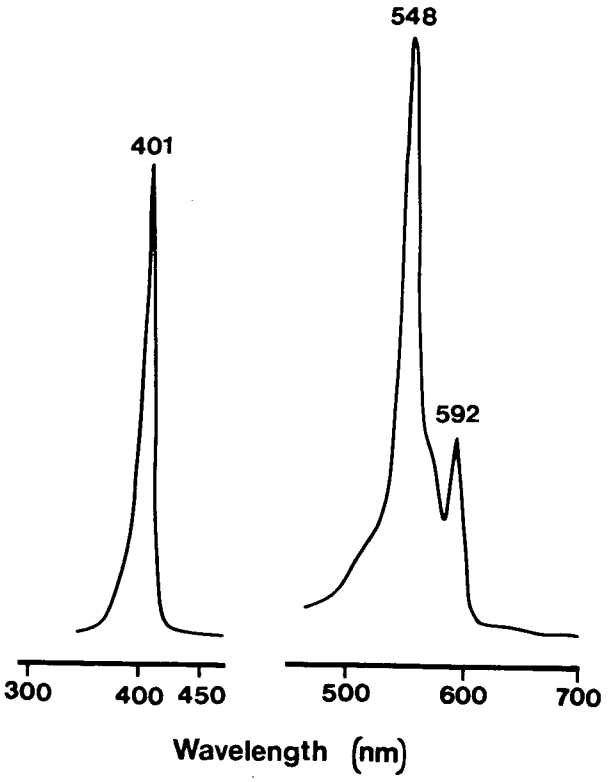


Figure III.3 Absorption spectrum of mesoporphyrin IX in formic acid.

The sodium salt was converted to mesohemin dihydrochloride as described by Corwin *et al.*[140] by the addition of boiling 25% hydrochloric acid (120mL) to the precipitate in the centrifuge tubes. The solid dissolved instantly and crystals of the dihydrochloride formed almost immediately. The crystalline mesoporphyrin dihydrochloride was collected by filtration, washed with a little 2.5% hydrochloric acid solution, and dried in air. The brown solid was stored at $\simeq 0^{\circ}C$. The yield of crude mesoporphyrin dihydrochloride was quantitative. The visible absorption spectrum in chloroform exhibited peaks of 400, 496, 530, 566 and 620nm (Literature values : 400, 499, 533, 567 and 621nm; Ref.136a).

Metallation of the mesoporphyrin dihydrochloride was carried out in refluxing N,N'-dimethylformamide (DMF) in the presence of ferrous chloride.[139] Reagent grade DMF (200mL) was brought to reflux in a 500mL round-bottom flask equipped with a reflux condenser. The solvent was heated on a stirring hot plate. The mesoporphyrin dihydrochloride prepared by the above procedure was added and the mixture allowed to stir for 5 min for complete solution of the porphyrin. Two mole equivalents of ferrous chloride (760mg) were powdered and then added to the solution. After a few minutes, completion of the reaction was checked by the loss of the free porphyrin's red fluorescence under long wave ultraviolet light, and spectrophotometrically by withdrawing a small aliquot for analysis of the mesohemin pyridine hemochrome. The metalation reaction was complete in 5 min.

The reaction vessel was removed from the hot plate and cooled to room temperature. Once cooled, the reaction mixture was added to an ice water bath (500mL) with stirring and the resulting precipitate filtered on a Buchner funnel until the filtrate was clear. The filtered material was washed with water and air dried. The yield of crude mesohemin was quantitative.

Crude mesohemin (600mg) was purified by chromatography on polyamide as described for deuterohemin in Section III.1.4 except that the solvent system used was BMF 110:15:1. Three impurities were present in the mesohemin dihydrochloride sample. The first two, which eluted from polyamide before mesohemin, appeared as a fast running red and a slower running pink band. These were collected but were not identified. The third impurity, a light brown band, eluted from the column after the dark brown mesohemin band. The impurity was discarded. The main product fractions were collected, taken to dryness, and crystallized as described for deuterhemin (see Section III.1.4). The yield of mesohemin chloride (chloro)mesoporphyrinatoiron(III) was 330mg or 55% from protohemin. TLC on silica gel (BMF 110:30:1) showed a single spot as did polyamide TLC (BMF 110:30:1 and methanol-acetic acid 100:2). Table III.2 lists absorbance data for the pyridine hemochrome of mesohemin while Figure III.4 shows the absolute absorption spectrum of the mesohemin pyridine hemochrome.

Table III.2

Absorbance data for the Pyridine Hemochrome Derived from Mesohemin.

Heme	λ_{max} (nm) ε_{mM}	Soret Band	β_{max}	α_{max}
Meso-[a]	λ	408	516	546
	ε	139.5	20.9	35.8
Meso-[b]	λ	408	516	546
	ε	140	21	34

a) Published λ_{max} and ε_{mM} values for the mesohemin pyridine hemochrome; Ref.136a.

b) Experimentally determined λ_{max} and ε_{mM} values for the mesohemin pyridine hemochrome.

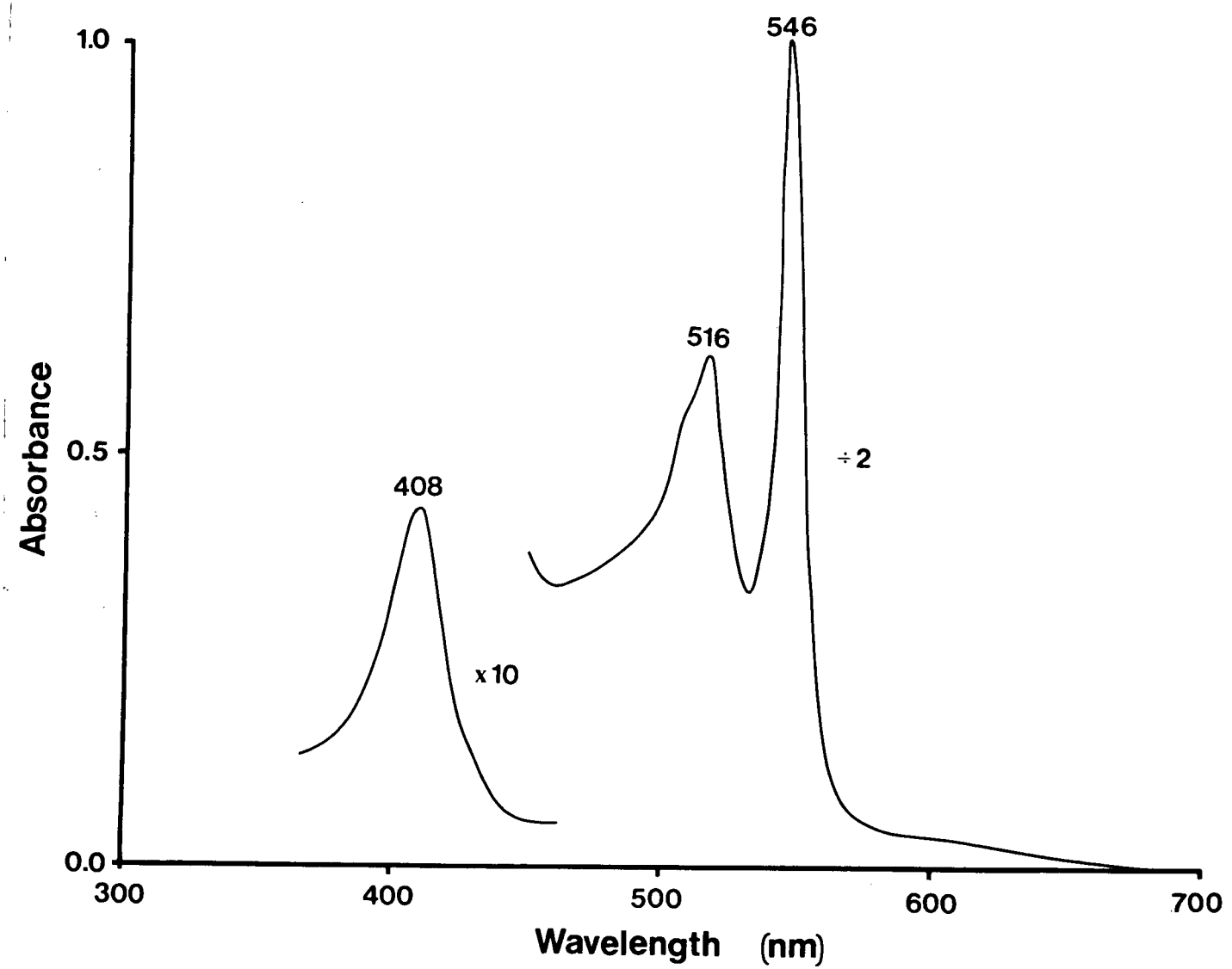
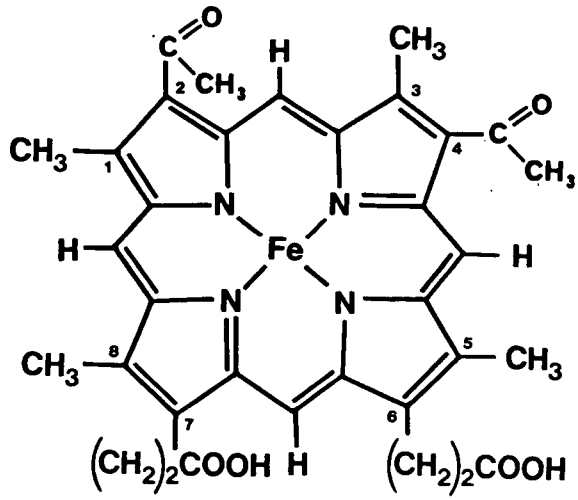


Figure III.4 Absorption spectrum of the mesohemin pyridine hemochrome.

III.1.6 Diacetyldeuterohemin (4)



(4)

Crude diacetydeuterohemin was prepared from crude deuterohemin (see Section III.1.4) using the original method of Fischer,[141] as modified by Dinello and Chang.[136a] One gram crude deuterohemin was dissolved in 200mL acetic anhydride in a 500mL round-bottom flask fitted with a drying tube and equipped with a magnetic stirring bar. The flask was placed in an icewater bath and the temperature brought to $0^{o}C$ with stirring. Fourteen millilitres of anhydrous $SnCl_4$ were then carefully added with stirring and the solution allowed to stir in the ice water bath for 7 min. Longer reaction times result in substantial decomposition and shorter times give substantial amounts of the mono-acetylated product.[136a] The reaction mixture was then carefully poured into 400mL of a mixture of ice and 1M HCl. The resultant mixture was allowed

to stir for 2h to destroy excess acetic anhydride. The crude product was then recovered by suction filtration, washed with water, and air dried. The yield was quantitative.

Crude diacetyldeuterohemin (400mg) was purified by polyamide chromatography as described for deuterohemin (see Section III.1.4) except that methanol-acetic acid 100:2 was used as the solvent system. Five bands were detected on the column. Diacetyldeuterohemin was the least mobile compound. The fractions corresponding to the main band were collected, evaporated to a volume of 10mL, and precipitated with water. The hemin was filtered and air dried for 30 min, then washed with ether and vacuum dried overnight. The yield was 120mg or 30% from protohemin.

Diacetyldeuterohemin is too soluble to crystallize using the procedure with pyridine, chloroform, acetic acid, and HCl, as described for crystallization of deuterohemin (see Section III.1.4). Substitution of propionic acid for acetic acid gave crystalline diacetyldeuterohemin, but nearly half of the pure material remained in solution. Attempts to work up the mother liquor resulted in substantial decomposition. The crystalline diacetyldeuterohemin showed a single spot on TLC on silica gel (BMF 110:30:1) and polyamide (BMF 110:30:1 and methanol-acetic acid 100:2). Table III.3 lists absorbance data for the pyridine hemochrome of diacetyldeuterhemin, while Figure III.5 shows the absolute absorption spectrum of the diacetyldeuterohemin pyridine hemochrome.

Table III.3

Absorbance Data for the Pyridine Hemochrome Derived from Diacetyldeuterohemin

Heme	λ_{max} (nm) ε_{mM}	Soret Band	β_{max}	α_{max}
Diacetyl-deutero (a)	λ	439	540	574
	ε	115	12.6	13.8
Diacetyl-deutero (b)	λ	439	537	573
	ε	110	13.8	16.5

a) Published λ_{max} and ε_{mM} values for the diacetyldeutero-hemin pyridine hemochrome; Ref.136a.

b) Experimentally determined λ_{max} and ε_{mM} values for the diacetyldeuterohemin pyridine hemochrome.

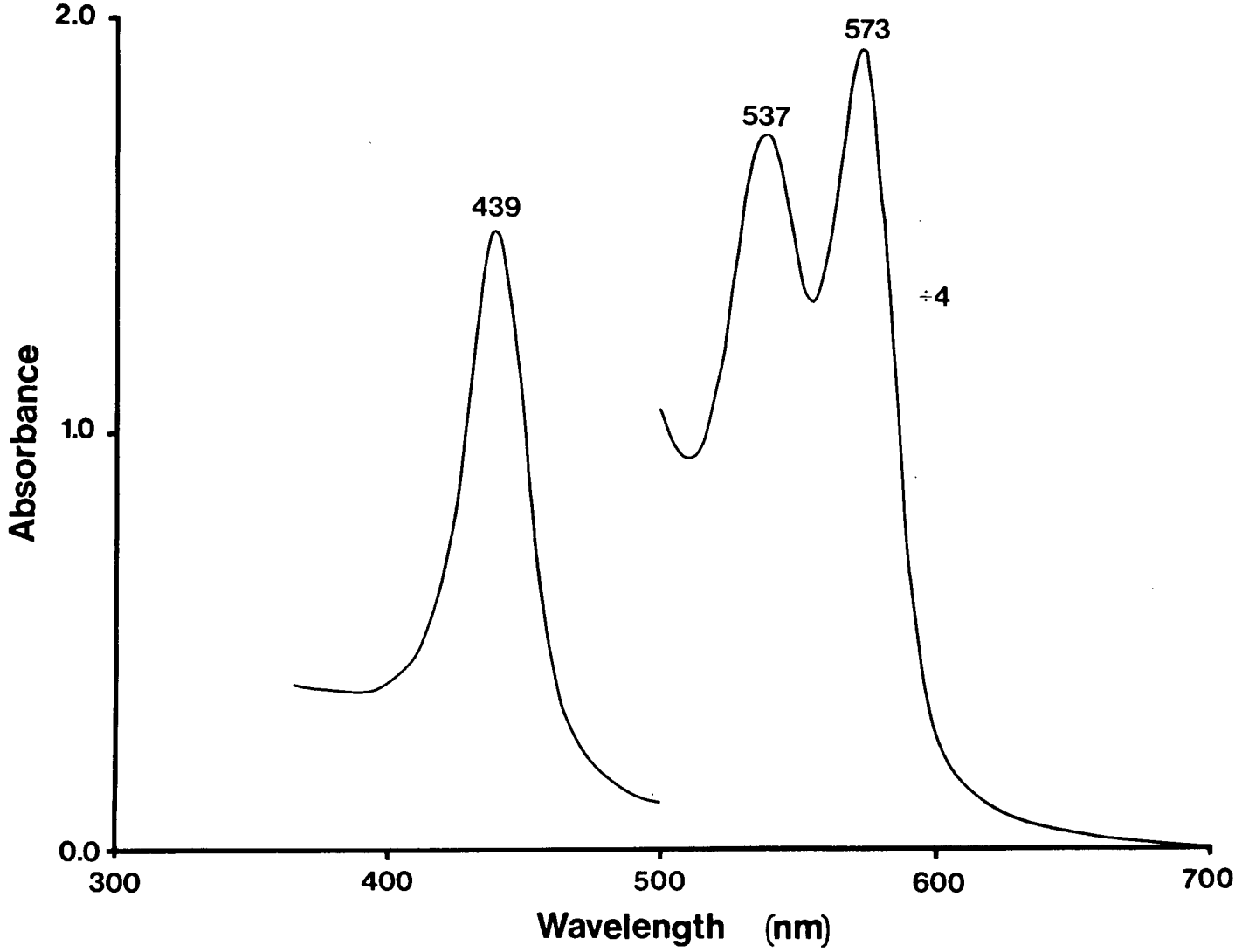
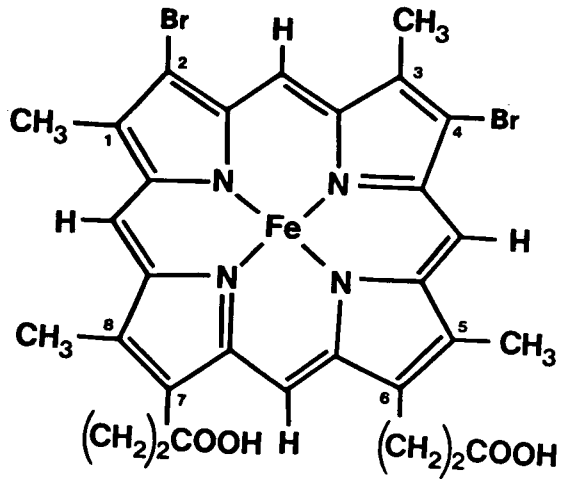


Figure III.5 Absorption spectrum of the diacetyldeutero-hemin pyridine hemochrome.

III.1.7 Dibromodeuterohemin (5)



(5)

Dibromodeuterohemin was prepared from crude deuterohemin (see Section III.1.4) using a four step procedure. Deuteroporphyrin dimethyl ester, produced by dematallation and esterification of crude deuterohemin, was brominated and then purified. The hemin was then prepared by insertion of iron into the purified dibromodeutero-porphyrin dimethyl ester followed by hydrolysis of the ester groups.

Deuteroporphyrin dimethyl ester was prepared from crude deuterohemin by the method of Caughey *et al.*[136b] which involved simultaneous iron removal and esterification with methanol. One gram of crude deuterohemin was suspended in a mixture of pyridine (2.5mL) and chloroform (10mL) in a 250mL two-necked round-bottom flask fitted with a bubbler and a fine glass frit for purging the solution with HCl gas. This brown mixture was

stirred at room temperature for 30 min to allow for complete solution of the hemin.

Chloroform (40mL), 8gm of finely powdered anhydrous ferrous sulphate, and 55mL of methanol were then added, and HCl gas was rapidly passed through the vigorously stirred solution until iron removal and esterification were complete. Iron removal was followed spectrophotometrically by withdrawing a small aliquot of the reaction mixture and then diluting with pyridine. Complete iron removal was determined by the appearance of the deuteroporphyrin spectrum. The visible absorption spectrum of deuteroporphyrin in pyridine exhibited peaks at 400, 496, 528, 565, and 619nm (literature values: 400, 497, 529, 566 and 620nm; Ref. 136a). A distinct color change of the reaction solution from brown to red was also associated with production of deuteroporphyrin. Deuteroporphyrin free acid and the dimethyl ester were distinguished by analytical thin layer chromatography on silica gel eluting with chloroform. Deuteroporphyrin dimethyl ester exhibited R_f values of ≈0.5 where as the free acid components remained near the origin of the chromatogram. Esterification was complete when no material remained at the origin of the chromatograms. Both iron removal and esterification were complete in 1h. The reaction mixture was extracted with water (200mL, three times), with 10% aqueous ammonia (200mL, twice) and again with water (200mL, twice). The washed chloroform solution was dried over anhydrous sodium sulphate (40gm) and taken to dryness.

The crude deuteroporphyrin dimethyl ester was brominated according to the method of Caughey *et al.*,[136b] using pyridinium hydrobromide perbromide prepared by the procedure described by Fieser.[142] Three millilitres of pyridine was added slowly to 6mL of 48% hydrobromic acid and the solution allowed to cool to room temperature. To this solution was added gradually 5g of bromine and again the solution was allowed to cool. The product was collected by suction filtration and washed thoroughly with acetic acid. The wet solid was then added to 20mL of acetic acid and left overnight to crystallize. The yield of orange needles was 6g.

Pyridinium hydrobromide perbromide (2g) was added over a 5 min period to the crude deuteroporphyrin dimethyl ester prepared above suspended in chloroform (100mL) in a 250mL round bottom flask. After 5 min acetone (35mL) was added, followed 5 min later by the addition of cold water (100mL). Up to and during the addition of water, the reaction was vigorously stirred and cooled to $0^{\circ}C$ in an icewater bath. The chloroform layer was washed with water, dried over anhydrous sodium sulphate (50g) and taken to dryness. The porphyrin ester was chromatographed on a silica gel (Woelm, 70-150 mesh, available from ICN) column (100g) and eluted with chloroform containing 1.5% methanol by volume. The eluted dibromodeuteroporphyrin dimethyl ester was recrystallized from chloroform : methanol (1:1, by volume). Analytical thin layer chromatography on silica gel eluting with chloroform revealed a single component and the visible absorption spectrum

in chloroform exhibited peaks at 499, 533, 568, and 623nm (literature values : 500, 534, 569, and 523nm; Ref. 136c).

Dibromodeuterohemin was prepared by insertion of iron into the purified dibromodeuteroporphyrin dimethyl ester, according to the procedure outlined for the metallation of mesoporphyrin dihydrochloride (see Section III.1.5). The ester groups were hydrolyzed in alcoholic KOH as described by Smith *et al.*[137b] Deuterohemin dimethyl ester was dissolved in 100mL of methanol containing 1% KOH by weight, the solution refluxed for 2h, and cooled to room temperature. The hemin free acid was precipitated in an ice-water bath containing 1M HCl solution (500mL), suction filtered, washed thoroughly with cold water, and air dried. The dibromodeuterohemin was then purified by column chromatography as described for diacetyldeuterohemin (see Section III.1.6). Two bands were detected on the column. Dibromodeuterohemin was the least mobile compound. The fractions corresponding to dibromodeuterohemin were collected, evaporated to a volume of 10mL, and precipitated with water. The hemin was filtered, washed thoroughly with water, and air dried. The yield of dibromodeuterohemin was 145mg or 15% from protohemin. TLC on silica gel (BMF 110:30:1) showed as single spot as did polyamide TLC (BMF 110:30:1 and methanol : acetic acid 100:2). Table III.4 lists absorbance data for the pyridine hemochrome of dibromodeuterohemin, while Figure III.6 shows the absolute absorption spectrum of the dibromodeuterohemin pyridine hemochrome.

Table III.4

Absorbance Data for the Pyridine Hemochrome Derived from Dibromodeuterohemin.

Heme	λ_{max}(nm) ε_{mM}	Soret Band	β_{max}	α_{max}
Dibromo-deutero (a)	λ	409	513	548
	ε	117	16	26
Dibromo-deutero (b)	λ	408	517	548
	ε	116	15	24

a) Published λ_{max} and ε_{mM} values for the dibromodeutero-hemin pyridine hemochrome; (Ref. 143).

b) Experimentally determined λ_{max} and ε_{mM} values for the dibromodeuterohemin pyridine hemochrome.

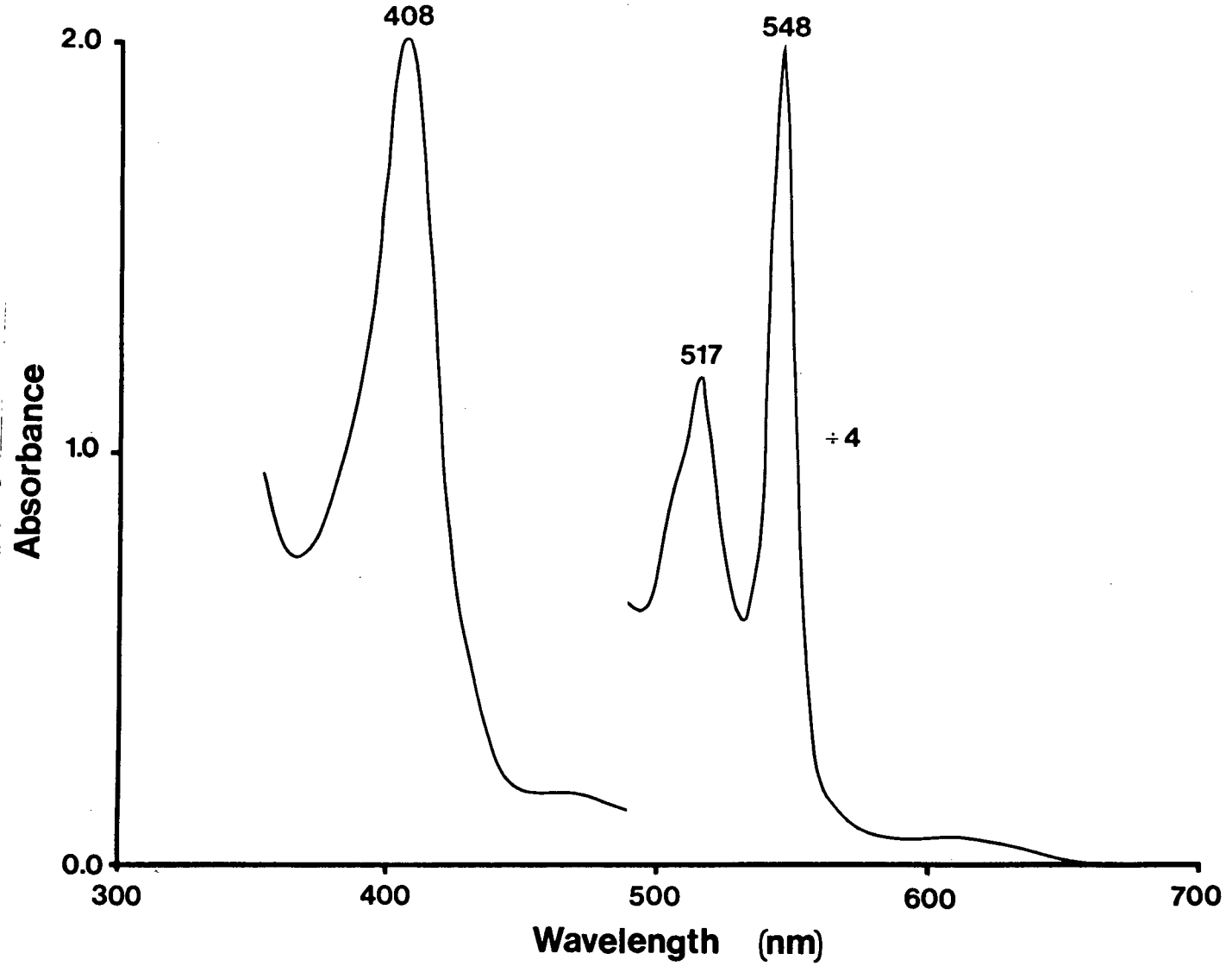


Figure III.6 Absorption spectrum of the dibromodeutero-hemin pyridine hemochrome.

III.2 Growth of *Pseudomonas putida* strain PpG 786

III.2.1 General Information

P. putida, strain PpG 786, (see Section III.2.3) was maintained and propagated using the combined methods of Gunsalus and Wagner[37] and Peterson.[33b] Sterile transfers to fresh minimal agar ensured the maintenance of a viable culture while a four-stage growth sequence ensured the most rapid large scale production of bacteria at the expense of camphor and liquid medium. The growth sequence (Section III.2.5) originated with a starter culture, progressed through two sets of 500mL shake-flask cultures, and concluded with a 14L fermentor culture. Excluding the 14L fermentors, all inoculation procedures were carried out in a laminar-flow clean air station. All shake-flask cultures were incubated at 35±1°C in a thermostated platform shaker (throw 1 7/8 inches) at a rotary speed of 200rpm. Both the laminar-flow unit and the rotary shaker were constructed in the mechanical shop of the Chemistry Department, U.B.C. The 14L cultures were grown three at a time in stirred-tank fermentors (Labroferm: New Brunswick Scientific). Within each tank the temperature was maintained at 30°C, the agitation rate at 320rpm and the aeration rate adjusted to 4.0L/min. Growth in liquid medium was measured turbidometrically on a Bausch and Lomb Spectronic 20 colorimeter at 660nm (OD660nm) using a cuvette of 1.0cm path length. Changes in pH of the medium during bacterial growth were monitored with an Instrumentation Laboratories Inc. Model 265 pH meter equipped with a glass pH electrode (Fisher).

For individual shake-flask stages, representative growth information was obtained (i.e. OD660nm and pH data) from only one of the inoculated flasks. The remaining flasks were left undisturbed. The data were then compared to a control flask containing uninoculated medium. In addition, representative growth data were obtained from one of the 14L fermentor cultures but control medium was not utilized at this stage. The turbidity data and pH profiles obtained were plotted for each stage (see Section III.2.5). The bacteria were harvested using a water-cooled, high-speed continuous centrifuge (Model LE, Carl Padberg, Schnell-Zentrifuge, Lahr/Raden) operated at 37,000rpm. Yields were expressed as wet weights of cells obtained.

III.2.2 Materials

All reagents utilized during the growth of *P. Putida* strain PpG 786, have been listed previously with the following exceptions: from American Scientific and Chemical Co., ammonium chloride, ammonium sulphate, calcium chloride, magnesium sulphate, manganese sulphate, monobasic and dibasic potassium phosphate (KH_2PO_4 and K_2HPO_4 respectively), and sodium chloride; from Difco Laboratories, Bactotryptone, Bacto yeast extract, and Bacto agar; from Dow Corning, antiform FG-10 emulsion; and from the Sigma Chemical Co., L-(+)-ascorbic acid, D-(+)-camphor, D-glucose, and L-glutamic acid.

The source and description of all equipment are provided in the text.

III.2.3 Organism

Pseudomonas putida, strain PpG 786 (ATCC 29607), obtained from Dr. I. C. Gunsalus, was the source of cytochrome P450 and related bacterial monooxygenase components (see Section II.2) in this study. This species of bacterium was derived from the parent Pseudomonad, PpG1 (ATCC 17453), isolated from soil by enrichment on D-(+)-camphor.[144]

Stock cultures were maintained at 30°C on minimal agar (see Section III.2.4.1) using D-(+)-camphor as the sole carbon and energy source, and were subcultured every two weeks.

III.2.4 Media

The media for all growth stages was prepared according to Gunsalus and Wagner[37] using singly distilled water. All solutions were sterilized at 121°C in an autoclave (American Sterilizer Co. Model AS-DIT616GE). The time required to sterilize the medium varied according to the total volume of solution per flask. For volumes of less than 200mL, sterilization was assured after 15 minutes, while volumes of 12L required a sterilization time of 45 minutes.

III.2.4.1 Minimal Agar

For the maintenance of the bacterium, a minimal agar containing minerals and a single carbon source was utilized. The medium required the following ingredients:

K_2HPO_4	7.0g
KH_2PO_4	2.0g
NaCl	0.12g
$MgSO_4 \cdot 7H_2O$	0.1g
$(NH_4)_2SO_4$	1.0g
Camphor	1.3g
Bacto agar	15g
Water	1.0L

Individual solutions containing the minerals, the carbon source, and the agar were prepared in separate 500mL Erlenmeyer flasks to a collective volume of 500mL. Poured and solidified medium was wrapped tightly in Saran Wrap and stored at 5°C. A single batch of minimal agar plates (20-30) was consumed every 3-4 months and contamination during the storage period was never observed.

III.2.4.2 Starter Media

For the starter cultures in which rapidly growing inocula were desired, a rich undefined medium of L-broth[145] was used. The L-broth contained the following ingredients:

Bactotryptone	10g
Bacto Yeast Extract	5.0g
NaCl	5.0g
Glucose	1.0g
Water	1.0L

The pH required adjustment to 7.0 with 1M NaOH. Eighty millilitres of L-broth was divided between four 50mL Erlenmeyer flasks (see Section III.2.5).

III.2.4.3 Large Scale Media

For the large scale production of the bacterium, a mineral salts medium was employed. The basal medium was prepared from a defined phosphate-ammonium (PA) solution containing the following ingredients:

K_2HPO_4	10.7g
KH_2PO_4	3.1g
NH_4Cl	4.0g
Water	1.0L

Essential mineral salts were added as a 100-fold concentrated stock solution (100 x Salts) containing the following ingredients:

$MgSO_4 \cdot 7H_2O$	19.5g
$MnSO_4 \cdot H_2O$	5.0g
$FeSO_4 \cdot 7H_2O$	5.0g
$CaCl_2 \cdot 2H_2O$	0.3g
Ascorbic acid	1.0g
Water	1.0L

The basal medium was supplemented with various carbon sources, antifoaming agent, and Bacto yeast extract, when applicable, during the growth sequence (see Section III.2.5). Camphor, the major carbon and energy source, was added as a finely ground solid or a liquid stock solution of 3M D- (+)-camphor in DMF. The various supplements were added to the basal PA solution before undergoing sterilization in the autoclave.

The pH of the freshly prepared medium ranged from 7.0-7.2.

III.2.5 Growth Procedure

The starter culture was prepared from 60mL (divided between three 50mL Erlenmeyer flasks) of L-broth medium inoculated with *P. Putida* and incubated for a 10h period with shaking. Growth in the starter medium was checked against 20mL of uninoculated L-broth. OD660nm and pH profiles for the L-broth cultures are shown in Figure III.7. The bacteria were visible as small billowy clouds in the media upon gentle swirling of the flasks. Subsequent to the 10h incubation period, the resulting late-logarithmic growth phase culture (OD660nm = 1.5±0.2) provided inocula for the first set of five 500mL shake-flasks. Four of the five 500mL Erlenmeyer flasks, containing 200mL of PA solution, 2mL of 100 x Salts solution and 10mM glutamic acid (the carbon source), were inoculated with 5.0mL of L-broth culture and incubated with continuous shaking. Initial growth reached mid-logarithmic growth phase in 2.0h (OD660nm = 0.4±0.1; see Figure III.8). Induction of cytochrome P450cam and related bacterial monooxygenase components was initiated at this point by the addition of 3M camphor in DMF to each flask. The final camphor concentration was adjusted to 5mM. After an OD660nm = 0.7±0.1 (≈4h) was obtained, stock camphor solution was again added to a final concentration of 5mM. The initial growth phase reached a maximum in ≈6h (OD660nm = 1.0±0.1) and was followed by a period of rapidly declining optical density of the medium (see Figure III.8). The

cultures were maintained through this lag period (≈6-12h) into a secondary growth phase in which camphor was actively metabolized. Growth was then continued until late-logarithmic growth phase was reached (≈25h). A 10mL aliquot of the late-logarithmic growth phase cells served as an inoculum for the second set of five 500mL shake-flasks. The flasks contained the same basal medium utilized in the previous shake-flasks but solid camphor was added as the only carbon source in place of the glutamic acid. All media were saturated with camphor to a final concentration of ≈8mM. Growth characteristics for this stage are represented in Figure III.9. At late-logarithmic growth phase (≈15h, OD660nm = 0.8±0.2) the shake-flask contents were added to the 14L fermentor jars containing 12L of PA solution, 120mL of 100 x Salts solution, 30mL of 10% (w/v) Bacto yeast extract, 2mL of antifoam and 15g of solid camphor (≈8mM). Once mid-logarithmic growth phase was attained in the 14L fermentors (≈7.0h, OD660nm = 0.4±0.1) the medium was kept saturated with camphor. Figure III.10 represents growth behavior during bacterial propagation at this stage. The camphor carbon source was added in both liquid (3M camphor in DMF) and solid form at a rate of 5g/h and incubation was maintained with vigourous aeration and agitation (see Section III.2.1). The total quantity of cells accumulated in the medium was estimated from the weight of bacteria collected in 40mL of culture using a Sorvall RC-2 refrigerated centrifuge equipped with an SS-34 rotor head. At late-logarithmic growth

phase (≈25±2h, OD660nm = 1.2±0.1) the maximal quantity of bacteria in solution was 150g per 36L of culture. Approximately 80% of the cells were removed by continuous centrifugation at a flow-rate of 1L/min. The medium was recycled with the addition of excess camphor to pH 6.0, below which no viable bacteria were obtained. Bacteria could be grown in the same medium for 72h and could be harvested 3-4 times without problems of contamination. This growth procedure yielded approximately 110g of bacteria per 10L of medium and an overall yield of 400g per growth cycle. Approximately 1.7g of camphor was consumed per gram of bacteria obtained. The pink cell pastes were stored in dry ice (-78^{o}C).

The pH of all media containing rapidly growing cultures decreased during active camphor metabolism but increased during the metabolism of other carbon sources, such as glucose and glutamic acid (see Figures III.7 - III.10).

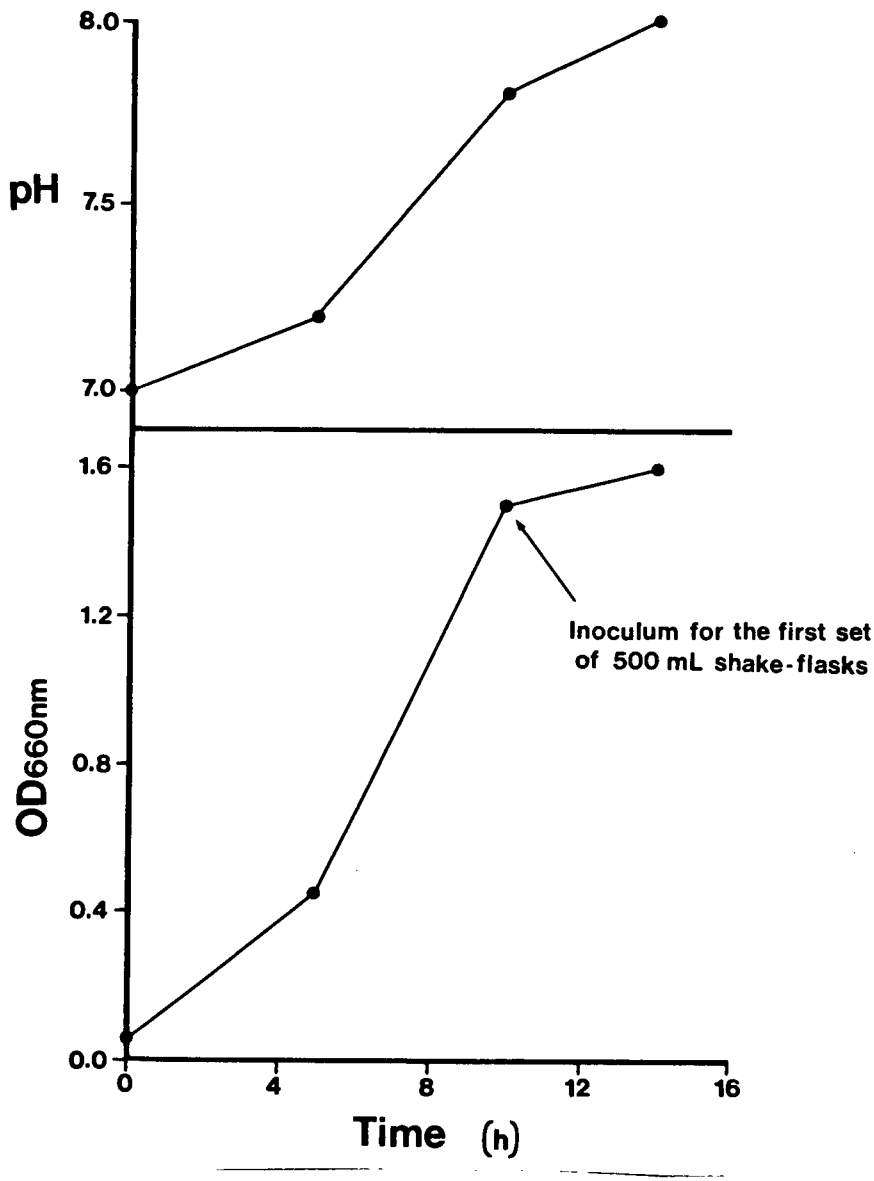


Figure III.7 OD660nm and pH profiles for bacterial growth in the L-broth medium.

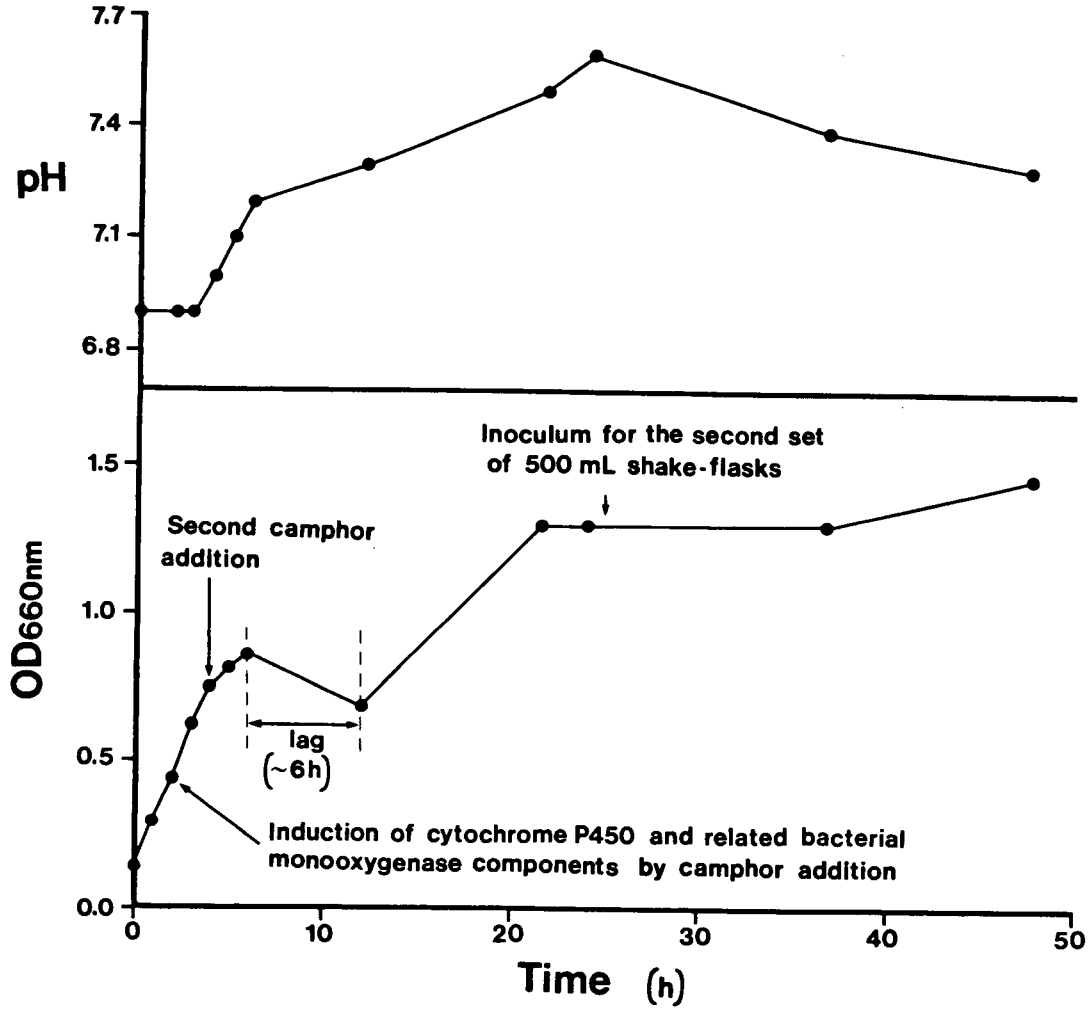


Figure III.8 OD660nm and pH profiles for bacterial growth in the first set of 500mL shake-flask media.

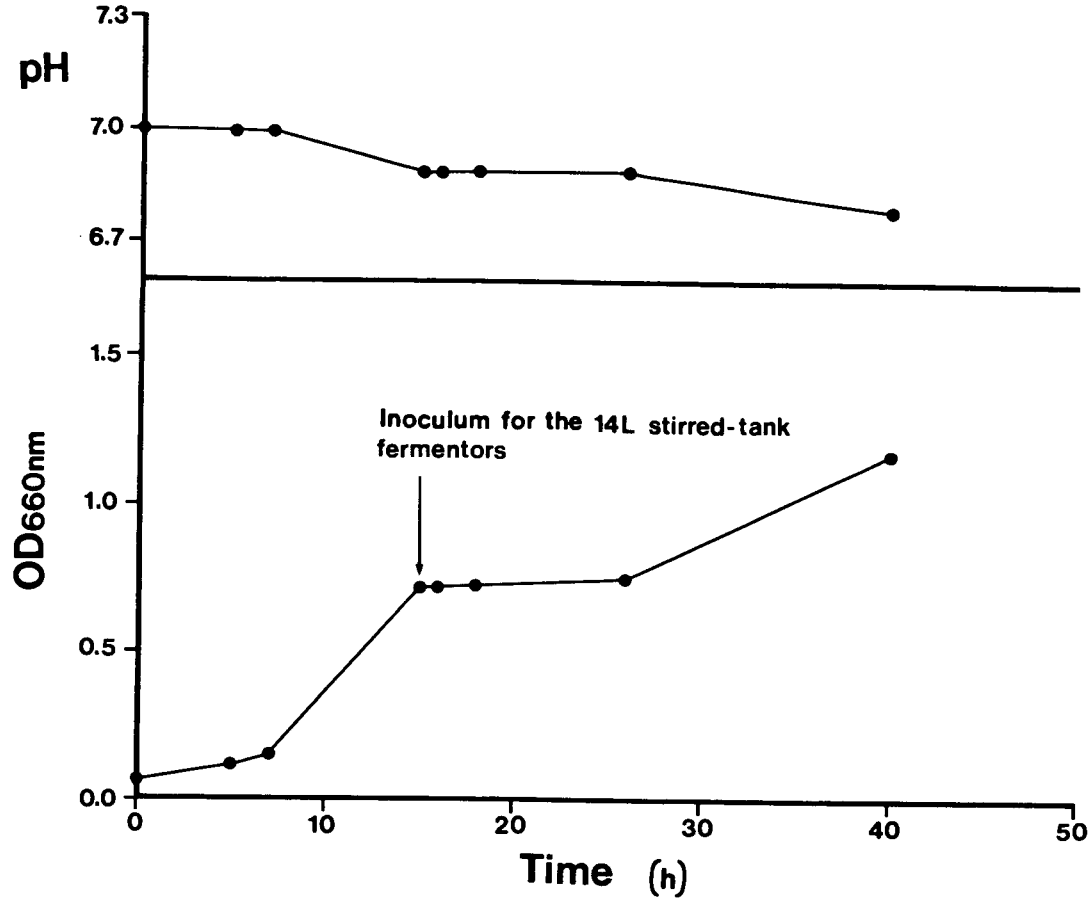


Figure III.9 OD660nm and pH profiles for bacterial growth in the second set of 500mL shake-flask media.

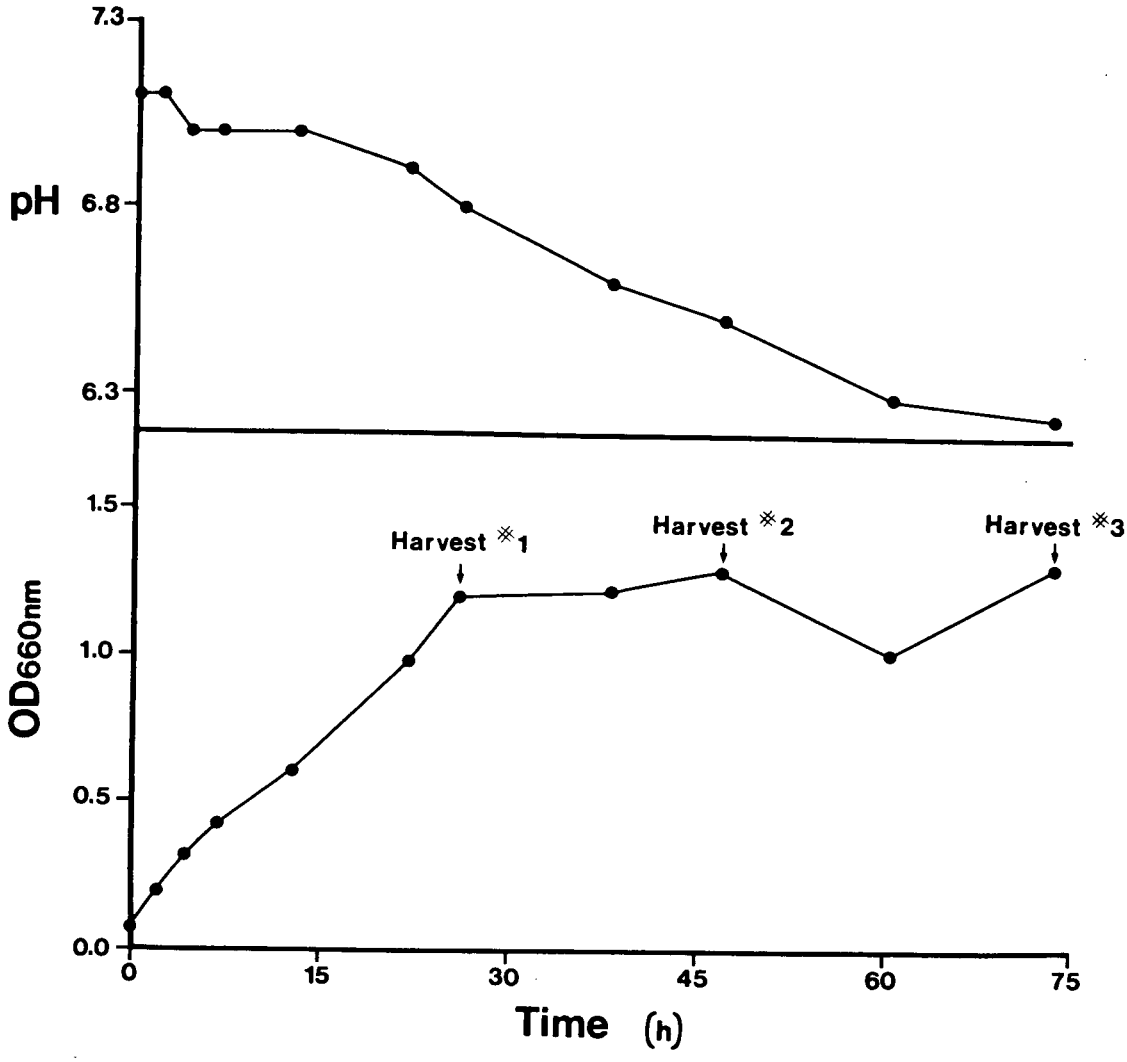


Figure III.10 OD660nm and pH profiles for bacterial growth in the 14L fermentor media.

III.3 Isolation and Purification of Cytochrome P450cam and Related Bacterial Monooxygenase Components

III.3.1 General Information

Cytochrome P450cam and related bacterial monooxygenase components (putidaredoxin and putidaredoxin reductase; see Section II.2) were extracted and purified from cells of *P. Putida*, strain PpG 786, by the methods of Gunsalus and Wagner,[37] and Peterson[33b] with slight modifications. An adapted procedure was developed to maximize the purity and not the yield of each protein component. A flow chart of the experimental design based on 400g of bacterial cell paste as obtained above is presented in Figure III.11.

III.3.1.1 Materials

Reagents were obtained as follows: from American Scientific and Chemical Co., glycerol and potassium chloride (KCl), from the Shwartz-Mann Chemical Co., enzyme grade ammonium sulphate ($(NH_4)_2SO_4$); and from the Sigma Chemical Co., β-mercaptoethanol (βME), deoxyribonuclease I (DNase) isolated from bovine pancreas, dithiothrietol (DTT), ribonuclease-A (RNase) isolated from bovine pancreas and tris(hydroxymethyl)aminomethane free base (Trizma Base). Chemicals not mentioned above were listed previously.

C.P. grade carbon monoxide (CO) was obtained from the Matheson Gas Co. Trace oxygen was removed as indicated previously for argon (see Section III.1.2) followed by drying through phosphorus pentoxide and Indicating Drierite. Carbon dioxide was removed with soda lime (Fisher). Complete removal

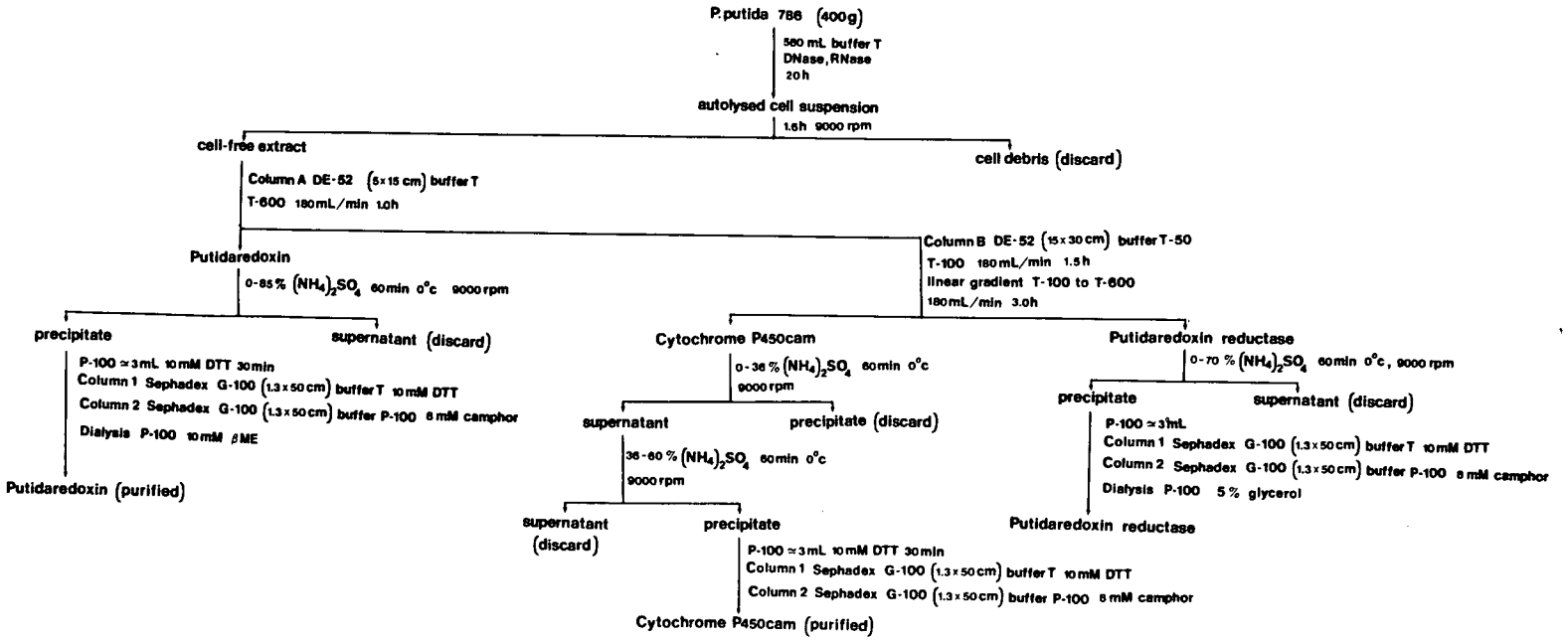


Figure III.11 Flow chart for the isolation and purifacation of cytochrome P450cam and related bacterial monooxygenase components from *P putida*, strain PpG786. Consult text for details.

of trace impurities was checked with mass spectrometry by Dr. G. Eigendorf of the Chemistry Department, U.B.C.

Seamless cellulose dialysis tubing with a 12,000 molecular weight cut-off was obtained from Fisher Scientific Co.

Plastipak disposable syringes (from 1.0 - 50mL sizes) were obtained from Becton, Dickinson and Co.

III.3.1.2 Buffers

The buffer solutions used during the isolation and purification procedures were prepared from singly distilled water, prefiltered with a Gelman filtration apparatus equipped with a 45μm Metricel membrane (Gelman Sciences Inc.) and deaerated by aspiration. All buffers were prepared at room temperature (23±2°C) and used immediately.

Tris(hydroxymethyl)aminomethane (Tris) buffers were prepared from a 1.0M stock solution of tris(hydroxymethyl)-aminomethane free base (Trizma Base), diluted to obtain a 50mM basal solution and carefully adjusted to pH 7.3 with 6M HCl. The following Tris buffers and simplified nomenclature[37] were used during the isolation and purification procedures: buffer T = 50mM Tris buffer, pH 7.3; the addition of 50, 100 and 600mM kCl were specified as buffers T-50, T-100 and T-600 respectively. All Tris buffers were made 10mM in βME prior to use unless noted otherwise. Other supplements included the addition of 10mM DTT and 5% (v/v) glycerol as required.

Potassium phosphate buffers were prepared by mixing equal volumes of 1.0M K_2HPO_4 and 1.0M KH_2PO_4 stock solutions

to obtain a 50mM basal solution of pH 7.0: buffer P = 50mM kCl was specified as buffer P-100 indicating the 100mM potassium ion concentration. Camphor was added as a solid to appropriate buffers to saturation levels (≈8mM), stirred overnight and filtered prior to use. Other supplements included the addition of 10mM βME and 5% (v/v) glycerol as required.

Approximate volumes of buffer solutions utilized throughout the isolation and purification procedure based on 400g of bacterial cell paste (as obtained above) are given in Table III.5; the approximate quantities of reagents follow in Table III.6.

III.3.1.3 Column Chromatography

In order to obtain uncontaminated and highly purified protein components, strict adherence to precision in the preparation of chromatographic resins and operation of the chromatography columns was essential. The Whatman DE-52 preswollen cellulose anion exchange (DE-52) and Sephadex G-100 resins (obtained directly from North American Scientific and Sigma Chemical Co. respectively) were prepared according to the manufacturer's recommendation. Chromatography columns and column ends for DE-52 anion exchange chromatography were obtained commercially from BioRad Laboratories (Model Bio-Rex). The columns for Sephadex G-100 chromatography were constructed from cast acrylic (Cadillac Plastics) in the mechanical shop of the Chemistry Department, U.B.C. (Figure III.12). The commercially obtained column ends were fitted with porous

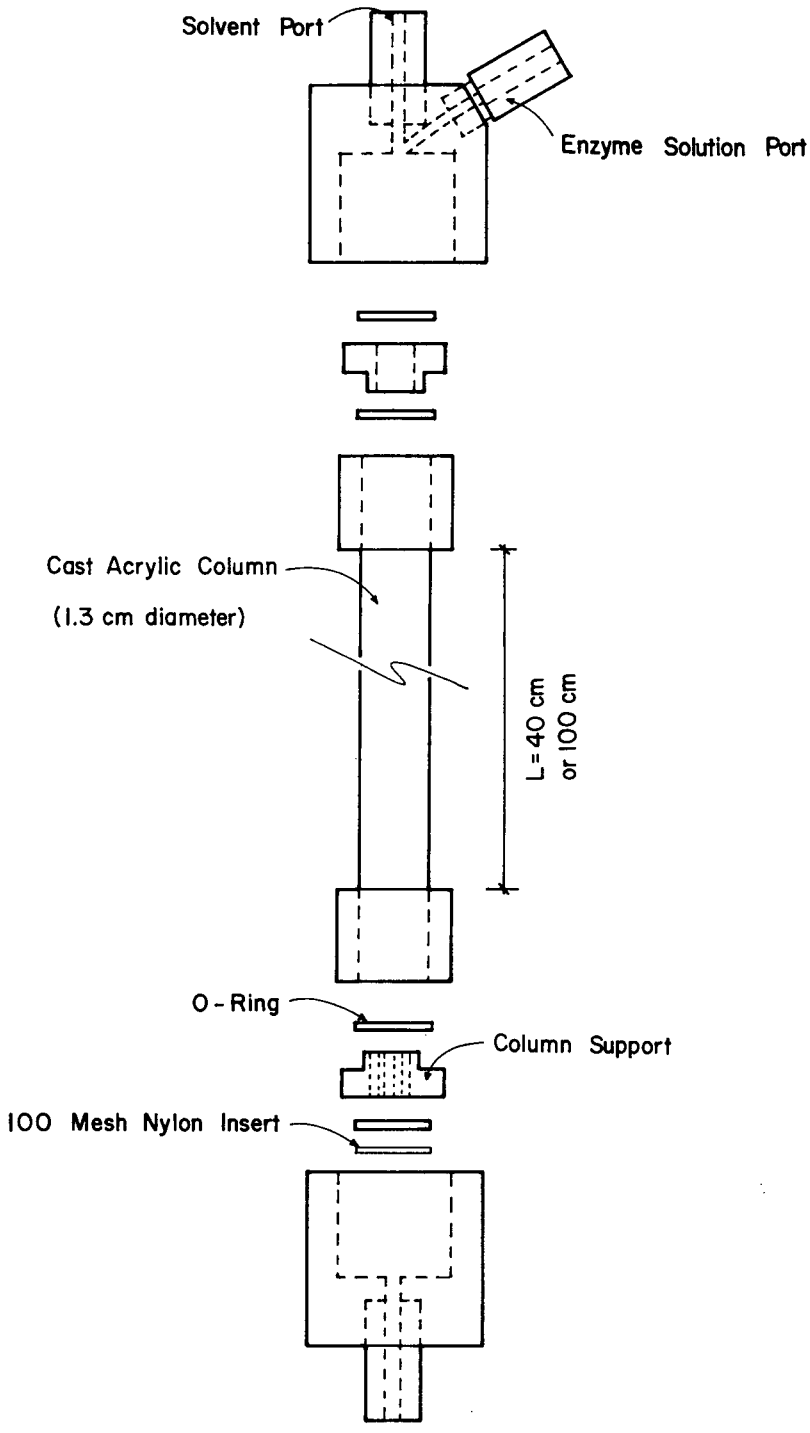


Figure III.12 A schematic diagram of the Sephadex G-100 columns.

Table III.5

Volumes of Buffers utilized during Protein Isolation and Purification

Step	Buffer Volumes
Cell-Free Extract	0.6L buffer T
DE-52 Chromatography	
a) Column A equilibration	4.0L buffer T, 10mM βME
b) Column B equilibration	4.0L buffer T-50, 10mM βME
c) Separation of protein components including linear salt gradient	4.0L buffer T-100, 10mM βME 4.0L buffer T-600, 10mM βME
Sephadex G-100 Chromatography	
a) Column 1 equilibration and elution	2.0L buffer T-100, 10mM DTT
b) Column 2 equilibration and elution	2.0L buffer P-100, 8mM camphor
Dialysis	
a) putidaredoxin reductase	2.0L buffer P, 5% (v/v) glycerol
b) putidaredoxin	2.0L buffer P, 10mM βME

Table III.6

Quantities of Reagents for Protein Isolation and Purification

Reagents	Quantities
Trizma Base, 1M	850mL
KH_2PO_4, 1M	60mL
K_2HPO_4, 1M	60mL
KCl	250g
$(NH_4)_2SO_4$	450g
NH_4OH, 14.8M	15mL
Glycerol	20mL
βME	15mL
DTT	0.4g
D-(+)-camphor	5.0g
DNase	1.0mg
RNase	1.0mg

polyethylene and 100 mesh nylon inserts while the constructed columns utilized only the 100 mesh nylon inserts. Columns were operated in the descending flow mode with constant-flow rates achieved using a Polystaltic Pump from Büchler Instruments or using gravity feed. Smaller diameter Tygon plastic (1/16 x 1/8 x 1/32 inches) or Intramedic polyethylene (0.045 x 0.062 inches) tubing were used for the transport of solution. Chromatography elution patterns were monitored visually and collected with a LkB Bromma, 7000 Ultrarac Fraction Collector. Concentration and centrifugation of protein solutions was achieved in an Amicon Ultrafiltration apparatus fitted with a YM-10 Diaflo Ultrafiltration membrane (>10,000 molecular weight cut-off), and in a Servall RC-2 refrigerated centrifuge equipped with a GSA or SS-34 rotor respectively.

Separation of the protein components on the DE-52 anion exchange columns (see Section III.3.2.2) was enhanced by gradually increasing the kCl concentration (i.e. ionic strength) of the eluting buffer from T-100 to T-600. This linear salt gradient was accomplished by the continuous addition of buffer T-600 to the buffer T-100 reservoir with vigorous stirring. Simultaneous with the addition of buffer T-600 was the continuous removal, *via* two exit tubes, of the buffer T-100 - T-600 mixture as both column elutent and waste buffer. Since the rate of removal of the buffer mixture was twice that of the addition rate of buffer T-600 a gradual increase in the ionic strength of the buffer was ensured.

III.3.2 Isolation of Cytochrome P450cam and Related Bacterial Monooxygenase Components

III.3.2.1 Cell-Free Extract

A single batch of cell paste (400g) frozen at dry ice temperatures for at least 10 days was thawed, combined with 280mL of buffer T,and homogenized using a variable speed electric mixer. The viscous pink suspension was stirred at 5°C for 8h. One mg each of DNase and RNase were added to the solution and stirring was continued at 5°C overnight (12h). A further 280mL of buffer T was then added and the solution thoroughly mixed. The cell suspension was centrifuged at 9,000rpm for 10 min to remove unlysed cells and cell debris, and then centrifuged at the same speed for another 1.5h to remove the cell membrane fraction. The resultant reddish-brown supernatant solution containing the three monooxygenase components was kept on ice at all times.

III.3.2.2 Isolation Procedure

All procedures were performed at 5°C unless otherwise specified. Constant-flow rates were maintained with a peristaltic pump (see Section III.3.1.3).

The cell-free extract derived from 400g of cell paste was applied at a flow rate of 180mL/h to DE-52 cellulose anion exchange column A (150g; 5 x 15cm), previously equilibrated with buffer T (see Table III.5 for volume of buffer T required for equilibration of Column A). During

application of the cell-free extract the effluent was discarded. Column A was washed with buffer T-100 at 180mL/h for 1.0h to promote the separation of the protein components. During this time the effluent was again discarded. Further effluent from Column A was applied to a second DE-52 cellulose anion exchange column, B, (300g; 5 x 30cm) equilibrated with buffer T-50 (see Table III.5 for volume of buffer T-50 required for equilibration of Column B). The DE-52 columns were washed continually with buffer T-100 at 180mL/min until ≈two-thirds of the red cytochrome band passed onto Column B (≈1.5h), leaving behind the trailing yellow putidaredoxin reductase and the brown putidaredoxin bands. A linear salt gradient with buffer T-100 to T-600 (see Section III.3.1.3) was then established at a flow rate of 180mL/min over a 3.0h period to allow for the elution and separation of the red cytochrome P450cam and yellow putidaredoxin reductase on Column B. Column A, containing the narrow dark brown putidaredoxin band, was disconnected at this point and the linear salt gradient was continued for the elution of Column B. The cytochrome P450cam and putidaredoxin reductase proteins were eluted over a period of 3.5h as separate highly visible bands. The putidaredoxin protein was then eluted from Column A with buffer T-600 over a 1.0h period. The protein effluent from each column was cooled through 6m of coiled polyethylene tubing at $0^{o}C$ and kept on ice at all times. Solutions of cytochrome P450cam and putidaredoxin were made 10mM in βME

while solutions of putidaredoxin reductase were made 5% (v/v) glycerol immediately after collection. Each protein fraction was precipitated and purified directly (see below).

III.3.2.3 Ammonium Salt Fractionation

All protein components were precipitated at 0°C with the addition of enzyme grade $(NH_4)_2SO_4$ according to the following procedure. The approximate requirements for precipitation of each protein component are provided in Table III.7.

Crystalline ammonium sulphate was added to the combined fractions of each protein with constant stirring over a 30 min period. For each 30g of ammonium sulphate added, 1.0mL of 14.8M NH_4OH was added for neutralization. The mixture was stirred for an additional 30 min and the precipitate collected by centrifugation. The supernatant, which often contained yellow flavin, was discarded. The protein pellets were resuspended in minimal buffer P-100 (≈3mL) and purified directly (see below). For precipitation of cytochrome P450cam an initial step was invoked to remove apo-cytochrome P450cam (see Table III.7). The protein contaminant was collected as a white solid and discarded.

Table III.7

Saturation Levels and Quantities of $(NH_4)_2SO_4$ required for the Precipitation of Cytochrome P450cam and Related Protein Components

Protein	$(NH_4)_2SO_4$ Saturation Level	$(NH_4)_2SO_4$ (g/L)
Putidaredoxin reductase	70%	500
Putidaredoxin	85%	560
Apo-cytochrome P450cam	36%	200
Cytochrome P450cam	60%	140

III.3.3 Purification of Cytochrome P450cam and Related Bacterial Monooxygenase Components

III.3.3.1 Purification Procedure

All procedures were performed at 5°C unless specified otherwise. Constant flow rates were maintained by gravity feed at not more than 250mm head pressure.

The protein solutions obtained from the ammonium salt fractionation procedure (see Section III.3.2.3) were centrifuged at 9,000rpm and concentrated to 1.0-2.0mL by ultrafiltration. The concentrates of putidaredoxin and cytochrome P450cam were made 50mM in DTT and incubated anaerobically for 30 min at room temperature (23±2°C) before purification.

Protein solutions were chromatographed on a sequence of two Sephadex G-100 columns (1.3 x 50cm) equilibrated with buffer T-100 made 10mM in DTT and P-100 made 8mM in camphor respectively; these are specified as Column 1 and Column 2. To avoid overloading of columns and to ensure maximum purification, each protein concentrate was chromatographed in two portions. Fractions were selected and purified further, on the basis of color density. About 70% of fractions from Column 1 were pooled, concentrated and re-chromatographed on Column 2. In each case, the purest protein was confined to the middle 30-40% of the fractions collected from Column 2. These fractions were then pooled and concentrated to 1.0-2.0mL aliquots. Putidaredoxin reductase and putidaredoxin were further dialysed for an

8h period against two changes of buffer P (2 x 1.0L) made 5% (v/v) in glycerol and 10mM in βME respectively. Putidaredoxin was dialysed under an argon atmosphere. All purified protein concentrates (stock solutions) were subjected to spectral analysis (see below) and stored in 3.0mL disposable plastic syringes at -78°C. Table III.8 summarizes the yields each protein component obtained from the isolation and purification procedure described above. Yields are calculated from the millimolar concentration of each protein in the stock solutions as determined by direct spectrophotometric measurement (see Section III.3.4), assuming protein molecular weights for putidaredoxin reductase, putidaredoxin and cytochrome P450cam of 47,000, 15,000 and 45,000 respectively.[30,37] Yields are quoted as mg of protein per 400g of bacterial cell paste.

Table III.8

Yields of Cytochrome P450cam and Related Protein Components

Protein	Yield (mg/400g cell paste)
Putidaredoxin reductase	none [a]
Putidaredoxin	91
Cytochrome P450cam	136

a) See Results and Discussion, Section IV.2.

III.3.4 Spectral Analysis of Cytochrome P450cam and Related Bacterial Monooxygenase Components

Generally, all liquids and solutions were handled under an argon atmosphere using Schlenk techniques.[146]

The electronic absorption spectrum of the prosthetic group of the holoprotein was the most convenient method of determining the concentration and purity of each of the purified stock protein solutions. The electronic spectra of putidaredoxin reductase and putidaredoxin in their oxidized and reduced states, and cytochrome P450cam (substrate-bound and substrate-free, and ferrous-CO) forms were recorded at room temperature ($23\pm2^{o}C$) from 700 to 250nm on a Cary spectrophotometer, model 17D. All spectroscopic measurements were carried out in the cell-tonometer shown in Figure III.13 against a reference cell containing only buffer. The cell-tonometer consisted of a clear quartz square cell (1 x 1 x 5cm), attached through 20cm of glass tubing to a sidearm reservoir fitted with a B-14 glass joint. A high vacuum O-ring joint (Kontes Glass Co.) with a B-14 sidearm socket were utilized for attachment to the vacuum/gas handling line. Total volume of the apparatus was 60mL. The reference cell was constructed from the same quartz cell but was attached through 5cm of glass tubing to a silicon rubber septum fitting and a high vacuum O-ring joint. The cell arrangements were made in the glass blowing shop of the Cheminstry Department, U.B.C.

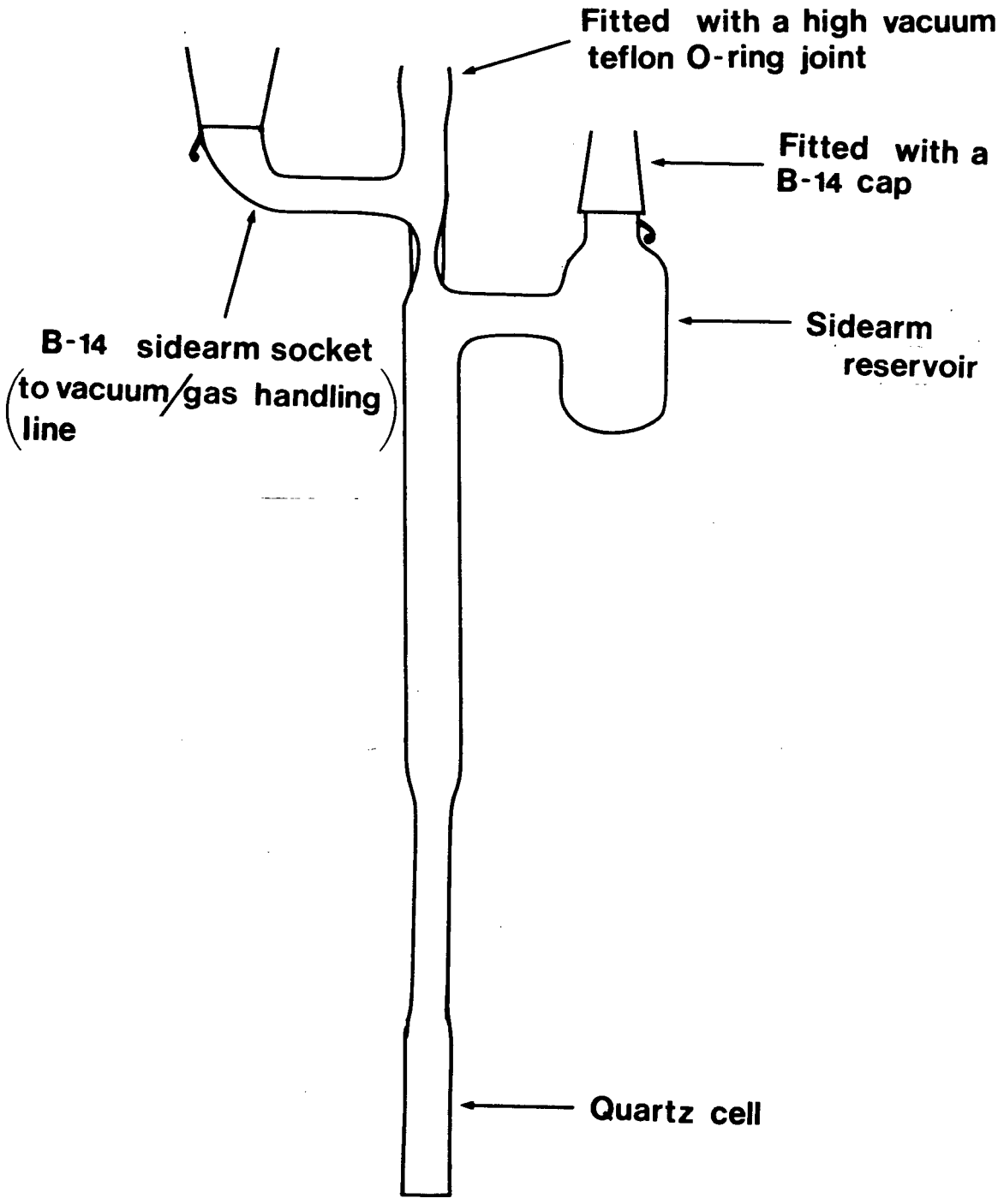


Figure III.13 The cell-tonometer

Preparation of the protein solutions for spectral observations involved 20-100 fold dilution of the stock samples in buffer P-100 (containing ≃8mM camphor for cytochrome P450cam solutions). Buffer (≃4.8mL) was dispensed into the tonometer reservoir and degassed by repeated evacuation and flushing with argon. A baseline spectrum was then obtained against the reference cell containing degassed buffer P-100. Stock protein solution (≃0.2mL) was then added to a final volume of 5.0mL (≃1 x 10^{-5}M protein; see Section III.5.3.3) and the spectrum of the oxidized state of each protein was obtained. The solution was transferred by tilting the liquid into the cell cavity from the reservoir. Reduction of ferric cytochrome P450cam to the ferrous state was achieved with sodium dithionite dissolved in deoxygenated buffer P-100 (≃4mg/mL, ≃1 x 10^{-2}M). Cytochrome solutions were stoichiometrically reduced by monitoring the dithionite absorption band at 314nm. An absorption maximum in the cytochrome spectrum at this wavelength indicated excess dithionite, and hence completion of the reduction process. The ferrous-CO complex of cytochrome P450cam was formed by gently bubbling carbon monoxide through the reduced cytochrome samples.

III.3.4.1 Concentration Determinations

The millimolar concentrations of the purified protein components were determined by direct spectoscopic measurement using published millimolar extinction coefficient data;[37,144]

for oxidized putidaredoxin reductase, λ_{max} 454, ε_{mM} = 10.0; for oxidized putidaredoxin, λ_{max} 455nm, ε_{mM} = 10.4; and for the ferrous-CO complex of cytochrome P450cam, λ_{max} 446nm, ε_{mM} = 120.

III.3.4.2 Purity Assay

The purity of the three monoxygenase components was determined based on the absorption ratio of prosthetic group to total protein in the oxidized state of each protein. These values were compared with homogeneous preparations reported in the literature; for native putidaredoxin reductase an A454/A275 absorption ratio of 0.14 was observed with samples estimated by sodium dodecyl sulphate (SDS) gel electrophoresis to be greater than 80% homogeneous.[144] Similarly, native putidaredoxin greater than 98% homogeneous in total protein mobility exhibited an A455/A275 optical absorption ratio of 0.44.[37] Finally, substrate cytochrome P450cam greater than 95% homogeneous by SDS gel electrophoresis was characterized by an A391/A280 absorption ratio of 1.45.[144]

III.4 Preparation of Reconstituted Cytochrome P450cam

III.4.1 General Information

The preparation of reconstituted cytochrome P450cam in this study involved the extraction of the heme prosthetic group from the native or parent enzyme followed by addition of protohemin chloride to the apoprotein to regenerate the enzyme. The method to be described can be used to reconstitute native cytochrome P450cam with any of the substituted hemins synthesized in Section III.1.

The heme group was removed from native cytochrome P450cam isolated and purified as in Section III.3 using acidified acetone at $-20^{o}C$ to give the apoprotein in a reconstitutable form with the procedure of Strittmatter[147] as adopted by Yu and Gunsalus.[148] Apocytochrome P450cam was reconstituted with protohemin chloride according to the method of Yu and Gunsalus.[148] All procedures were performed in an argon atmosphere.

III.4.1.1 Materials

All reagents utilized during the reconstitution experiments have been listed previously with the following exceptions: from Fisher Scientific Co., 2-butanone, disodiumethylenediaminetetraacetate ($Na_2(H_2EDTA)$), ethanol and sodium bicarbonate; and from the Sigma Chemical Co.,cysteine (free base) and horse heart myoglobin (salt-free lyophilized powder).

All solvents were used directly without further purification.

III.4.2 Extraction of the Heme Group from Native Cytochrome P450cam

III.4.2.1 Extraction Procedure

Acetone (2.5mL per mg of enzyme) was acidified by adding 0.1mL of concentrated HCl per 50mL of acetone and the mixture cooled to -20°C in a dry ice-30% ethanol slush bath. The solution was allowed to equilibrate with stirring, and then 1.0-2.0mL of enzyme solution (buffer P-100, 8mM camphor, $\simeq 10^{-3}$M cytochrome) was added dropwise with constant stirring. The solution was stirred for 10 min and the white protein precipitate was collected at 9,000rpm in a refrigerated centrifuge equilibrated to -20°C. The pink supernatant, containing extracted heme, was removed for analysis (see Section III.4.2.2) and the white protein pellet was immediately dissolved in deoxygenated 0.06M kOH ($\simeq$20mL) made 20% (v/v) in glycerol and equilibrated to 0°C in an ice-water bath. The apoprotein solution was dialysed at 5°C against deoxygenated water (1.0L) for 6h and then in deoxygenated buffer P-100 for 12h. A steady flow of argon, passed through a fine sintered glass frit, was used to displace oxygen from solution during the dialysis. The dialysate was centrifuged to remove any denatured protein that had precipitated and concentrated by ultrafiltration to 1.0-2.0mL. The apoprotein was kept on ice at all times and used immediately to prepare the protohemin-reconstituted cytochrome. The millimolar concentration of apocytochrome P450cam was determined based on its absorbance

at 280nm using millimolar extinction coefficient data determined in the present work;[149] ε_{mM} = 91.1, see Section IV.2.3. Residual absorption in the Soret region (≈400nm) of the apoprotein spectrum, indicative of intact cytochrome P450cam, was removed by repeating the extraction procedure. The yield of apocytochrome P450cam was estimated as up to 80% from native P450cam.

III.4.2.2 Analysis of the Heme Prosthetic Group

The pink acid-acetone supernatant solution obtained from the heme extraction procedure was evaporated under reduced pressure in an aluminum foil-wrapped flask to yield a black residue. The residue was dissolved in 1.0mL of pyridine and subjected to analysis by TLC on silica gel and polyamide, and by spectral observation of the pyridine hemochrome complex. Chromatograms were developed with BMF (110:30:1) and methanol-acetic acid (100:2) solvent systems and the hemochrome complex was prepared and analysed as described in Section III.1.3. TLC on silica gel (BMF 110:30:1) showed a single spot as did polyamide TLC (BMF 110:30:1) and methanol-acetic acid (100:2). Table III.9 lists absorption data for the pyridine hemochrome of the extracted heme along with analogous data obtained from the literature. The amount of heme removed from the native cytochrome was determined based on the heme absorbance at 557nm (ε_{mM} = 34.4).[136a] For comparison, this value was checked against the concentration of starting enzyme. The values agreed within 20%.

Table III.9

Absorbance Data for the Pyridine Hemochrome Derived from Extracted Heme.

Heme	λ_{max}(nm) ε_{mM}	Soret	β_{max}	α_{max}
Extracted	λ	418	524	556
	ε	181	20	32
Proto- [a]	λ	418	524	557
	ε	191.4	17.5	34.4

a) Published literature data; (Ref.136a).

III.4.3 Reconstitution of Apocytochrome P450cam

III.4.3.1 Reconstitution Procedure

The apoprotein was converted to the biologically inactive P420 form by the addition of a stock solution of protohemin chloride. This stock solution was made up in a 10mL volumetric flask by dissolving ≈2.0mg of hemin chloride in 0.5mL of deoxygenated 0.06M KOH containing 4% methanol, the volume being brought to 10mL with deoxygenated buffer P-100. Fresh stock hemin solutions were prepared before each reconstitution experiment to avoid degradation or aggregation of the hemin on standing.[148]

Using a 50mL pear-shaped flask, the hemin solution was added dropwise, with gentle swirling, at a hemin-replaced to heme-removed ratio of 1.1; 10% more hemin was added to the apocytochrome than was removed from the native enzyme. The amount of heme removed from the native cytochrome was calculated from both the parent enzyme (see Section III.3.4.1) and the pyridine hemochrome spectrum (see Section III.4.2.2). Treatment of the reconstituted P420 solution with an equal volume of buffer P-100 containing camphor (8mM), cysteine (100mg/mL) and glycerol (40%(v/v)) converted the P420 forms to the P450 form as determined by Soret absorption maxima of the reduced-CO complex. Equal volumes of the buffer P-100 (camphor)-cysteine solution (≈5mL) were added twice, at two hour intervals, during the 6h incubation period at room

temperature (23±2°C). Following spectral analysis of the crude reconstituted enzyme solution (Section III.3.4), each sample was cooled to 0°C in ice and purified immediately.

III.4.4 Purification of Reconstituted Cytochrome P450cam

III.4.4.1 DE-52 Anion Exchange Chromatography

The reconstituted cytochrome solution (Section III.4.3.1) (≈15mL) was centrifuged at 9,000rpm for 5 min and the supernatant solution absorbed, at 5°C, onto a DE-52 cellulose anion exchange column (2 x 8cm), equilibrated with 3mM phosphate buffer, pH 7.0, made 8mM in camphor. Flow rates were maintained by gravity feed and the DE-52 column was constructed from a 50mL Plastipak disposable syringe as shown in Figure III.14. After absorption, the column was washed with at least 5 bed volumes of equilibrating buffer (≈250mL) to remove excess cysteine reagent as well as glycerol. The eluent was then changed to buffer P-100 made 8mM in camphor and the protein (red band), which immediately moved down the column, was collected. The enzyme solution was concentrated by ultrafiltration to 1.0-2.0mL and subjected to spectral analysis (see Section III.3.4). Samples exhibiting an absorbance at 420nm in the reduced-CO spectrum were subjected to a second procedure designed to remove this impurity (see below).

III.4.4.2 Removal of P420 Impurities

The use of excess hemin chloride during the reconstitution procedure promoted impurity formation in the form of "non-specifically" bound or "non-regenerated" heme. The impurity was manifested as an absorption at 420nm in the reduced-CO spectrum of the crude reconstituted enzyme.[133a] Pure samples of the reconstituted cytochrome required for spectroscopic

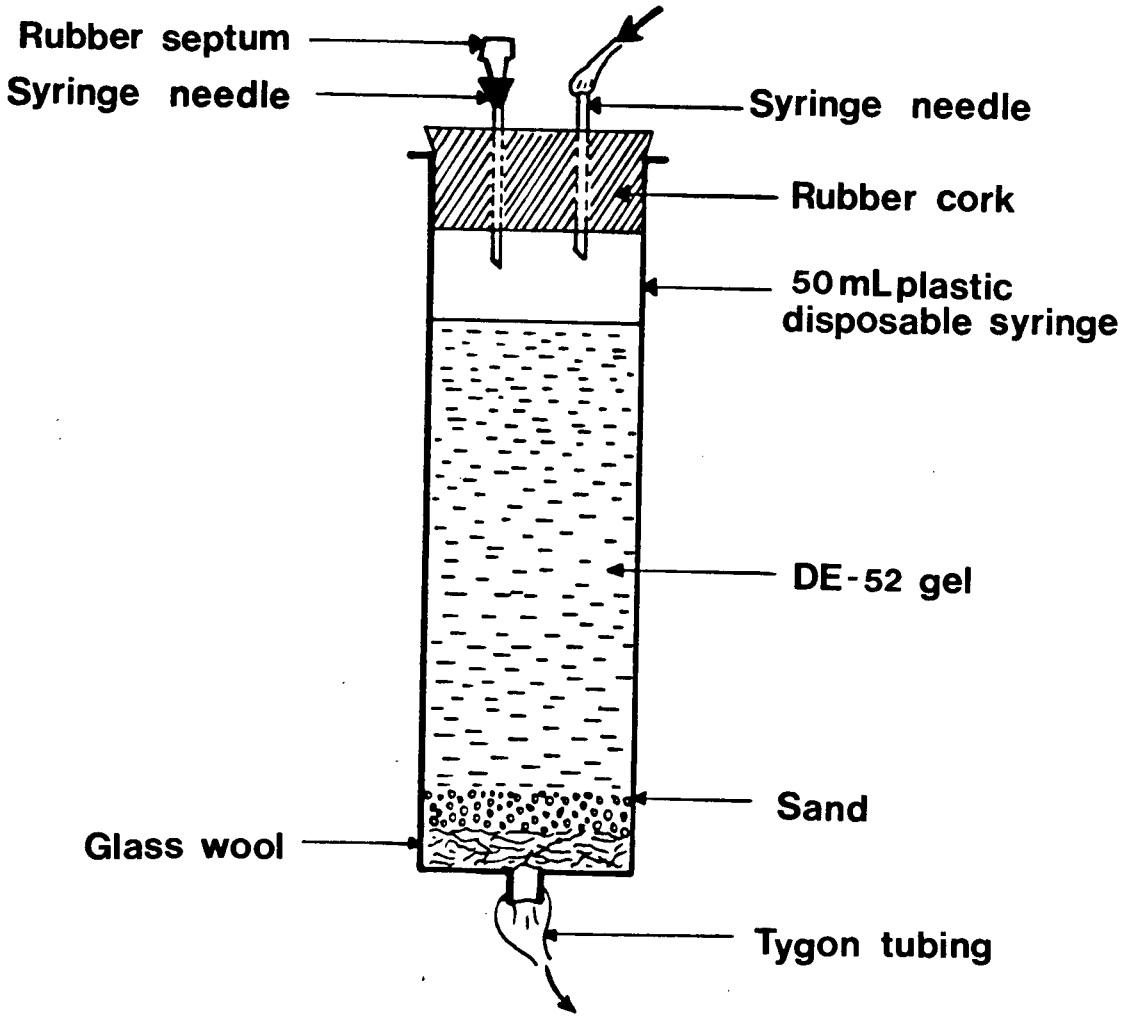


Figure III.14 A schematic drawing of the DE-52 column constructed from a 50mL disposable syringe.

Leaf 159 missed in numbering.

and kinetic studies were prepared by adding apomyoglobin to the crude cytochrome solutions. Since apomyoglobin has a higher affinity for the heme group than does apocytochrome P450cam,[150] the unregenerated heme (P420 type) was efficiently stripped from the cytochrome P450cam solution and disposed of in a form (myoglobin-bound) that was easily removed by Sephadex G-100 chromatography.

III.4.4.3 Procedure for Removal of P420 Impurities

From the spectrum of the ferrous-CO adduct of the crude reconstituted cytochrome solutions, the amount of unregenerated protoheme was estimated using $\varepsilon_{mM}^{420} = 179$.[37] The preparation of apomyoglobin is described in Section III.4.4.4.

Heme transfer was accomplished by incubating the crude reconstituted P450cam prepared as in Section III.4.3.2 with apomyglobin in a 50mL pear-shaped flask at a mole ratio of heme-receptor to P420 of 1.2. Incubation was done at room temperature (23±2°C) under an argon atmosphere for 1.0-3.0 min. The proteins were then separated at 5°C on a Sephadex G-100 column (1.3 x 100cm) equilibrated with buffer P-100 containing 8mM camphor. Flow rates were maintained by gravity feed. Column construction was identical to that in Figure III.12. The protein solution was applied to the column in not more than 2.0mL volumes and was developed with the same buffer system at 250mm head pressure. The proteins eluted as separate but diffuse bands (brown) with the reconstituted myoglobin eluting first. The cytochrome P450 band was

collected after 4.0-5.0h and concentrated by ultrafiltration to 1.0-2.0mL. Following spectral analysis (see Section III.3.4) the enzyme solution were used immediately for kinetic experiments. Samples were stored under argon at -78°C in 3.0mL disposable syringes.

III.4.4.4 Preparation of Apomyoglobin

Procedure:

The procedure was similar to that reported by Breslow.[151] A 100mg sample of myoglobin was dissolved in 10mL of deionized water (1% solution) at 0°C, and the pH carefully adjusted to 1.5 with 1M HCl. The removal of the heme from myoglobin was ensured if the pH of the initial ferrimyoglobin solution was near 1.5 which is a critical value for the cleavage of the protein-heme link.[151] The solution was then extracted at 5°C first with an equal volume of 2-butanone, then twice more with a half-volume of 2-butanone to remove the heme. The resulting slightly straw-colored solution was then immediately dialysed at 5°C against 4 changes (4 x 500mL) of sodium bicarbonate solution (50mg/mL) and then against several changes (5 x 500mL) of deionized water. Solution changes were made every 6h. The apomyoglobin solution was further dialysed against 2 changes (2 x 500mL) of 1 x 10^{-4}M $Na_2(H_2EDTA)$ solution, and against several changes (5 x 500mL) of deionized H_2O. The apomyoglobin solution was centrifuged to remove denatured protein that had precipitated, and then cencentrated to ≈5.0mL using an Amicon UM-2 Ultrafiltrator (>1000MWt). Finally,

the concentrated protein solution was dialysed against 4 changes (4 x 250mL) of buffer P-100 and concentrated to 2.0 - 3.0mL. The myoglobin solution was used immediately for the removal of unregenerated heme from reconstituted cytochrome P450cam. The solution could be stored for up to 1 month at 5°C without appreciable denaturation. The millimolar concentration of apomyoglobin was determined based on the absorbance at 280nm (ε_{mM} = 15.5).[151]

III.5 Kinetic Study of the Reaction of Carbon Monoxide with the Ferrous Cytochrome P450cam and Myoglobin Systems by Flash Photolysis

III.5.1 The Flash Photolysis Apparatus

The flash photolysis apparatus utilized in these experiments was designed and constructed by Chang[152] and included the general features described by Gibson[132] and Porter.[134] The apparatus consisted of four subunits: (1) a monochromatic light source (i.e. a tungsten lamp and monochromator), the light from which was collimated and passed through the reaction mixture to monitor transient intermediates; (2) a thermostated reaction chamber (i.e. flash and sample compartment), with associated filters to select the appropriate monitoring and flashing wavelengths of UV-VIS light: (3) a photolysis flash (i.e. photographic flashgun) for producing short pulses of intense light along with charging and triggering equipment; and (4), an electronic detector and a rapid recorder (i.e. photomultiplier cell and oscilloscope) for the physical detection and estimation of transient intermediates. The arrangement of these components is illustrated in the block diagram of Figure III.15. The essential characteristics of each subunit are described presently.

Since the flash photolysis apparatus had not been operated for several years all subunits were dismantled, examined thoroughly and repaired when necessary. The original circuitry was analysed, cleaned, and recalibrated as required. For convenience, a small vacuum line fitted with CO gas

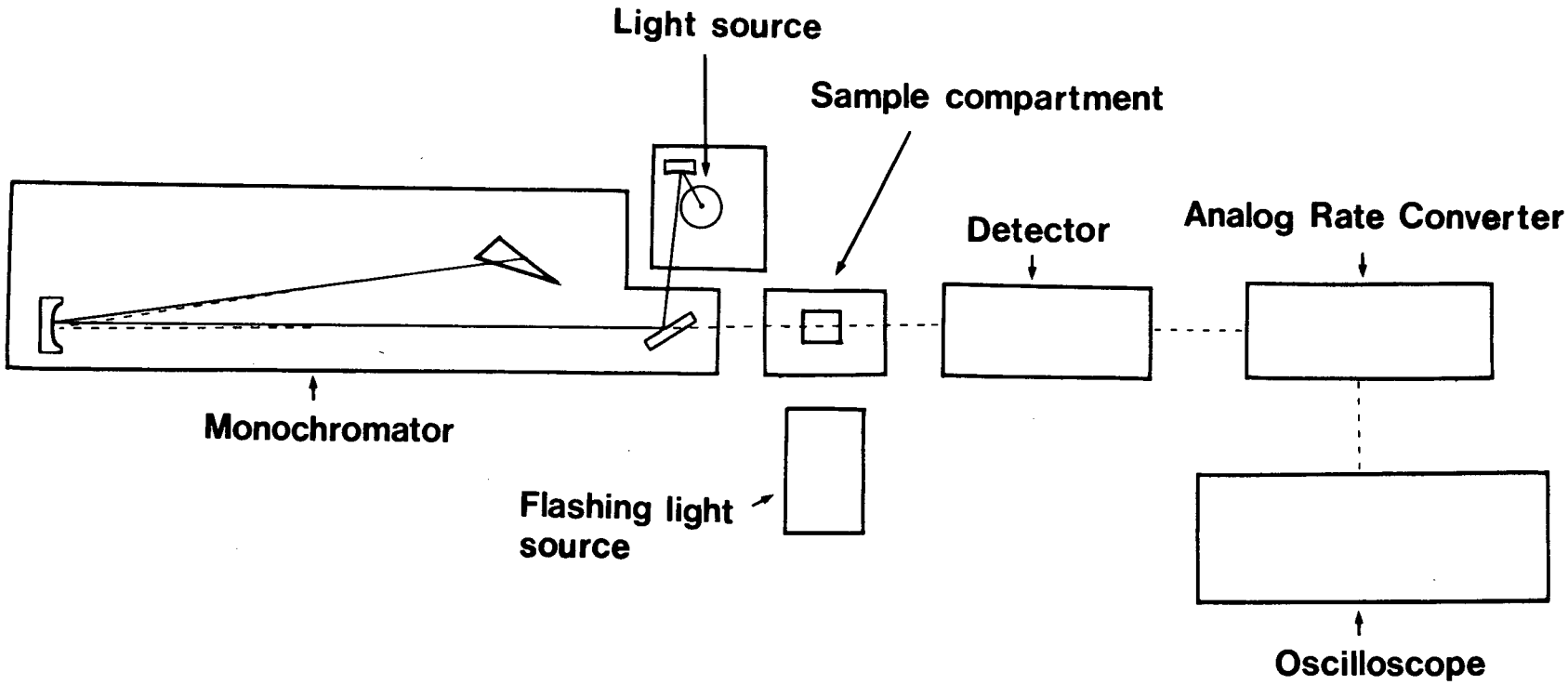


Figure III.15 Block diagram of flash photolysis apparatus.

handling equipment was constructed adjacent to the flash unit. All equipment repairs were performed in the electrical and mechanical shops of the Chemistry Department, U.B.C. The vacuum/CO handing line was made in the glassblowing shop, also, of the Chemistry Department, U.B.C.

III.5.1.1 Monitoring Light Source

The monochromator of a Beckman DU Spectrophotometer (Model 2400) equipped with a standard 24 watt tungsten filament automobile headlamp, provided the continuous monochromatic monitoring source as well as the basic framework of the flash photolysis apparatus. The lamp was operated from an external D.C. regulated power supply (6V., 3.2amps) and was enclosed in the original lamp compartment of the Beckman Spectrophotometer. Under these operating conditions, the noise level in the monitoring beam was kept to a minimum and the lamp was assured a greater lifetime.[134] The lamp was thoroughly cleaned of all debris before and after each set of flash experiments.

III.5.1.2 Flash and Sample Compartment

The original sample holder of the Beckman Spectrophotometer was replaced with a flash and sample compartment adapted for carrying out the flash photolysis experiments. Structural details of the subunit are presented in Figure III.16. All parts were constructed from brass metal and darkened with a brass bluing solution.

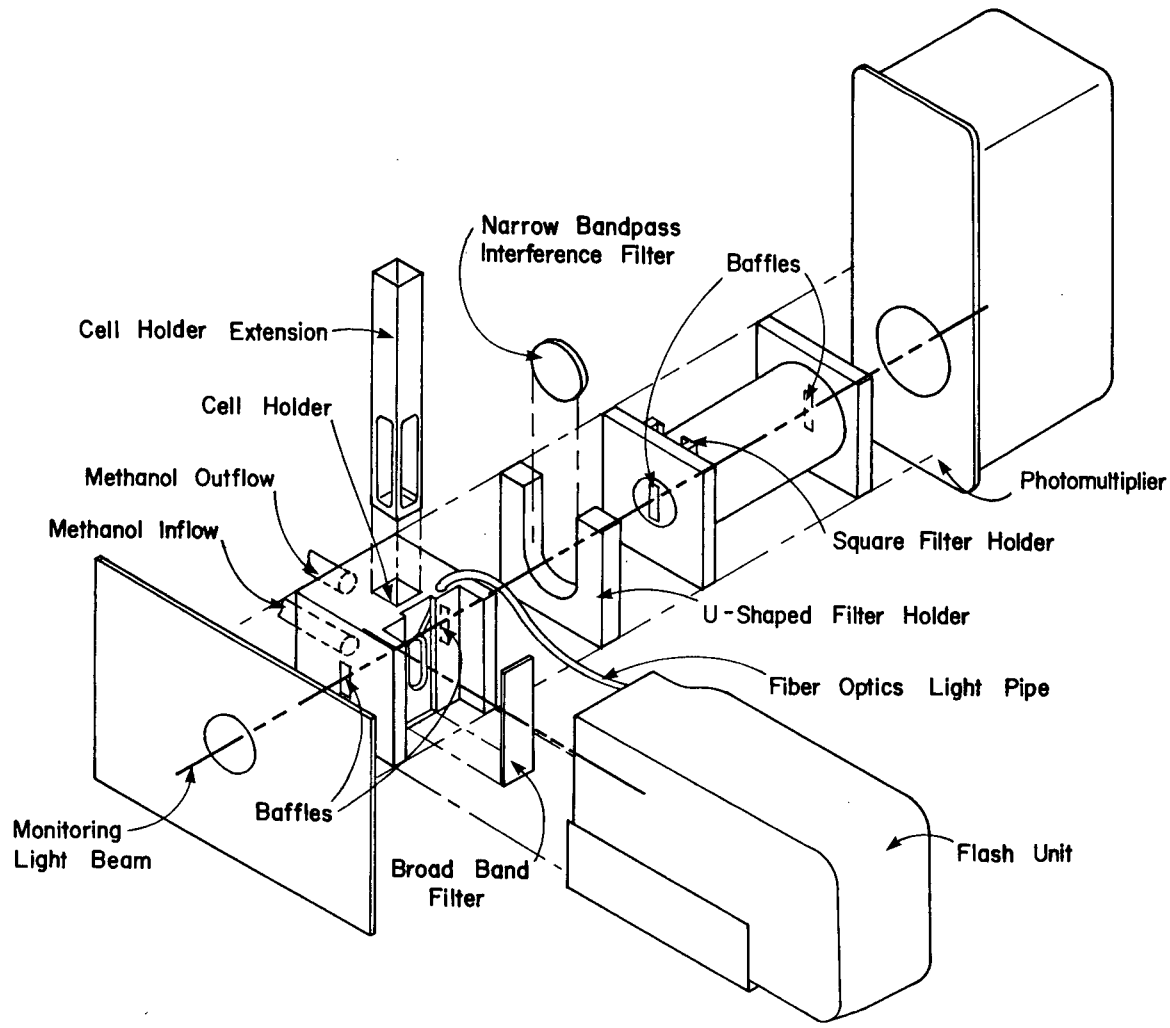


Figure III.16 Structural details of the flash and sample compartment of the flash photolysis unit.

The flash and sample compartment, containing the sample cell holder, was supplemented with an extension to conveniently house the cell-tonometers (see Figure III.13) as well as effectively block all external light from the reaction chamber. Three windows were cut in the extension tube for the flashing and monitoring light (see Figure III.16). The photolyzing flash light was arranged at 90^{o} to the monitoring light and completely illuminated the solution in the sample cell. The flashing light source (see Section III.5.1.3) was mounted on a bracket fixed to the exit slit face of the Beckman monochromator. To prevent "blinding" the photomultiplier detector from the blast of the light pulse, a crossover filtering system was utilized in which essentially all light from the flash was blocked from entering the PMT (see Section III.5.3.1). Inexpensive broadband cutoff filters were placed in front of the flashing light source to select the desired waveband output, while costly 10nm bandpass interference filters were placed between the flashing chamber and the PMT to pass only the monitoring wavelengths. Filters were obtained from the Oriel Corporation and Esco Products, and criterion for the selection of the crossover filtering system is described in Section III.5.3.1. Baffles with long rectangular windows were incorporated into the flash and sample compartment to achieve collimation of the monitoring and flashing light before reaching the interference filters. Between the interference filter and the PMT the light beam was collimated further by means of a blackened tube ($\simeq$10cm)

containing baffles with small rectangular windows at each end (see Figure III.16). Temperature control was provided by a Haake model Fk circulating thermostating bath capable of circulating temperature-equilibrated methanol through the flash and sample compartment as well as an external cylindrical water-bath simultaneously (Figure III.17). Hemoprotein solutions for kinetic analysis were equilibrated in the cylindrical water-bath while attached to the vacuum/CO handling line and then placed in the flash and sample compartment to perform the flash photolysis experiment (see Section III.5.2).

III.5.1.3 Flashing Light Source

The flash pulse was provided by a Braun 2000 model F027 automatic photographic flashgun operated from an external regulated D.C. power supply (6V., 2 amps). The desired light pulse characteristics, specifically intense flashes with rapid extinguishing, were readily obtained with this source. The single xenon flash lamp dissipated approximately 40 joules per flash[94c] in an effective time of 250±20 μsec (see Section III.5.3.2) and was sufficiently powerful to photodissociate up to 30% of the carbonylated myoglobin and P450cam systems (see Section III.5.3.4). To obtain the correct pulse time, the flasher was equipped with a fibre-optics feedback system. This system utilized the light sensing circuit of the Braun flashgun, which measures reflected light and cuts off the flash output. One end of the fibre-optics tube (0.3 x 25cm) was fixed immediately adjacent to the flash tube while the other was attached to the sensor (see Figure III.16). Flash

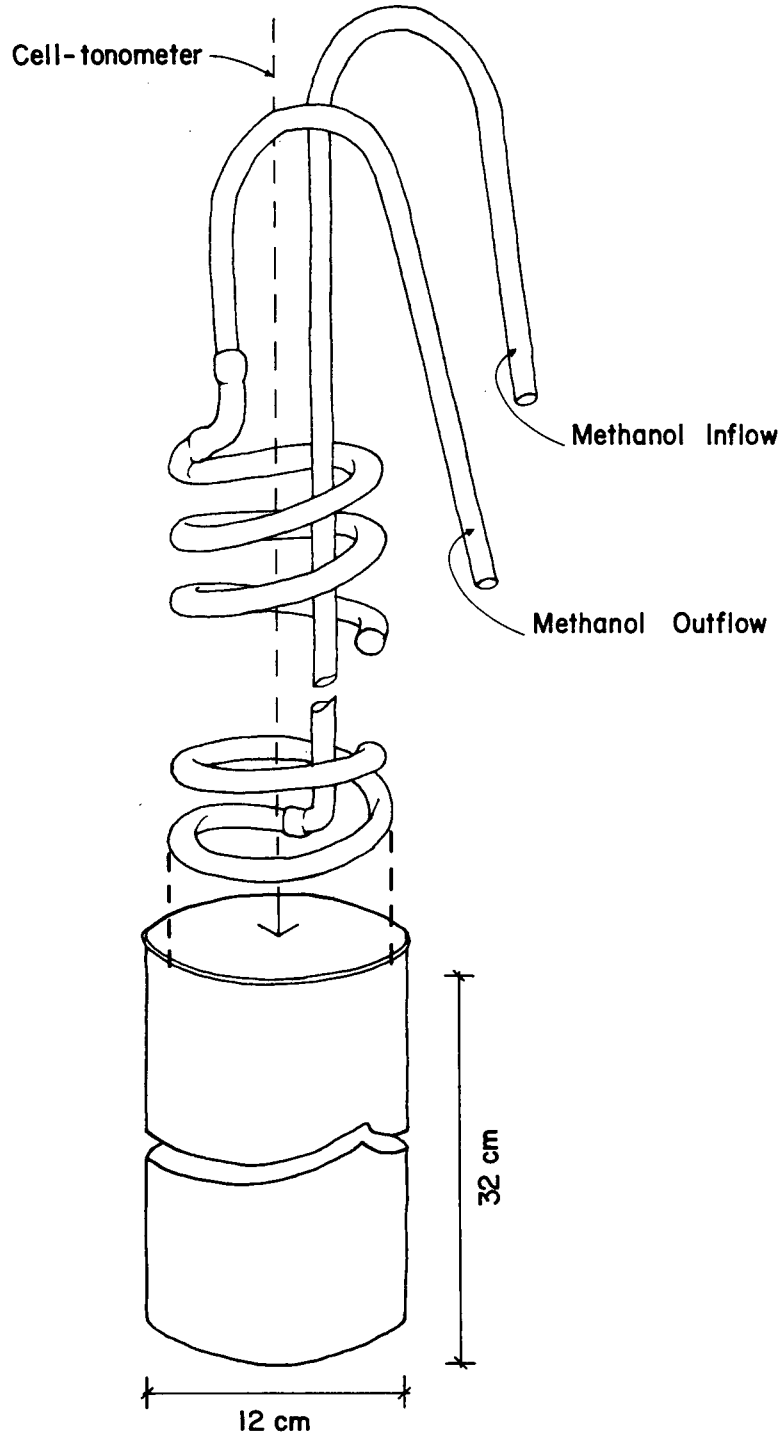


Figure III.17 Schematic diagram of the cylindrical water-bath used for equilibration of protein solutions while attached to the vacuum/CO-handling line.

light was fed back to the sensor *via* the light pipe cutting of the light pulse. The light duration was easily controlled by adjusting the position of the tube relative to the sensor. The closer the optics tube to the sensor, the sooner the flash output was cut off. Adjustments of 1.0-3.0mm in this distance shifted the flash duration from ≈8msec to the desired range (≈250 μsec; see Section III.5.3.2).

Since the "dead time" of the flash photolysis apparatus (see Section II.5) depends on the characteristics of the light pulse, the sharper the cutoff edge of the pulse the lesser the "dead time". The "dead times" of ≈250 μsec mentioned above were sufficiently short to successfully study the kinetics of carbon monoxide binding to the cytochrome P450cam and myoglobin systems. The flashgun was fired independently of, or simultaneously with, a storage oscilloscope (see Section III.5.1.4) through an external triggering circuit.[134] Approximately 15 seconds were required for recharging between flashes but unlimited numbers of flashes were obtained from the on-line power supply.

To obtain photodissociation of the carbonylated hemoproteins it was essential to remove the protective plastic convex flash tube cover in order to align the flash tube as close to the sample cell as possible. The distance between the flash tube and sample cell was ≈1.0cm. The light pulse was collimated using black tape to enclose all but the flash tube and reflecting system. Extreme care was taken when handling the unprotected flash lamp so that grease and dust

would not dull the flash output. The flash tube was carefully cleaned and stored after each use.

III.5.1.4 Detector and Recording System

The original Beckman detector and high voltage power supply components were replaced with a 1P28 photomultiplier housed in a *PMT* package (manufactured by Products for Research Inc., Danvers, Mass.) and regulated D.C. power supply adjustable from 300-500 volts. The transmission output from the PMT was processed directly through an on-line electronic analog "computer"[153] to avoid tedious data acquisition for absorbance conversion and fitting of the rate constant. The Analog Rate Converter contained two log amplifier circuits which could independently give both an exponential decay curve of the absorbance change and a linear trace whose slope *vs.* time was the rate constant for the reaction. The complete working circuit[152] of the Analog Rate Converter is shown in Figure III.18. The output from the Analog Rate Converter was connected directly to channel 1 of a dual trace amplifier (Tektronix 5A18N) in a Tektronix Type R5103N storage oscilloscope. The sweep time was controlled with a Tektronix 5B10N time base amplifier and the signal was registered and stored with a Tektronix D-11 single beam storage unit. The oscilloscope trace was initiated independently of, or simultaneously with, the flashgun (see Section III.5.1.3) through an external triggering circuit.[134] All exponential decay curves and first order rate plots were

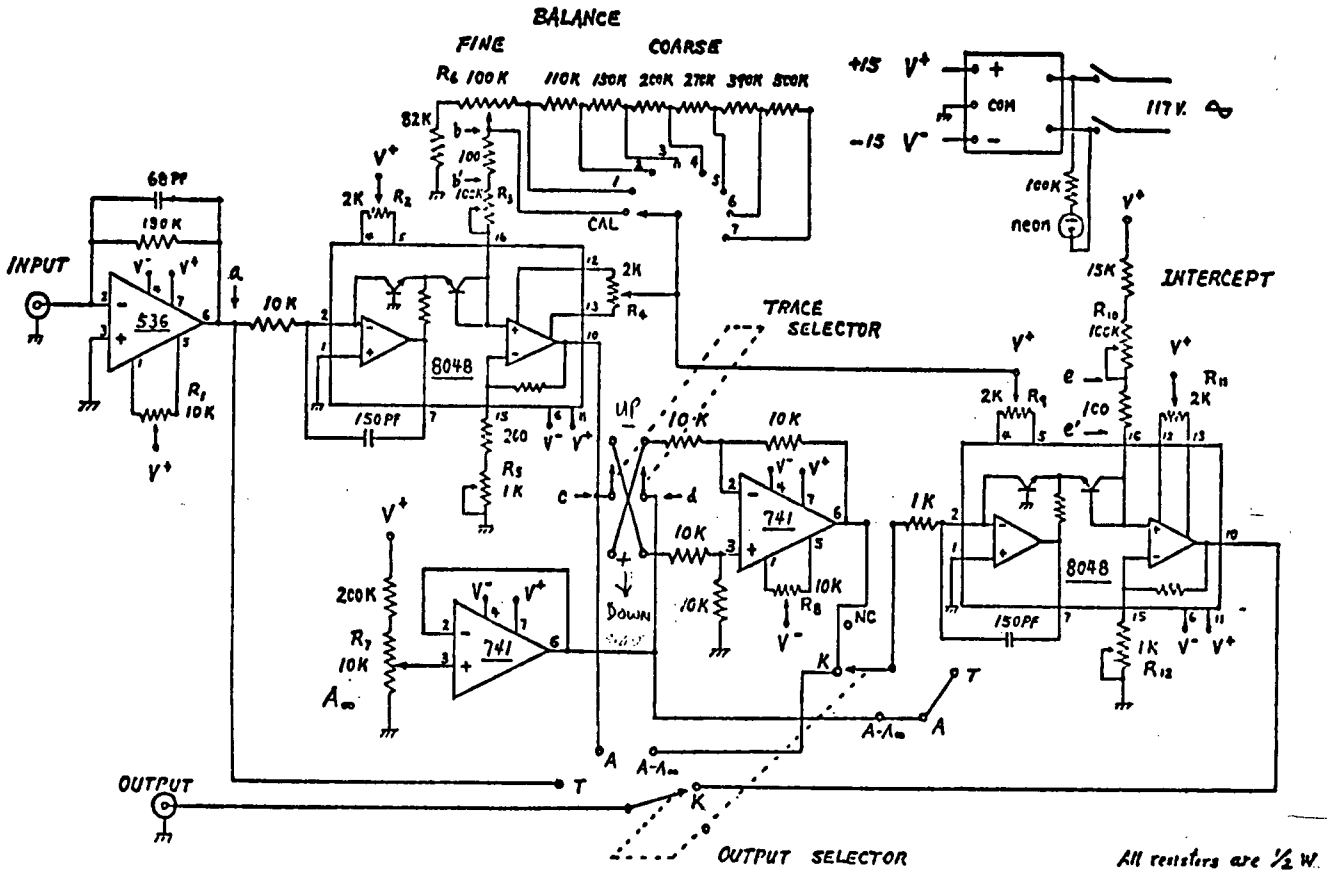


Figure III.18 Complete working circuit of the Analog Rate Converter.

photographed with a Tektronix C-5 oscilloscope camera loaded with Polaroid 3000 Land Film, Type 107. Photographs were developed and protected according to the manufacturer's directions.

III.5.1.5 Operation of the Flash Photolysis Apparatus

Detailed step-by-step instructions are given in Appendix I.

III.5.2 The Flash Photolysis Experiment

III.5.2.1 General Information

The flash photolysis experiments were performed at 20°C on the ferrous-CO complexes of horse-heart myoglobin and native and protohemin-reconstituted *P. putida* cytochrome P450cam. Hemoprotein solutions for kinetic measurements were prepared in the cell-tonometer shown in Figure III.13 by dilution of stock hemoprotein solutions in buffer P-100 (made 8mM in camphor for the P450cam systems). The final volume of the protein solutions were 5.0mL and protein concentrations, $\simeq 1 \times 10^{-5}$M. Stock myoglobin solutions were prepared by dissolving ≃10mg of myoglobin in 2.0mL buffer P-100, while myoglobin solutions for spectral and kinetic analyses required addition of ≃0.7mL of the stock solution to ≃4.3mL of degassed buffer P-100. Stock cytochrome P450cam solutions, as prepared in Sections III.3 and III.4, were diluted by addition of ≃ 0.2mL stock to ≃4.8mL degassed buffer P-100, 8mM camphor. All hemoprotein solutions for kinetic measurements were prepared under CO while attached to the vacuum/CO handling line adjacent to the flash unit, and all buffers were degassed three times by employing a freeze and thaw static vacuum technique followed by CO saturation. Complete kinetic analysis of each hemoprotein required the preparation of different protein solutions for each of three separate kinetic runs; the concentration of these protein solutions varied by ≃ 5%.

A typical flash photolysis experiment involved an initial spectral analysis of the hemoprotein in the ferric, ferrous and ferrous-CO states followed by compilation of kinetic data at several partial pressures of CO from 180 to 750mm Hg. To avoid protein denaturation, separate hemoprotein solutions were prepared for both the spectral and kinetic analyses. Reaction mixtures for spectral analysis were prepared under argon as described in Section III.3.4, while solutions for flash photolysis experiments were prepared under CO by a similar method differing only in the buffer-degassing mechanism. Approximate dilutions required for the myoglobin and P450cam solutions have been mentioned above. The UV-VIS spectra of the hemoproteins were obtained at 20^{o}C on a Cary 17D spectrophotometer equipped with a thermostated cell compartment. Protein solutions for spectrophotometric measurements were thermally equilibrated for 10 min (before the spectra were obtained), in a rectangular water-bath set up adjacent to the spectrophotometer (see Figure III.19). Protein solutions for kinetic measurements were prepared at room temperature (23±2^{o}C) and then transported to the spectrophotometer for equilibration and to record the spectra. For subsequent changes in the CO pressures as required during the flash photolysis experiments, the hemoprotein solutions were equilibrated for 10 min at 20^{o}C in a cylindrical water-bath (Figure III.17) while attached to the vacuum/CO handling line. The final CO pressure was adjusted following this equilibration period.

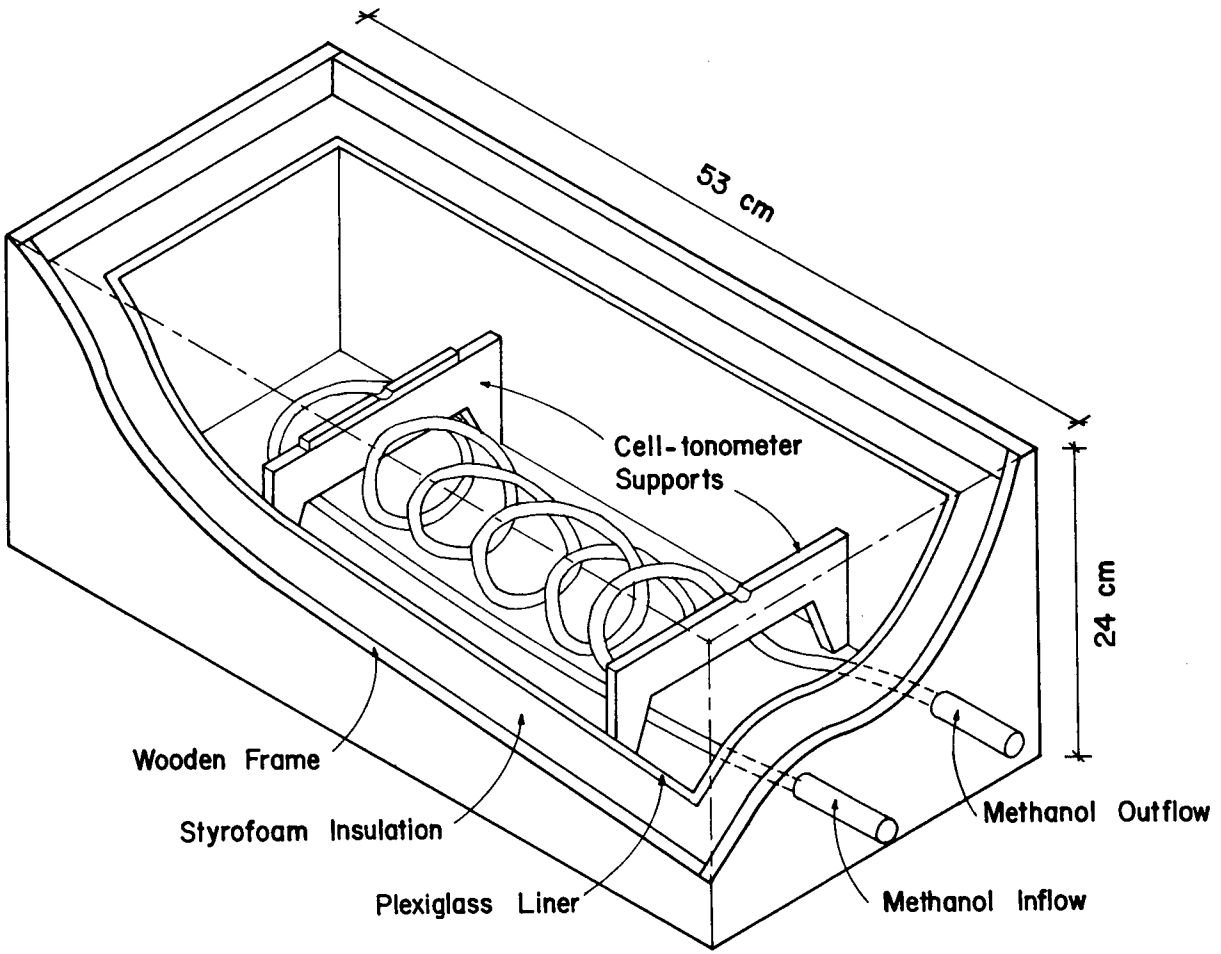


Figure III.19 Schematic diagram of rectangular water-bath used for equilibration of protein solutions at the Cary spectrophotometer.

The solutions were gently swirled for ≈1 min to allow for gas equilibration and immediately transferred to the flash photolysis apparatus for kinetic measurements. Two Haake model Fk circulating thermostating bath were therefore required during the flash photolysis experiments; one for the simultaneous equilibration of the cell compartment and external water-bath at the spectrophotometer and the other for the equilibration of the flash and sample compartment of the flash unit and the cylindrical water-bath utilized at the vacuum/CO handling line. The spectroscopic cells were labelled to ensure that they were placed in the cell holders of the flash unit and the spectrophotometer in the same direction for every experiment.

In order to monitor the concentration of each hemoprotein complex throughout the flash photolysis experiments, as well as impurity formation in the cytochrome P450cam samples (i.e. P420 type),[148] the spectrum of the ferrous-CO complex was taken before and after kinetic data acquisition at each CO pressure. These spectra were used to calculate the concentration of the hemoprotein throughout the kinetic experiment as well as compare absorption data (i.e. λ_{nm} and ε_{mM} values) with the initial spectral analysis of the hemoprotein. Complete data were collected for three different samples of each hemoprotein and tabulated on the data acquisition sheets shown in Figure III.20. For data analysis partial pressures of CO were converted to gas concentrations in solution; at 20°C, 1.0mm Hg of partial pressure corresponds

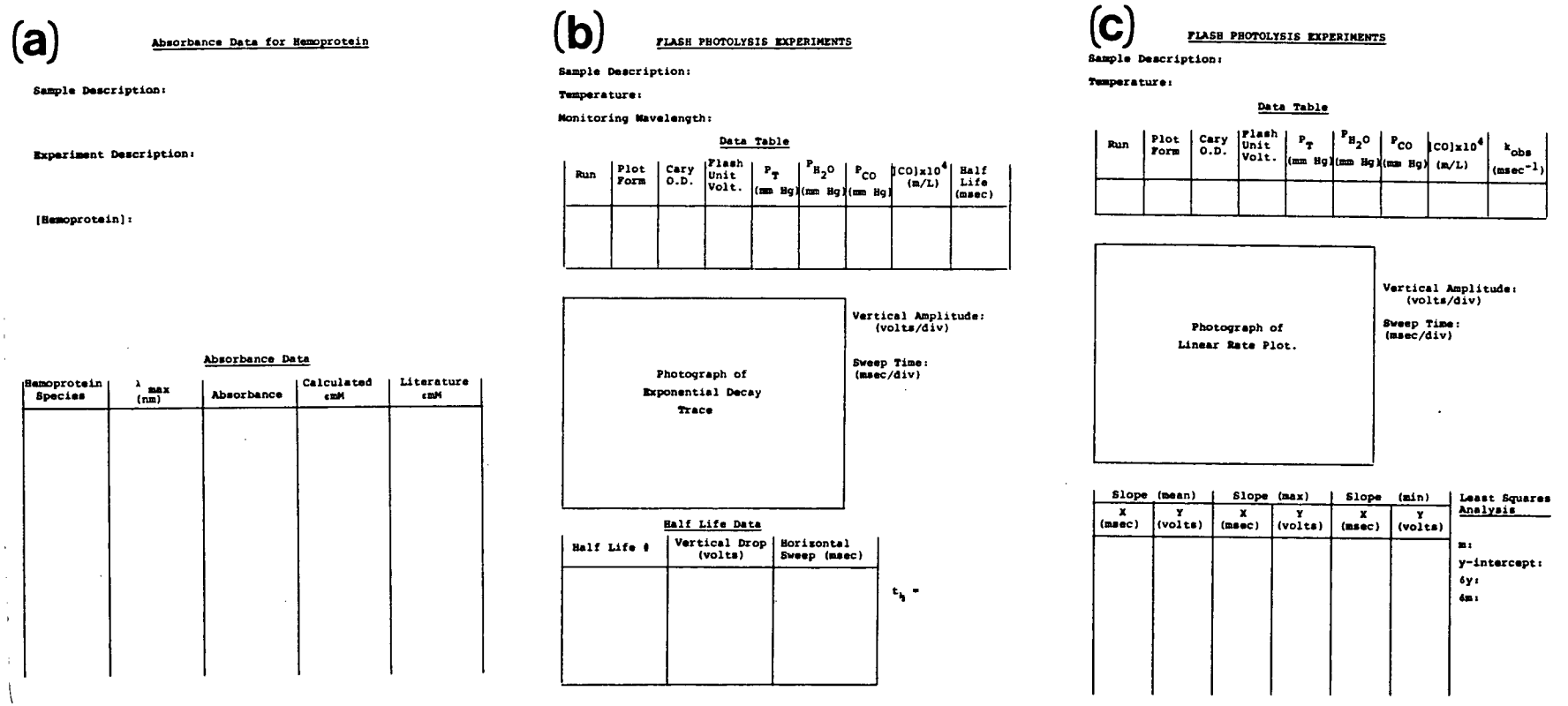


Figure III.20 Data acquisition sheets utilized for the collection of kinetic data; (a) was used for the collection of absorbance data, (b) for the collection of exponential decay data and (c) for the collection of linear plot data (δy and δm of linear rate plot data are the errors in the y-intercept and slope, respectively, obtained from the least squares analysis of data points).

to 1.36×10^{-6}M for CO.[109] Since the protein concentrations were very low and the solubility of carbon monoxide was of the order of 1×10^{-3}M, the gas concentration in solution and the partial pressure of the gas over the solution remained essentially constant throughout the experiments. All pressures were measured with a mercury manometer and corrected for the vapour pressure of water.

The concentration of the myoglobin solutions was determined from the concentration of the stock solution and checked by direct spectroscopic measurement of the ferrous-CO myoglobin complex at 540nm ($\varepsilon_{mM} = 15.4$).[109]

III.5.2.2 Procedure

Absorbance data obtained from the initial spectral analysis were recorded on data acquisition sheet Figure III.20a and used to calculate protein concentrations, as well as estimate the purity of the protein preparation. These spectra were also used to select the proper flashing and monitoring light filters for the flash photolysis experiment (see Section III.5.3.1). Protein solutions for kinetic measurements were then prepared under CO (1 atm). Prior to the addition of stock protein solution degassed buffers were equilibrated at the Cary spectrophotometer and then placed in the thermostated cell compartment to obtain a baseline spectrum. Stock protein solution was then added and again the solution equilibrated before the ferric hemo-protein spectrum obtained. Stoichiometric $Na_2S_2O_4$-reduction

of this solution produced the fully carbonylated hemoprotein complex, which was equilibrated before the spectrum obtained. Spectra were recorded from 700 to 250nm. The sample cell was then immersed in the cylindrical water bath, attached to the vacuum/CO handling line and carefully evacuated three times being careful to avoid boiling of the solution. The cell was then left to equilibrate for a further 10 min period after which the CO pressure was carefully adjusted over the solution. Following calibration of the flash photolysis apparatus (see Section III.5.1.5), the sample solution was removed from the vacuum/CO handling line and placed in the sample compartment of the flash unit to obtain an exponential decay curve for the CO-ferrous-hemoprotein recombination reaction at the specified CO pressure. The trace was photographed and all parameters recorded as on data acquisition sheet Figure III.20b. The flash unit was then recalibrated and the pseudo first-order rate plot obtained. The trace was again photographed and all parameters recorded as on Figure III.20c. The sample cell was then removed from the flash unit and transported to the spectrophotometer to obtain a spectrum of the ferrous-CO complex. The CO pressure was then readjusted over the solution with equilibration and the above procedure repeated. Exponential decay curves and pseudo first-order rate plots were obtained at seven different partial pressures of CO between 180 to 750mm Hg. Approximately 2.0 min were required to produce each trace and an entire kinetic run was completed in 3-4h.

III.5.3 Preliminary Experiments

III.5.3.1 Selection of Filtering System

The crossover filtering system utilized in the flash and sample compartment of the flash unit (see Section III.5.1.2) was selected in conjunction with the UV-VIS spectra of the ferrous and ferrous-CO complexes of myoglobin and cytochrome P450cam (i.e. from the initial spectral analysis). The photodissociation of carbon monoxide from the ferrous-CO species was initiated (i.e. flashed) from either the VIS (450-600nm) or near-UV (350-380nm) band regions, while the relaxation process was followed by monitoring the Soret absorption peaks (420-450nm) of the ferrous-CO or intermediate five-coordinate ferrous species. The input flashing light and the monitoring wavelengths were isolated with broadband cutoff and narrowline interference filters respectively. Figure III.21 shows the absorption spectra of the ferrous and ferrous-CO states of both proteins along with the broadband cutoff and narrowline interference filter combinations most suited for the flash photolysis of these systems.

The broadband cutoff filters were selected to utilize the highest energy regions of the flash lamp output (300-700nm)[157] and to flash the absorption peaks of maximum intensity within the VIS (450-600nm) and near-UV (350-380nm) regions. The photodissociation reaction was promoted using all of the broadband cutoff filters shown in Figure III.21; however, at protein concentrations of $\simeq 1 \times 10^{-5}$M the

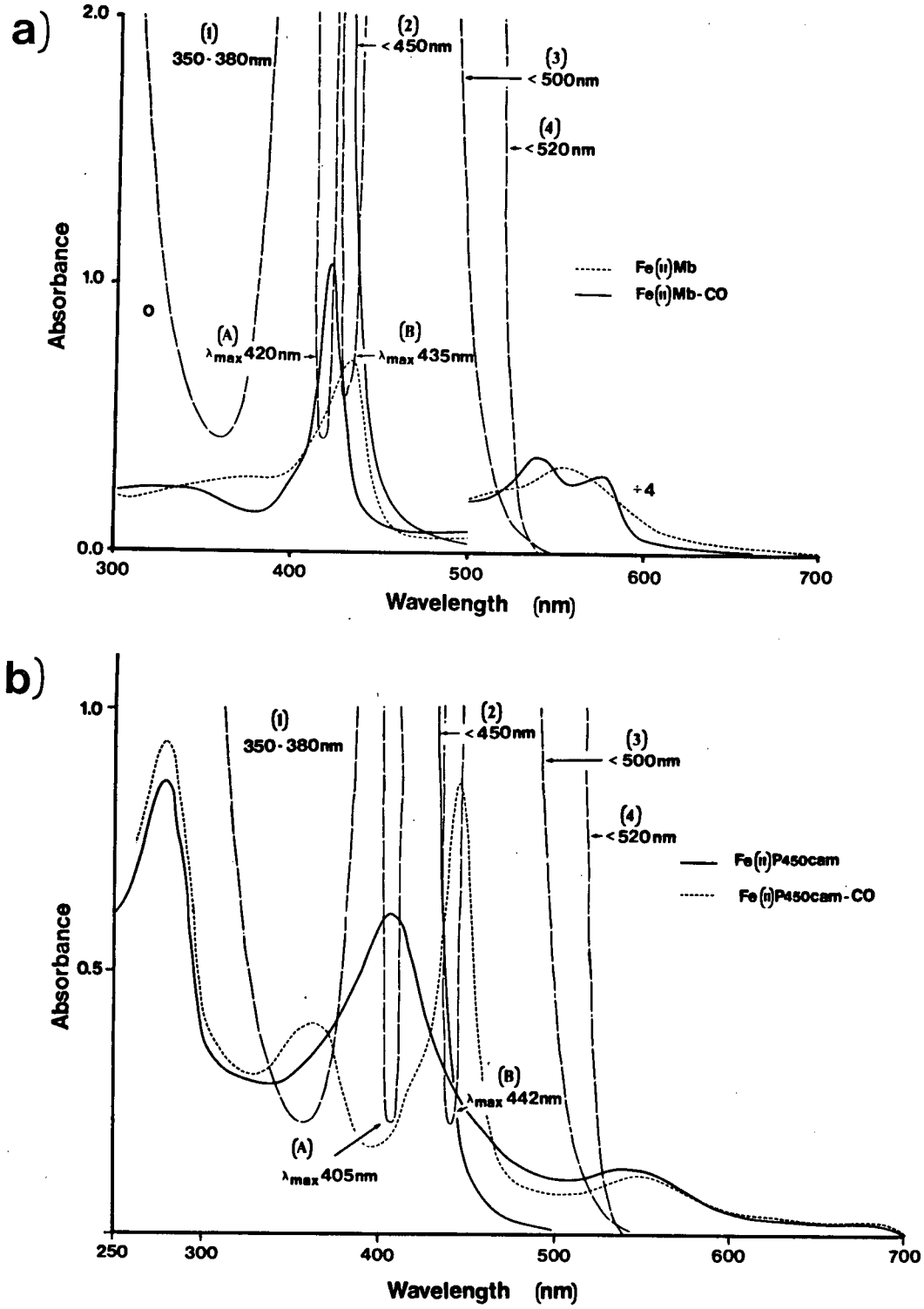


Figure III.21 Absorption spectra of the ferrous and ferrous-CO states of myoglobin and cytochrome P450cam along with the broad-band cutoff and narrowline interference filters most suited for the flash photolysis of these systems (Figures III. 21a and III.21b respectively).

perturbations were most noted when the myoglobin system was flashed below 450nm (cutoff filter #2, Figure III.21a; Esco #S133870) and the cytochrome P450cam systems in the 350 to 380nm region (cutoff filter #1, Figure III.21b; Oriel Model G-774-3550).

The narrowline interference filters were chosen to monitor the Soret absorption band which fell within the calibration limit (O.D. $\simeq$ 1.0) of the flash photolysis apparatus at protein concentrations of $\simeq 1 \times 10^{-5}$M (see Section III.5.3.3). For the myoglobin system, the intermediate ferrous Soret peak at 432nm (interference filter B, Figure III.21a; Esco #S904358) was selected while the ferrous-CO peak at 446nm (interference filter B, Figure III.21b; Oriel Model G-522-4416) was chosen for the P450cam species. The interference filter bandpass maxima passed as close to the Soret maxima as possible and maximal efficiency of the cross-over system was achieved if the bandpass maxima of both filters did not overlap (see Section III.5.3.2). Table III.10 summarizes the most effective filter combinations used for the study of ferrous myoglobin and cytochrome P450cam with CO by flash photolysis.

III.5.3.2 Light Pulse Characteristics

The light pulse characteristics were obtained on the flash photolysis apparatus as indicated in Section D of the operating instructions (see Section III.5.1.5).

Table III.10

Most Effective Filter Combinations for the Flash Photolysis Study of Ferrous Myoglobin and Cytochrome P450cam with CO

Hemoprotein	Soret Peak (nm)	Cutoff Filter (nm)	Interference Filter (nm)
Myoglobin (ferrous species)	432	>450	432
Cytochrome P450cam (ferrous-CO species)	446	350-380	442

The time-based characteristics of the light pulse (i.e. rise time, flash duration, and dacay time) were adjusted with the fibre-optics feedback system described in Section III.5.1.3. With the appropriate broadband cutoff filter in place (see Table III.10), a neutral density filter (O.D. = 3.0) was inserted between the flash and sample compartment and the PMT. The position of the light pipe was adjusted until a reproducible flash trace exhibiting a rise time of 30±10 μsec, a flash duration time of 140±20 μsec, and a decay time of 60±10 μsec was obtained. The time-based characteristics of the flash output from a typical photographic flashgun[154] are described in Figure III.22, while Figure III.23 shows the characteristics of the Braun flashgun output. The peak shape of the flash pulse was examined using all the broadband cutoff filters indicated in Figure III.21 and no distinct changes in peak shape were observed; the flash lamp gave a reproducible flash output that was independent of wavelength of the flashing light.

To check the efficiency of the crossover filtering system, the neutral density filter was replaced with the interference filters listed in Table III.10. Light leakage to the PMT was manifested in a trace with similar pulse characteristics as outlined above; however, the filtering efficiency was increased (i.e. shorter time-based characteristics of the flash trace) as the bandpass maxima of the cutoff and interference filters became further separated. Removal of the interference filter caused "blinding" of

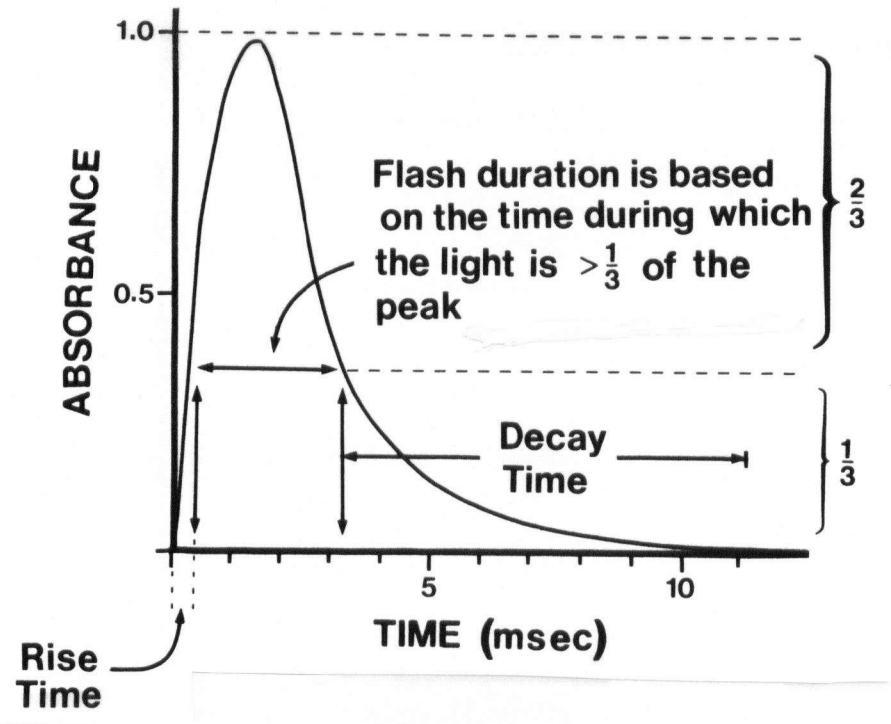


Figure III.22 Time-based characteristics of the flash output from a typical photographic flash gun; Ref.154.

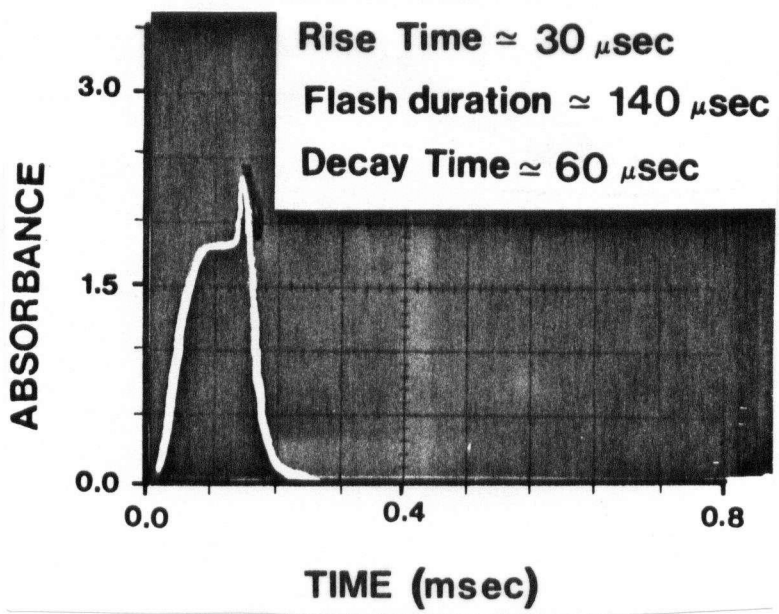


Figure III.23 Pulse characteristics of the flash output from the Braun flashgun.

the photomultiplier (manifested in a square trace of amptitude 8V and duration 250μsec) indicating that the majority of flashing light was blocked by the interference filter.

III.5.3.3 Calibration Check

Under the calibration parameters of the Analog Rate Converter,[153] the photomultiplier tube anode current was converted into a voltage linear with absorbance, with 1V equal to 1 OD unit.

In order to determine whether there was a direct proportionality between optical density of the test solutions and the voltage scale of the flash photolysis apparatus a calibration curve was constructed over a wide range of protein concentrations. Solutions of reduced myoglobin and the ferrous-CO complex of cytochrome P450cam were prepared (≈1.2 x 10^{-4}M; see Section III.3.4) and the appropriate filters were selected for the flash unit (Table III.10). The Soret absorbance of each species was obtained on the Cary Spectrophotometer at the bandpass maxima of the interference filter (i.e. 432nm for reduced myoglobin and 442nm for reduced-CO P450cam species) and then transferred to the flash photolysis unit, which was calibrated at the same respective wavelengths, to obtain the corresponding voltage reading. The concentration of each solution was diluted by removing one half of the solution and replacing the volume with degassed buffer. The corresponding optical density and voltage readings were

recorded. Solutions were further diluted several times and the corresponding readings obtained. The graph of OD Cary *vs.* V Flash Unit (Figure III.24) indicated that the calibration limit of the flash apparatus is OD ≃ 1.0 above which the direct proportionality was not obeyed. The protein solutions for spectral and kinetic measurements were therefore prepared as $\simeq 1 \times 10^{-5}$M solutions in order to keep the Soret maxima of the ferrous myoglobin and ferrous-CO P450 complexes at an OD ≃ 1.0.

III.5.3.4 Extent of Photodecomposition

In order to determine the extent of photodecomposition of the CO complexes of ferrous myoglobin and cytochrome P450cam by the flashing light pulse, the spectra of the kinetic intermediates produced by the flash were obtained. Protein solutions were prepared to a concentration of $\simeq 1 \times 10^{-5}$M as described in Section III.3.4 and carbon monoxide was added to a final pressure of 1 atm. Electronic absorption spectra of the ferrous and ferrous-CO complexes were obtained for both hemoproteins. Solutions of the fully carbonylated species were then placed in the flash photolysis machine and exponential decay curves for the CO recombination reaction were obtained at six different wavelengths between 400-450nm (the Soret region of both the myoglobin and cytochrome P450cam complexes). Selection of the particular wavelength was done with various narrow line interference filters with 10nm bandpass maxima at 400,

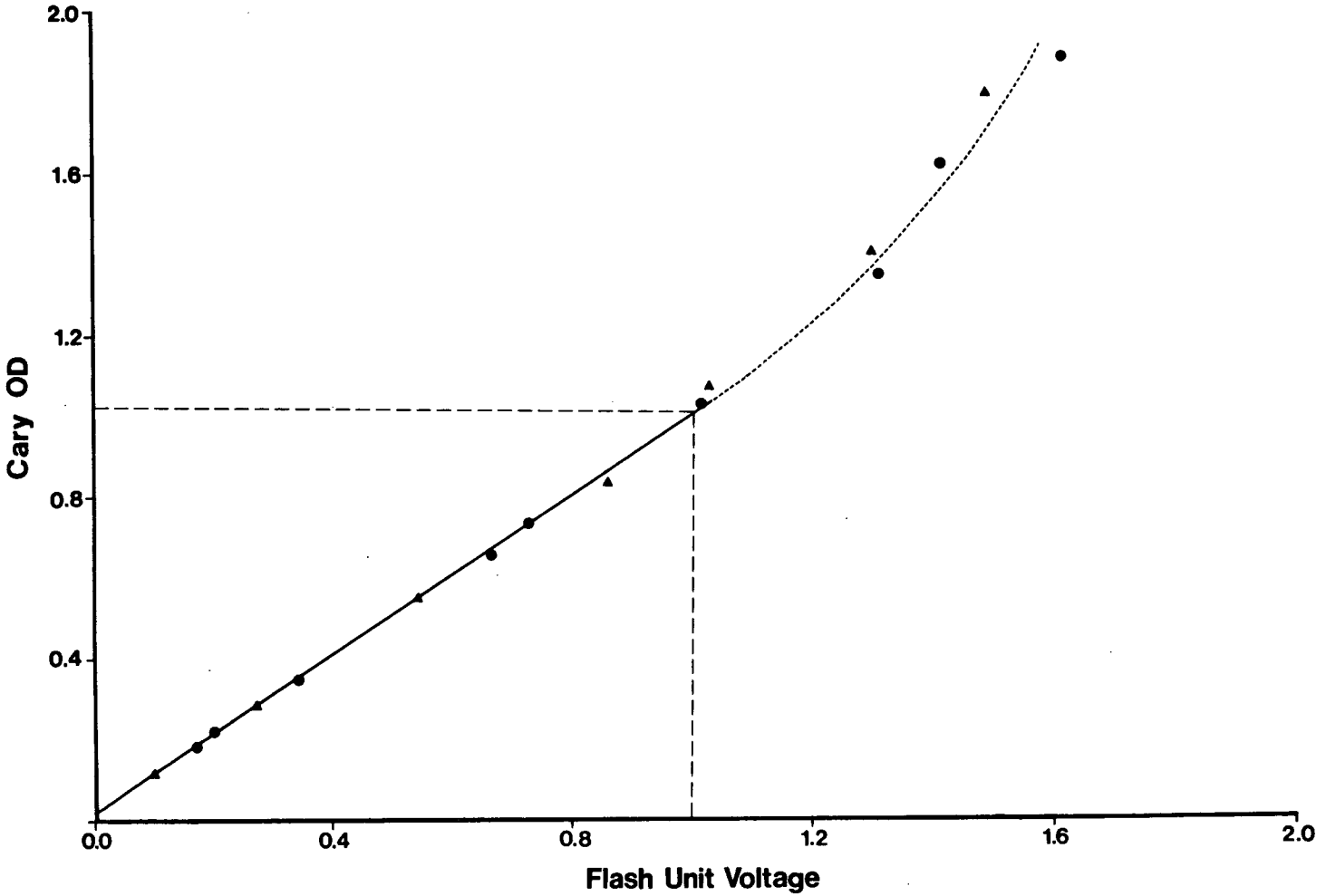


Figure III.24 Graph of optical density measured on the Cary Spectrophotometer *vs*. Voltage on the flash unit.

405, 420, 430, 435, 442, and 450nm (available from Oriel and Esco). Broadband cutoff filters for selection of flashing light were those listed in Table III.10. The initial absorbance (at time = 0) on the exponential decay traces was taken as the maximal absorbance change in solution at the precise moment the CO was flashed off. These absorbance values were then plotted on the electronic absorption spectra of ferrous and ferrous-CO myoglobin and cytochrome P450cam (see Figure III.25a,b). For both proteins the resulting spectra of the kinetic intermediates showed ≈30% photodecomposition, as calculated by the absorbance change of the ferrous-CO Soret absorption. As well these spectra passed directly through the spectrophotometric isosbestic points of the ferrous and ferrous-CO complexes of myoglobin (at, 407, 427, and 457nm; see Figure III.25a) and cytochrome P450cam (at 429 and 465nm; see Figure III.25b), indicating that dissociation of the CO was the only effect of the photodecomposition process (raw data are given in Appendix III). All measurements were obtained at 20°C.

III.5.3.5 Kinetic Study of CO Binding the Ferrous Myoglobin

In order to determine whether the flash photolysis apparatus described previously was operable, the unit was applied to the well-documented and theoretically simple reaction of carbon monoxide with methmyoglobin. The kinetic results obtained using the experimental procedure outlined in Section III.5.2 were in excellent agreement with those reported in the literature and are described in detail later (see Section IV.4.2).

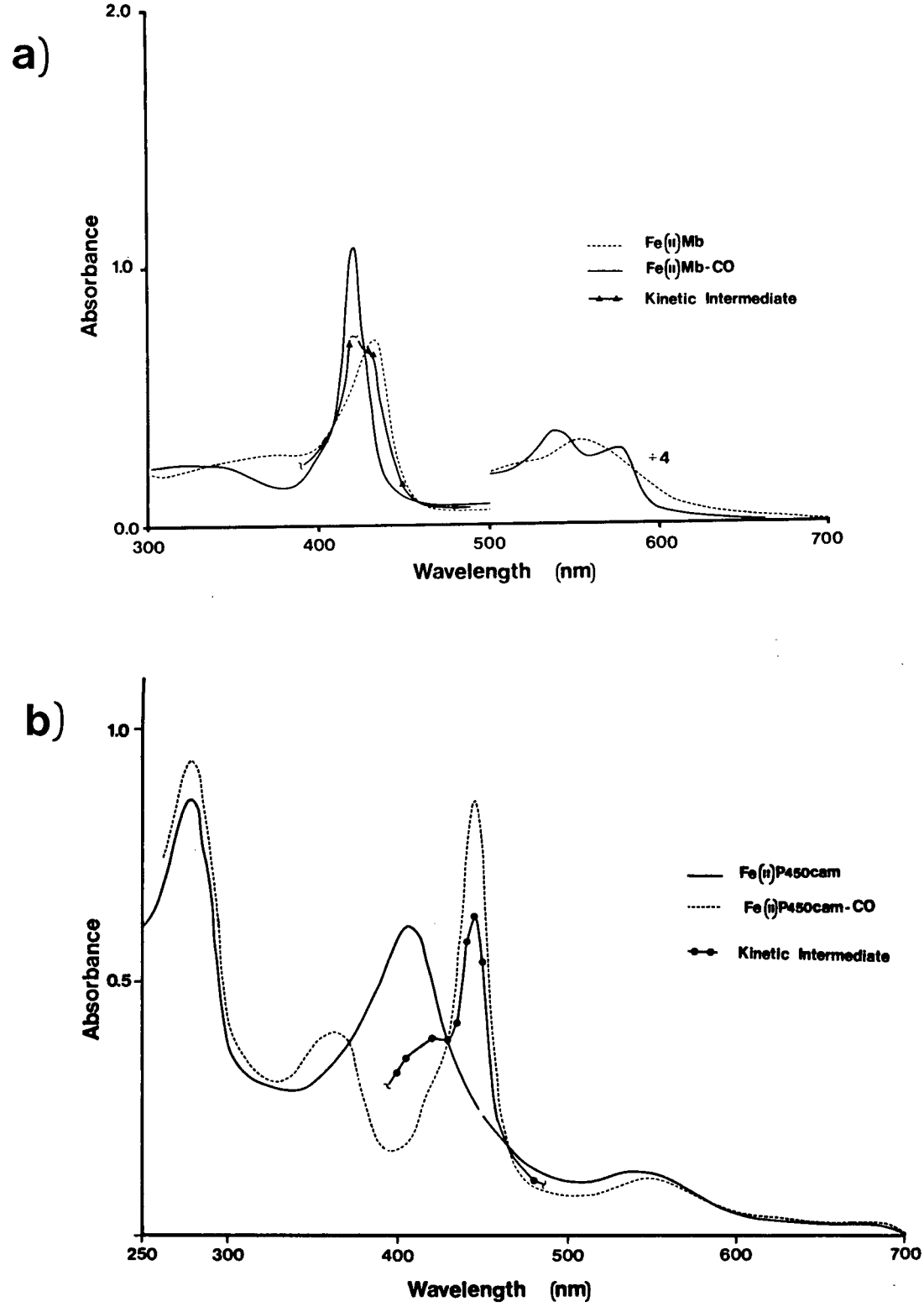


Figure III.25 Spectra of the kinetic intermediates formed by photodecomposition of the ferrous-CO complexes of myoglobin (a) and cytochrome P450cam (b).

III.6 Spectrophotometric Determination of the Equilibrium Constant for the Reaction of Carbon Monoxide with Ferrous Cytochrome P450cam

III.6.1 General Information

Equilibrium constant (Kco) measurements for Reaction II.5 were made by following VIS and near UV (e.g. the Soret bands) spectral changes with changes in the concentration of the carbon monoxide ligand. The equilibrium experiments were performed at 20°C with the native reduced cytochrome P450cam complex using standard spectrophotometric techniques.[8] Following the initial spectral analysis of the enzyme, separate protein solutions were prepared under argon for the equilibrium constant measurements (see Section III.3.4). The experimental format, including equipment, followed closely that outlined for the flash photolysis experiments in Section III.5.2. For data analysis, partial pressures of CO were converted to gas concentrations in solution (see Section III.5.2.1). Equilibrium data was tabulated on data acquisition sheets shown in Figures III.26 a and b while absorbance data was tabulated as in Figure III.18a. CO pressures were measured with a di-n-butylphthalate (oil) manometer and corrected for the vapour pressure of water. Partial pressures of CO in mm oil were converted to mm Hg for data analysis (i.e. (mm oil) 7.73×10^{-2} = mm Hg).

III.6.2 Materials

All reagents have been obtained as previously listed except for the following; from Fisher Scientific, di-n-butylphthalate.

(a)

Equilibrium Data

Sample Description:

Temperature:

Vapour Pressure of H_2O:

	Theoretical[155]	Experimental

Data Table

Species #	Wanted Pco mm Hg(oil)	P_{Total} (mm oil)	Pco (mm oil)	A446nm	A408nm

(b)

Data Analysis

Wavelength Maxima :

Absorbance of Pure Species: Ao =

A_∞ =

Data Table

Pco (mm Hg)	$[CO]x10^6$ (M)	Log [CO]	A-Ao	A_∞-A	$\frac{A-Ao}{A_\infty-A}$	log $\frac{A-Ao}{A_\infty-A}$

Figure III.26 Data aquisition sheets utilized for the collection of equilibrium data (a) and data analysis (b).

III.6.3 Procedure

Prior to addition of stock cytochrome solution, buffers for the equilibrium measurements were degassed three-times with a freeze-thaw static vacuum technique followed by argon saturation. The degassed buffer was equilibrated for 10 min in the rectangular water-bath adjacent to the Cary Spectrophotometer (see Figure III.19) and then transferred to the thermostated cell compartment of the spectrophotometer to obtain a baseline spectrum. Spectra were recorded from 500 to 250nm. The enzyme solution was then reduced with the addition of $Na_2S_2O_4$ solution (see Section III.3.4) and equilibrated for another 10 min in the external water-bath. The equilibrated solution was again transferred to the thermostated cell compartment of the spectrophotometer to obtain the initial ferrous cytochrome P450cam spectrum. The sample cell was then emersed in the cylindrical water-bath (see Figure III.17) and attached to the vacuum/CO handling line. Following evacuation of the sample solution, known pressures of carbon monoxide (2-20 torr) were admitted to the argon-free system. The argon atmosphere was removed by gradual evacuation of the sample cell and care was taken to avoid boiling of the protein solution. Complete evacuation of the cell was determined by measuring the vapour pressure of the aqueous buffer with the manometer; at 20°C vapour pressure of water is 17.5 torr (228mm oil).[155] The system was evacuated up to three times to obtain a constant water vapour

pressure reading. Once evacuated, the system was allowed to equilibrate for 10 min in the cylindrical water-bath while still attached to the vacuum/CO handling line. Changes in internal pressure of the system (due to leakage) were closely monitored during the equilibration period and if the manometer readings remained stationary throughout this time CO pressures were carefully let into the system. The solutions were gently swirled for ≈1 min to allow for gas equilibration, transported to the water-bath set up next to the Cary spectrophotometer for a further 5 min equilibration period, and then immediately transferred to the spectrophotometer to obtain a spectrum of the partially carbonylated system. Once the spectrum was obtained the cell was returned to the vacuum/CO handling line, the pressure of CO readjusted over the solution with equilibration and another spectrum of the partially carbonylated system was taken. Approximately nine different spectra were obtained at CO pressures up to 45 torr. The final spectrum of the fully carbonylated cytochrome complex was obtained at 1 atm CO pressure. Data analyses for the equilibrium studies were recorded on the data acquisition sheet in Figure 26a and analysed according to data acquisition sheet in Figure 26b.

CHAPTER IV

RESULTS AND DISCUSSION

IV.1 Growth of *P. putida* strain PpG 786

P. putida, strain PpG 786, was utilized in this study because it possesses several advantages over the parent strain, PpG 1.[37] These include shorter generation times on D-(+)-camphor, resistance to lysis by bacteriophage, and release of the hydroxylase proteins by simple freeze-thaw autolysis. The advantages of using the mutant strain PpG 786 not only allowed for rapid and quantitative production of the bacterium but also provided easy access to the P450cam enzyme and related monooxygenase components. Although the growth sequence described in Section III.2 provided the most reliable method for obtaining large amounts of the bacteria, and in turn the monooxygenase components, problems were initially encountered in obtaining a smooth progression in bacterial growth from the maintenance stage to harvestable quantities in the 14L fermentors. These problems elucidated several important growth as well as general characteristics of this strain of bacteria.

Early experiments invoked a similar growth sequence to that described in Section III.2.5, except the bacteria were maintained on minimal agar containing glucose, citrate (sodium salt), and l-asparagine as the carbon and energy sources and inocula for the 14L fermentor cultures were started in L-broth medium and developed in a single set of 1.0L shake-flasks, which contained PA solution (500mL), 100 x salts (5mL) and glutamic acid (10mL). Induction of the camphor monooxygenase components

was initiated in the 1.0L shake-flasks at mid-logarithmic growth phase by the addition of 3M camphor in DMF, and the culture allowed to progress to late-logarithmic growth phase (≈7h, see Figure IV.1). The culture, which was assumed to be metabolizing camphor, was then used to inoculate the 14L fermentor media prepared as in Section III.2.5. Rapid initial growth in the 14L fermentors was followed by a period of rapid decline in optical density at 660nm, either ending in complete necrosis of the culture or remaining stationary at an intermediate level (i.e. a lag phase, see Figure IV.2). This drop in optical density was accompanied by accumulation of large amounts of cell debris indicative of cell lysis and death. Growth in the 14L fermentors was not followed for more than 25h. Several experiments were then performed at the shake-flask stage to determine the growth characteristics of the bacterium over extended lengths of time. Results obtained from the experiments showed that the lag phase could last as long as 60h before the bacteria began to actively metabolize the camphor substrate, but more commonly, the lag times ranged from 20-40h (Figure IV.3). All growth curves obtained were characterized by the same distinct profile as that indicated in Figure IV.3; an initial rapid growth phase eventually gave way to a larger secondary growth phase attributed to the utilization of camphor. Active camphor metabolism was recognized by a marked increase in optical density of the medium following the lag period, production of a distinct odour peculiar to the camphor-

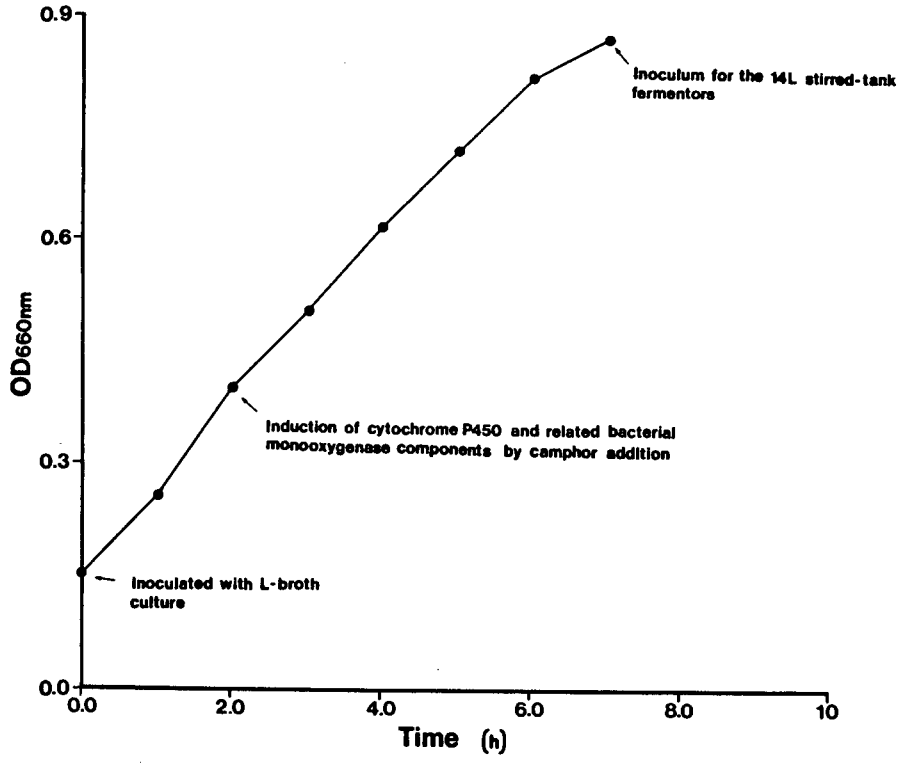


Figure IV.1 Growth of *P. putida*, strain PpG786, at the 1.0L shake-flask stage during early growth experiments.

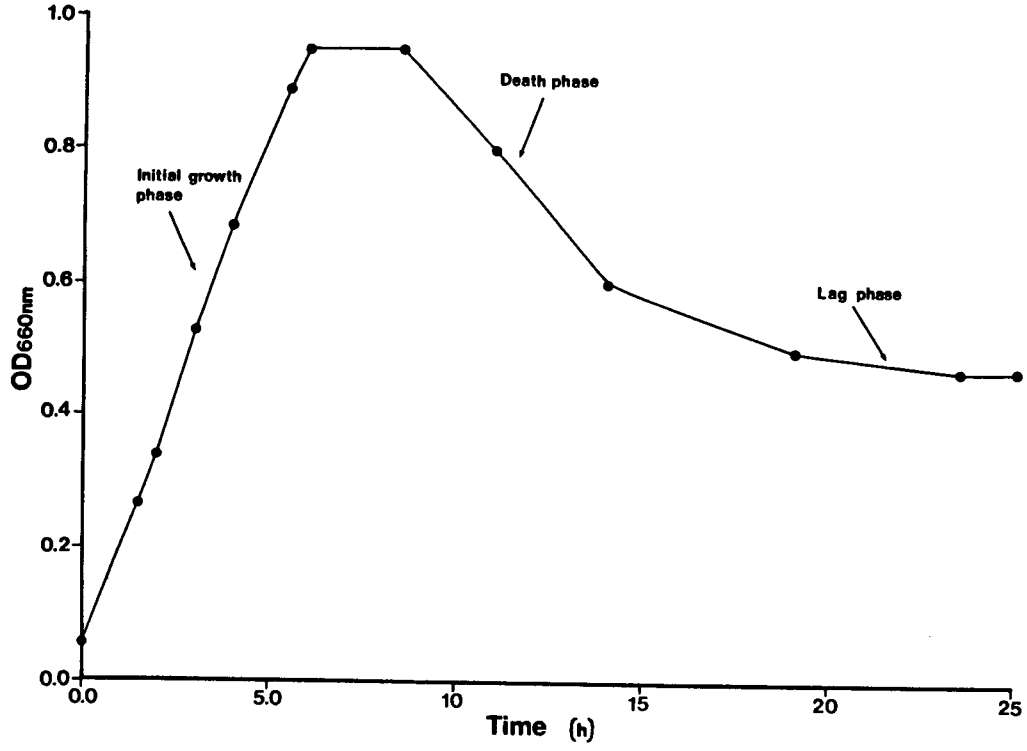


Figure IV.2 Growth of *P. putida*, strain PpG786, at the 14L fermentor stage during early growth experiments.

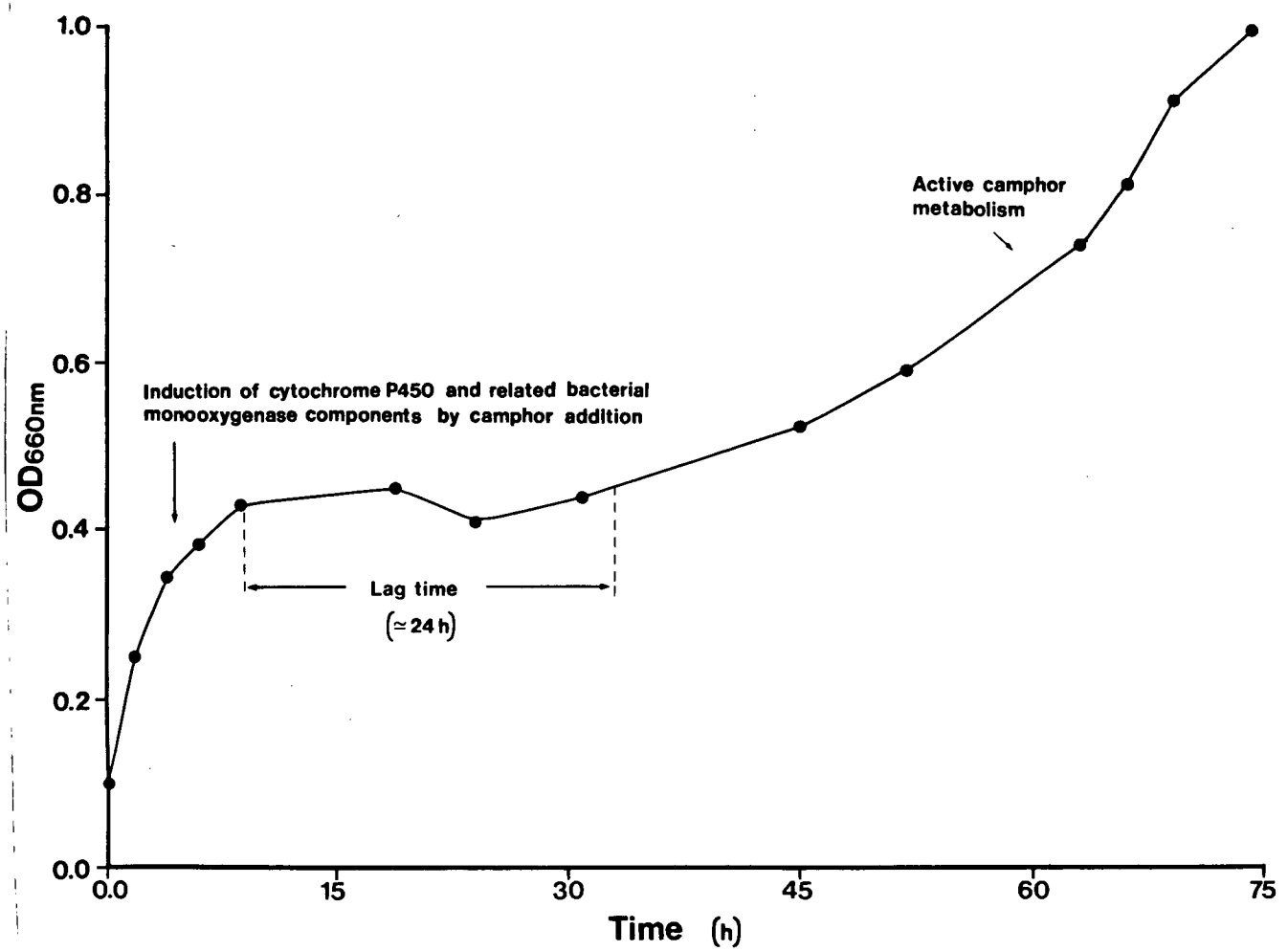


Figure IV.3 Growth characteristics of *P. putida*, strain PpG786, over extended lengths of time in shake-flask media.

metabolizing bacteria, and the accumulation of pinkish-colored bacteria (due to high cytochrome P450cam content).[37] As well, distinct trends in pH of the medium were ascribed to bacterial metabolism of camphor *vs*. the simpler organic substrates such as glucose and glutamate. Growth on glucose and glutamic acid, such as at the L-broth stage and initial growth in the 1.0L shake-flasks (see Figures III.7 and IV.1, respectively), was accompanied by an increase in pH of the medium while camphor-metabolism was associated with a gradual decrease in pH (Figure III.9). A rationale for the observed trends in pH is difficult without closer examination of metabolites and changes in medium composition; however, the decrease in pH of the medium during camphor metabolism is known to be due to the accumulation of organic acid metabolites of camphor degradation by *P. putida*.[158,159]

Following these experiments, the growth sequence was modified to that described in Section III.2. Active camphor-metabolizing bacteria were plated on minimal agar containing camphor as the only carbon and energy source (see Section III.2.4.1) and a second set of shake-flasks, containing only PA solution and camphor (see Section III.2.5), was included. The size of the shake-flask containers and the volume of media were reduced to promote better aeration of the media (see Section III.2.5). These changes ensured that the shake-flask inoculum for the 14L fermentor medium was actively metabolizing camphor. Subsequent results showed growth in the first set of 500mL shake-flasks followed the same biphasic nature as

observed previously in the 1.0L shake-flasks (Figure IV.3), except the lag time was shortened (6-12h, see Figure III.8). Inoculum for the second set of 500mL shake-flasks was obtained therefore following established growth on camphor in the first set of shake-flasks (≈25h). Near logarithmic growth on camphor was then observed reproducibly in the second shake-flask cultures as well as in the 14L fermentor media (Figures III.9 and III.10). These experiments formed the basis of the bacterial growth procedure described in Section III.2.

The biphasic nature of the growth curve observed during the growth of *P. putida*, strain PpG 786, (Figure III.8) is called diauxie[160] and is a common phenomena exhibited by growing bacteria. Under certain circumstances, the adaptive response of a growing culture to an added substrate may be blocked by the presence of a more favoured substrate, that supports faster growth. The mechanism, which promotes metabolic economy, was first discovered in 1940 by Kluyver[160] but the most classic example was reported in 1942 by Monod[160] for growth of *Escherichia coli* on glucose and sorbitol. In this case *E. coli* consumed the glucose first and then, after a short lag period, resumed growth on sorbitol. Further analysis showed that glucose repressed the induction of the enzymes and membrane transport systems required for the utilization of sorbitol. This diauxic growth behavior exhibited by *E. coli* was manifested in a biphasic growth curve similar to that observed for growth of *P. putida*, strain PpG 786, in the presence of glutamic acid and camphor (Figure III.8, see Section III.2.5). The initial growth phase

of Figure III.8 can be attributed to utilization of glutamic acid since this was the only carbon source present in the medium prior to induction of the camphor monooxygenase components. As well, analysis of Figure III.8 and IV.1 indicates that the initial growth rate (i.e. initial slope of the growth curve) was unaffected by the addition of camphor and was much faster than the growth rate on camphor alone (Figure III.10). This behavior seems reasonable by analogy to the *E. coli* system, since the simple carbon source, glutamic acid, would likely be utilized before the complex camphor molecule as well as be favourable for faster growth. Whether or not glutamic acid metabolism represses the utilization of camphor would involve a more detailed investigation into the growth characteristics of *P. putida*, strain PpG 786. The observed growth profile in Figure III.8 may be in fact the resultant of two superimposed growth curves; one for initial growth of glutamic acid and the other for slower growth on camphor. It should be noted that diauxic growth curves such as these have been reported by Gunsalus *et al.*[159] for growth of *P. putida*, strain PpG 1, (parent strain) on camphor and camphor metabolites; however, the mechanism of the observed diauxic growth was not probed.

Another important feature of the growth curves for *P. putida*, strain PpG 786, is the lag period between the initial growth phase and established growth on camphor. Lag periods of up to 60h are probably not due entirely to the physiological changes required for camphor metabolism but to the selection and propagation of those bacteria capable of metabolizing

camphor. This feature of the growth curves for *P. putida*, strain Ppg 786, on camphor exemplifies some important characteristics of this microbe.

The Pseudomonas family of bacteria are known to have the ability to utilize an extremely wide variety of carbon substrates as their sole energy source. More specifically, *P. putida*, strain PpG 786, classified as Biotype A according to the nutritional characteristics outlined by Stanier *et al.*,[161] has the ability to metabolize and grow on a complex organic substrate such as D-(+)-camphor as well as 80-100 other carbon sources. Much of this observed metabolic diversity and adaptability has been attributed to the presence of plasmids,[5,6] which are small circular molecules of extra chromosomal double-stranded DNA found in the cytoplasm of the bacterial cell. These plasmids, which represent only a small fraction of the cell's genome (1-3%), code for important accessory genetic traits that are not ordinarily encoded by the bacterial chromosomes. The traits, which are manifested as active enzymes synthesized by the cell's metabolic machinery, are usually crucial for the adaptation of the bacterium to its environment. In *P. putida* the ability to adapt to growth on camphor as the sole carbon and energy source is mediated by the "CAM-plasmid", which specifically codes for the production of the cytochrome P450cam monooxygenase system as well as several other enzymes involved in the camphor oxidation pathway.[162] In general, however, the plasmids are not essential to the everyday metabolism of the bacterial host

and can be lost or gained without harm to the cell. Furthermore, under conditions which do not involve the use of the plasmid genes, it is possible to isolate a variant bacterium that no longer has the plasmid; once the plasmid is lost it cannot be regenerated by the cell and therefore this genetic information can be partially or totally lost from an isolated bacterial population.[163] Partial loss of the "CAM-plasmid" from *P. putida* during storage could account for the extended lag periods observed during the early growth experiments. Prolonged storage on minimal agar containing only simple carbons sources such as glucose, citrate, or ℓ-asparigine, would promote selection of those bacteria without the "CAM-plasmid" since the plasmid genes would not specifically be utilized. Bi-monthly replating of the bacteria would speed the selection process. Subsequent growth in media containing glucose or glutamic acid would be expected to be logarithmic, predominantly in those bacteria without the plasmid, even after the additions of camphor. However, once the simple carbon sources were exhausted the initial rapid growth phase would be expected to give way to rapid decline in cell number and death to the bacteria without the "CAM-plasmid". The long lag times observed then could be attributed to the selection and propagation of the percentage of the bacterial population that still contained the genetic information for camphor metabolism. The fact that growth in some cultures stopped completely indicated that the "CAM-plasmid" could have been almost entirely eliminated from the population. Although this hypothesis

cannot be proven without further investigation into the growth characteristic of *P. putida*, strain PpG 786, it serves to point out that the bacteria must be maintained on minimal agar containing camphor as the only carbon source. As might be expected, the bacteria do not grow quite as well under these conditions; however, maintainence on camphor will allow for the most rapid access to the bacteria and in turn to the cytochrome P450 monooxygenase enzyme components.

IV.2 Properties of Cytochrome P450cam and Related Monooxygenase Components

IV.2.1 Putidaredoxin Reductase

IV.2.1.1 Spectral Analysis

The absorption spectra of various oxidation states of putidarexodin reductase, isolated and purified as in Section III.3, are given in Figure IV.4. The spectrum of the oxidized protein exhibited a strong protein absorption at 272nm together with weaker absorptions at 370, 414, 470, 530 and 570nm. Reduction of the yellow protein solution with $Na_2S_2O_4$ under anaerobic conditions produced an essentially colorless solution with a small absorption maxima at 411nm. Addition of carbon monoxide did not visibly affect the color of the solution but resulted in the formation of two new peaks at 418 and 444nm. The absorption peak at 444nm suggested that the purified putidaredoxin reductase contained a cytochrome P450cam impurity. Analysis of the oxidized and reduced spectra as well indicated that the impurity was the substrate-free cytochrome. Figure IV.5 shows a reported absorption spectrum of purified putidaredoxin reductase and Table IV.1 gives literature absorbance data for both the reductase and substrate-free cytochrome P450cam. Although the strong absorption peak at 272nm as well as the weak absorption at 470nm were indicative of the reductase enzyme, the other more characteristic peaks (i.e. 378 and 454nm) were presumably lost under the strong cytochrome absorptions in these regions.

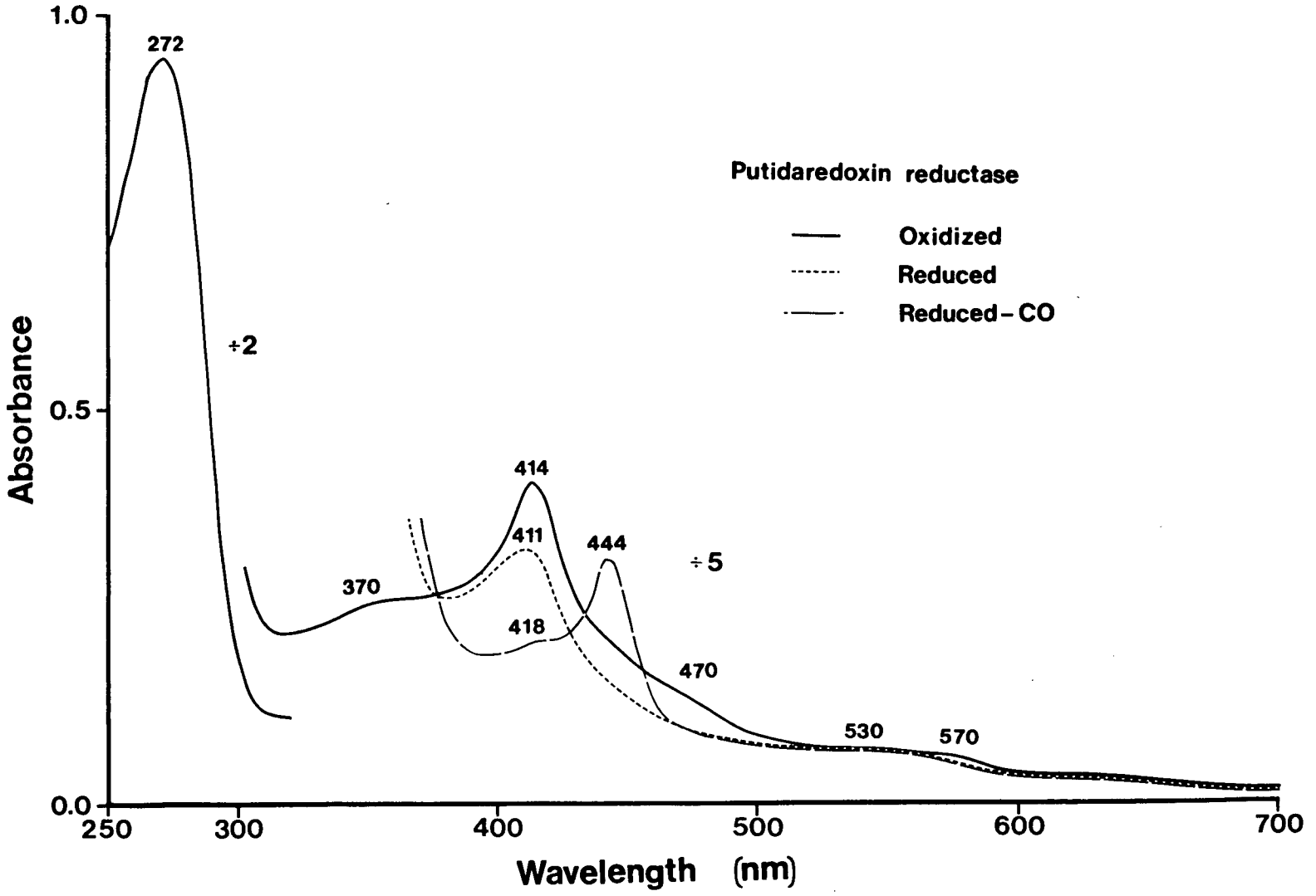


Figure IV.4 Absorption spectra of putidaredoxin reductase isolated and purified as in Section III 3.

Table IV.1

Absorbance Data for Putidaredoxin reductase and Substrate-free Cytochrome P450cam

Form	(a) Cytochrome P450cam (substrate-free)		(b) Putidaredoxin reductase	
	λ_{nm}	ε_{mM}	λ_{nm}	ε_{mM}
Oxidized	280	68.3	275	72
	360	36.7	378	9.7
	417	115	454	10.0
	535	11.6	480	8.5
	569	11.9		
Reduced	408	76.7		
	540	15.1		
Reduced-CO	447	121		
	550	14.3		

a) Ref.37

b) Ref.30

Incorporation of the impurity in the putidaredoxin reductase preparations was unexpected since the flavoprotein was isolated as a distinct yellow solution apparently free of brown putidaredoxin and red cytochrome P450cam. As well, all attempts to isolate the flavoprotein using the procedure described in Section III.3 resulted in the incorporation of the same cytochrome P450cam impurity in each purified protein sample. Further purification of the reductase protein was attempted using careful $(NH_4)_2SO_4$ fractionation and Sephadex G-100 chromatography (1.3 x 100cm); however, the similarity in molecular weights of these two proteins (putidaredoxin reductase, 45,000 Daltons; cytochrome P450cam, 47,000 Daltons[37]) prevented removal of the cytochrome contaminant. The inability to isolate contaminant-free putidaredoxin reductase using the described procedures (Section III.3) shows that complete separation on the Whatman DE-52 cellulose anion exchange resin did not occur. Even though the protein appeared to elute as a separate band, residual cytochrome P450cam enzyme trailing behind the major cytochrome band must have been eluted along with the flavoprotein. These results emphasize the importance of the precise preparation of the anion exchange resin and buffer solutions for the initial separation of the protein components. Small inconsistencies in the pH of the buffer solutions, as well as improper degassing of the anion exchange resin, promote the formation of diffuse protein bands rather than narrow

concentrated bands and make it difficult to obtain discrete separation of the protein components. Complete separation could be enhanced presumably with the use of larger bed-volumes of the anion exchange resin; however, modification of the eluting buffer systems would probably be more effective. The rate of separation of the protein components, *via* increased ionic strength of the buffer, must be slowed down to allow for more complete separation. Replacement of buffer T-100, used to promote the initial protein separation on Column A, with buffer T or T-50 would provide a much smaller increase in ionic strength and possibly a greater control of the initial separation of putidaredoxin reductase and cytochrome P450cam. The isolation of pure putidaredoxin reductase requires modification of the present procedure and may involve the development of a completely different isolation procedure such as that reported by Gunsalus and Wagner.[37]

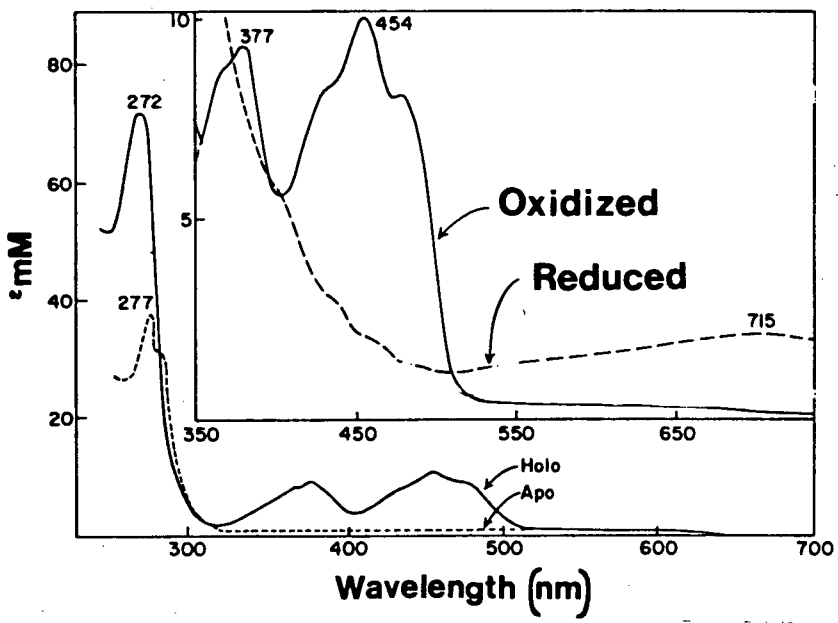


Figure IV.5 Absorption spectra of purified putidaredoxin reductase; Ref.30.

IV.2.2 Putidaredoxin

IV.2.2.1 Spectral Analysis

The absorption spectra of various oxidation states of putidaredoxin isolated and purified as described in Section III.3 are given in Figure IV.6. The spectrum of the oxidized $Fe_2S_2Cys_4$ iron-sulphur protein (Fe(III)-Fe(III)) showed a strong protein absorption at 276nm followed by the characteristic weaker peaks of the prosthetic group at 324, 412 and 454nm. Sodium dithionite reduction of the brown protein solution under anaerobic conditions converted one of the iron atoms to the ferrous state (Fe(II)-Fe(III)) with a bleaching of the absorption fairly uniformly above 500nm.[30] Formation of a faint pink solution accompanies the reduction process as well as the formation of a residualmaximum at 550nm. Flushing the solution with carbon monoxide produced no observable changes in the reduced spectrum. The experimentally determined absorbance data are shown in Table IV.2 along with those reported in the literature. The experimentally determined values are in excellent agreement with the literature values.

IV.2.2.2 Purity

The iron-sulphur protein was approximately 95% homogeneous (see Section III.3.4.2) and contained negligible contamination by the cytochrome P450cam or putidaredoxin reductase proteins. The absorption ratio of $A_{454}/A_{276} = 0.42$ is comparable to the homogeneous preparations reported in the literature: 0.30,[35] 0.43,[30] 0.44.[37]

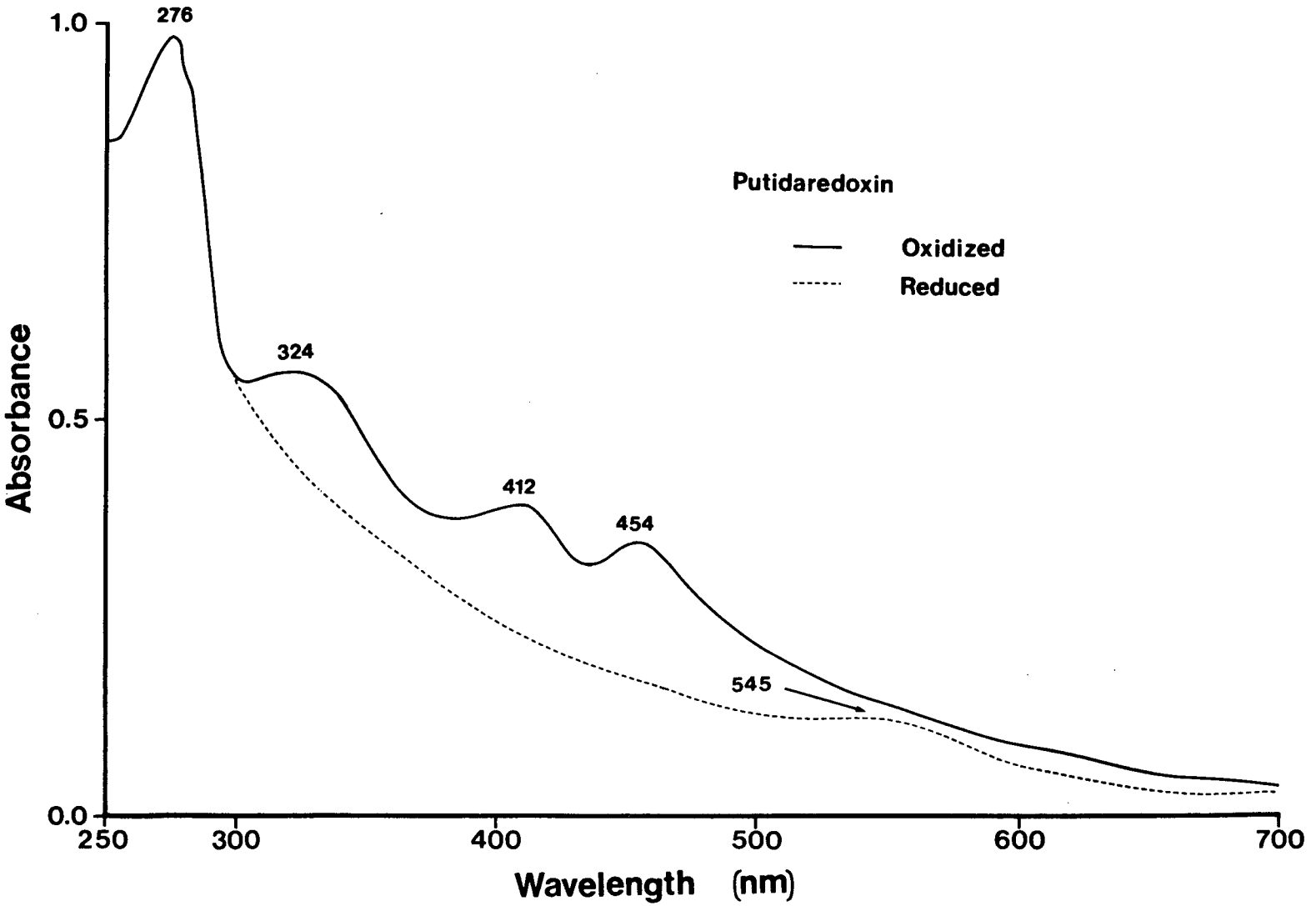


Figure IV.6 Absorption spectra of various states of putidaredoxin isolated and purified as in Section III.3.

Table IV.2

Absorbance Data[a] for Putidaredoxin

Form	(b) Experimental Preparation		(c) Literature Preparation		(d) Literature Preparation	
	λ_{nm}	ε_{mM}	λ_{nm}	ε_{mM}	λ_{nm}	ε_{mM}
Oxidized (Fe^{3+}-Fe^{3+})	276	24.6	280	22.5	275	23.6
	324	15.6	325	15.0	325	15.6
	412	11.0	415	10.0	415	11.1
	454	10.3	455	9.6	455	10.4
Reduced (Fe^{2+}-Fe^{3+})	545	4.0	545	5.0		

a) The experimental absorbance data listed above were averaged over three samples of putidaredoxin, estimated error 5%.

b) Determined in buffer P-100, pH 7.0, at room temperature ($23\pm2^{o}C$) using published millimolar extinction coefficient data for oxidized putidaredoxin at 455nm, ε_{mM} = 10.4; Ref.37.

c) Ref. 30.

d) Ref. 37.

IV.2.2.3 Stability

The purified protein was stable for about 1 month when stored at -78°C under argon and in the presence of 10mM βME. The original dark brown protein solution gradually turned colorless with no retention of characteristic absorption spectra. At 4°C, decomposition of the protein occurred rapidly producing a colorless solution in ≃1 week.

IV.2.3 Cytochrome P450cam

IV.2.3.1 Spectral Analysis of Substrate-Bound P450cam

The absolute absorbance spectra of various forms of substrate-bound cytochrome P450cam, isolated and purified as in Section III.3, are shown in Figure IV.7. The spectrum of the oxidized cytochrome exhibited a protein absorption at 280nm and absorptions of the heme-prosthetic group at 391 and 643nm. Less well-defined absorptions of the heme-group are evident at 510 and 540nm. This ferric substrate-bound state of the enzyme is associated with a high-spin configuration of the heme-iron.[105] Stoichiometric dithionite addition to the brown protein solution under anaerobic conditions resulted in the one-electron reduction of the heme-iron with concomitant formation of a pink solution with absorption maxima at 408 and 544nm. The small absorption at 314nm was indicative of a slight excess of dithionite. Purging $Na_2S_2O_4$-reduced solution with CO intensified the pink color and resulted in the formation of the carbon monoxide complex with the characteristic Soret absorption maximum at 445nm. As well, the high energy Soret maxima in the near-UV region and weaker absorption peaks in the 500-600nm region were located at 365 and 550nm, respectively. The absorbance data obtained experimentally are given in Table IV.3 along with absorbance data reported from the literature. Comparison of the data indicates that those determined experimentally are in excellent agreement, within experimental error, with the literature values.[37,33b]

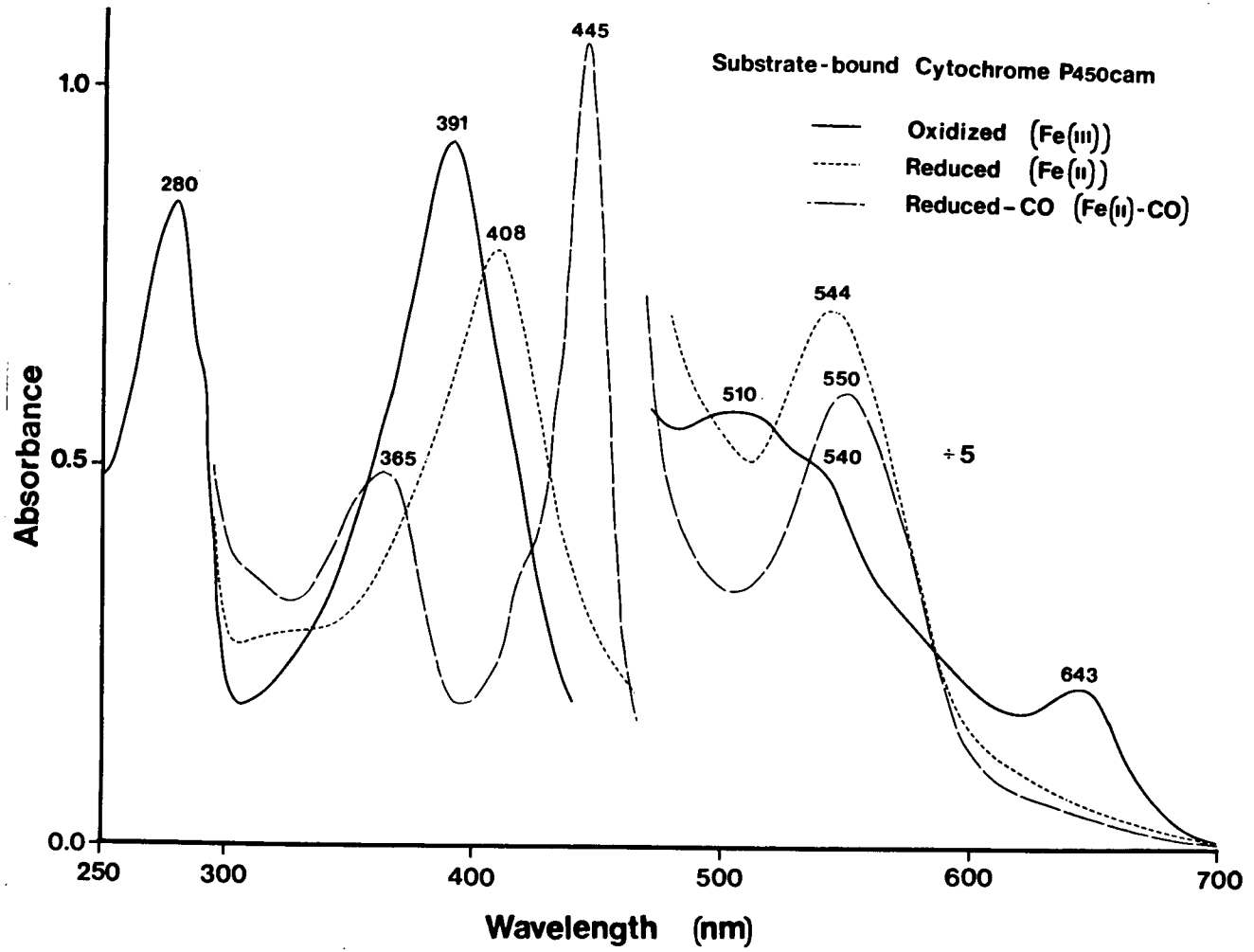


Figure IV.7 Absorption spectra of various states of substrate-bound cytochrome P450cam isolated and purified as in Section III.3

Table IV.3

Absorbance Data[a] for Substrate-bound Cytochrome P450cam

Form	(b) Experimental Preparation		(c) Literature Preparation		(d) Literature Preparation	
	λ_{nm}	ε_{mM}	λ_{nm}	ε_{mM}	λ_{nm}	ε_{mM}
Oxidized	280	91.1			280	63.3
	391	101	391	101	391	102
	510	13.0	510		510	13.0
	540	11.3	540		540	11.2
	643	4.6	645	5.0	645	5.4
Reduced	408	86.3	408	83	408	86.5
	544	15.9	542	15.2	542	16.0
Reduced-CO	365	56.1			364	60.8
	445	120	446	119	446	120
	550	14.0	550	13.0	550	14.0

a) Averaged over three sets of data; estimated error 5%

b) Determined in buffer P-100, pH 7.0, ≈8mM camphor at room temperature (23±2°C). Data determined using published millimolar extinction coefficients at 446nm,[37] ε_{mM} = 120.

c) Ref. 33b.

d) Data quoted for precrystalline cytochrome samples, Ref. 37.

The most notable differences amongst the data are found in the extinction coefficient values of the protein absorption at 280nm, the 645nm peak and the near-UV peak at 365nm of the ferrous-CO complex. Discrepancies in εmM values for the protein absorbance are due to the presence in the experimental cytochrome preparations of residual apo-cytochrome P450cam that represents a common artifact of the enzyme isolation procedure. Values obtained for precrystalline enzyme samples (Table IV.3) exhibit much lower ε_{mM} values for the protein absorbance (ε_{mM}^{280} = 63.3) due to total elimination of the apoprotein which requires subsequent gel filtration and anion exchange chromatographic steps, as outlined by Gunsalus and Wagner.[37] The millimolar extinction coefficients for the 645 and 365nm peaks were found to be consistently low in all enzyme preparations and again seem to be an artifact of the isolation and purification procedure described in Section III.3.

IV.2.3.2 Spectral Analysis of Substrate-Free P450cam

Figure IV.8 shows the unusual bathochromic (red) shift of the Soret maximum of substrate-bound cytochrome P450cam upon removal of the camphor-substrate. Camphor was removed by chromatography at 5°C on a Sephadex G-10 (1x20 cm) column with buffer P-100, pH 7.0, not containing camphor. The Soret maximum at 391nm was red-shifted by 25nm to 416nm upon removal of substrate to yield the spectrum of the oxidized resting enzyme. The removal of substrate was also accompanied by the formation of distinct α and β absorption peaks at 570 and

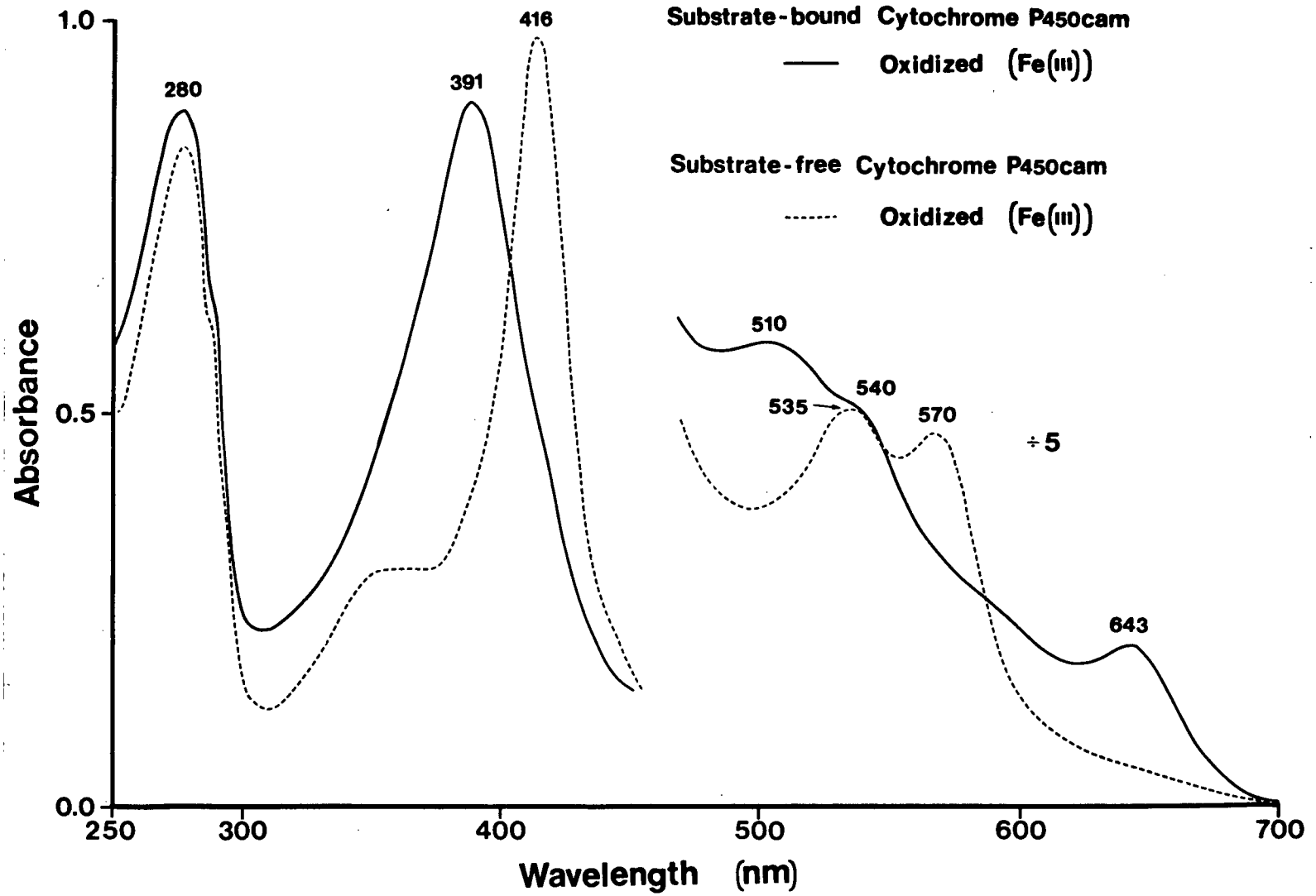


Figure IV.8 Absorption spectra of the ferric state of substrate-bound (----) and substrate-free (———) cytochrome P450cam.

535nm, respectively. These spectral changes are associated with a spin-state conversion at the heme-iron center[105] from high-spin (substrate-bound, S=5/2) to low-spin (substrate-free, S=½) Addition of a few crystals of solid camphor regenerates the high-spin substrate-bound form with the Soret maximum at 391nm.

Figure IV.9 shows the absorption spectra of the various forms of substrate-free cytochrome P450cam. That of the oxidized cytochrome in the absence of camphor has absorption maxima at 280, 416, 535 and 570nm while subsequent $Na_2S_2O_4$ reduction yielded a spectrum very similar to that of the ferrous substrate-bound enzyme (Figure IV.7), although the peak at 408 and 540nm were characterized by lower intensities (see Table IV.4). The spectrum of the carbon monoxide complex was identical to that of the reduced-CO complex of the substrate-bound enzyme with maxima at 365, 445 and 550nm. Table IV.4 lists typical absorbance data determined experimentally for various forms of substrate-free cytochrome P450cam along with literature data;[33b,37] agreement is excellent. It is important to note at this point that the reduced substrate-free enzyme binds camphor very strongly.[33b] Camphor-binding during $Na_2S_2O_4$-reduction of the enzyme often led to extinction coefficients at 408nm that were closer to those of the reduced substrate-bound enzyme (see Table IV.3). Care was taken to avoid incorporation of camphor during preparation of the substrate-free enzyme solution; since the spectra of the reduced-CO complexes of both the substrate-free and substrate-bound

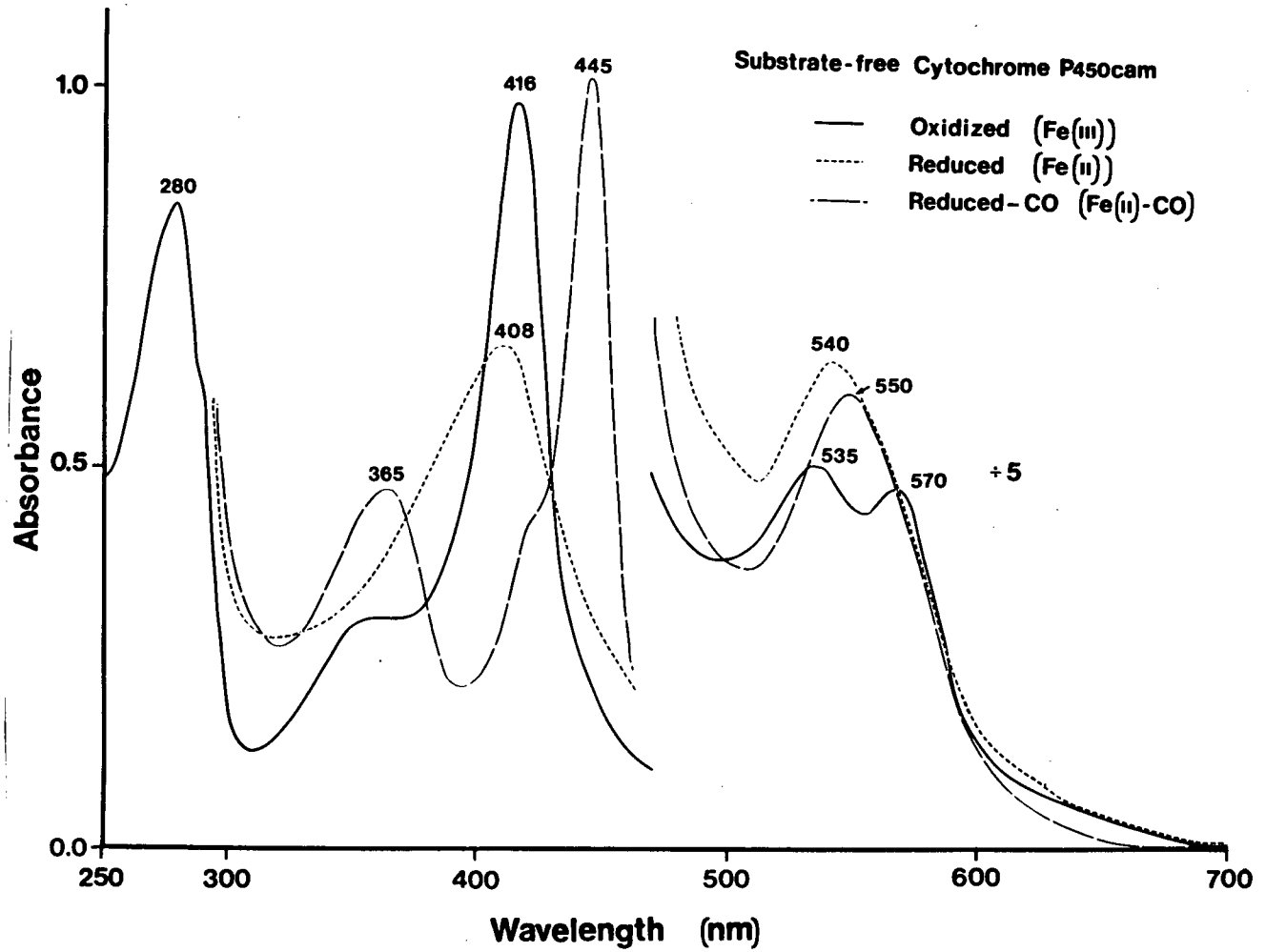


Figure IV.9 Absorption spectra of various states of substrate-free cytochrome P450cam.

Table IV.4

Absorbance Data[a] for Substrate-free Cytochrome P450cam

Form	Experimental Preparation		(b) Literature Preparation		(c) Literature Preparation	
	λ_{nm}	ε_{mM}	λ_{nm}	ε_{mM}	λ_{nm}	ε_{mM}
Oxidized	279	96.5			280	68.3
	360	34.2			360	36.7
	416	116	418	104	417	115
	535	11.8	535	10.3	535	11.6
	568	11.2	570	10.4	569	11.9
Reduced	408	76.5	408	69	408	76.7
	542	15.2	540	13.5	540	15.1
Reduced-CO	365	54.6				
	445	119	447	104	447	120
	550	14.1	550	12.1	550	14.3

a) Determined in buffer P-100, pH 7.0, at room temperature ($23\pm2^{o}C$) using published millimolar extinction coefficient data for ferrous-CO, substrate-free cytochrome P450cam at 445nm; $\varepsilon_{mM} = 120$; Ref. 37. Estimated error 5%.

b) Ref. 33b.

c) Ref. 37.

enzymes were identical, there was no way of determining the extent of substrate binding once the CO-adducts were formed. Close examination of the published extinction coefficients of the bands in the 500-600nm region for the oxidized substrate-free cytochrome reveals that the α-band should be slightly more intense than the β-absorption band. This trend, however, was reversed for all experimental preparations in the present work and can be attributed to an artifact of cytochrome P450cam as isolated and purified according to Section III.3.

IV.2.3.3 Purity

Substrate-bound cytochrome P450cam, isolated and purified as in Section III.3, provided the most convenient form of the enzyme to assay the purity of the experimental preparations (see Section III.3.4.2). The deep-red enzyme solution was approximately 80% homogeneous and contained negligible contamination by putidaredoxin reductase and putidaredoxin. The absorption ratio of A391/A280 = 1.13 is comparable to those of other cytochrome P450cam preparations reported in the literature : 1.0,[33b] 1.37,[87] 1.45.[37]

IV.2.3.4 Stability

The stability of the purified cytochrome P450cam enzymes is dependent on the potassium ion concentration and on the absence or presence of camphor.[47] In the presence of 100mM

K^+ and ≃8mM camphor the substrate-bound enzyme preparations could be stored anaerobically at 5°C for at least six months with no apparent loss of the observed spectral characteristics (Figure IV.7). However, at $[K^+] \leq 100$mM and in the absence of camphor the enzyme degraded in about one month at 5°C to yield large amounts of cytochrome P420, the process being accompanied by protein precipitation. The importance of potassium ions and camphor to the stability of the enzyme was emphasized during early purification experiments which invoked buffers containing 20-50mM K^+ and no camphor. Figure IV.10 shows the spectra of the various forms of the substrate-free cytochrome, purified according to Section III.3.3.1 using buffer T containing 20mM KCl and buffer P on Column 1 and Column 2, respectively. The spectrum of the oxidized form of the enzyme is not markedly different from that of the camphor-free form in the presence of 100mM potassium ions shown in Figure IV.9; however, $Na_2S_2O_4$-reduction of the cytochrome P450cam solution in the absence of dioxygen results in a distinct spectrum quite different from that of reduced substrate-free P450cam shown in Figure IV.9. Figure IV.10 shows Soret maxima of the reduced cytochrome at 414 and 441nm and prominent α and β absorption maxima at 565 and 536nm, respectively. Adding CO produced the expected hyper-spectrum with absorbance maxima at 365, and 445nm, and caused coalescence of the distinct α and β bands to yield a maximum at 548nm. There was also a prominent absorption maximum at 420nm of the reduced-CO complex, which represents cytochrome P420, a degraded form of cytochrome P450. The enzyme samples isolated

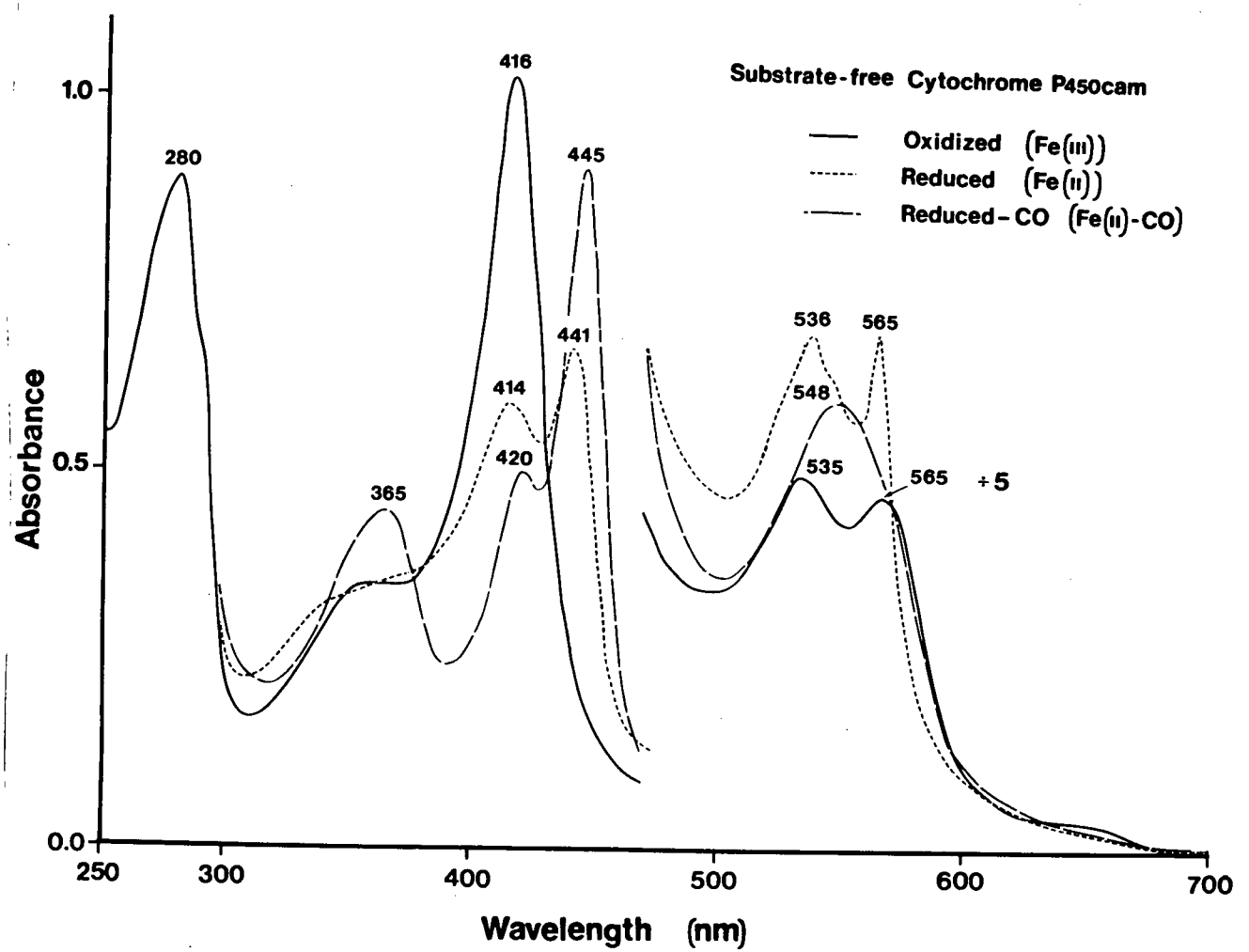


Figure IV.10 Cytochrome P450cam purified in the presence of 20-50mM potassium ions and in the absence of substrate.

under these conditions readily degraded further and were generally too unstable for extensive spectroscopic or kinetic measurements. The effects of the $[K^+]$ and camphor on the stability of the enzyme have been reported by Peterson *et al.*[33b] but no explanation has been given. The important results from this information, however, are that manipulations of the enzyme must be done in the presence of 100mM potassium ions, and storage must be in the camphor-bound form.

During the storage period, the P450cam enzyme solutions must be kept strictly anaerobic because the enzyme readily dimerizes in the presence of air.[164] Figure IV.11 shows the absorption spectra of various forms of substrate-bound cytochrome P450cam after prolonged exposure to air. In the oxidized state the spectrum exhibited a Soret peak at 414nm with a well-defined shoulder at 395nm; visible bands appeared at 535, and 565nm while the 645nm peak was indicative of the substrate-bound enzyme. Initially, this spectrum suggested that the enzyme solution was a mixture of substrate-bound and substrate-free cytochrome species (Figure IV.7 and IV.9); however, upon $Na_2S_2O_4$-reduction the spectrum was exclusively that of the substrate-bound ferrous cytochrome P450 enzyme. Absorption maxima were found at 408 and 543nm, with εmM values identical to those quoted in Table IV.3 for the substrate-bound ferrous enzyme. Treatment with carbon monoxide produced the ferrous-CO complex with absorption peaks at 365, 445 and 550nm. The millimolar absorptivities were again

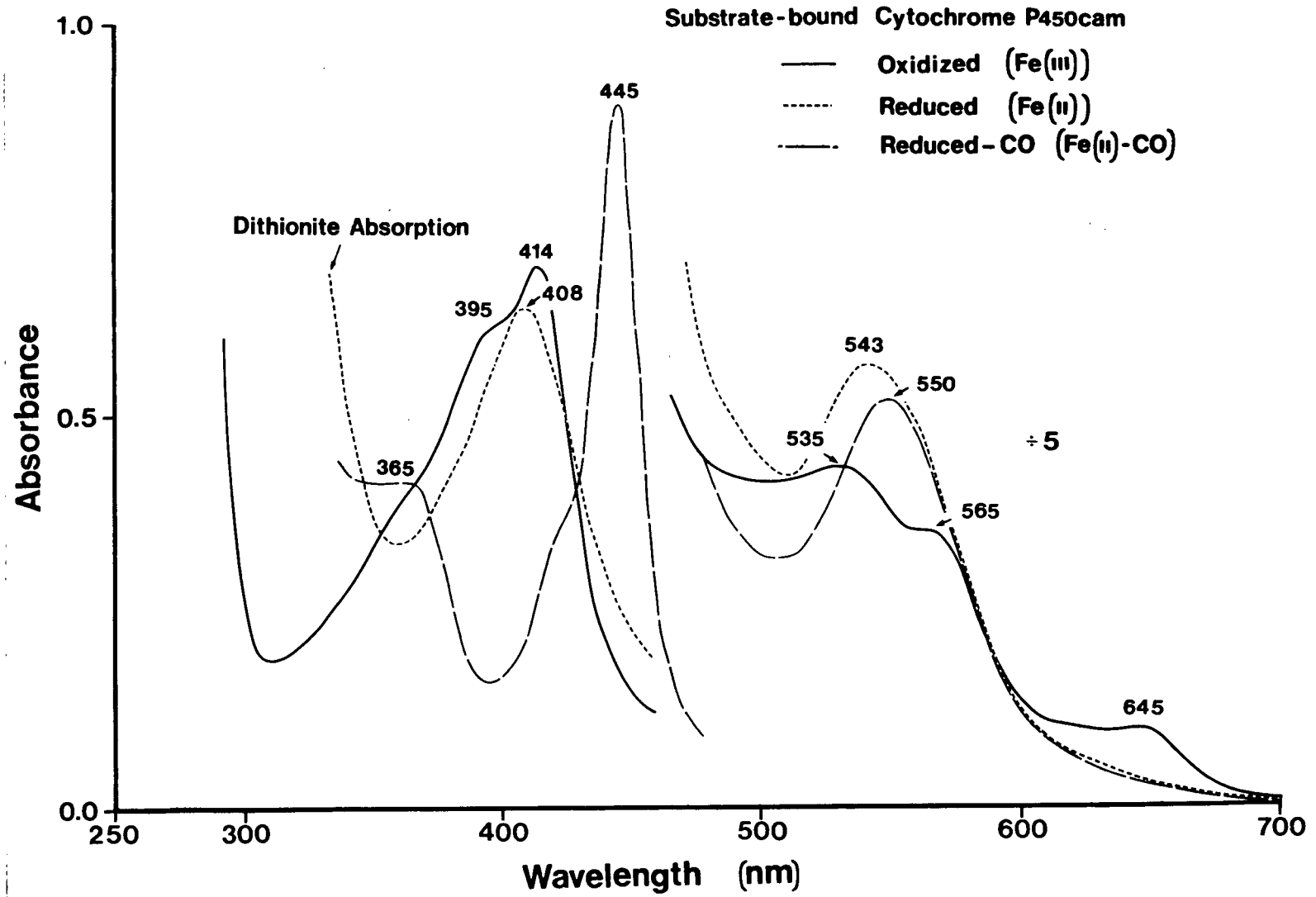


Figure IV.11 Various spectra of partially dimerized substrate-bound cytochrome P450cam.

identical to those quoted in Table IV.3 for the substrate-bound ferrous-CO complex. The lack of a peak at 420nm suggested as well that the peak at 414nm in the oxidized state was not due to some form of degraded enzyme. The formation of the dimeric enzyme complex has been reported[164] and is thought to occur via the slow oxidation of the free-sulphydryl moieties (-SH) to form a disulphide bridge (-S-S-) between the monomeric cytochromes.[164] Reversal of dimerization is accomplished in ≈30min by anaerobic incubation at room temperature with reduced sulphydryl reagents such as dithiothreitol (DTT) lends support to the idea of dimerization through disulphide bridge formation between protein monomers. The disulphide bridges would also be reduced by dithionite and give rise to the expected ferrous and ferrous-CO spectra for the enzyme system.

IV.2.4 Myoglobin

IV.2.4.1 Spectral Analysis

The absorption spectra of various forms of myoglobin are given in Figure IV.12. The spectrum of the oxidized (ferric) state exhibited an aromatic protein absorption at 275nm and major absorption bands of the heme prosthetic group at 408, 505, 540 and 630nm. $Na_2S_2O_4$-reduction of the brown protein solution produced a pink solution with maxima at 370, 434, and 555nm. Gassing the solution with carbon monoxide produced another distinct color change to intense pink-yellow, indicative of the ferrous-CO myoglobin complex. The spectrum exhibited absorption maxima in the near-uv region at 342nm, in the Soret region at 423nm and distinct α and β visible peaks at 578 and 540nm, respectively. Absorbance data for the various forms of myoglobin agree well with the literature values (Table IV.5).

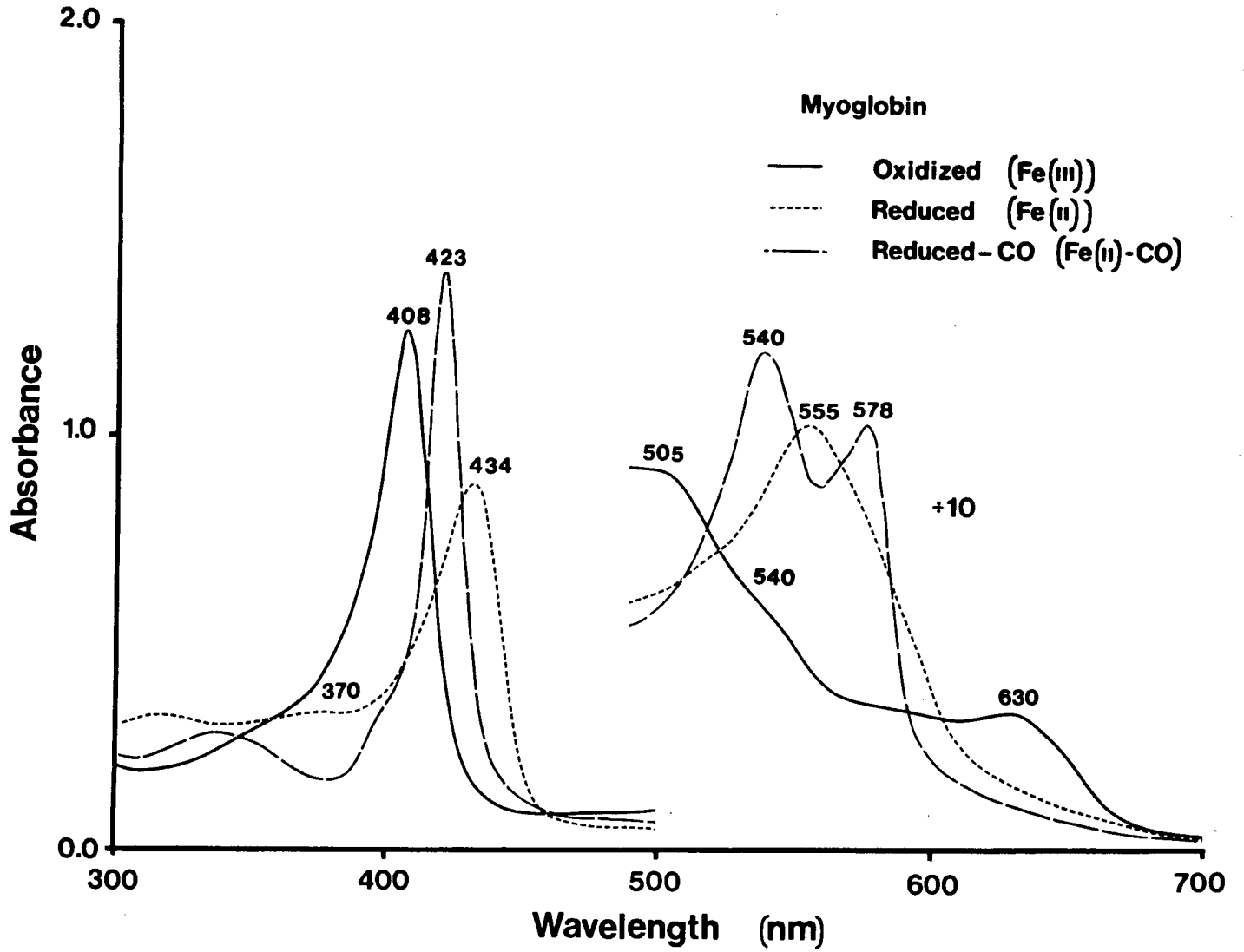


Figure IV.12 Absorption spectra of various states of myoglobin.

Table IV.5

Absorbance Data[a] for the Various Forms of Myoglobin

Form	(b) Experimental		(c) Literature	
	λ_{nm}	ε_{mM}	λ_{nm}	ε_{mM}
Oxidized	275	34.6		
	408	180	408	188
	505	9.98	502	10.2
	630	4.00	630	3.9
Reduced	370	39.7		
	434	130	435	131
	554	12.0	560	13.8
Reduced-CO	342	30.2		
	423	207	424	207
	540	15.7	540	15.4
	578	14.2	579	13.9

a) Averaged over three sets of absorbance data; estimated error, 5%.

b) Determined in buffer P, pH 7.0, at room temperature ($23\pm2^{o}C$) by dilution of stock myoglobin solution of known concentration (see Section III.5.2.1).

c) Ref. 109, p.44.

IV.3 Reconstitution of Cytochrome P450cam with Hemin chloride

Removal and replacement of the heme group of cytochrome P450cam, isolated and purified as in Section III.3, was followed spectrophotometrically by removing small aliquots of the reaction mixture for spectral analysis (see Section III.3.4). Spectrophotometric measurements provided a reliable basis for qualitative examination of reaction intermediates at each stage in the reconstitution procedure and for quantitative calculations where required. Results from a typical reconstitution procedure are described below.

IV.3.1 Apocytochrome P450cam

Apocytochrome P450cam, prepared by the method described in Section III.4.2, was characterized by the absorption spectra given in Figure IV.13. The spectrum of the oxidized apoprotein exhibited only the protein absorption at 280nm and was free of the Soret, the visible and the near-IR absorption maxima indicative of the oxidized ferric state of the heme-prosthetic group (see Section IV.2.3). The spectrum of the apoprotein was unchanged by reduction with $Na_2S_2O_4$, or by $Na_2S_2O_4$-reduction followed by CO addition. Occasionally, however, the spectrum of apocytochrome P450cam prepared by a single acidified-acetone treatment showed a small absorption band in the Soret region (≃400nm) due to incomplete removal of the heme-prosthetic group. This

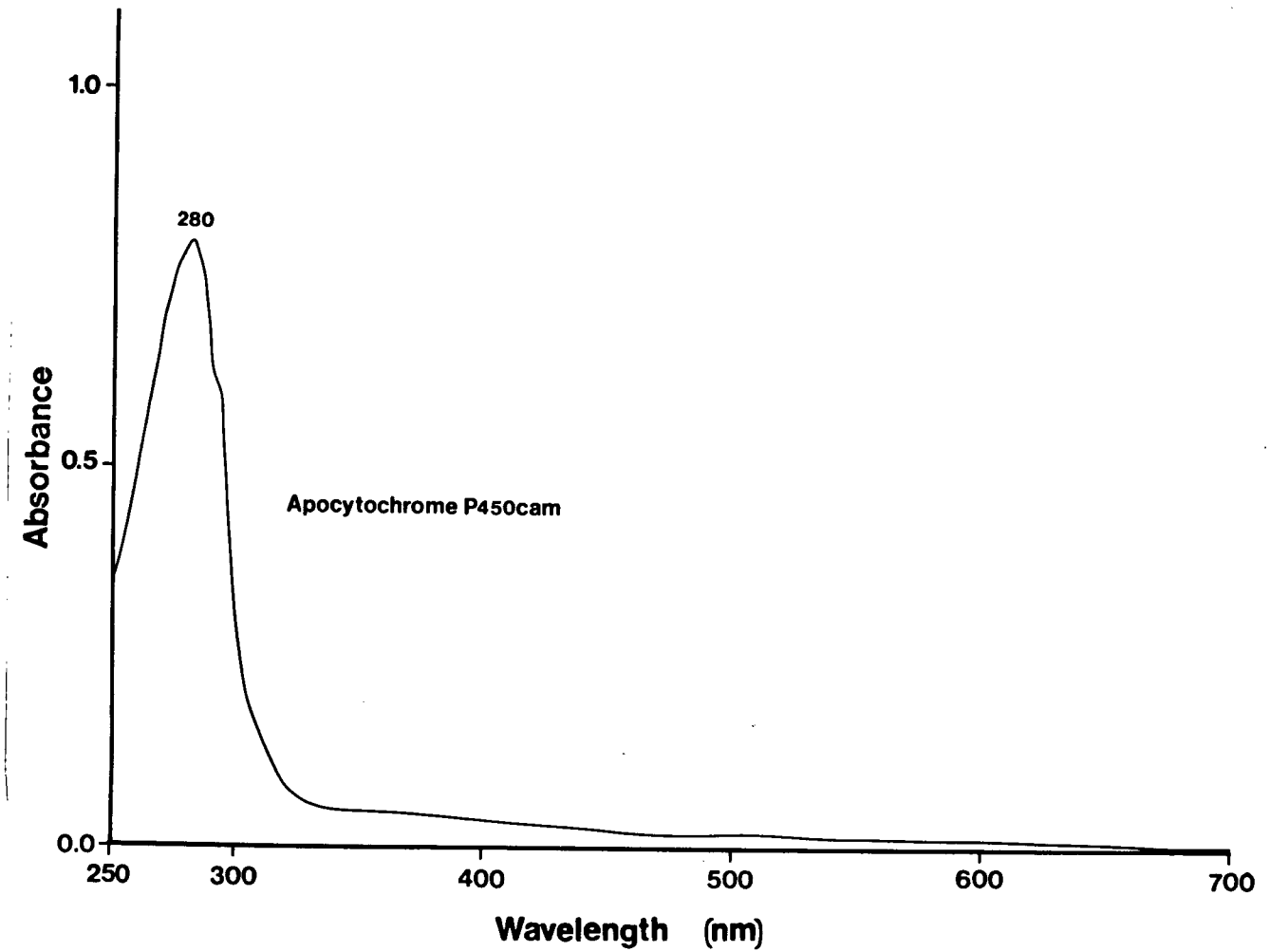


Figure IV.13 Absorption spectra of apocytochrome P450cam.

correlated to a 2-3% residual concentration of the native enzyme as estimated from the small absorption increase at 445nm of the CO adduct of the reduced apoprotein. A second acidified-acetone treatment prior to dissolution of the protein in dilute alkaline solution removed these traces of the heme at the expense of lower overall yields of the apoprotein. The ultraviolet absorption of the apoprotein closely resembled that of native cytochrome P450cam (Figure IV.7) and was attributed to the absorbance of the aromatic tyrosine and tryptophan amino acid residues of the protein polypeptide.[165] Apocytochrome P450cam prepared in this manner was obtained in high yields and could be satisfactorily reconstituted with protohemin chloride to give the identical spectral properties of the parent enzyme.

Although the procedure described in Section III.4.2.1 produced good yields of apocytochrome P450cam in a reconstitutable form, major difficulties were encountered during dissolution of the white protein pellet collected from the acidified acetone solution. The pellet dissolved only reluctantly in the dilute KOH-glycerol solvent system, and required exhaustive trituration and excessive volumes of solvent for subsequent dialysis. Dissolution of the apoprotein was especially difficult for parent enzyme solutions of lower purity (<75% homogeneous, A391/A280 <1.0; see Section III.3.4.2). Addition of up to 40% (v/v) glycerol increased the apoprotein solubility slightly but extensive trituration was still required.

Recently, Wagner *et al.*[165] have found the apoprotein to be soluble in an aqueous histidine-glycerol co-solvent system. In these experiments, heme removal was accomplished *via* the acid-butanone liquid-phase technique of Breslow[151] used for heme-extraction from myoglobin in the present work (Section III.4.4.4). Apocytochrome P450cam prepared by this method was found to have limited solubility in H_2O, 0.1M solutions of neutral potassium phosphate, KCl or His at pH8.0, and 20% (v/v) glycerol. The combination of 20% glycerol and 0.1M His at pH8.0 however, was found to fully solubilize the apoprotein. The distinct advantage of this method[165] was that the protein is solubilized at all times during the heme-extraction process, thus avoiding the difficulties encountered on redissolving the solid apoprotein pellet. Whether the histidine/glycerol system would allow for rapid dissolution of the apoprotein pellet collected from the acidified-acetone extraction process utilized in this study awaits further investigation. The acid-butanone, liquid-phase method was not utilized for the heme-removal step in this study because previous reports[166] suggested that gross denaturation of the apocytochrome accompanied the heme-extraction. Denaturation was thought to be due principally to the low pH value (1.5) needed for heme-removal from cytochrome P450cam; however, addition of histidine ·HCl to the aqueous phase as reported by Wagner *et al.*[165] has created milder conditions for the heme-extraction process (pH2.5)

and has enabled this technique to yield the apoprotein in high yields with little problem of protein denaturation.

IV.3.2 Pyridine Hemochrome of Extracted Heme

Heme extracted from cytochrome P450cam was analysed by silica gel and polyamide TLC and by preparation of the pyridine hemochrome complex, and the data compared with those reported in the literature (see Section III.4.2.2).

Analysis of the spectrum of the pyridine hemochrome complex of the extracted heme from native cytochrome P450cam provided the most reliable method for determining the amount of commercial hemin to be reinserted into the apoprotein. Calculations based on the extinction coefficients of the apoprotein absorbance at 280nm were generally felt to be unreliable because of the ambiguity in the coefficients for the apoprotein prepared in this study (see Section IV.2.3.1). Generally, the amount of heme removed from the native enzyme, plus 10% excess, was added to the apocytochrome solution for reconstitution of the native enzyme (i.e. the heme-replaced to heme-removed ratio equalled 1.1; see Section III.4.3.1).

IV.3.3 Reconstitution of Cytochrome P450cam

Protohemin recombination with apocytochrome P450cam produced initially a precursor(s) to the holoprotein which was characterized in the ferric, ferrous and ferrous-CO states by the absorption spectra shown in Figure IV.14. The spectrum of the protohemin-apocytochrome solution showed a protein absorption at 275nm followed by a broad maximum at 365nm. Dithionite-reduction of this solution produced a broad absorption band (slightly red-shifted) with defined maxima at 380 and 423nm. Spectral changes in the 500-700nm region were not recorded but have been reported in the literature.[148] Treatment of the $Na_2S_2O_4$-reduced solution with carbon monoxide produced the CO-adduct with an intense Soret absorption maximum at 420nm indicative of the P420 cytochromes.[13,14] Comparison of the hemin-apoprotein spectra (Figure IV.14) with those of the protohemin complexes prepared in aqueous buffer (Figure IV.15) indicated the spectral changes that occurred upon interaction of the isolated heme group with the apoprotein. Interaction of the hemin with the apoprotein in the oxidized state (Figure IV.14) produced a slight broadening of the 365nm band (Figure IV.15); in the reduced state, the distinct absorption maxima at 380 and 423nm (Figure IV.14) were generated from a shoulder region around 400nm (Figure IV.15). In the reduced-CO state the Soret maximum of the heme (Figure IV.15) exhibited a 12nm red shift (408 to 420nm) upon addition to the apocytochrome solution. Although not recorded in Figure IV.14, the interaction of the hemin with the apoprotein

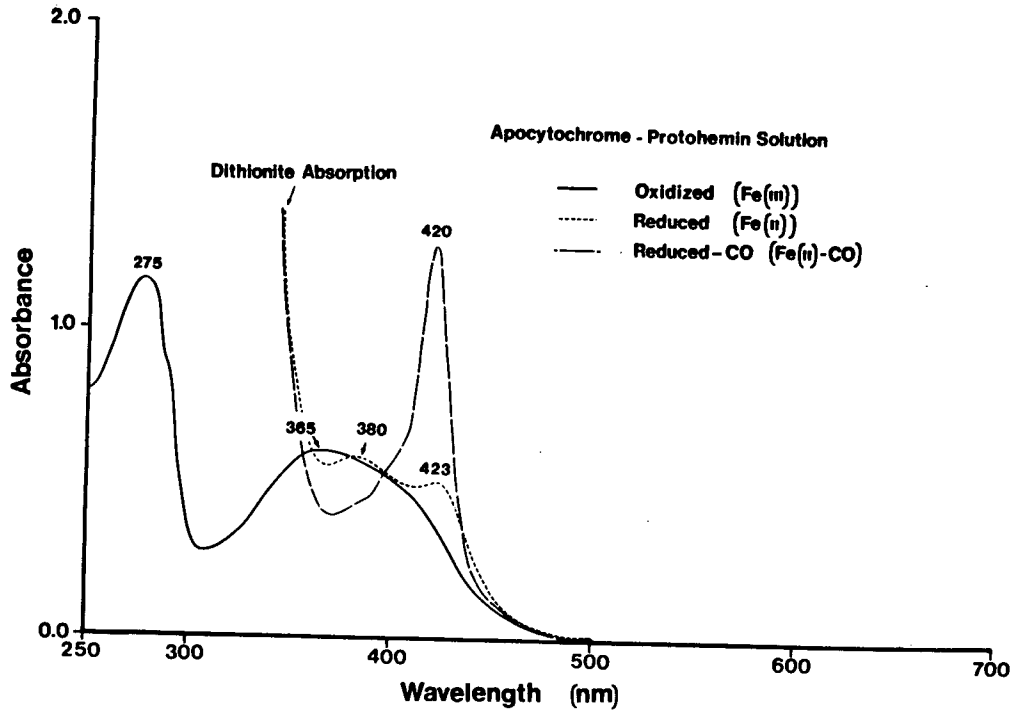


Figure IV.14 Absorption spectra of various states of the protohemin-apocytochrome solution.

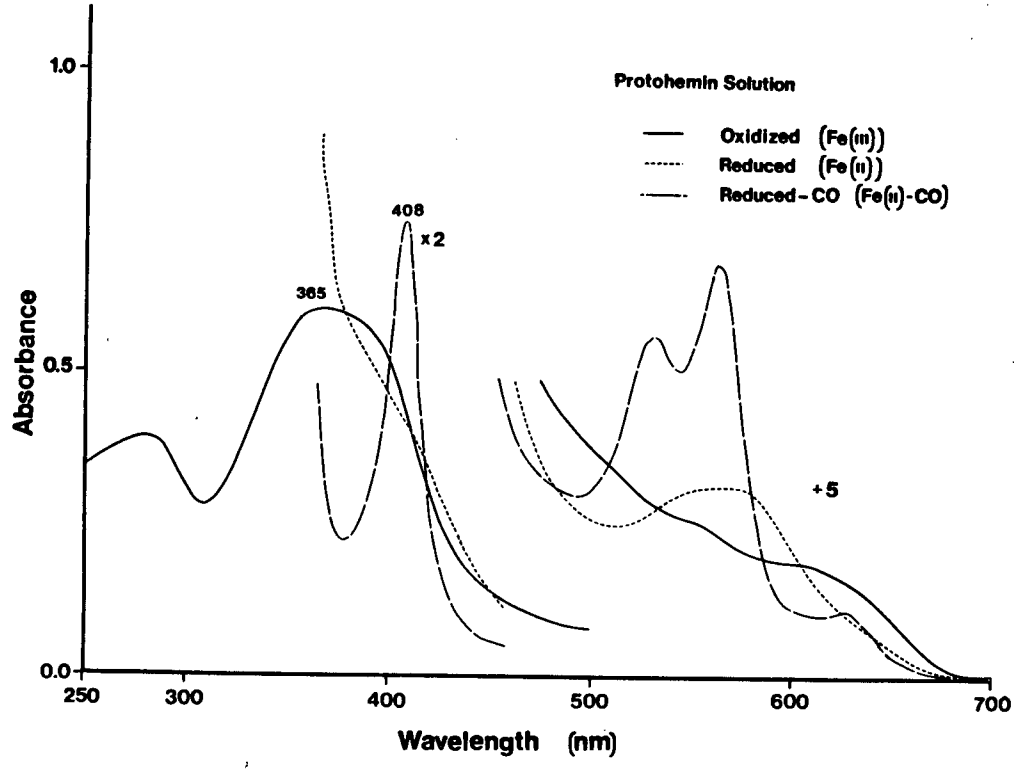


Figure IV.15 Absorption spectra of various states of protohemin in aqueous buffer P at room temperature (23±2°C).

was accompanied also by a coalescence of the distinct α and β bands in the 500-600nm region of the reduced-CO hemin complex (Figure IV.15).[148] Changes in the absorption spectra of the reduced-CO complexes were attributed to changes in axial coordination of the heme moiety upon interaction with the apoprotein, and probably represent several forms of "non-specifically" bound heme. Since the Soret maximum at 420nm is analogous to that of the reduced-CO complex of myoglobin,[109] the P420 precursors may have in fact coordinated imidazole.

Incubation of the heme-apoprotein solution in the presence of camphor and high concentrations of cysteine and glycerol for 6h (see Section III.4.3.1) converted the cytochrome P420 species into the native enzyme as characterized by the cytochrome P450 optical spectrum (Figure IV.16). The crude reconstituted cytochrome P450cam exhibited a Soret maximum of the oxidized substrate-bound enzyme at 391nm, a Soret maximum of the $Na_2S_2O_4$-reduced complex at 409nm, and the hyper-spectrum of the reduced-CO complex with Soret maxima at 445 and 370nm; the latter was manifested as a shoulder at 370nm and the protein absorption at 280nm was not observed because of the strong absorbance of the excess cysteine. The absorption spectra of the cysteine-incubated hemin-apoprotein solution also showed a residual maximum of the reduced-CO complex at ≈420nm, indicative of "non-regenerated" heme. Purification of the crude reconstituted enzyme solution by anion-exchange chromatography (see Section III.4.4.1) removed the excess cysteine and glycerol reagents, and

produced absorption maxima in the oxidized, reduced and reduced-CO complexes (Figure IV.17) identical to those observed in the native substrate-bound enzyme (see Section IV.2.3.1). The absorption at 314nm was indicative of excess $Na_2S_2O_4$ reducing agent. Again the spectrum of the reduced-CO complex exhibited a residual peak at 420nm, that was used to calculate the approximate concentration of "non-regenerated" heme in the reconstituted protein solution (see Section III.4.4.2). Following incubation with apomyoglobin and Sephadex G-100 chromatography (Section III.4.4.3), the final spectra of substrate-bound, hemin-reconstituted cytochrome P450cam are shown in Figure IV.18. The spectrum of the oxidized reconstituted enzyme exhibited the protein absorption at 280nm which closely resembled that of apocytochrome P450cam (Figure IV.14), and absorptions of the heme-prosthetic group at 391 and 645nm; less well-defined absorptions of the heme-group were found at ≈510 and ≈540nm. Stoichiometric dithionite-reduction of the oxidized cytochrome solution produced the ferrous complex with maxima at 408 and 544nm. Excess dithionite was manifested in the peak at 314nm. Flushing the system with carbon monoxide produced the ferrous-CO complex with the Soret bands at 445 and 365nm and a peak at 550nm. All traces of the absorption at 420nm indicative of the P420 contaminants were removed following apomyoglobin incubation. The experimental absorbance data for substrate-bound system given together with literature data in Table IV.6; agreement is excellent. Absorbance data for the native (Table IV.3) and

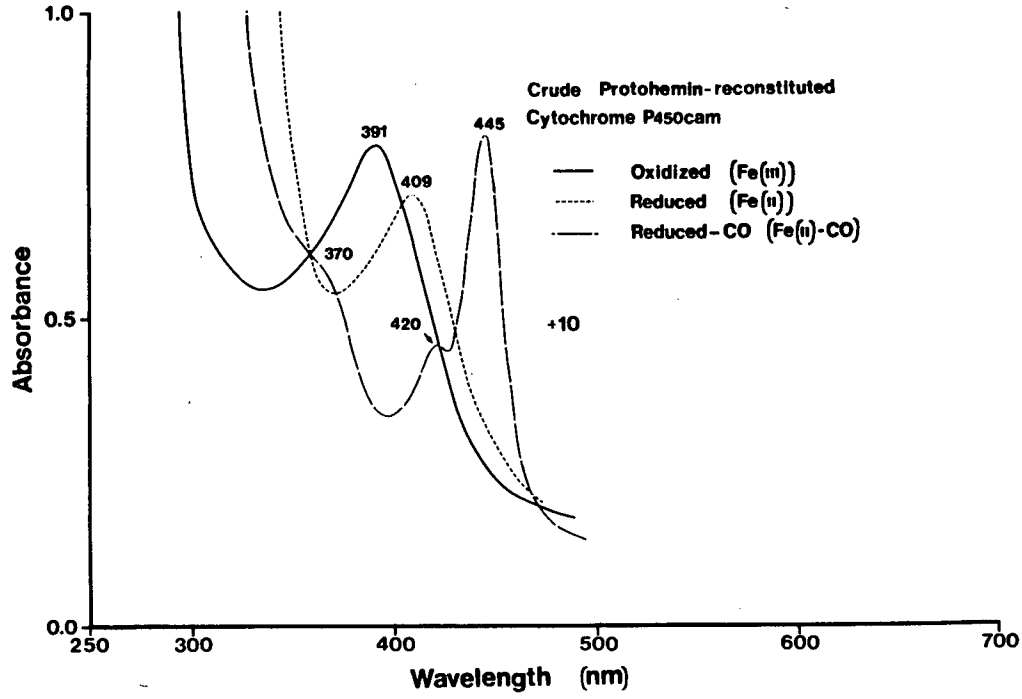


Figure IV.16 Absorption spectra of the cysteine-incubated protohemin-apoprotein solution.

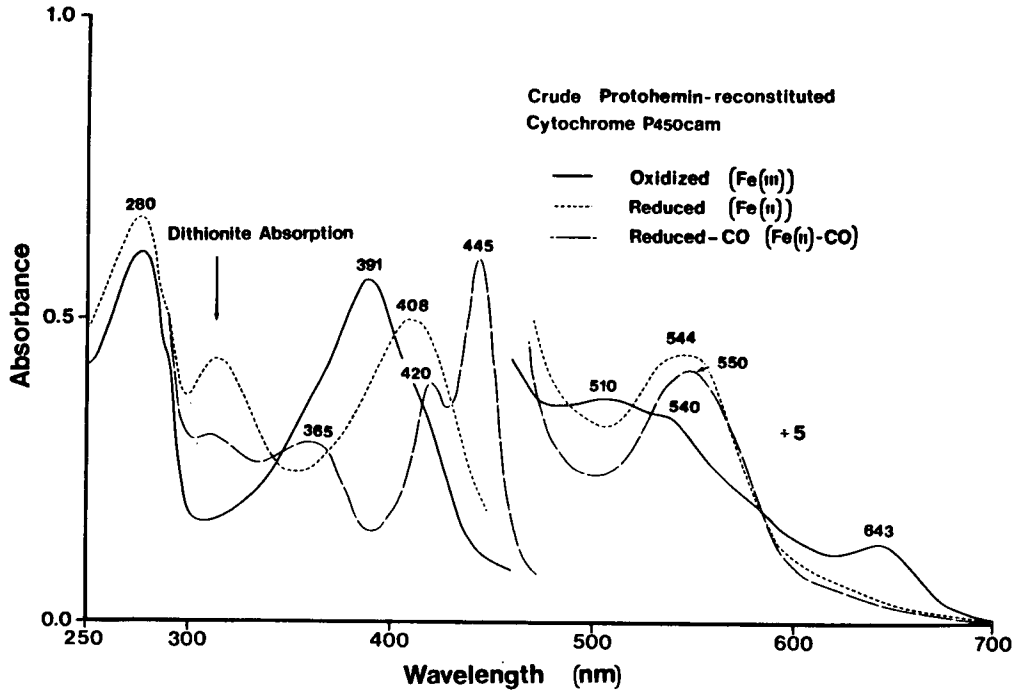


Figure IV.17 Absorption spectra of the reconstituted cytochrome P450cam following DE-52 anion exchange chromatography.

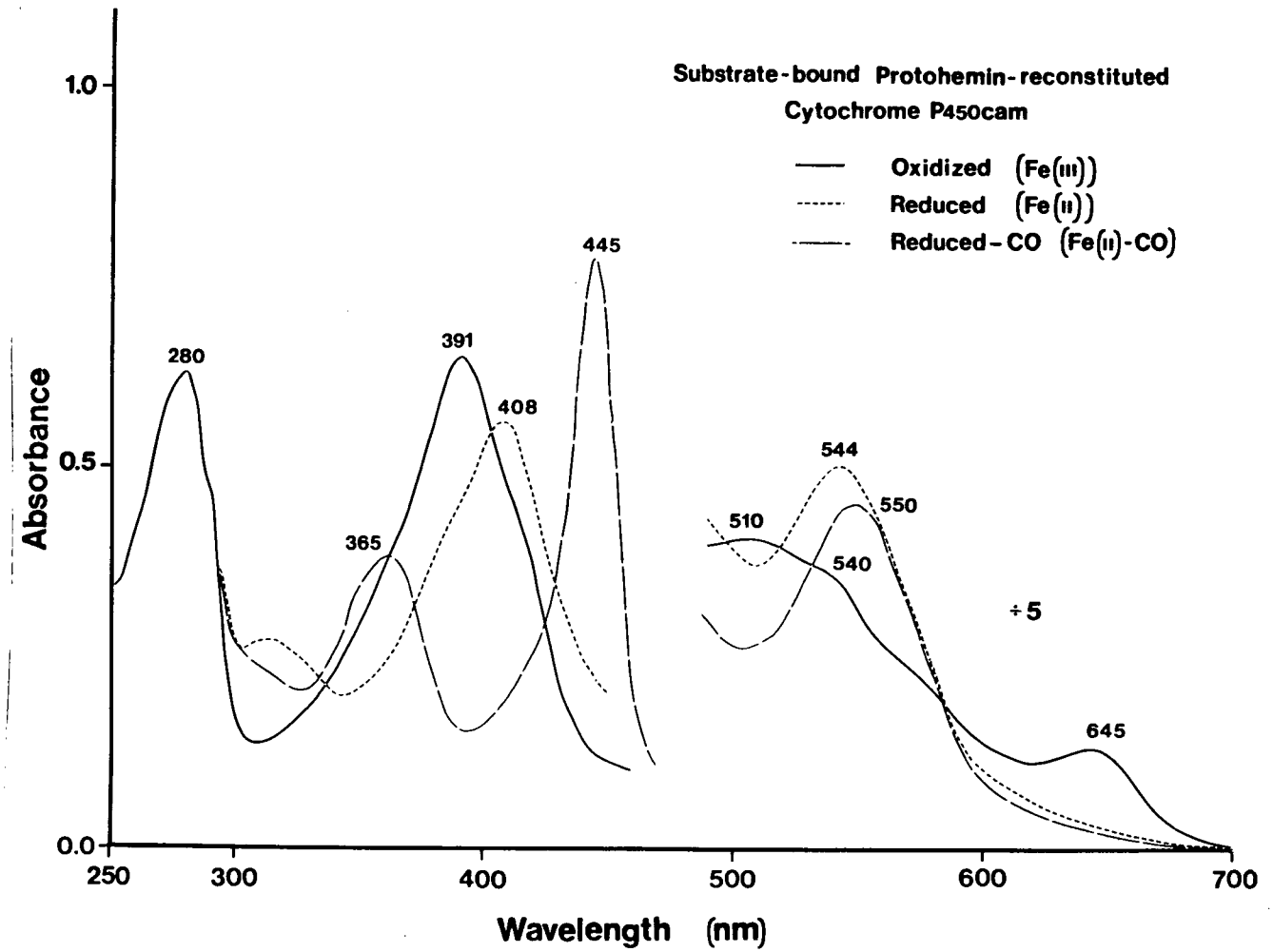


Figure IV.18 Absorption spectra of various states of the substrate-bound protohemin-reconstituted cytochrome P450cam.

Table IV.6

Absorbance Data[a,b] for Substrate-bound Reconstituted Cytochrome P450cam

Form	Experimental Preparation		(c) Literature Preparation		(d) Literature Preparation	
	λ_{nm}	ε_{mM}	λ_{nm}	ε_{mM}	λ_{nm}	ε_{mM}
Oxidized	280	91.3			280	65
	391	99.8	391	102	391	99
	417	shoulder				
	510	12.6	510	13.0	510	12.5
	540	11.5	540	11.2	540	10.5
	645	4.2	645	5.4	646	5.0
Reduced	408	86.5	408	86.5	408	84.0
	544	15.6	542	16.0	542	15
Reduced-CO	365	56.7	364	60.8		
	445	120	446	120	446	120
	550	14.0	550	14.0	550	13.0

a) Averaged over three sets of data; estimated error 5%.

b) Determined in buffer P-100, pH 7.0, ≈8mM camphor at room temperature (23±2°C) using published extinction coefficient data of the reduced-CO complex at 446nm, ε_{mM}=120; Ref.10.

c) Ref. 10

d) Ref. 165.

reconstituted substrate-bound cytochromes were very similar except for a small shoulder at 417nm on the Soret maximum of the ferric reconstituted complex. This shoulder absorption was seen in all reconstituted cytochrome preparations (Fe(III) state) and was thought to be indicative of a substrate-free cytochrome P450 impurity. No attempts were made to remove the impurity.

The major draw-back to the reconstitution procedure described in Section III.4 was the low yields (≈15%) of reconstituted cytochrome P450cam obtained from the native enzyme. Areas of significant protein loss were in the production of the apoprotein, where trituration in the KOH-glycerol solvent system often led to incomplete dissolution and denaturation of the apoprotein, and in the cysteine incubation, which was always accompanied by precipitate formation due to possible "salting-out" of the protein component by excess cysteine and hemin in solution. Yields of reconstituted cytochrome P450cam reaching 30% have been reported by Wagner *et al.*[165] using the acid-butanone liquid-phase technique with the aqueous histidine/glycerol co-solvent system mentioned earlier (Section IV.3.1), as well as longer incubation periods (36-48h) for the conversion of the P420 species to the native enzyme. This procedure appears to avoid the complications of apoprotein dissolution and precipitation during the cysteine incubation and generally seems to be better suited for the reconstitution experiments. It is of interest to note that the longer incubation periods were

thought to reflect a dynamic equilibrium established between two isomeric P420 species that differ only by the sidedness of the heme plane in the protein pocket (180° of rotation about the α-γ meso-carbon axis);[165] formation of the native enzyme was thought to occur from only one of the particular P420 isomers. The longer incubation periods in the presence of thiol reagents could possible alleviate the use of apomyoglobin for removal of the P420 contaminants from the reconstituted P450cam preparations.

IV.3.4 Purity of Reconstituted Cytochrome P450cam

The deep-red, substrate-bound, reconstituted cytochrome P450cam solution was approximately 80% homogeneous and contained a slight impurity likely in the form of substrate-free P450cam. The impurity was manifested as a shoulder absorption at 417nm in the spectra of the oxidized substrate-bound reconstituted enzyme (Figure IV.18). The absorption ratio of A_{391}/A_{280} = 1.10 was comparable to that of the parent enzyme purity (see Section IV.2.3.3), as well as that of another reconstituted cytochrome P450cam preparation reported in the literature : 1.52.[165]

IV.3.5 Stability of Reconstituted Cytochrome P450cam

In the presence of 100mM potassium ions and ≈8mM camphor the reconstituted enzyme solutions could be stored anaerobically, at 5°C, for at least six months with no apparent loss of the observed spectral characteristics (Figure IV.18).

IV.4 Study of the Reaction of CO with the Ferrous State of Myoglobin and the P450cam Systems by Flash Photolysis

IV.4.1 Treatment of Data

The reaction of CO with the ferrous state of myoglobin and the P450cam systems, as described by Reaction II.5, was successfully studied by the flash photolysis method. Since the light-pulse enhanced the reverse of Reaction II.5 for both hemoprotein systems (i.e. Fe(II)-CO $\longrightarrow$ Fe(II)+CO; see Section III.5.3.4), information about the subsequent CO-binding kinetics was readily obtained by observing the decrease in the intensity of the Soret band of the intermediate CO-free hemoprotein complexes or the increase in the Soret band of the CO-bound complexes. Kinetic analysis of the recombination reaction following the flash was simplified by performing the experiments under conditions in which the CO ligand was in great excess. Absorbance *vs.* time decay traces, obtained *via* the Analog Rate converter of the flash unit, were used to estimate the reaction rate dependence on hemoprotein concentration, and the observed rate constants were determined by standard relationship IV.1 derived in Appendix II:

$$\ln \frac{A_o - Ae}{A - Ae} = k_{obs}t \qquad \text{(IV.1)}$$

where A is the absorbance at time, t.

Ae is the absorbance at equilibrium

A_o is the absorbance at the start of the reaction

and k_{obs} is the observed rate constant.

Since the observed reaction rate constant, k_{obs}, corresponded to the sum of the forward, k_{on}, and reverse, k_{off}, rate constants as given in equation IV.2 (see Appendix II), changing the CO concentration allowed for the determination

$$k_{obs} = k_{on}[CO] + k_{off} \qquad (IV.2)$$

of the second-order rate constant for the forward of Reaction II.5, k_{on}, and the first-order rate constant for the reverse of Reaction II.5, k_{off}.

IV.4.2 Study of the Reaction of CO with the Ferrous State of Myoglobin by Flash Photolysis

As mentioned in Section III.5.3.5, the reaction of CO with ferrous myoglobin was studied with the flash photolysis apparatus in order to test and develop the unit. Complete kinetic runs, including compilation of data at seven different CO concentrations, were performed at $20^{o}C$ on three different myoglobin samples at protein concentrations of $6.43 \times 10^{-6}M \pm 5\%$. Only one set of data (kinetic Run 2) will be analysed in detail here but the results will be compared with analogous data compiled for kinetic Runs 1 and 3. Raw data for kinetic Run 2 (i.e. exponential decay curves, linear rate plots and spectral data) can be found in Appendix IVa; tabulated data for kinetic Runs 1 and 3 are included in Tables IV.7 and IV.8 of this section.

Figure IV.19 shows representative data from kinetic Run 2 for the CO-myoglobin system obtained at a protein concentration of $6.43 \times 10^{-6}M$ and CO concentration of $8.58 \times 10^{-4}M$; Figure IV.19A shows the absorbance *vs.* time exponential decay plot while Figure IV.19B shows the corresponding linear rate trace. For the ferrous state of myoglobin, the reaction with CO was monitored by observing the exponential decrease in intensity of the Soret band of the CO-free intermediate at 432nm produced upon photodissociation of the ferrous-CO complex (Figure IV.19A). Monitoring of the

A)

FLASH PHOTOLYSIS EXPERIMENTS

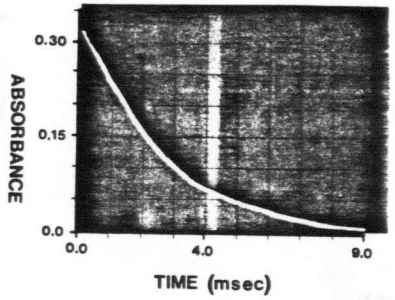
Sample Description: Myoglobin -CO complex

Temperature: 20 ± 0.2°C

Monitoring Wavelength: 432nm

Data Table

Run	Plot Form	Cary O.D.	Flash Unit Volt.	P_T (mm Hg)	P_{H_2O} (mm Hg)	P_{CO} (mm Hg)	$[CO]\times10^4$ (m/L)	Half Life (msec)
2.2	Exp. Decay	0.48	0.50	648	17.5	631	8.58	1.6



Vertical Amplitude: 0.05 (volts/div)

Sweep Time: 1.0 (msec/div)

Half Life Data

Half Life #	Vertical Drop (volts)	Horizontal Sweep (msec)
0	0.325	0
1	0.163	1.9 (1.9)
2	0.081	3.5 (1.6)
3	0.041	5.3 (1.8)
4	0.020	6.7 (1.4)

$t_{\frac{1}{2}}$ = 1.6 msec

B)

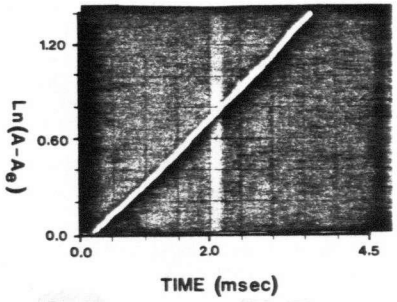
FLASH PHOTOLYSIS EXPERIMENTS

Sample Description: Myoglobin-CO complex

Temperature: 20±0.2°C

Data Table

Run	Plot Form	Cary O.D.	Flash Unit Volt.	P_T (mm Hg)	P_{H_2O} (mm Hg)	P_{CO} (mm Hg)	$[CO]\times10^4$ (m/L)	k_{obs} ($msec^{-1}$)
2.2	Rate Plot	0.48	0.50	648	17.5	631	8.58	4.0×10^{-1}



Vertical Amplitude: 0.2 (volts/div)

Sweep Time: 0.5 (msec/div)

Slope (mean)		Slope (max)		Slope (min)	
X (msec)	Y (volts)	X (msec)	Y (volts)	X (msec)	Y (volts)
0.5	0.13	0.5	0.10	0.5	0.15
1.0	0.33	1.0	0.30	1.0	0.33
1.5	0.53	1.5	0.52	1.5	0.53
2.0	0.73	2.0	0.73	2.0	0.73
2.5	0.94	2.5	0.94	2.5	0.92
3.0	1.13	3.0	1.14	3.0	1.12

Least Squares Analysis

m: $4.0\times10^{-1}msec^{-1}$

y-intercept: -7.8×10^{-2}

$\delta y: 1.3\times10^{-2}$

$\delta m: 3.5\times10^{-3}msec^{-1}$

Figure IV.19 Representative data from kinetic Run 2 for the reaction of CO with the ferrous state of myoglobin; (A) gives absorbance *vs.* time exponential decay plot and (B) gives the corresponding linear rate plot.

Table IV.6.1

Kinetic Data from kinetic Run 2 for the Reaction of CO with Ferrous Myoglobin at 20°C.

Run	$[CO]x10^4$ (M)	$t_{½}$ (msec) (a)	$k_{obs}x10^1$ ($msec^{-1}$) (a)	$k_{obs}x10^1$ ($msec^{-1}$) (b)	$t_{½}$ (msec) (c)	$k_{obs}x10^1$ ($msec^{-1}$) (c)
2.1	10.1	1.5	4.6	5.1	1.5	4.6
2.2	8.58	1.6	4.3	4.0	1.7	4.1
2.3	7.21	1.8	3.9	3.6	1.8	4.0
2.4	5.86	2.1	3.3	3.3	2.2	3.2
2.5	4.53	2.6	2.7	2.9	2.6	2.7
2.6	3.21	3.7	1.9	2.2	3.6	2.1
2.7	2.68	4.5	1.5	1.6	4.4	1.5

(a) Directly determined experimentally from the absorbance *vs.* time plots; k_{obs} values determined using the relationship $k = \frac{\ln 2}{t_{½}}$

(b) Determined experimentally from the ln(A-Ae) *vs.* time plots *via* the analog converter.

(c) Determined experimentally over approximately four half-lives of the absorbance *vs.* time plots by computer analysis; Ref.168.

Table IV.7

Kinetic Data from Kinetic Run 1 for the Reaction of CO with Ferrous Myoglobin[a] at 20°C.

Run	$[CO]x10^4$ (M)	$t_{1/2}$ (msec) (b)	$k_{obs}x10^1$ ($msec^{-1}$) (b)	$k_{obs}x10^1$ ($msec^{-1}$) (c)	$t_{1/2}$ (msec) (d)	$k_{obs}x10^1$ ($msec^{-1}$) (d)
1.1	10.0	1.4	5.0	4.7	1.5	4.6
1.2	8.55	1.5	4.6	4.4	1.6	4.3
1.3	7.20	1.8	3.9	3.5	1.8	3.8
1.4	5.85	2.2	3.2	3.1	2.1	3.3
1.5	4.50	2.5	2.8	2.7	2.5	2.6
1.6	3.20	3.3	2.1	2.1	3.2	2.0
1.7	2.60	4.2	1.7	1.7	4.3	1.6

a) Kinetic data were obtained at a protein concentration of $6.19x10^{-6}$M. Kinetic constants are tabulated in Table IV.9.

b) Directly determined experimentally from the absorbance *vs.* time plots; k_{obs} values determined using the relationship $k = \frac{\ln 2}{t_{1/2}}$

c) Determined experimentally from the ln(A-Ae) *vs.* time plots *via* the analog converter.

d) Determined experimentally over approximately four half-lives of the absorbance *vs.* time plots by computer analysis; Ref.168.

Table IV.8

Kinetic Data from kinetic Run 3 for the Reaction of CO with Ferrous Myoglobin[a] at 20°C.

Run	$[CO]x10^4$ (M)	$t_{1/2}$ (msec) (b)	$k_{obs}x10^1$ ($msec^{-1}$) (c)	$k_{obs}x10^1$ ($msec^{-1}$) (b)	$t_{1/2}$ (msec) (b)	$k_{obs}x10^1$ ($msec^{-1}$) (d)
3.1	10.1	1.5	4.6	4.9	1.5	4.6
3.2	8.50	1.6	4.3	4.5	1.7	4.1
3.3	7.23	1.8	3.9	3.7	1.9	3.6
3.4	5.83	2.1	3.3	3.2	2.0	3.5
3.5	4.53	2.8	2.5	2.5	2.8	2.4
3.6	3.25	3.4	2.0	2.0	3.5	2.0
3.7	2.64	4.3	1.6	1.6	4.4	1.6

a) Kinetic data were obtained at a protein concentration of $6.62x10^{-6}$M. Kinetic constants tabulated in Table IV.9.

b) Directly determined experimentally from the absorbance *vs.* time plots; k_{obs} values determined using the relationship $k = \frac{\ln 2}{t_{1/2}}$

c) Determined experimentally from the ln (A-Ae) *vs.* time plots *via* the analog converter.

d) Determined experimentally over approximately four half-lives of the absorbance *vs.* time plots by computer analysis; Ref.168.

intermediate CO-free complex was felt essential since the absorbance of the Soret band at protein concentrations of $\simeq 1 \times 10^{-5}$M ($OD_{432nm} \simeq 1.0$) fell within the calibration limit of the flash unit (see Section III.5.3.3). The direct proportionality between optical density measured on the Cary spectrophotometer and voltage on the flash unit can be seen by comparison of the values tabulated in the Data Table listed at the top of Figure IV.19A; the values represent the absorbance of the ferrous-CO complex at 432nm (see myoglobin spectra, Appendix IVa). The initial absorbance on the exponential decay plot ($\simeq$0.3 OD units) represents a 30% photodecomposition of the CO-bound complex (refer to myoglobin spectra, Appendix IVa). Based on $t_{\frac{1}{2}}$ half-life data recorded over the entire exponential decay curve (up to four half-lives; Half-Life Data table at bottom of Figure IV.19A), the reaction showed a pseudo first-order dependence on hemoprotein concentration. The $t_{\frac{1}{2}}$ values obtained directly from the absorbance *vs.* time plots and from a separate computer analysis[168] of the exponential decay curves for kinetic Run 2 for myoglobin are given in Table IV.6.1. Tables IV.7 and IV.8 give the corresponding $t_{\frac{1}{2}}$ data for kinetic Runs 1 and 3. All absorbance *vs.* time plots indicated the same pseudo first-order dependence on hemoprotein concentration and over the three kinetic runs the $t_{\frac{1}{2}}$ values varied by about 10%.

Analysis of the exponential decay data (Figure IV.19A) *via* relationship IV.1 gave the linear rate plot shown in

Figure IV.19B. Plots of ln (A-Ae) *vs.* time obtained from the Analog Rate Converter of the flash unit were linear over one to two half-lives and of positive slope; the positive slope was due to electronic manipulation of the data through the analog device and was common to all rate plots for the myoglobin system. k_{obs} values were obtained from a least squares fit[168] of data points from the maximum, minimum and mean slopes of the rate plots as tabulated at the bottom of Figure IV.19B. The y-intercept, which equalled-ln(A_o-Ae), was generally ignored since accurate measurement of this value required precise tuning of the analog device and did not always afford an analysable rate plot (see Appendix I, section D). Figure IV.20 shows how the linear rate plots varied with changes in CO concentrations for kinetic Run 2 while the corresponding k_{obs} values are tabulated in Table IV.6 Since analysis of rate data *via* the analog converter over more than two half-lives resulted in noisy or badly smeared traces, the k_{obs} values were compared with a second set of k_{obs} values obtained from a computer analysis[168] of the absorbance *vs.* time plots over three to four half-lives. These data, tabulated in Table IV.6.1 for kinetic run 2, agreed within 10% with the corresponding k_{obs} values obtained from the analog device as did the $t_{½}$ values. As well, the k_{obs} values obtained from the analog converter were in excellent agreement (within 10%) with those calculated from the $t_{½}$ values obtained directly from the absorbance *vs.* time plots (see Table IV.6.1). Excellent agreement was also observed between the analog-derived, the calculated and the computer-derived k_{obs} values for kinetic Runs 1 and 3 (Tables IV.7

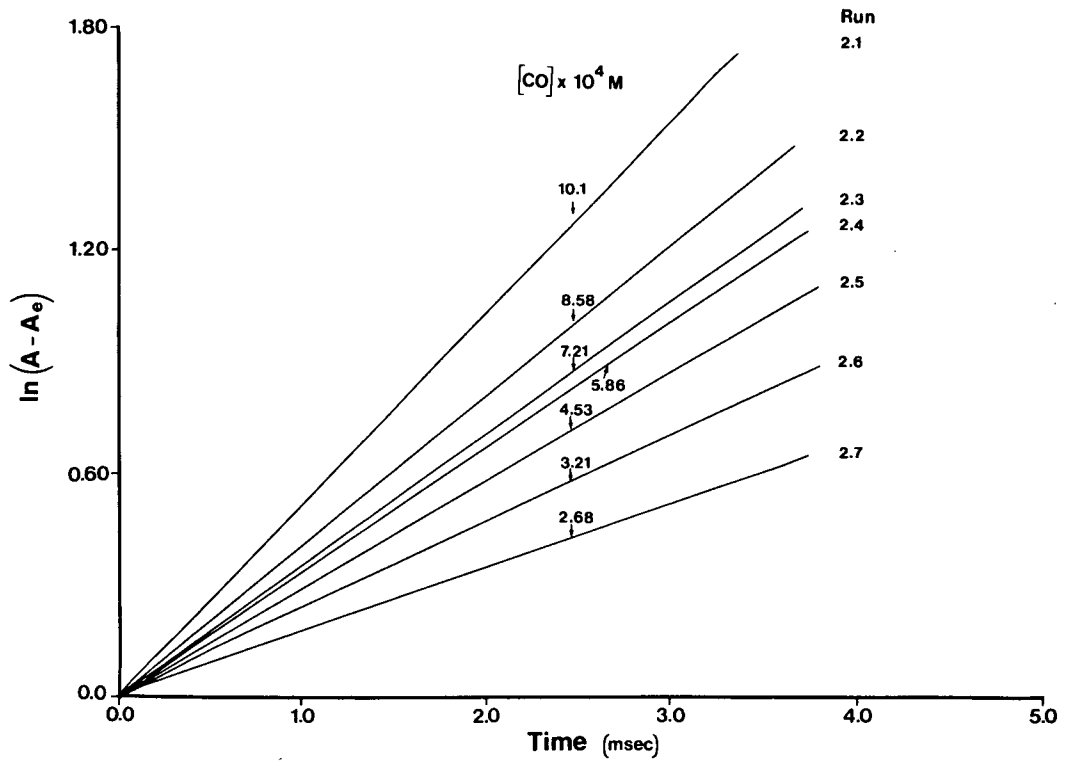


Figure IV.20 Variation in the slope of the ln(A-Ae)*vs.* time plots with changes in CO concentration for kinetic Run 2 of the myoglobin system.

and IV.8, respectively). The approach to a first-order reaction in hemoprotein concentration with the use of a large excess of the CO ligand is evident from Figure IV.21, which shows the plots of $t_{\frac{1}{2}}$ values from the absorbance *vs.* time plots *vs.* k_{obs}^{-1} obtained from k_{obs} values measured *via* the analog converter for kinetic Runs 1, 2 and 3; the plots represent straight lines of slope 0.74 ± 0.02, 0.76 ± 0.06 and 0.67 ± 0.2, respectively which are comparable to the expected value of ln2 for a first-order reaction. Plotting the k_{obs} values *vs.* concentration of CO as described in equation IV.2 produced straight lines for all kinetic runs as shown in Figure IV.22; however, Run 2 showed a higher fluctuation in the data points due possibly to the greater fluctuation in protein concentration throughout the run as suggested by the overall decrease in concentration of the CO-bound hemoprotein (Figure IV.23). A least squares fit of the k_{obs} *vs.* CO concentration data gave slope, k_{on}, and intercept, k_{off}, for the reaction of CO with ferrous myoglobin, and Table IV.9 summarizes the kinetic constants obtained at 20°C from all three kinetic runs for the myoglobin-CO system. Comparison of the data shows a 10% variation in the kinetic constants derived *via* the Analog Rate Converter that is not observed amongst the computer-derived constants; however, the mean kinetic constants are very close for the two sets of data. Averaging the data in Table IV.9 gives a second-order rate constant for the CO-recombination reaction, k_{on}, of $4.1 \times 10^{5} M^{-1} S^{-1}$ ± 10% at 20°C which is in excellent agreement with published literature

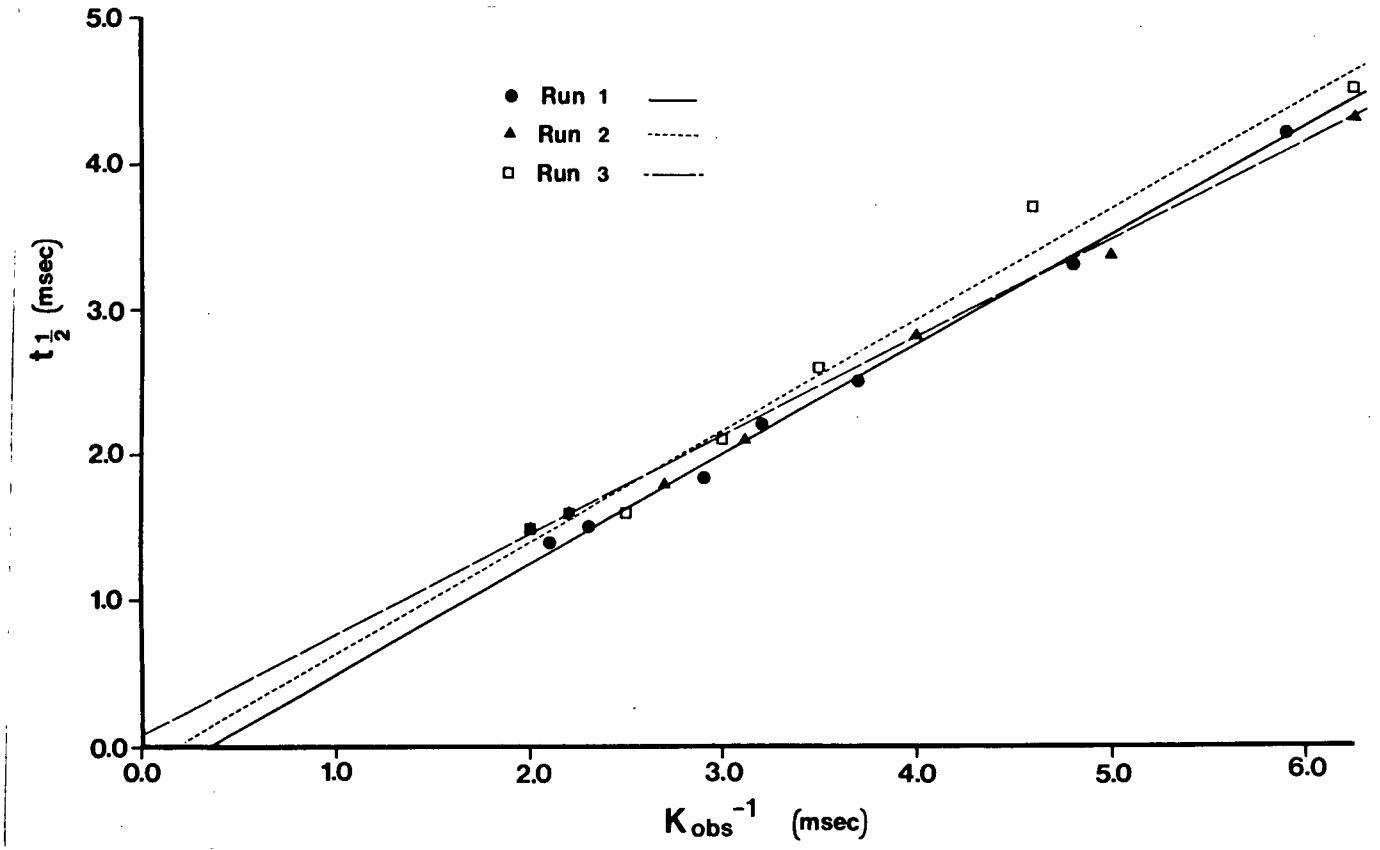


Figure IV.21 Plots of $t_{\frac{1}{2}}$ *vs.* k_{obs}^{-1} data from kinetic Runs 1, 2 and 3 for the myoglobin-CO system.

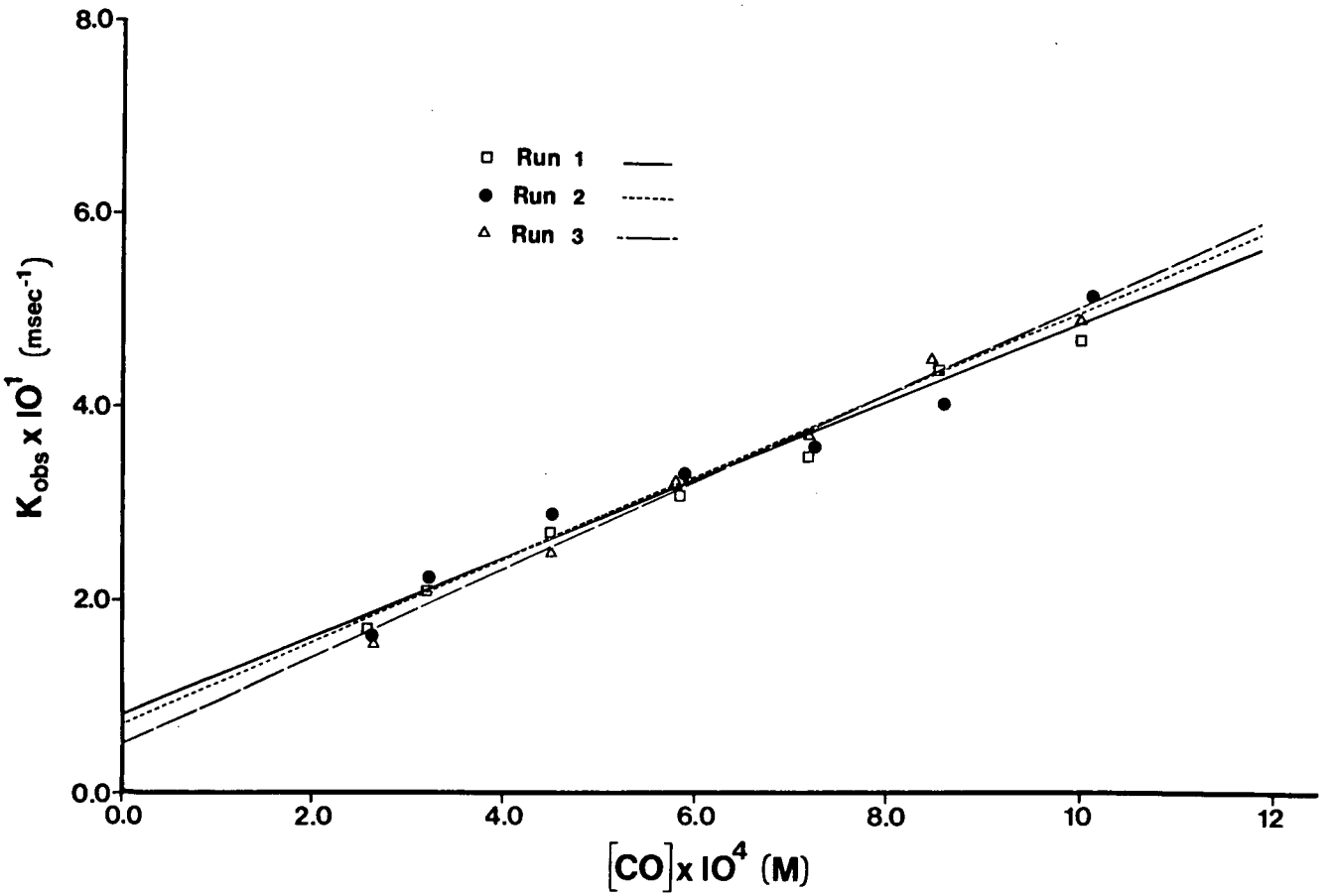


Figure IV.22 Plot of k_{obs} *vs.* CO concentration data from kinetic Runs 1, 2 and 3 for the myoglobin-CO system.

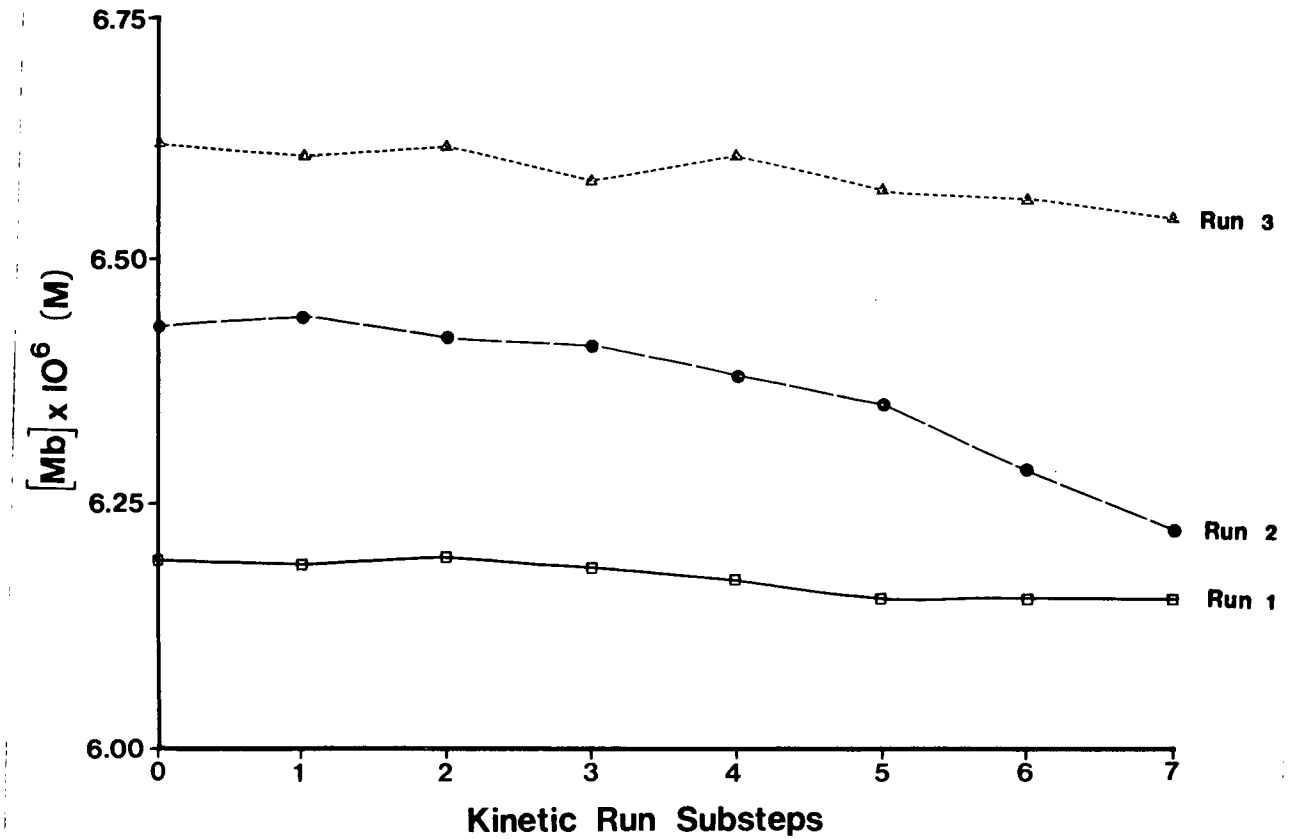


Figure IV.23 Fluctuation in protein concentration during kinetic Runs 1, 2 and 3 for the myoglobin-CO system.

Table IV.9

Kinetic Constants obtained for the Reaction of CO with Ferrous Myoglobin at 20°C.

Kinetic Run	[Protein] (M)	k_{on}(a) ($M^{-1}S^{-1}$)	k_{off}(a) (S^{-1})	Kco(b) (M^{-1})
1	6.19×10^{-6}	$4.0\pm0.2\times10^{5}$	80±10	5.0×10^{3}
		$4.1\pm0.2\times10^{5}$	70±15	5.9×10^{3}
2	6.43×10^{-6}	$4.2\pm0.3\times10^{5}$	70±30	6.0×10^{3}
		$4.0\pm0.4\times10^{5}$	75±20	5.3×10^{3}
3	6.62×10^{-6}	$4.5\pm0.2\times10^{5}$	50±10	9.0×10^{3}
		$4.0\pm0.3\times10^{5}$	70±20	5.7×10^{3}

a) The upper kinetic constants for each kinetic run was obtained from a least squares fit of the analog converter-derived k_{obs} values *vs.* CO concentration data; the lower kinetic constant from the computer-derived k_{obs} values *vs.* CO concentration plots. Quoted errors obtained from least squares fit of k_{obs} *vs.* CO concentration data.

b) Equilibrium constant, Kco, calculated from the expression $Kco = k_{on}/k_{off}$. Estimated error, ± 40%.

data obtained between 4-24°C of from 3.0-5.0 x $10^5 M^{-1} S^{-1}$.[94e,109,151,133h] The average k_{off} value of $69S^{-1}$ ± 30% at 20°C can be compared with the published value at the same temperature of $0.02S^{-1}$.[109] The apparently inaccurate k_{off} value leads to a calculated equilibrium constant, Kco of 6.2 x $10^3 M^{-1}$ which is comparable with the published value of 2.7 x $10^7 M^{-1}$.[109] Clearly the method described for the determination of k_{off} is unreliable; the value of k_{off} has to be obtained by an independent method (i.e. stopped-flow analysis). The apparent enhanced off rate measured might presumably result from the photosensitivity of the decarbonylation reaction which is known to proceed with high quantum yield;[109] the monitoring of the reaction at the 432nm position could then in principle enhance the off rate. The determination of k_{on} for the CO-myoglobin system was apparently quite accurate and served to show that the flash unit could be utilized for the study of the P450cam-CO systems.

IV.4.3 Study of the Reaction of CO with the Ferrous State of Native Cytochrome P450cam by Flash Photolysis

Kinetic data for the reaction of CO with the ferrous state of native substrate-bound cytochrome P450cam were collected at 20°C in a fashion similar to that used for the myoglobin system using three different enzyme solutions (see above); protein concentrations were fixed at 8.59×10^{-6}M ± 2% and CO concentrations ranged from $0.2\text{-}1.0 \times 10^{-3}$M. The results from kinetic Run 3 are analyzed in detail below and compared with the other two kinetic runs as well as with the myoglobin system. Raw data for kinetic Run 3 (i.e. exponential decay curves, linear rate plots and spectral data) are shown in Appendix IV.b and tabulated in Table IV.10; kinetic data from Runs 1 and 2 are tabulated in Tables IV.11 and IV.12.

Figure IV.24 shows a typical set of kinetic data from kinetic Run 3 for the native P450cam-CO system obtained at a protein concentration of 8.75×10^{-6}M and a CO concentration of 8.60×10^{-4}M; Figure IV.24A shows the exponential decay curve for the reaction of CO with the ferrous state of native P450cam while Figure IV.24B gives the corresponding linear rate plot. The interaction of CO with ferrous P450cam was monitored at 442nm by observing the increase in intensity of the edge of the 445nm Soret band of the ferrous-CO complex; Figure IV.24A shows the exponential decay curve for the process. The 445nm peak was chosen to monitor the recombination reaction since the peak fell within the calibration limit of the flash unit at protein concentrations of $\simeq 1 \times 10^{-5}$M (see Section III.5.3.3).

A) FLASH PHOTOLYSIS EXPERIMENTS

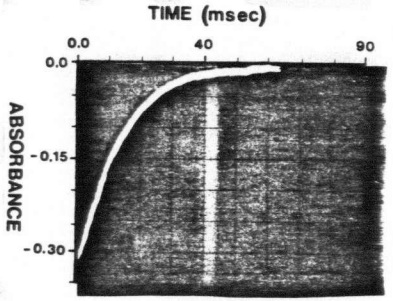
Sample Description: Native P450cam-CO complex

Temperature: 20±0.2°C

Monitoring Wavelength: 442nm

Data Table

Run	Plot Form	Cary O.D.	Flash Unit Volt.	P_T (mm Hg)	P_{H_2O} (mm Hg)	P_{CO} (mm Hg)	[CO]x10^4 (m/L)	Half Life (msec)
3.2	Exp. Decay	0.975	0.980	650	17.5	633	8.60	9.3



Vertical Amplitude: 0.05 (volts/div)

Sweep Time: 10 (msec/div)

Half Life Data

Half Life #	Vertical Drop (volts)	Horizontal Sweep (msec)
0	0.32	0
1	0.16	9 (9)
2	0.08	18 (9)
3	0.04	27 (9)
4	0.02	37 (10)

$t_{\frac{1}{2}}$ = 9.3 msec

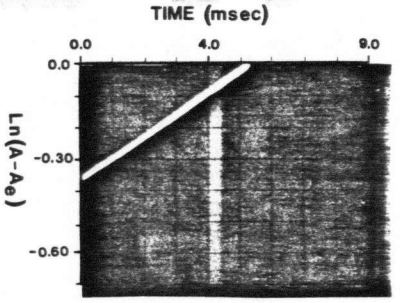
B) FLASH PHOTOLYSIS EXPERIMENTS

Sample Description: Native P450cam-CO complex

Temperature: 20±0.2°C

Data Table

Run	Plot Form	Cary O.D.	Flash Unit Volt.	P_T (mm Hg)	P_{H_2O} (mm Hg)	P_{CO} (mm Hg)	[CO]x10^4 (m/L)	k_{obs} (msec^{-1})
3.2	Rate Plot	0.975	0.980	650	17.5	633	8.60	7.1×10^{-2}



Vertical Amplitude: 0.1 (volts/div)

Sweep Time: 1.0 (msec/div)

Slope (mean)		Slope (max)		Slope (min)	
X (msec)	Y (volts)	X (msec)	Y (volts)	X (msec)	Y (volts)
0	-0.370	0	-0.370	0	-0.360
1.0	-0.295	1.0	-0.295	1.0	-0.295
2.0	-0.230	2.0	-0.230	2.0	-0.230
3.0	-0.155	3.0	-0.150	3.0	-0.160
4.0	-0.085	4.0	-0.075	4.0	-0.090
5.0	-0.015	5.0	-0.005	5.0	-0.025

Least Squares Analysis

m: 7.1×10^{-2} msec^{-1}

y-intercept: -3.7×10^{-1}

δy: 1.9×10^{-3}

δm: 7.7×10^{-4} msec^{-1}

Figure IV.24 Typical set of kinetic data obtained from kinetic Run 3 for the reaction of CO with the ferrous, substrate-bound state of native cytochrome P450cam; (A) shows the exponential decay curve while (B) gives the corresponding linear rate plot.

Table IV.10

Kinetic Data from kinetic Run 3 for the Reaction of CO with the Ferrous State of Native Substrate-bound, Cytochrome P450cam at 20°C.

Run	$[CO]x10^4$ (M)	$t_{1/2}$ (msec) (a)	$k_{obs}x10^2$ ($msec^{-1}$) (a)	$k_{obs}x10^2$ ($msec^{-1}$) (b)	$t_{1/2}$ (msec) (c)	$k_{obs}x10^2$ ($msec^{-1}$) (c)
3.1	9.96	8.5	8.2	7.1	8.0	8.7
3.2	8.60	9.3	7.5	7.1	8.9	7.8
3.3	7.24	10	6.9	5.9	9.9	7.0
3.4	5.88	12	5.8	5.3	11	6.3
3.5	4.52	14	5.0	4.3	14	4.9
3.6	3.16	21	3.3	3.1	21	3.3
3.7	2.48	27	2.7	3.0	28	2.5

a) Determined directly from the absorbance *vs.* time plots; k_{obs} values determined using the relationship $k = \frac{\ln 2}{t_{1/2}}$

b) Determined experimentally from the ln(A-Ae) *vs.* time plots *via* the analog converter.

c) Determined experimentally over approximately four half-lives of the absorbance *vs.* time plots by computer analysis; Ref.168.

Table IV.11

Kinetic Data[a] from kinetic Run 1 for the Reaction of CO with the Ferrous State of Native Substrate-bound, Cytochrome P450cam at 20°C.

Run	[CO]x10^4 (M)	$t_{½}$ (msec) (b)	k_{obs}x10^2 (msec^{-1}) (b)	k_{obs}x10^2 (msec^{-1}) (c)	$t_{½}$ (msec) (d)	k_{obs}x10^2 (msec^{-1}) (d)
1.1	9.96	11	6.3	5.5	10.6	6.5
1.2	8.60	12	5.8	5.9	10	6.7
1.3	7.24	13	5.3	5.2	13	5.3
1.4	5.88	14	5.0	4.5	16	4.4
1.5	4.52	18	3.9	3.7	18	3.9
1.6	3.16	22	3.2	3.5	21	3.3
1.7	2.48	30	2.3	2.7	30	2.4

a) Kinetic data obtained at a fixed protein concentration of 8.42×10^{-6}M. Kinetic constants are tabulated in Table IV.13.

b) Determined directly from the absorbance *vs.* time plots; k_{obs} values determined using the relationship $k = \frac{\ln 2}{t_{½}}$

c) Determined experimentally from the ln (A-Ae) *vs.* time plots *via* the analog converter.

d) Determined experimentally over approximately four half-lives of the absorbance *vs.* time plots by computer analysis; Ref.168.

Table IV.12

Kinetic Data[(a)] from kinetic Run 2 for the Reaction of CO with the Ferrous State of Native Substrate-bound, Cytochrome P450cam at 20°C.

Run	$[CO]x10^4$ (M)	$t_{1/2}$ (msec) (b)	$k_{obs}x10^2$ ($msec^{-1}$) (b)	$k_{obs}x10^2$ ($msec^{-1}$) (c)	$t_{1/2}$ (msec) (d)	$k_{obs}x10^2$ ($msec^{-1}$) (d)
2.1	9.96	10	6.9	6.8	9.2	7.5
2.2	8.60	9.3	7.5	6.8	9.4	7.4
2.3	7.24	11	6.3	5.9	11	6.5
2.4	5.88	13	5.3	5.0	12	5.8
2.5	4.52	15	4.6	4.1	15	4.7
2.6	3.16	19	3.7	4.0	19	3.7
2.7	2.48	28	2.5	2.8	27	2.5

a) Kinetic data obtained at a fixed protein concentration of $8.42x10^{-6}$M. Kinetic Data are tabulated in Table IV.13

b) Determined directly from the absorbance *vs.* time plots; k_{obs} values determined using the relationship $k = \frac{\ln 2}{t_{1/2}}$

c) Determined experimentally from the ln (A-Ae) *vs.* time plots *via* the analog converter.

d) Determined experimentally over approximately four half-lives of the absorbance *vs.* time plots by computer analysis; Ref.168.

The voltage measured on the flash unit at 442nm was equivalent to the absorbance of the P450cam-CO complex at the same wavelength (see initial P450cam-CO spectrum, Appendix IV.6) and the initial absorbance on the absorbance *vs.* time plot of Figure IV.24A (≃-0.3) represented ≃30% photodecomposition of the P450cam-CO complex (see Section III.5.3.4). Based on $t_{\frac{1}{2}}$ half-life data obtained directly from the absorbance *vs.* time curves, the reaction of CO with the ferrous state of native P450cam approximated a first-order process (see Half-Life Data table Figure IV.24A). Computer analysis[168] of the exponential decay curves also indicated a pseudo first-order dependence on hemoprotein concentration and gave $t_{\frac{1}{2}}$ values in good agreement (within 10%) of those derived directly from the exponential decay curve (see Table IV.10); similar results were observed for kinetic Runs 1 and 2 (Tables IV.11 and IV.12, respectively). Comparison of the half-life data shows an ≃20% variation in the $t_{\frac{1}{2}}$ values between kinetic runs and comparison with the corresponding $t_{\frac{1}{2}}$ data for the myoglobin system (see Table IV.6.1, IV.7 and IV.8) indicates about a 6-fold decrease in the half-life of the reaction of CO for the P450cam system.

Analysis of the exponential decay data (Figure IV.24A) *via* relationship IV.1 gave the linear analog converter-derived ln(A-Ae) *vs.* time plots shown in Figure IV.24B; the variation of the plots with CO concentration for kinetic Run 3 is shown in Figure IV.25. The ln(A-Ae) *vs.* time plots were linear for all kinetic runs but represented only ≃0.5 half-lives of the absorbance *vs.* time curves (see Figure IV.24B) due to limitations

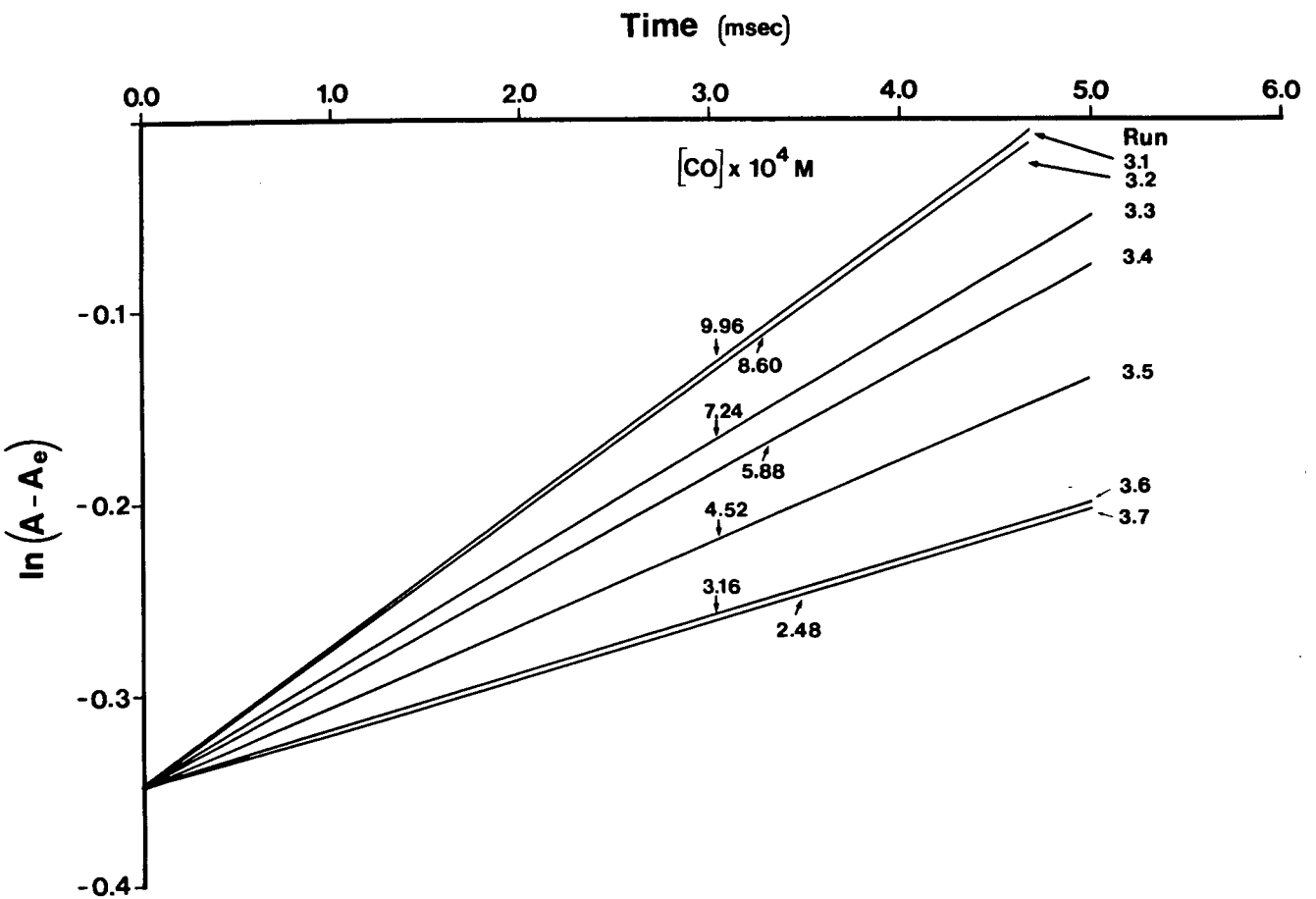


Figure IV.25 Variation in the slope of the ln(A-Ae) *vs.* time plots with changes in CO concentration for kinetic Run 3 of the native P450cam-CO system.

of the flash unit oscilloscope; longer sweep times resulted in noisy and badly smeared ln(A-Ae) *vs.* time plots. A least squares fit[168] of data points taken from the maximum, minimum and mean slopes of the plots gave observed rate constants that deviated by ≈25% from both the k_{obs} values calculated from the $t_{½}$ values obtained directly from the exponential decay curves and the computer-derived k_{obs} values (see Tables IV.10, IV.11 and IV.12); the calculated and computer-derived k_{obs} values on the other hand varied by only 10%. Plots of the $t_{½}$ values obtained directly from the absorbance *vs.* time plots *vs.* k_{obs}^{-1} data from the analog device gave straight lines of slope 0.93±0.07, 0.87±0.06 and 0.84±0.01 for kinetic Runs 1, 2 and 3, respectively (see Figure IV.26), while the analogous straight line plots for the computer-derived k_{obs} values gave slopes that were much closer to the expected values of ln2 for a first-order reaction; kinetic Runs 1, 2 and 3 gave slopes of 0.73±0.01, 0.67±0.02 and 0.70±0.01, respectively (see Figure IV.26). Inspection of the $t_{½}$ *vs.* k_{obs}^{-1} graphs in Figures IV.26 and IV.27 also showed less deviation in the plots between kinetic runs for the computer-derived k_{obs} data. Since the computer analysis of the absorbance *vs.* time plots appeared to give more reliable analysis of the exponential decay data, the kinetic constants for the reaction of CO with ferrous P450cam were derived from the computer-derived k_{obs} values. These k_{obs} values varied by ≈20% between kinetic runs and were again approximately 6 times smaller than the corresponding k_{obs} values for the myoglobin-CO system (see Tables IV.6.1, IV.7 and IV.8). Subsequent plotting of the computer-derived k_{obs} values *vs.* CO

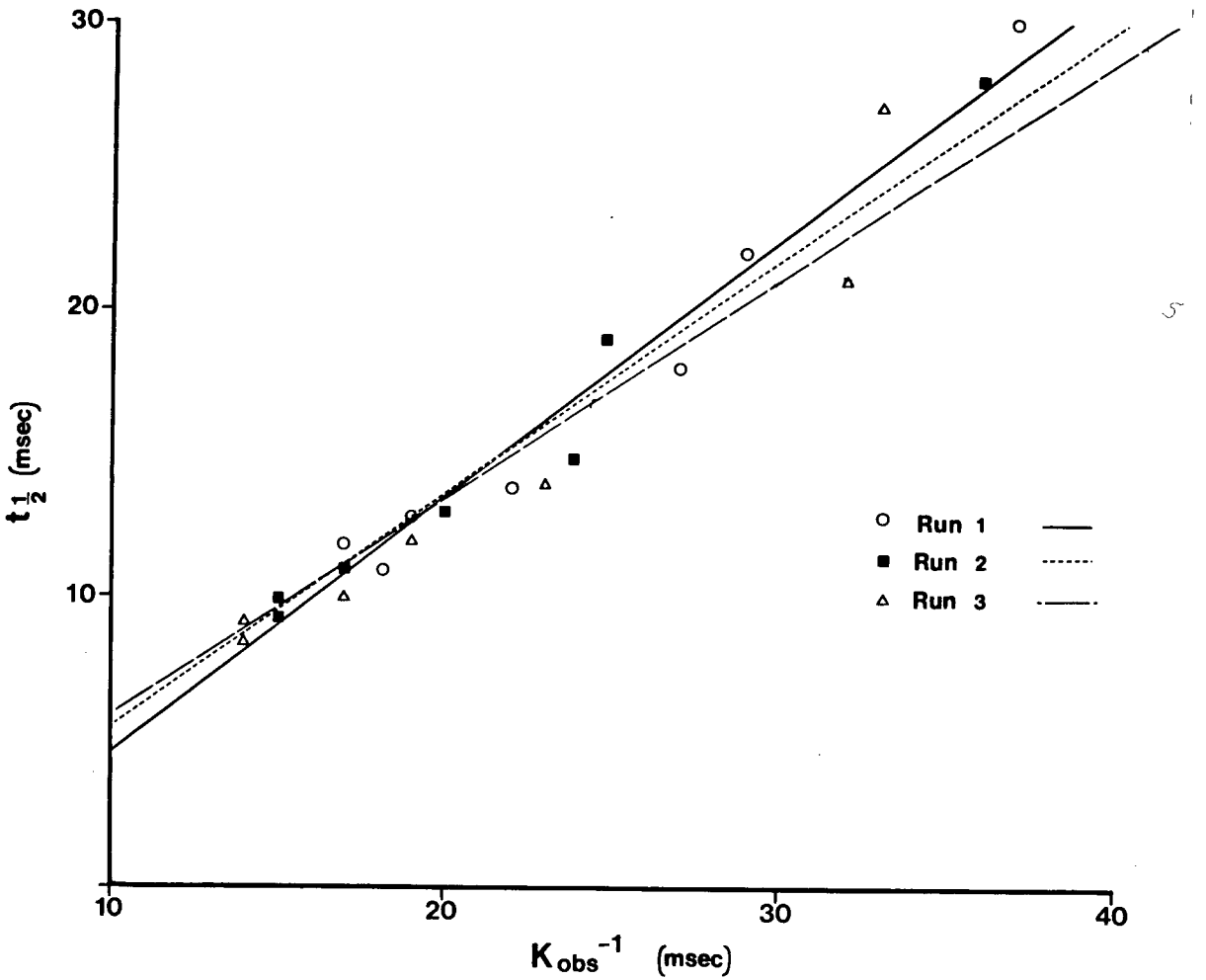


Figure IV.26 Plot of $t_{\frac{1}{2}}$ *vs.* analog-derived k_{obs}^{-1} values from kinetic Runs 1, 2 and 3 for the native P450cam-CO system.

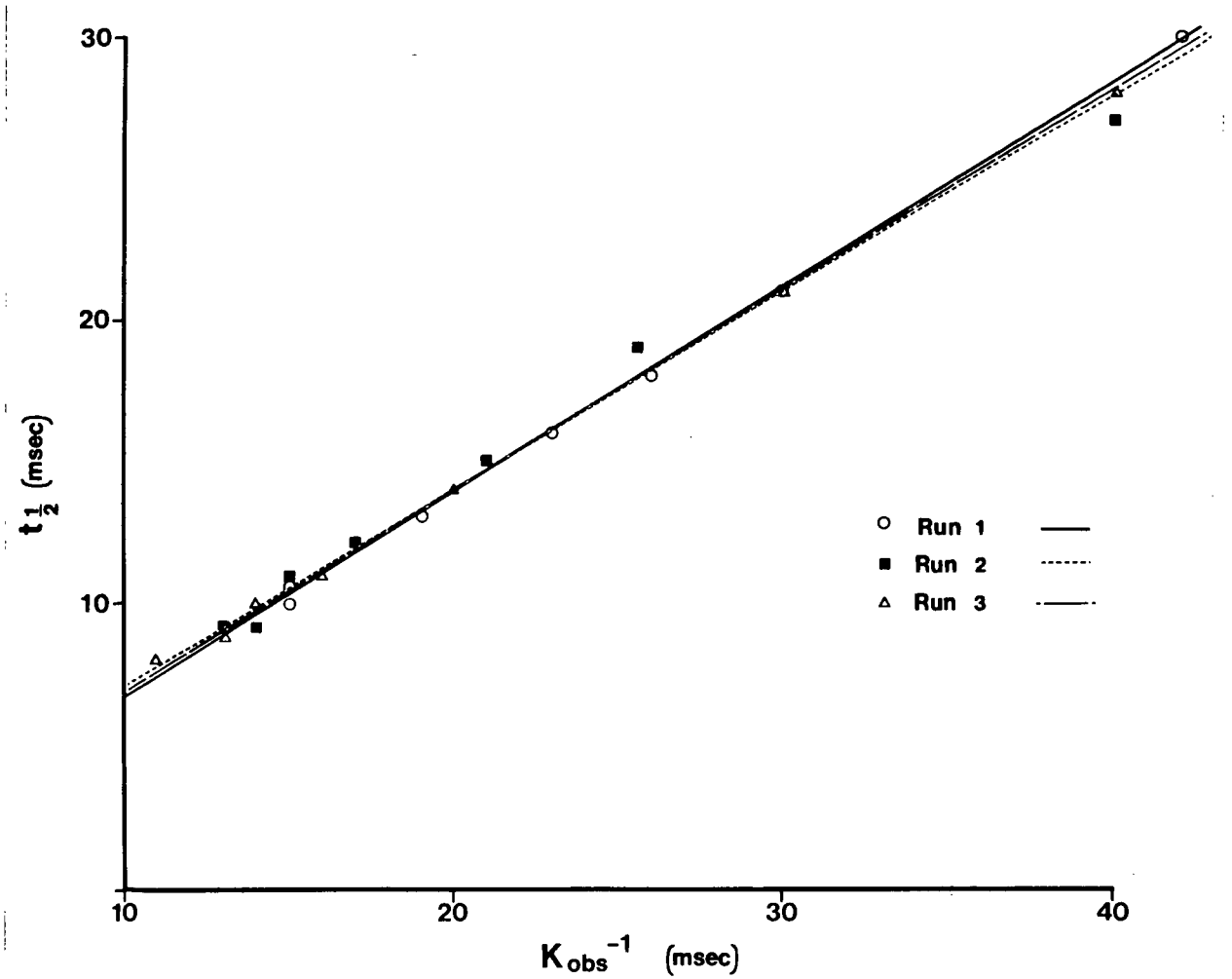


Figure IV.27 Plots of $t_{\frac{1}{2}}$ *vs.* computer-derived k_{obs}^{-1} values for kinetic Runs 1, 2 and 3 for the native P450cam-CO system.

concentrations (Figure IV.28) gave straight lines in accordance with equation IV.2 and allowed for the determination of the kinetic constants for the interaction of CO with the ferrous state of native, substrate-bound, cytochrome P450cam (Table IV.13). The smaller fluctuation in data points of the k_{obs} *vs.* CO concentration plot for kinetic Run 3 was likely due to the stability of the protein concentration throughout the run as indicated in Figure IV.29. Analysis of the data in Table IV.13 gives an average value for the second-order rate constant for the recombination of CO with ferrous substrate-bound P450cam at 20°C of $6.8 \times 10^4 M^{-1} S^{-1}$ ± 20% which is comparable with published literature values obtained for the substrate-bound enzyme *via* flash photolysis ($3.5 \times 10^4 M^{-1} S^{-1}$ at 12°C[133e] and $8.0\text{-}23 \times 10^4 M^{-1} S^{-1}$ between 5 and 25°C[30]) and *via* stopped-flow analysis ($3.8 \times 10^4 M^{-1} S^{-1}$ at 4°C[33e] and $2.2\text{-}3.6 \times 10^5 M^{-1} S^{-1}$ between 20 and 25°C[10,133a]). Comparison of the k_{on} values determined for the myoglobin and substrate-bound P450cam ($4.1 \times 10^5 M^{-1} S^{-1}$ *vs.* $6.8 \times 10^4 M^{-1} S^{-1}$) indicates that the ferrous state of myoglobin reacts approximately 6 times faster with CO than does the P450cam system; the camphor substrate is though to restrict access of the CO molecule to the heme moiety in the P450cam enzymes (see Section II.5). The first-order rate constant for the dissociation of CO from ligand-bound P450cam in the presence of substrate at 20°C of 12 ± 20% can be compared with the stopped flow measurements of $1.7 S^{-1}$ and $2.8 S^{-1}$ between 20 and 24°C.[10,133a] On analogy with the myoglobin system, which also showed enhancement of the k_{off} value, the monitoring light at

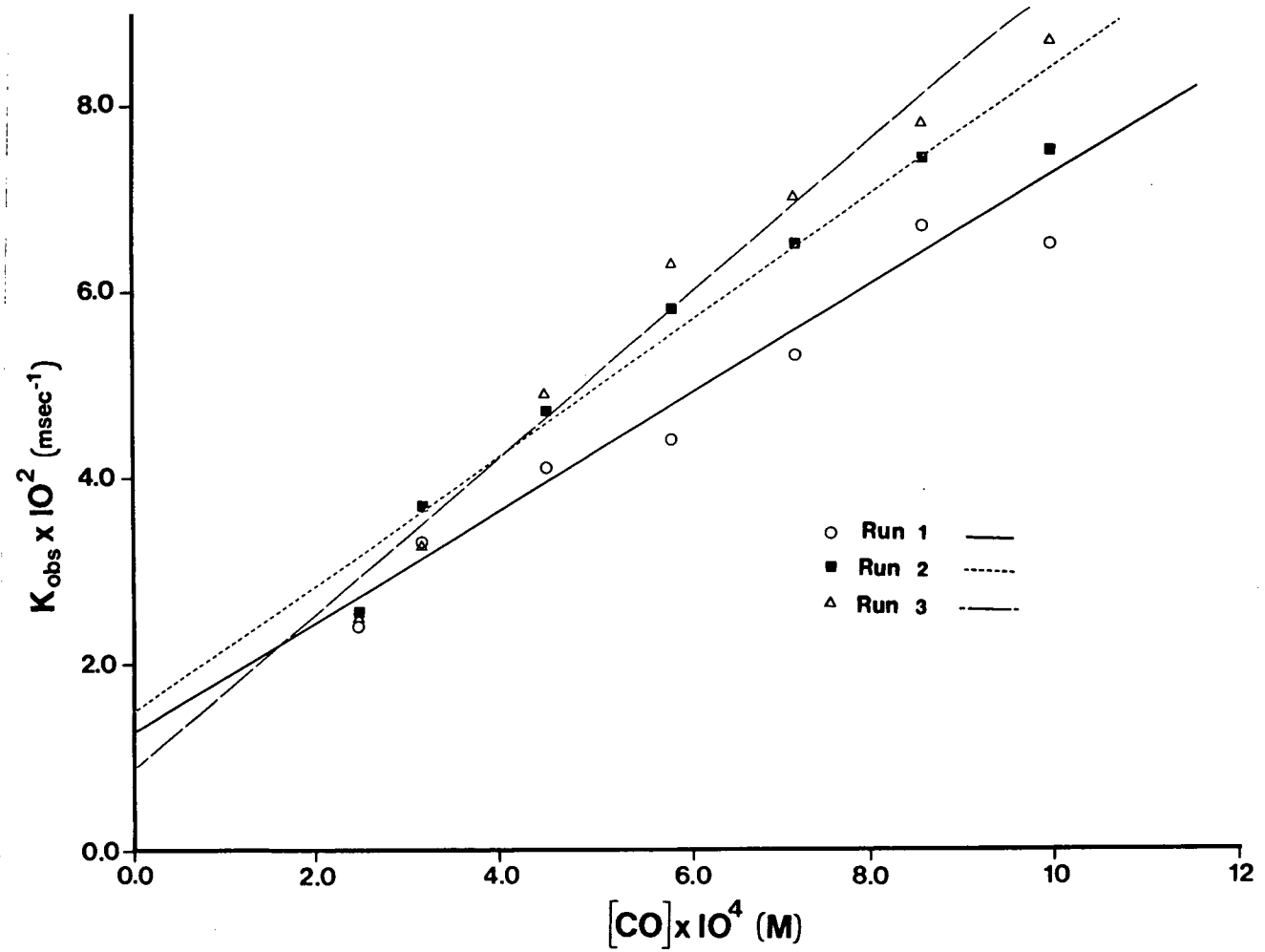


Figure IV.28 Plots of k_{obs} *vs.* CO concentrations for kinetic Runs 1, 2 and 3 for the substrate-bound native P450cam-CO system.

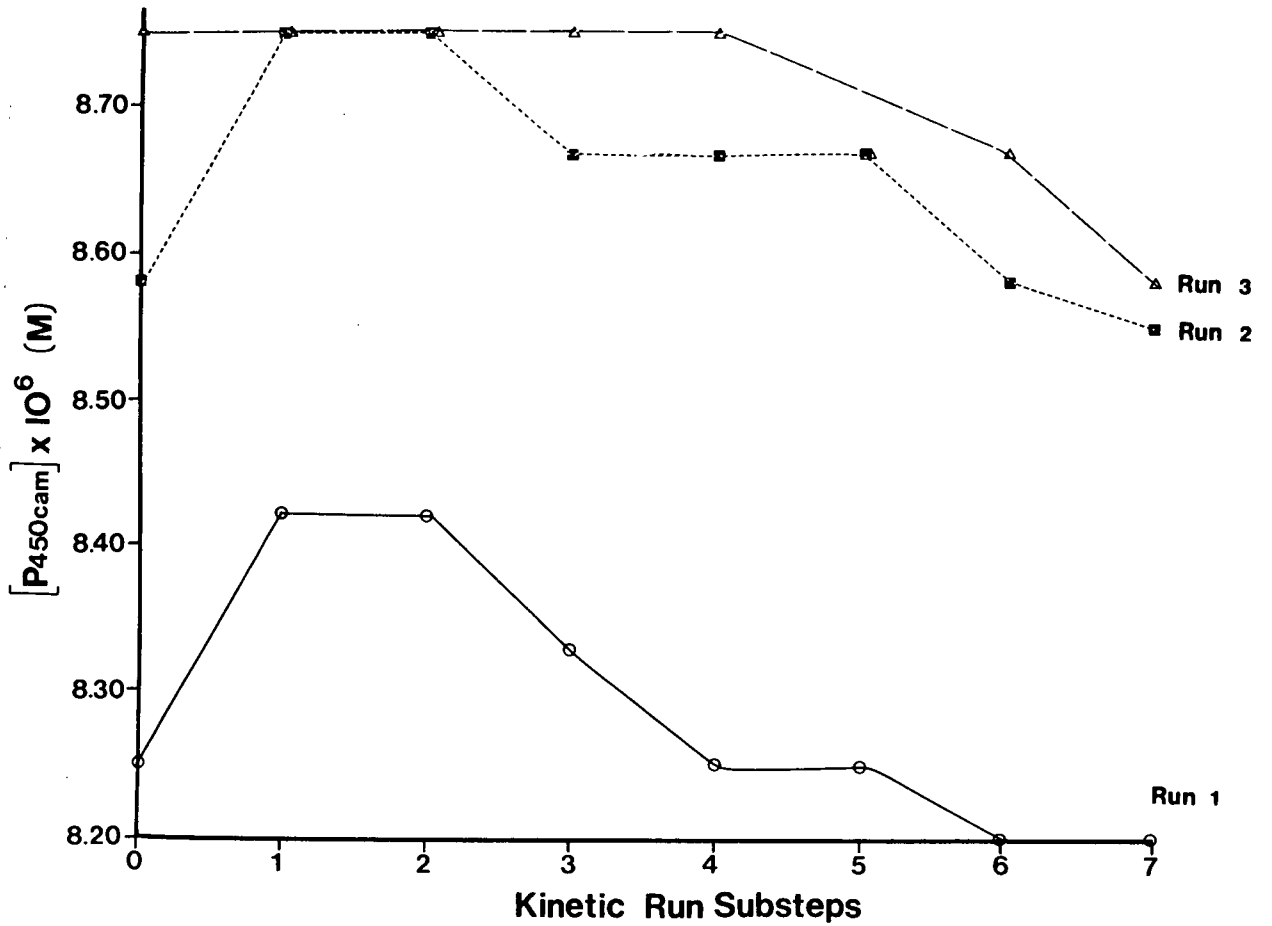


Figure IV.29 Fluctuation in protein concentration throughout kinetic Runs 1, 2 and 3 for the native P450cam system.

442nm appears to have enhanced the photodecomposition rate of CO-bound hemoprotein. The resulting equilibrium constant, Kco, at 20°C of $6.0 \times 10^{3} M^{-1}$ is thus apparently low when compared with the literature value of $1.3 \times 10^{5} M^{-1}$ obtained at the same temperature.[99]

Table IV.13

Kinetic Constants[(a)] obtained for the Reaction of CO with the Ferrous State of Native Substrate-bound Cytochrome P450cam at 20°C.

Kinetic Run	[Protein] (M)	k_{on}(c) ($M^{-1}S^{-1}$)	k_{off}(c) (S^{-1})	Kco(b) (M^{-1})
1	8.42×10^{-6}	$5.7 \pm 0.5 \times 10^{4}$	13±3	4.4×10^{3}
2	8.60×10^{-6}	$6.6 \pm 0.7 \times 10^{4}$	15±4	4.4×10^{3}
3	8.75×10^{-6}	$8.2 \pm 0.6 \times 10^{4}$	9±4	9.1×10^{3}

a) Kinetic constants obtained from the computer analysis of the absorbance *vs.* time plots.

b) Equilibrium constant calculated from the expression

$$Kco = \frac{k_{on}}{k_{off}}$$

. Estimated error, ± 40%.

c) Quoted errors derived from the least squares analysis of the k_{obs} *vs.* concentration plots.

IV.4.4 Study of the Reaction of CO with the Ferrous Substrate-bound State of Protohemin-reconstituted Cytochrome P450cam by Flash Photolysis

Kinetic data for the reaction of CO with the ferrous substrate-bound state of protohemin-reconstituted cytochrome P450cam were collected at 20°C on three different reconstituted protein samples; protein concentrations were fixed at 7.50×10^{-6}M ± 5% and the CO concentrations varied from 0.2 - 1.0×10^{-3}M. Typical data from kinetic Run 2 for the reconstituted P450cam system are analyzed in detail below along with comparison with analogous data from kinetic Runs 1 and 3 for the reconstituted enzyme system and the results from the myoglobin and native substrate-bound P450cam system described above (see Sections IV.4.2 and IV.4.3 respectively). Raw data for kinetic Run 2 for reconstituted P450cam (i.e. exponential decay curves, linear rate plots and spectral data) are given in Appendix IV.c and tabulated in Table IV.14; kinetic data for kinetic Runs 1 and 3 are tabulated in Tables IV.15 and IV.16 respectively.

Figure IV.30 shows a typical set of kinetic data from kinetic Run 2 for the reaction of CO with the ferrous-reconstituted P450cam system at a fixed protein concentration of 7.50×10^{-6}M and CO concentration of 7.24×10^{-4}M. The absorbance *vs.* time trace shown in Figure IV.30A was obtained by following the increase in intensity of the ferrous-CO adduct of the reconstituted enzyme at 442nm as described for native P450cam (see Section IV.4.3) and direct proportionality was again observed between the spectral absorbance and the flash unit voltage of the ferrous-

A) FLASH PHOTOLYSIS EXPERIMENTS

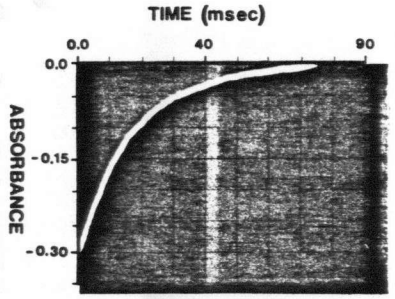
Sample Description: Protohemin-reconstituted P450cam-CO complex

Temperature: 20±0.2°C

Monitoring Wavelength: 442nm

Data Table

Run	Plot Form	Cary O.D.	Flash Unit Volt.	P_T (mm Hg)	P_{H_2O} (mm Hg)	P_{CO} (mm Hg)	$[CO]\times10^4$ (m/L)	Half Life (msec)
2.3	Exp. Decay	0.824	0.820	550	17.5	533	7.24	13



Vertical Amplitude: 0.05 (volts/div)

Sweep Time: 10 (msec/div)

Half Life Data

Half Life #	Vertical Drop (volts)	Horizontal Sweep (msec)
0	0.300	0
1	0.150	11.5 (12)
2	0.075	23 (11)
3	0.038	36 (13)
4	0.019	50 (14)

$t_{\frac{1}{2}}$ = 13msec

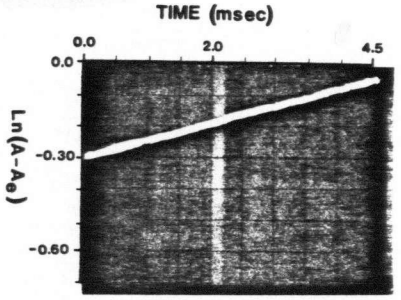
B) FLASH PHOTOLYSIS EXPERIMENTS

Sample Description: Protohemin-reconstituted P450cam-co complex

Temperature: 20±0.2°C

Data Table

Run	Plot Form	Cary O.D.	Flash Unit Volt.	P_T (mm Hg)	P_{H_2O} (mm Hg)	P_{CO} (mm Hg)	$[CO]\times10^4$ (m/L)	k_{obs} ($msec^{-1}$)
2.3	Rate Plot	0.824	0.820	550	17.5	533	7.24	5.3×10^{-2}



Vertical Amplitude: 0.1 (volts/div)

Sweep Time: 0.5 (msec/div)

Slope (mean)		Slope (max)		Slope (min)	
X (msec)	Y (volts)	X (msec)	Y (volts)	X (msec)	Y (volts)
0	-0.300	0	-0.305	0	-0.280
0.5	-0.265	0.5	-0.270	0.5	-0.260
1.0	-0.240	1.0	-0.245	1.0	-0.240
1.5	-0.210	1.5	-0.210	1.5	-0.210
2.0	-0.190	2.0	-0.190	2.0	-0.190
2.5	-0.160	2.5	-0.155	2.5	-0.165
3.0	-0.130	3.0	-0.130	3.0	-0.140
3.5	-0.080	3.5	-0.070	3.5	-0.090
4.0	-0.080	4.0	-0.070	4.0	-0.090

Least Squares Analysis

m: 5.3×10^{-2} $msec^{-1}$

y-intercept: -2.9×10^{-1}

δy: 1.9×10^{-3}

δm: 9.7×10^{-4} $msec^{-1}$

Figure IV.30 Typical set of kinetic data obtained from kinetic Run 2 for the reaction of CO with the ferrous substrate-bound state of protohemin-reconstituted cytochrome P450cam; (A) shows the exponential decay curve while (B) indicates the linear rate plot.

Table IV.14

Kinetic Data[(a)] from kinetic Run 2 for the Reaction of CO with the Ferrous Substrate-bound State of Protohemin-reconstituted Cytochrome P450cam at 20°C.

Run	$[CO]x10^4$ (M)	$t_{1/2}$ (msec) (a)	$k_{obs}x10^2$ ($msec^{-1}$) (a)	$k_{obs}x10^2$ ($msec^{-1}$) (b)	$t_{1/2}$ (msec) (c)	$k_{obs}x10^2$ ($msec^{-1}$) (c)
2.1	9.96	10.5	6.6	6.6	10.6	6.7
2.2	8.60	11	6.3	6.1	11	6.3
2.3	7.24	13	5.3	5.3	13	5.2
2.4	5.88	15	4.6	4.1	15	4.7
2.5	4.52	18	3.9	3.5	18	3.9
2.6	3.16	25	2.8	2.3	24	2.9
2.7	2.48	30	2.3	1.4	30	2.3

a) Determined directly from the absorbance *vs.* time plots; k_{obs} values determined using the relationship $k = \frac{\ln 2}{t_{1/2}}$

b) Determined experimentally from the ln(A-Ae) *vs.* time plots *via* the analog converter.

c) Determined experimentally over approximately four half-lives of the absorbance *vs.* time plots by computer analysis; Ref.168

Table IV.15

Kinetic Data[a] from kinetic Run 1 for the Reaction of CO with the Ferrous Substrate-bound State of Protohemin-reconstituted Cytochrome P450cam at 20°C.

Run	$[CO]x10^4$ (M)	$t_{1/2}$ (msec) (b)	$k_{obs}x10^2$ ($msec^{-1}$) (b)	$k_{obs}x10^2$ ($msec^{-1}$) (c)	$t_{1/2}$ (msec) (d)	$k_{obs}x10^2$ ($msec^{-1}$) (d)
1.1	9.96	10	6.9	7.0	10.5	7.4
1.2	8.60	11	6.3	6.1	11	6.6
1.3	7.24	12	5.8	5.4	13	5.7
1.4	5.88	15	4.6	4.0	15	4.8
1.5	4.52	18	3.9	3.6	18	3.9
1.6	3.16	25	2.8	2.2	25	2.8
1.7	2.48	30	2.3	1.6	29	2.2

a) Kinetic Data determined at a protein concentration of $7.80x10^{-6}$M; kinetic constants are tabulated in Table IV.17.

b) Determined experimentally from the absorbance *vs.* time plots; k_{obs} values determined using the relationship $k = \frac{\ln 2}{t_{1/2}}$

c) Determined experimentally from the ln(A-Ae) *vs.* time plots *via* the analog converter.

d) Determined over approximately four half-lives of the absorbance *vs.* time plots by computer analysis; Ref.168.

Table IV.16

Kinetic Data[a] from kinetic Run 3 for the Reaction of CO with the Ferrous Substrate-bound State of Protohemin-reconstituted Cytochrome P450cam at 20°C.

Run	$[CO]x10^4$ (M)	$t_{1/2}$ (msec) (b)	$k_{obs}x10^2$ ($msec^{-1}$) (b)	$k_{obs}x10^2$ ($msec^{-1}$) (c)	$t_{1/2}$ (msec) (d)	$k_{obs}x10^2$ ($msec^{-1}$) (d)
3.1	9.96	9.5	7.3	7.1	10	7.0
3.2	8.60	10	6.9	6.5	11	6.4
3.3	7.24	13	5.3	5.0	12	5.5
3.4	5.88	14	5.0	4.5	14	4.8
3.5	4.52	17	4.1	3.8	18	4.0
3.6	3.16	24	2.9	2.5	24	2.8
3.7	2.48	30	2.3	1.3	30	2.3

a) Kinetic data obtained at a protein concentration of $7.20x10^{-6}$M; kinetic constants tabulated in Table IV.17.

b) Determined experimentally from the absorbance *vs.* time plots; k_{obs} values determined using the relationship $k = \frac{\ln 2}{t_{1/2}}$

c) Determined experimentally from the ln (A-Ae) *vs.* time plots *via* the analog converter.

d) Determined over approximately four half-lives of the absorbance *vs.* time plots by computer analysis; Ref.168.

CO adduct at 442nm (see Data Table Figure IV.30A). As observed with the myoglobin (Figure IV.19A) and native P450cam (Figure IV.24A) systems, the initial absorbance on the absorbance *vs.* time plot represented ≈30% photodecomposition of the CO adduct (Figure IV.30A). Based on $t_{\frac{1}{2}}$ half-life data derived directly from the exponential decay plot (see Half-Life Data table Figure IV.30A) and from a separate computer analysis of the curve (see Table IV.14) the reaction of CO with the ferrous, substrate-bound state of protohemin-reconstituted P450cam again approximated a first-order process, and $t_{\frac{1}{2}}$ values derived by both methods were in excellent agreement (see Table IV.14); similar results were observed for kinetic Runs 1 and 3 (see Table IV.15 and IV.16 respectively). Comparison of the half-life data for the reconstituted P450cam system indicated a 10% variation in the $t_{\frac{1}{2}}$ values between kinetic runs and showed good agreement with $t_{\frac{1}{2}}$ values for the native enzyme (see Section IV.4.3); the $t_{\frac{1}{2}}$ values were again approximately 6 times larger than the corresponding values for the myoglobin system (see Tables IV.6.1, IV.7, and IV.8).

Analysis of the absorbance *vs.* time plots *via* the analog converter of the flash unit (in accordance with equation IV.1) gave linear plots (kinetic Run 2 data given in Figure IV.30B) that varied with CO concentration (Figure IV.31); however, since the plots contained only up to 0.5 half-lives of the absorbance *vs.* time plots (see Figure IV.30B), the resultant k_{obs} values calculated from the linear rate plots were apparently unreliable when compared with either the k_{obs} values calculated

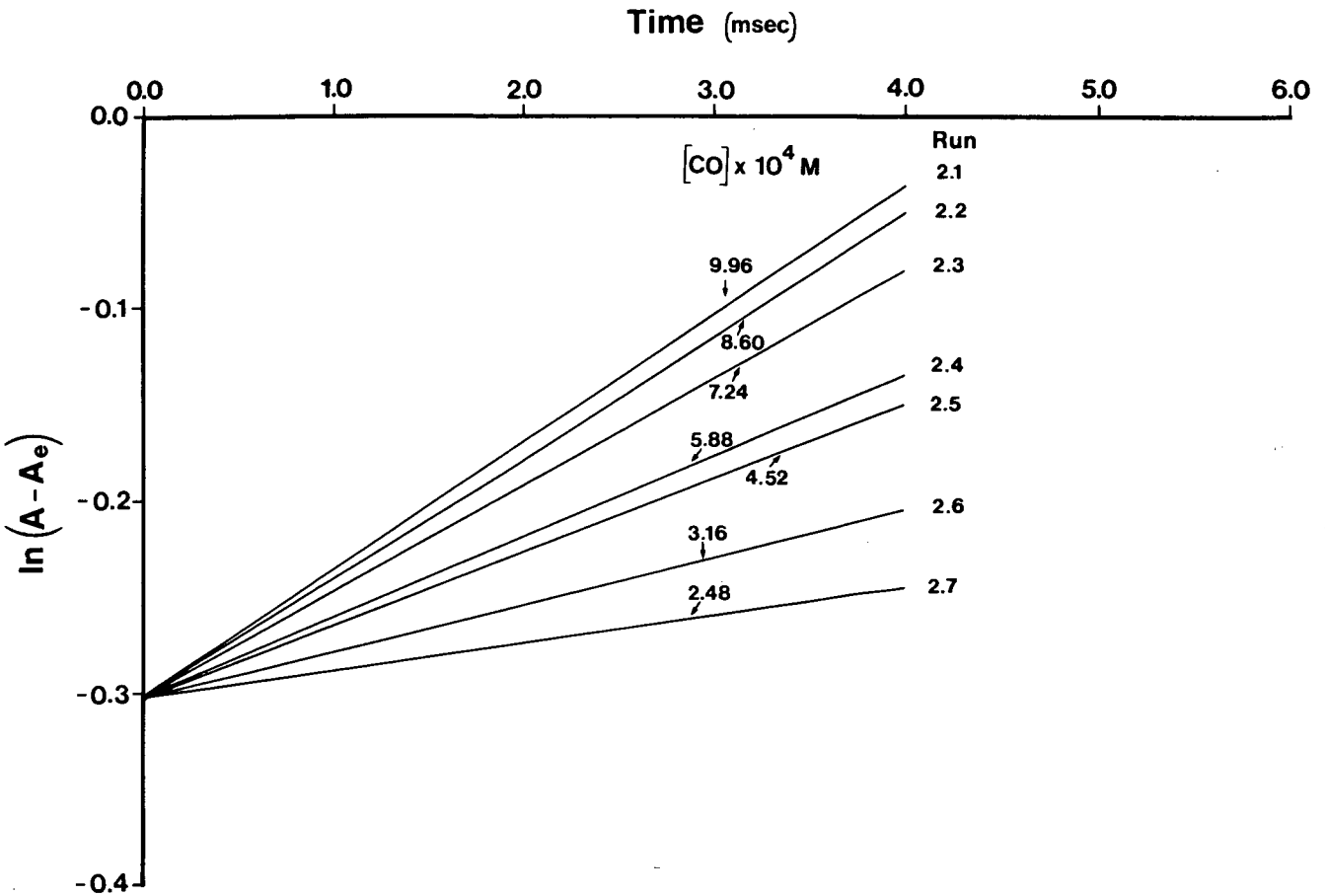


Figure IV.31 Variation of the slope of the ln(A-Ae) *vs.* time plots with CO concentration for kinetic Run 2 of the protohemin-reconstituted P450cam-CO system.

from $t_{\frac{1}{2}}$ values obtained directly from the exponential decay curves or the computer-derived k_{obs} values (see Table IV.14) Plotting the $t_{\frac{1}{2}}$ values obtained directly from the exponential decay curves *vs.* k_{obs}^{-1} data from the analog device gave straight lines with slopes that deviated by up to 50% from the expected value of ln2 for a first-order reaction; kinetic Runs 1, 2 and 3 gave slopes of 0.42 ± 0.03, 0.36 ± 0.04 and 0.33 ± 0.05 respectively for k_{obs} values obtained *via* the analog device (see Figure IV.32), while slopes of 0.64 ± 0.02, 0.70 ± 0.02 and 0.69 ± 0.02 for the respective kinetic Runs were obtained for the plots utilizing the computer-derived k_{obs} data (Figure IV.33). Subsequent determination of the kinetic constants for the reaction of CO with the reconstituted P450cam system was done using the computer-derived data; these data varied by ≈10% between kinetic runs, showed good agreement with the corresponding k_{obs} data obtained for the native enzyme system (see Section IV.4.3), and indicated an ≈6-fold decrease in the observed rate of reaction when compared with the myoglobin system (see Section IV.4.2).

Graphing of the computer-derived k_{obs} values *vs.* CO concentration as shown in Figure IV.34 for kinetic Runs 1, 2 and 3 gave straight lines in accordance with equation IV.2 and provided the corresponding k_{on} and k_{off} values for the reconstituted P450cam system (Table IV.17); the close correlation of the data to a straight line may have been due to the stability of the protein concentration throughout the kinetic runs (Figure IV.35). Analysis of the data in

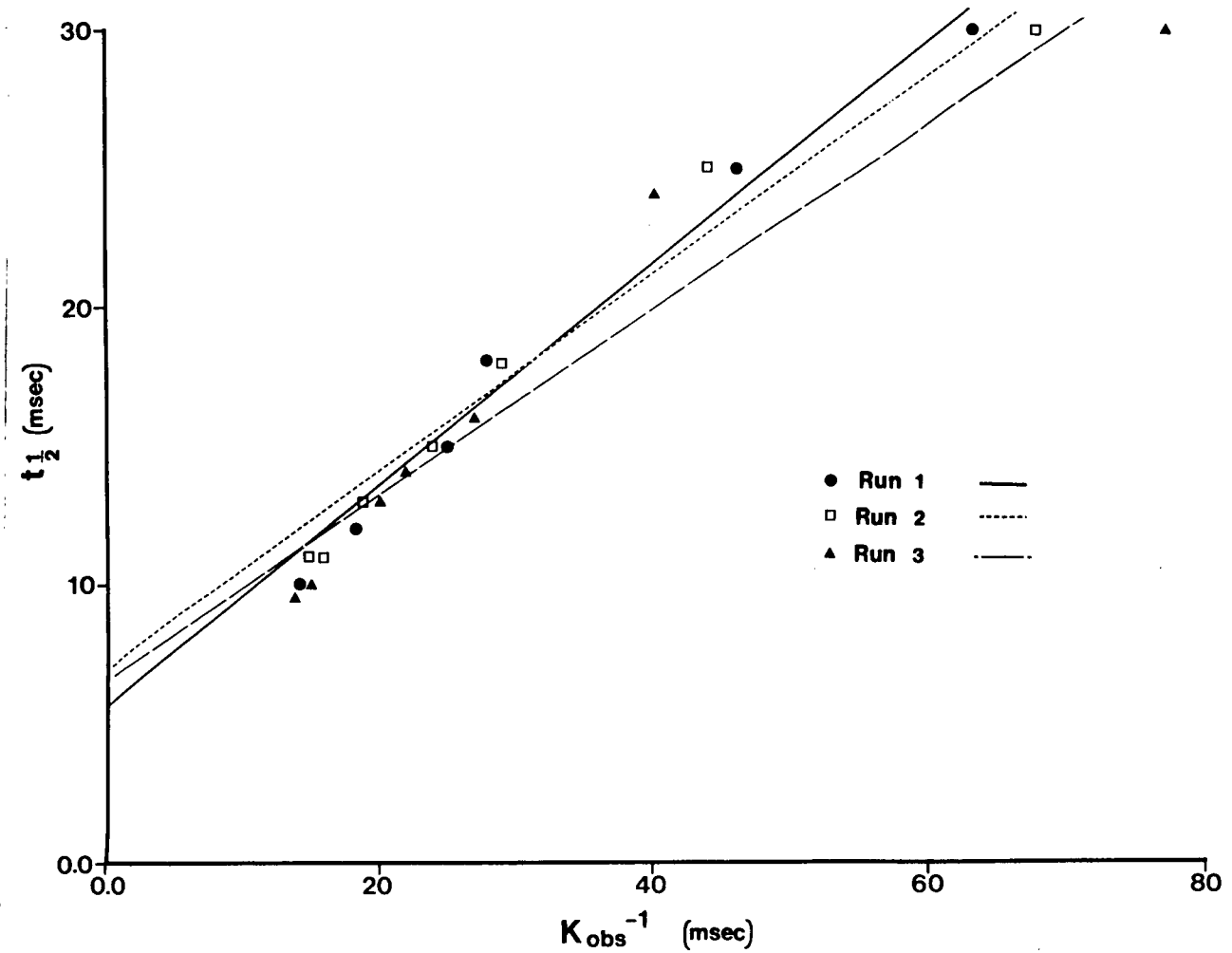


Figure IV.32 Plots of $t_{\frac{1}{2}}$ *vs.* analog-derived k_{obs}^{-1} data for kinetic Runs 1, 2 and 3 for the protohemin-reconstituted P450cam-CO system.

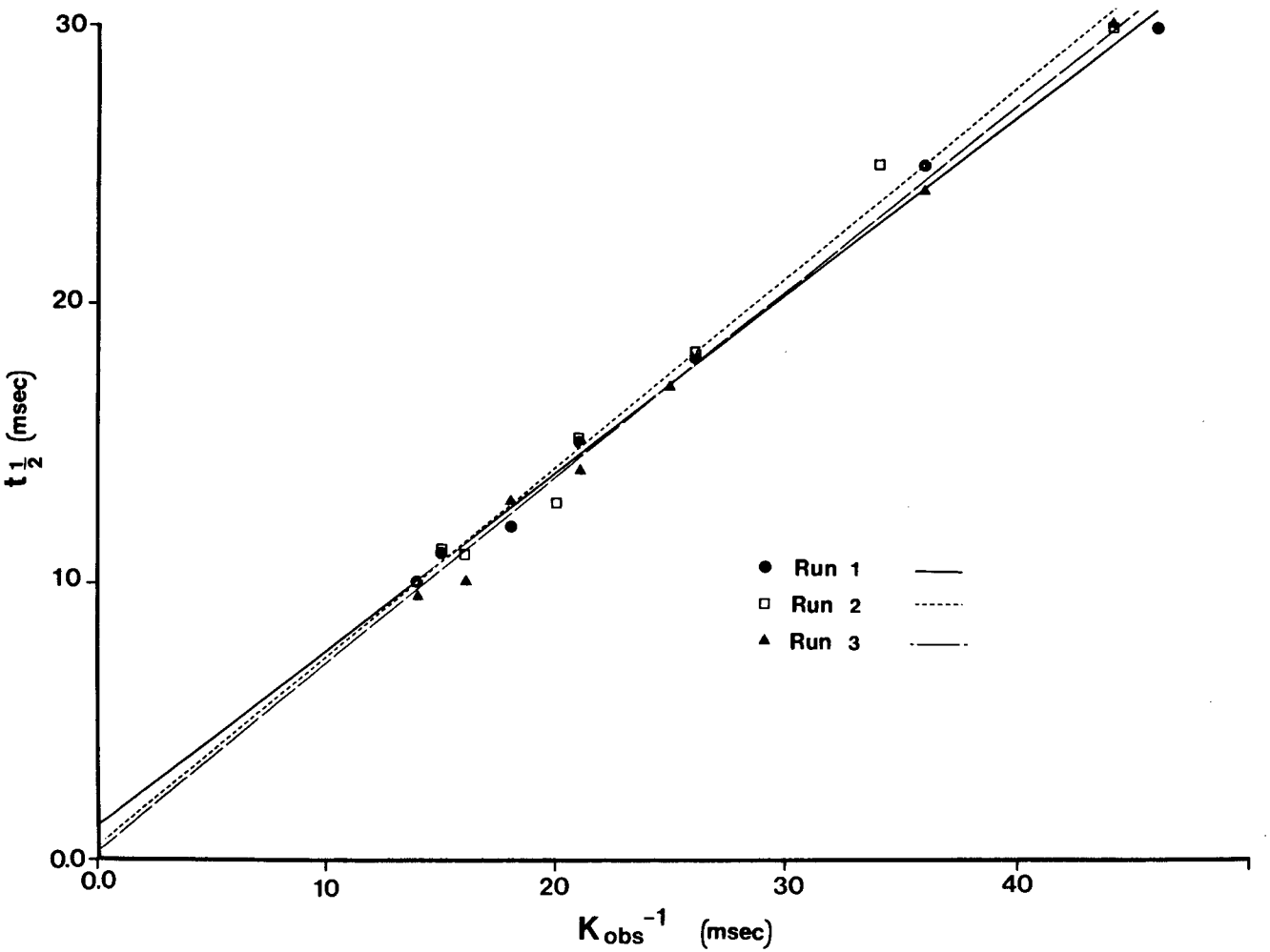


Figure IV.33 Plots of $t_{\frac{1}{2}}$ *vs.* computer-derived k_{obs}^{-1} data for kinetic Runs 1, 2 and 3 for the protohemin-reconstituted P450cam-CO system.

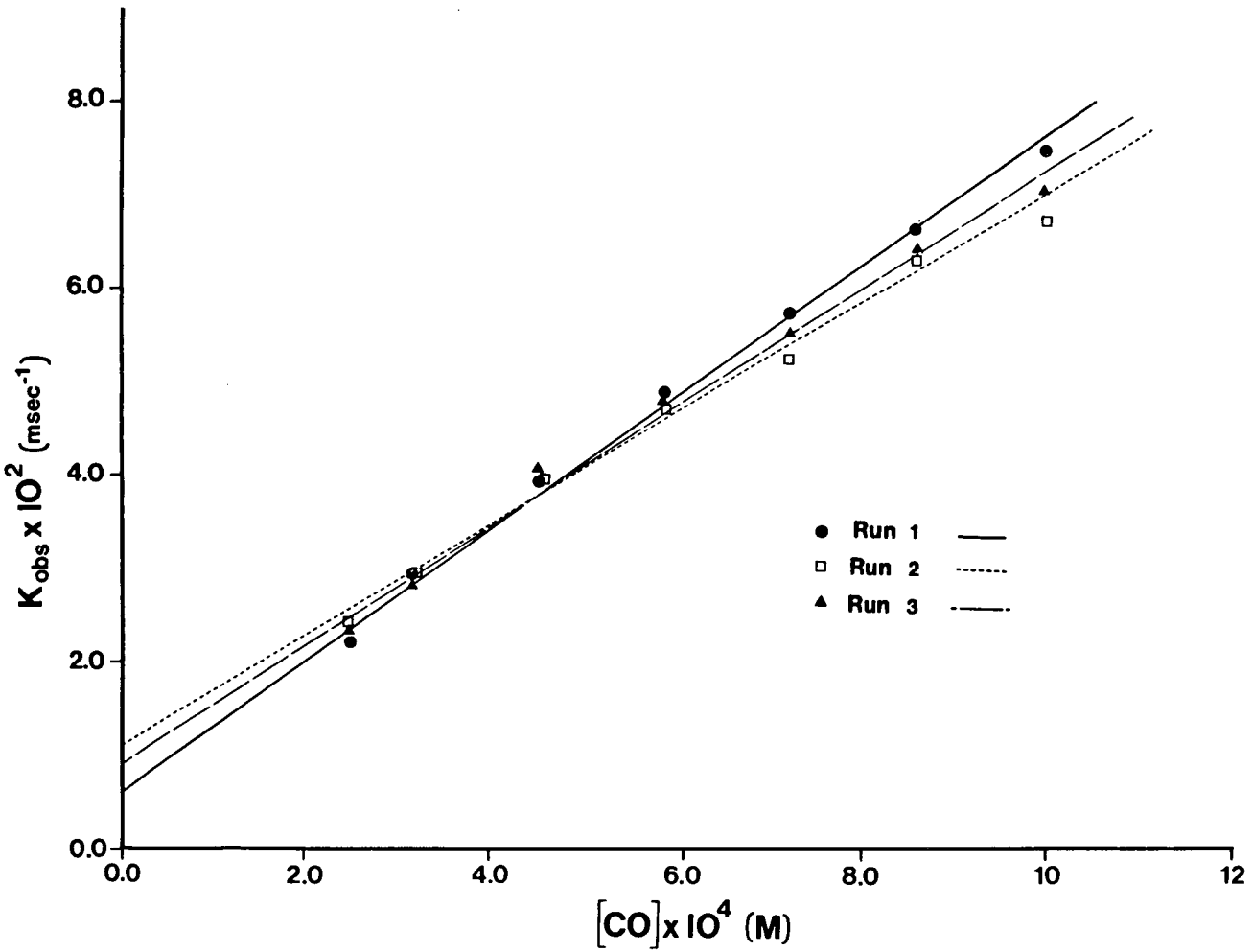


Figure IV.34 Plot of k_{obs} *vs.* CO concentration data for kinetic Runs 1, 2 and 3 for the substrate-bound protohemin-reconstituted P450cam-CO system.

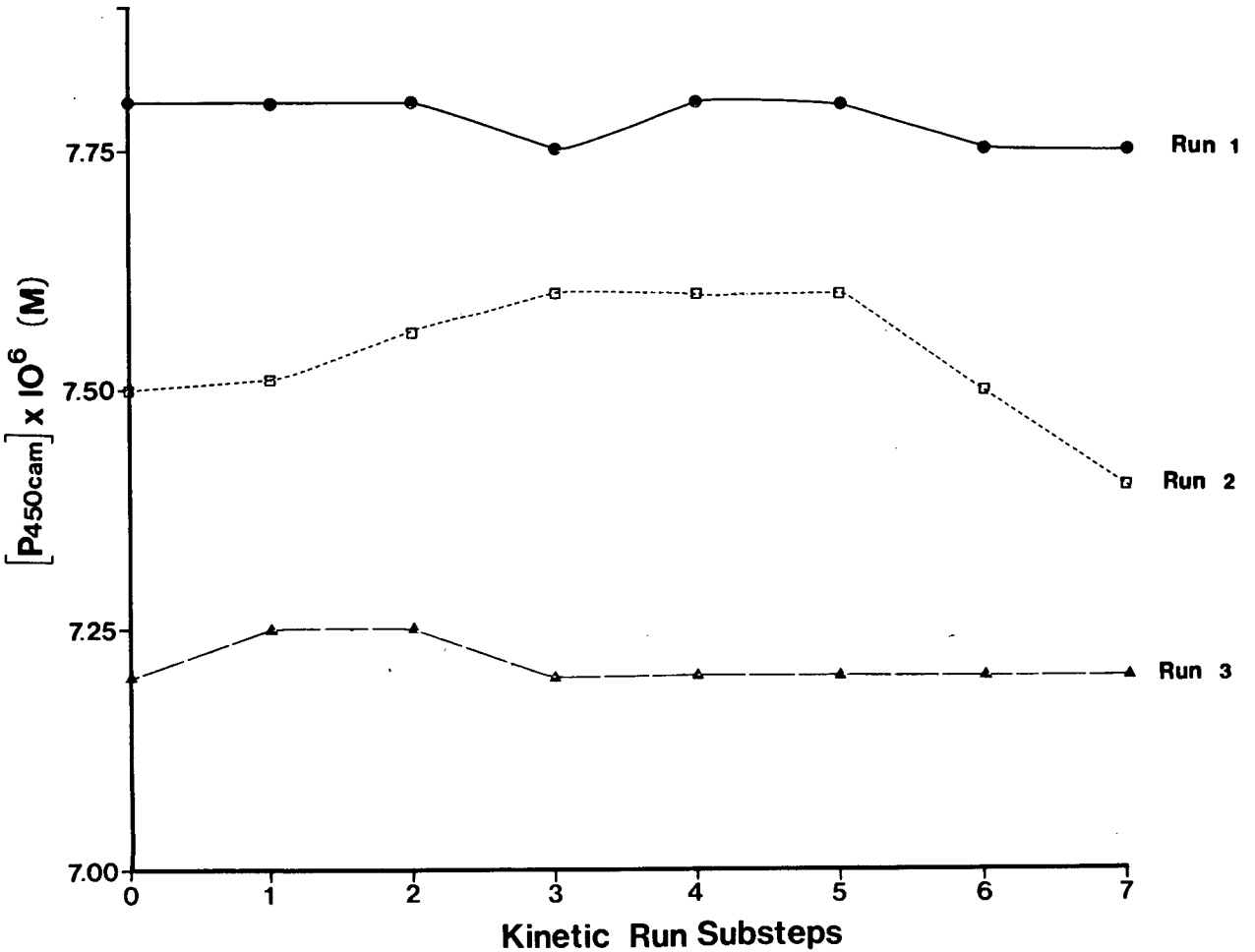


Figure IV.35 Fluctuation in protein concentration during kinetic Runs 1, 2 and 3 for the substrate-bound protohemin-reconstituted P450cam-CO system.

Table IV.17

Kinetic Constants[a] obtained for the Reaction of CO with the Ferrous State of Protohemin-Reconstituted Cytochrome P450cam at 20°C.

Kinetic Run	[Protein] (M)	k_{on} ($M^{-1}S^{-1}$)	k_{off} (S^{-1})	Kco[b] (M^{-1})
1	7.8×10^{-6}	$6.9\pm0.2\times10^{4}$	6 ± 1	1.2×10^{4}
2	7.5×10^{-6}	$5.9\pm0.3\times10^{4}$	11 ± 2	5.4×10^{3}
3	7.2×10^{-6}	$6.3\pm0.3\times10^{4}$	9 ± 2	7.0×10^{3}

a. Kinetic constants derived from plots of k_{obs} values from a computer analysis of the absorbance *vs.* time plots *vs.* CO concentrations. Quoted errors obtained from least squares fit of k_{obs} *vs.* CO concentration data.

b. Equilibrium constant obtain from the expression $K \doteq \frac{k_{on}}{k_{off}}$. Estimated error, ± 30%.

Table IV.17 gives an average value of the second-order rate constant for CO-association with the ferrous substrate-bound state of protohemin-reconstituted P450cam at 20°C of $6.4 \times 10^{4} M^{-1} S^{-1}$ ± 10% which is in excellent agreement with the k_{on} value derived for the native enzyme, as is the average first-order rate constant for CO dissociation from the reconstituted enzyme at 20°C of $8.7 S^{-1}$ ± 20% (see Section IV.4.3); reconstitution of the native enzyme apparently has little effect on the reactivity of the enzyme towards CO.

IV.5 Spectrophotometric Determination of the Equilibrium Constant for the Reaction of CO with the Ferrous State of Native Substrate-bound Cytochrome P450cam.

IV.5.1 Treatment of Data

As determined in the previous section, the flash photolysis study of the reaction of CO with the ferrous state of myoglobin and the P450cam systems was an unreliable method for the accurate determination of the CO-dissociation constant, k_{off}. More reliable k_{off} values were obtained, however, from the equilibrium constant for the CO reaction, , as calculated in expression IV.3.

$$Kco = \frac{k_{on}}{k_{off}} \qquad (IV.3)$$

Equilibrium constant values for the native P450cam system were obtained by following the changes in intensity of the 408 or 445nm Soret band of the CO-free or CO-bound adduct, respectively, with changes in concentration of CO; Kco values for the reconstituted P450cam system were not obtained, and Kco values for the myoglobin system are not readily obtainable by this method due to the very high CO-affinity of this hemoprotein system.[109]

The formation of the ferrous P450cam-CO complex obeys the reaction:

$$Fe(II)P450cam + CO \underset{}{\overset{Kco}{\rightleftharpoons}} Fe(II)P450cam\text{-}CO \qquad (IV.4)$$

The fraction, Y, of Fe(II)P450cam-CO present at a known CO concentration was calculated from the following expression:[8]

$$Y = \frac{A-Ao}{A_\infty-A} \qquad \text{(IV.5)}$$

where A is the absorbance at a known free ligand concentration

Ao is the absorbance observed when no ligand is present

A_∞ is the absorbance of the fully formed carbonyl complex

The equilibrium constant, Kco, was determined from a plot of log $\frac{A-Ao}{A_\infty-A}$ *vs.* log [CO] as derived below.

$$Kco = \frac{[Fe(II)P450cam\text{-}CO]}{[Fe(II)P450cam][CO]} = \frac{Y}{(1-Y)[CO]} = \frac{A-Ao}{(A_\infty-A)[CO]} \qquad \text{(IV.6)}$$

$$\text{and} \quad \log Kco = \log \frac{A-Ao}{A_\infty-A} - \log[CO] \qquad \text{(IV.7)}$$

where [CO] is the molar concentration of the free ligand studied.

For such plots of log $\frac{A-Ao}{A_\infty-A}$ *vs.* log [CO] the slope is theoretically equivalent to the number of CO ligands bound to ferrous enzyme (i.e. one for the P450cam-CO system), and the intercept on the abscissa gives a value of -log Kco. Experimental scatter often occurred at either extreme of the plot, and where possible, the range of $\frac{A-Ao}{A_\infty-A}$ values used was kept from 0.2 to 4.0 (see below). $P_{\frac{1}{2}}^{CO}$ values, which represent the partial pressure of CO at which the ferrous-CO adduct is half formed, are related to the equilibrium constant by the expression:

$$Kco = \frac{1}{P_{\frac{1}{2}}^{CO}} \qquad \text{IV.8}$$

IV.5.2 CO-Binding to Native P450cam

Equilibrium constant measurements were obtained on four different samples of native, substrate-bound cytochrome P450cam at protein concentrations of 7.50×10^{-6}M ±5% and at CO concentrations ranging from ≃2.0 to 60×10^{-6}M (i.e. from ≃2.0-45mm Hg partial pressure of CO); absorbance data (i.e. λ_{max} and εmM values) for the oxidized, reduced, and reduced-CO enzyme species showed excellent agreement (within 10%) with data listed in Table IV.3 for the native substrate-bound enzyme and all samples were estimated as 80% homogeneous by the A391/A280 absorption ratio (see Section III.3.4.2). Equilibrium data for Run 3 are detailed below while the corresponding data for the remaining experiments (Runs 1, 2 and 4) are tabulated in Appendix Va; results from all equilibrium experiments are discussed below.

Figure IV.36 shows the set of spectral changes observed for Equilibrium Run 3 by the addition of CO to ferrous, substrate-bound cytochrome P450cam; the protein concentration was fixed at 7.48×10^{-6}M and the CO concentration varied from ≃$4.0\text{-}30 \times 10^{-6}$M (i.e. partial pressures of CO ranging from ≃3.0-20mm Hg). Spectrum 1, representing the initial CO-free P450cam species with a Soret maximum at 408nm, decreased with increasing CO concentration (≃$4.0\text{-}30 \times 10^{-6}$M), and gave final spectrum 10 for the fully carbonylated enzyme system (at 1.0×10^{-3}M CO) with Soret maxima at 445 and 365nm. Clean isosbestic points were observed at 465, 429 and 373nm, although

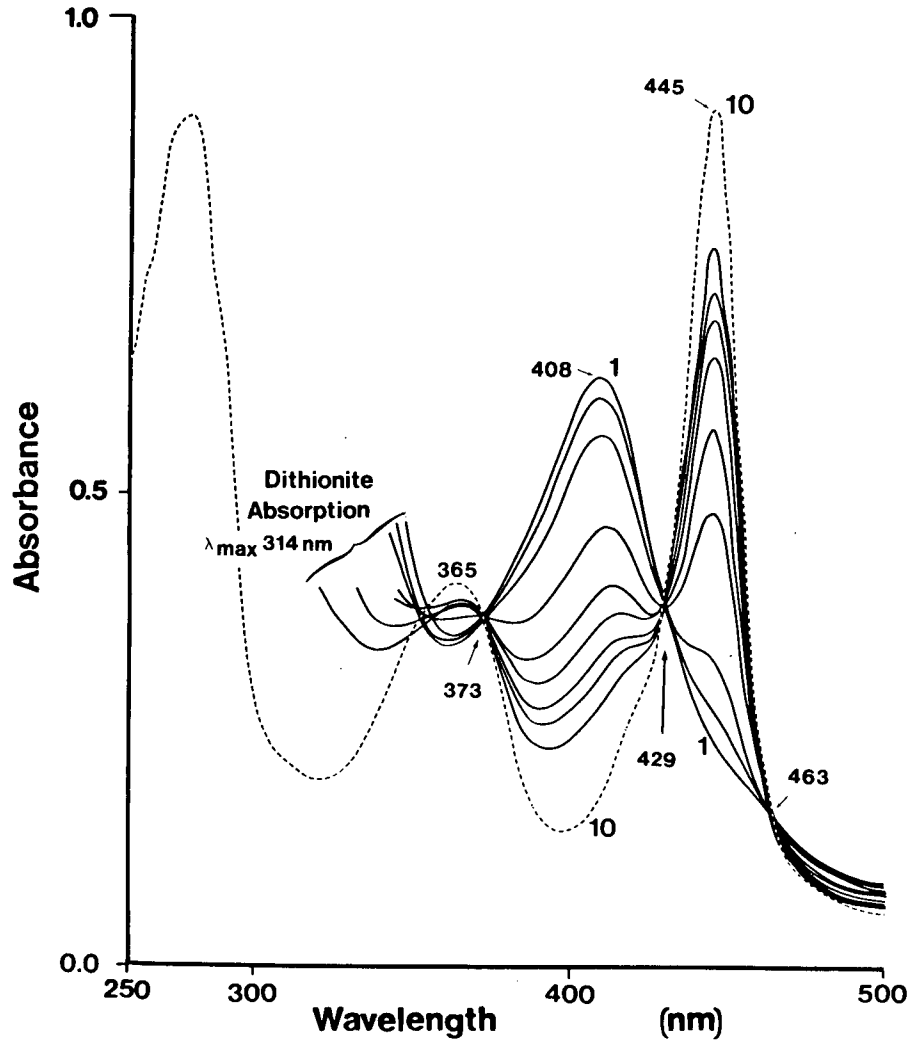


Figure IV.36 Spectral changes observed for Equilibrium Run 3 by the addition of CO to the ferrous substrate-bound state of native cytochrome P450cam.

that around 373nm was often not as well defined because of interference of excess dithionite which has a peak at 314nm; analogous spectral data were obtained for all four equilibrium experiments. Figure IV.37 shows the set of raw data obtained for Equilibrium Run 3; Figure IV.37A gives CO partial pressure data along with the corresponding absorbance readings taken directly off the spectra (Figure IV.36) at the Soret maxima at 408 and 445nm while Figure IV.37B indicates a typical analysis of these data at the 445nm Soret band. Data at the 408nm Soret peak gave essentially the same analysis.

Graphing of the log $\frac{A-Ao}{A_\infty-A}$ *vs.* log [CO] data tabulated in Figure IV.37B for Equilibrium Run 3, along with analogous data from Runs 1, 2 and 4, gave the plots shown in Figure IV.38. These plots showed a distinct curve in the data points for each run, with the most linear region found between log $\frac{A-Ao}{A_\infty-A}$ values of -0.3 to 0.6 (corresponding to $\frac{A-Ao}{A_\infty-A}$ values of 0.5 to 4.0); data points obtained at low CO concentrations (i.e. log $\frac{A-Ao}{A_\infty-A}$ values <-0.3) showed large deviations from linearity particularly for Runs 3 and 4. A least squares fit of data points in the -0.3 to 0.6 log $\frac{A-Ao}{A_\infty-A}$ value range (5-6 points of each run) gave slopes of 1.5 - 1.6 and intercepts on the abscissa of -4.90 - -4.96, corresponding to an average equilibrium constant for reaction IV.4 at 20°C of $8.7 \times 10^4 M^{-1}$ ±10%; the value may be compared to the three reported K_{CO} values for substrate-bound bacterial cytochrome P450cam of $2.6 \times 10^5 M^{-1}$ at 4°C,[133c] $6.6 \times 10^5 M^{-1}$ at 20°C[133a] and $1.3 \times 10^5 M^{-1}$

A)

Equilibrium Data

Sample Description: Native P450cam-CO Complex

Temperature: 20±0.2°C

	Theoretical[155]	Experimental
Vapour Pressure of H_2O:	228 mm oil	229 mm oil
	17.5 mm Hg	17.7 mm Hg

Data Table

Species #	Wanted Pco mm Hg(oil)	P_{Total} (mm oil)	Pco (mm oil)	A445nm	A408nm
1	0	229		0.237	0.613
2	3.00 (39)	271	42.0	0.267	0.589
3	4.00 (52)	279	50.0	0.325	0.550
4	6.00 (78)	303	73.5	0.475	0.453
5	8.00(104)	332	103	0.563	0.388
6	10.0 (130)	360	131	0.641	0.348
7	12.0 (156)	386	157	0.678	0.316
8	14.0 (182)	412	184	0.707	0.294
9	20.0 (260)	489	261	0.751	0.263
10	∞ 1 atm			0.898	0.163

B)

Data Analysis

Wavelength Maxima : 445nm

Absorbance of Pure Species: A_o = 0.237

A_∞ = 0.898

Data Table

Pco (mm Hg)	$[CO]\times10^6$ (M)	Log [CO]	A-Ao	A_∞-A	$\frac{A-A_o}{A_\infty-A}$	log $\frac{A-A_o}{A_\infty-A}$
3.25	4.42	-5.35	0.03	0.631	4.75×10^{-2}	-1.32
3.87	5.26	-5.28	0.088	0.573	1.54×10^{-1}	-8.14×10^{-1}
5.68	7.73	-5.11	0.238	0.423	5.63×10^{-1}	-2.50×10^{-1}
7.96	10.8	-4.96	0.326	0.335	9.73×10^{-1}	-1.18×10^{-2}
10.1	13.8	-4.86	0.404	0.257	1.57	1.96×10^{-1}
12.1	16.5	-4.78	0.441	0.220	2.01	3.02×10^{-1}
14.2	19.3	-4.71	0.470	0.191	2.46	3.91×10^{-1}
20.2	27.4	-4.56	0.514	0.147	3.50	5.44×10^{-1}

Figure IV.37 Raw data obtained for Equilibrium Run 3; (A) gives CO partial pressure and absorbance data while (B) gives the data analysis.

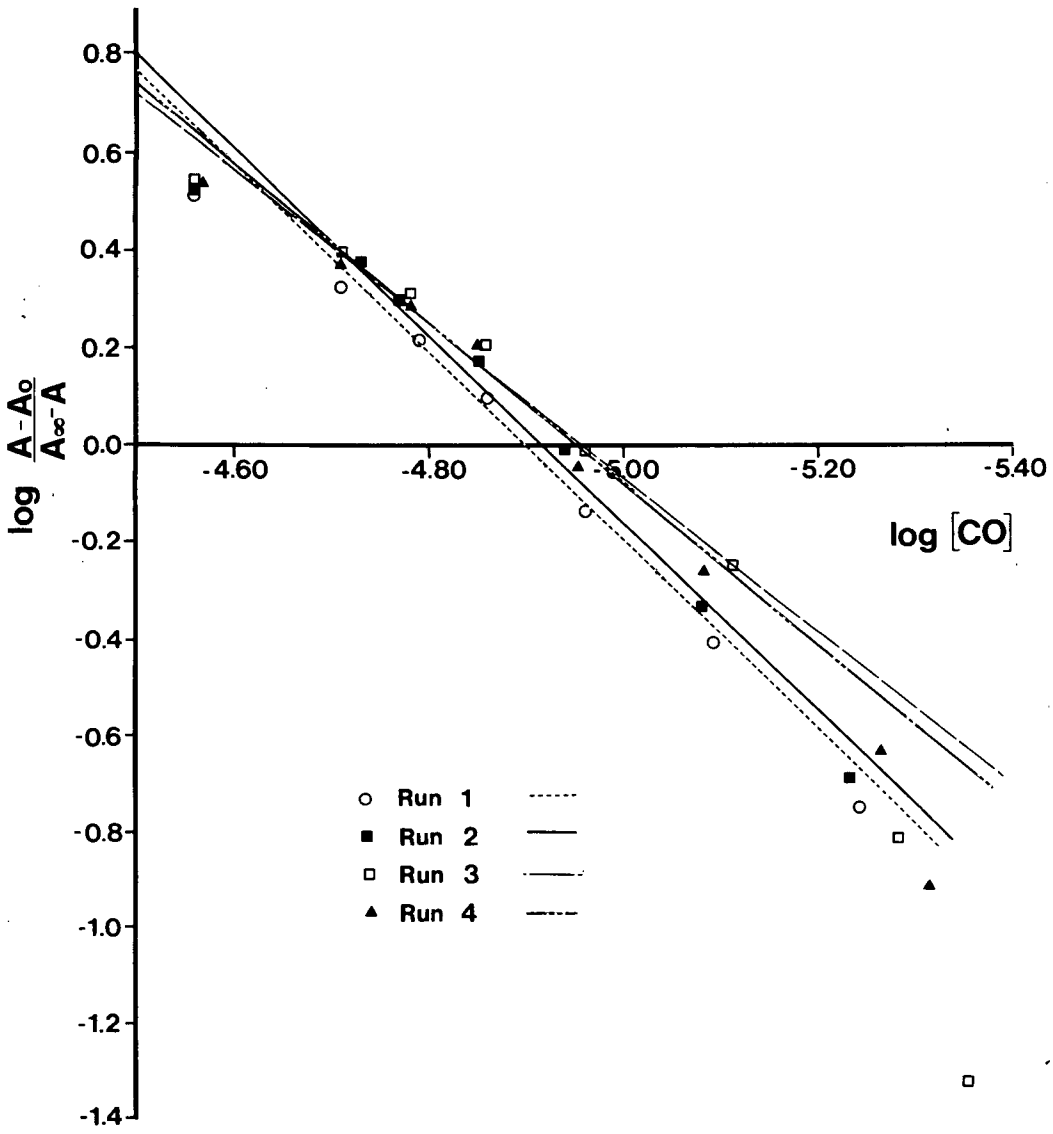


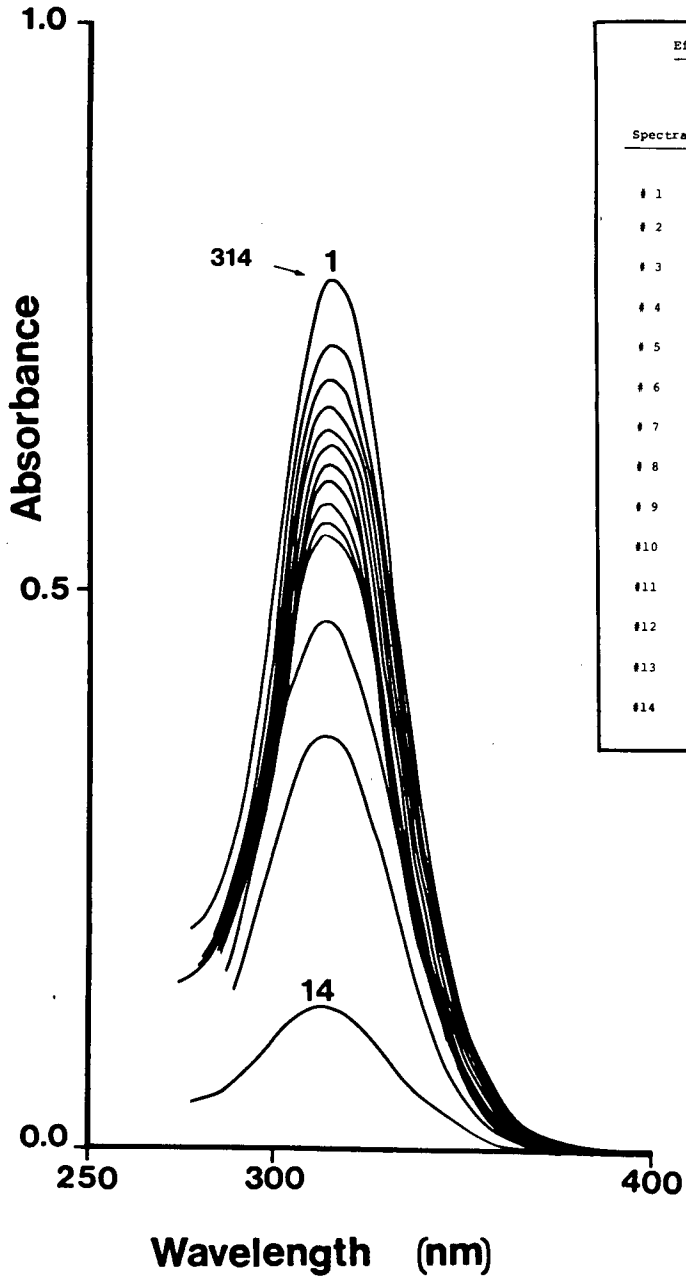
Figure IV.38 Plots of log $\frac{A-Ao}{A_\infty-A}$ *vs.* log[CO] for Equilibrium Runs 1-4.

at 24°C[99] (see Table II.1). The Kco value obtained in the present work, however, was felt to be somewhat unreliable because of the consistently high slope values (≃1.5) obtained from the log-log plots, indicative of the interaction of more than one CO molecule, and the reproducible curvature in the data points for each plot (see Figure IV.38). Since the P450cam samples used for the equilibrium experiments showed identical properties (i.e. λ_{max}, ε_{mM} and purity) to those of the enzyme preparations utilized for the literature Kco measurements, the enzyme samples were felt not to be the source of the experimental errors. More detailed studies on the equilibrium did show however, that at lower concentrations of the dithionite reducing agent, as assessed by the residual 314nm absorption, the equilibrium data (above $\log \frac{A-Ao}{A\infty-A}$ values of 0.0 or ≲8mm Hg CO partial pressure) gave linear plots of slope closer to one (≃1.0-1.3) and corresponding Kco values more consistent with the literature values; dithionite, initially present in large excess (≃50-fold excess reducing equivalents), was thought to be interfering with the CO-binding process during the initial experimental readings. Several semi-quantitative experiments were then performed to determine the behavior of dithionite in aqueous buffer P and the effect, if any, of the reducing agent on the intensity of the Soret maximum at 408nm of the CO-free ferrous enzyme and at 445nm of the fully and partially carbonylated enzyme; the apparatus and techniques were those employed for the CO-equilibrium measurements (see

Section III.6). Dithionite itself ($\simeq 2.0 \times 10^{-4}$M) was shown to decompose in phosphate buffer, pH 7.0, at 20°C under 1 atm argon likely in accordance with the equilibrium:[169]

$$2S_2O_4^{-2} + H_2O \rightleftharpoons S_2O_3^{2-} + 2HSO_3^{-1}$$

the rate of decomposition was increased by shaking (Figure IV.39). Essentially the same data were obtained for the decomposition under vacuum or 1 atm CO. Excess dithionite ($\simeq 2.0 \times 10^{-4}$M) had no observable effect on the intensity of the 408 and 445nm Soret maxima of the reduced and reduced-CO enzyme complexes (Figures IV.40 and IV.41, respectively), but in the presence of the reduced enzyme alone (under 1 atm argon) the rate of dithionite decomposition was essentially unaffected by shaking of the solution (Figure IV.40); shaking of the fully carbonylated system (under 1 atm CO), however, did lead to increased decomposition rate (Figure IV.41) as with dithionite itself. The spectra of the Fe(II) and Fe(II)-CO enzymes were unchanged up to 48h after disappearance of the dithionite peak. Each of these experiments (Figure IV.39-IV.41) were performed at least three times with identical results. Figure IV.42 shows the absorbance changes observed for the partially carbonylated system at 5.64mm Hg (i.e. 7.67×10^{-6}M CO) while allowing the dithionite peak to disappear over a 24h period. The initial spectrum shows an absorbance at 445nm ($\simeq 0.425$) very similar to that observed for Equilibrium Run 3 (see Figure IV.37A) as wellas



Effect of $Na_2S_2O_4$ on Standing

Spectra #	Time (min)	Comments
# 1	0	No shaking
# 2	5	No shaking
# 3	10	No shaking
# 4	15	No shaking
# 5	20	No shaking
# 6	25	No shaking
# 7	30	No shaking
# 8	35	No shaking
# 9	40	No shaking
#10	45	No shaking
#11	50	No shaking
#12	55	10S shake
#13	60	30S shake
#14	65	1.0 min shake

Figure IV.39 Decomposition of dithionite in phosphate buffer, pH 7.0, at 20°C under 1 atm. argon. Inset gives absorbance *vs.* time data.

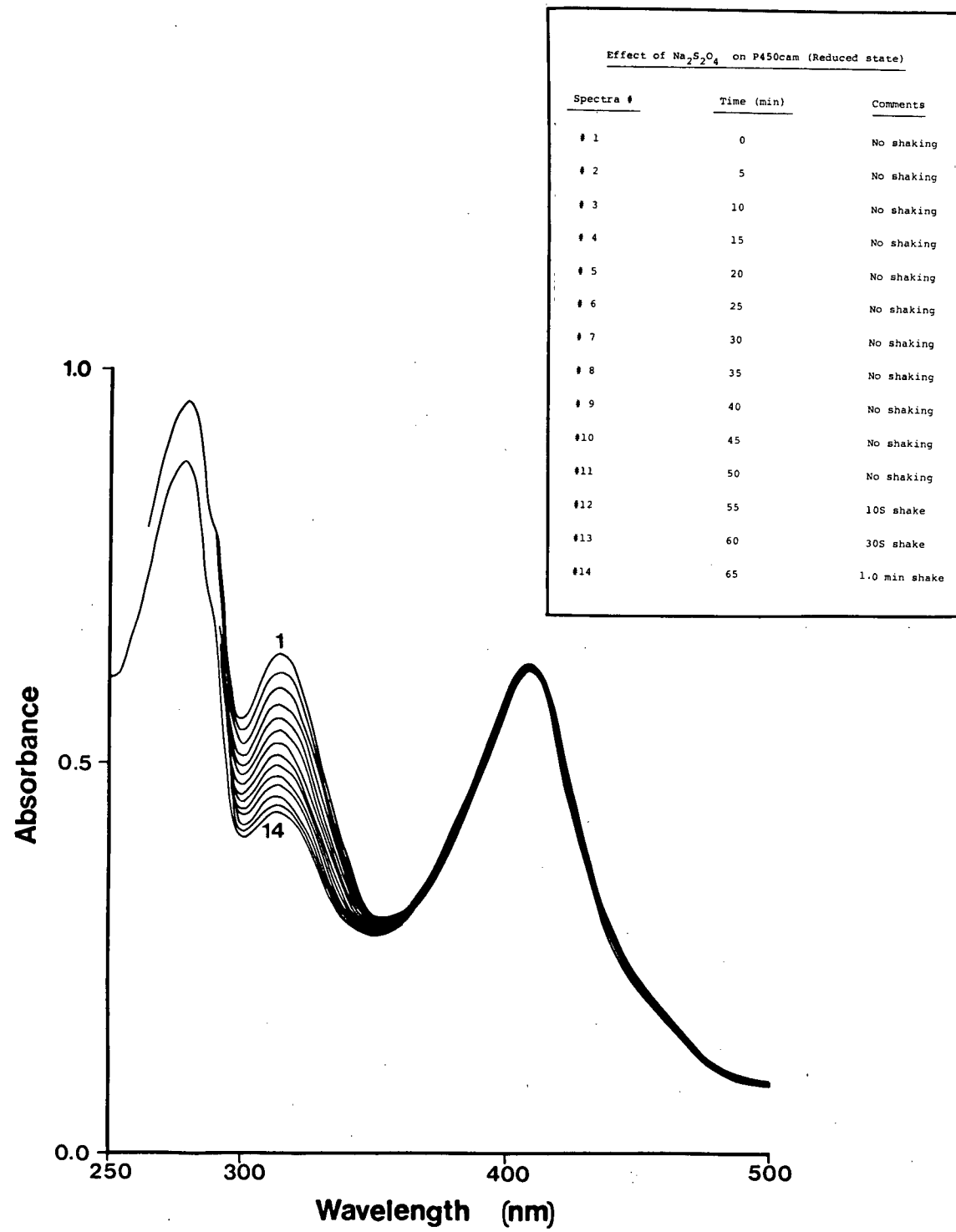
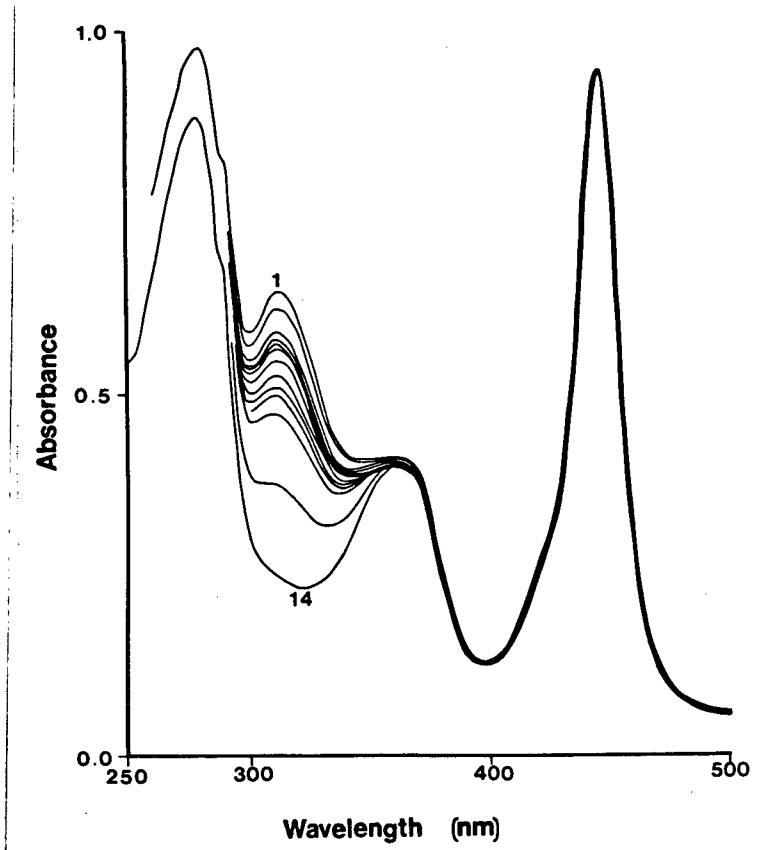


Figure IV.40 Decomposition of dithionite in the presence of ferrous cytochrome P450cam. Inset gives absorbance *vs.* time data.



Effect of $Na_2S_2O_4$ on P450cam-CO Complex

Spectra #	Time (min)	Comments
# 1	0	No shaking
# 2	5	No shaking
# 3	10	No shaking
# 4	15	No shaking
# 5	20	No shaking
# 6	25	No shaking
# 7	30	No shaking
# 8	35	No shaking
# 9	40	No shaking
#10	45	No shaking
#11	50	No shaking
#12	55	10S shake
#13	60	30S shake
#14	65	1.0 min shake

Figure IV.41 Decomposition of dithionite in the presence of the fully carbonylated enzyme. Inset gives absorbance *vs.* time data.

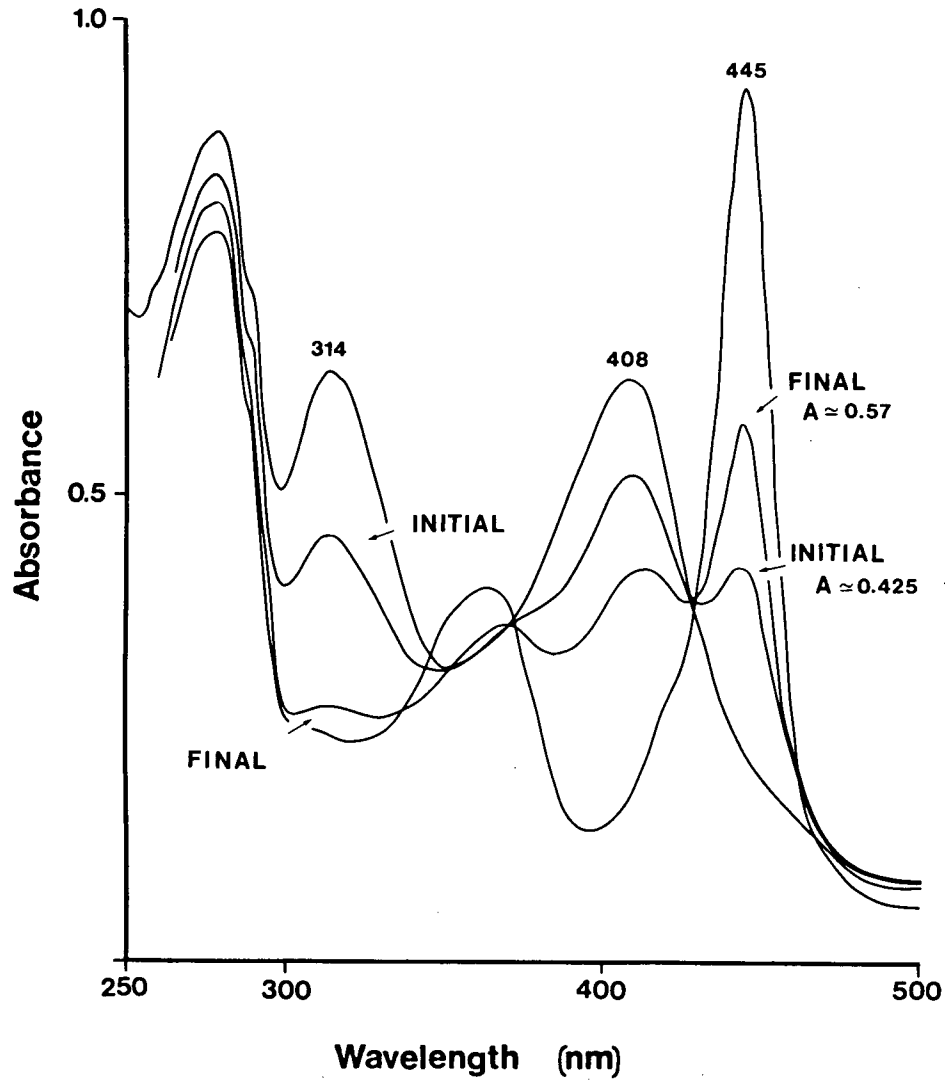


Figure IV.42 Absorbance change observed at 445nm of the partially carbonylated cytochrome P450cam following the disappearance of the dithionite peak.

Runs 1, 2 and 4 (Appendix V.a) at the same CO concentration and indicated about 46% formation of the carbonyl; the final absorbance of ≃0.57 at 445nm indicated the CO-bound complex was about 61% formed, more in accordance with the literature value of $P_{\frac{1}{2}}^{CO}$ = 5.5mm Hg at 24°C for the substrate-bound P450cam system.[99] This experiment was repeated at lower CO concentrations with the same result; loss of the dithionite peak at 314nm was accompanied by an increase in concentration of the ferrous-CO adduct. Two further equilibrium experiments were then performed under conditions of only a slight excess of dithionite (small 314nm peak); the spectral changes are shown in Figure IV.43 and the resultant log $\frac{A-Ao}{A_\infty-A}$ *vs.* log [CO] data are plotted in Figure IV.44, while raw data for these experiments are tabulated in Appendix V.b. The plots are reasonably linear with slope 1.3-1.4 and intercepts on the X-axis of -5.01 and -5.17, corresponding to an average Kco value of $1.3 \times 10^5 M^{-1}$ ± 15% and a $P_{\frac{1}{2}}^{CO}$ value of 5.6mm Hg at 20°C. Although these experiments gave Kco values closer to the literature values measured for bacterial P450cam,[33c,99,133a] further experiments are needed to verify the effect of dithionite or its decomposition byproducts on the equilibrium constant determination. Such dithionite-effects have not been reported in the literature and were obviously not observed in the equilibrium constant measurements for the bacterial system where NADH was used as the reductant.[99,133a] Dithionite was used in the equilibrium measurements of Peterson and Griffin[33c]; however, since the enzyme was "reduced with a

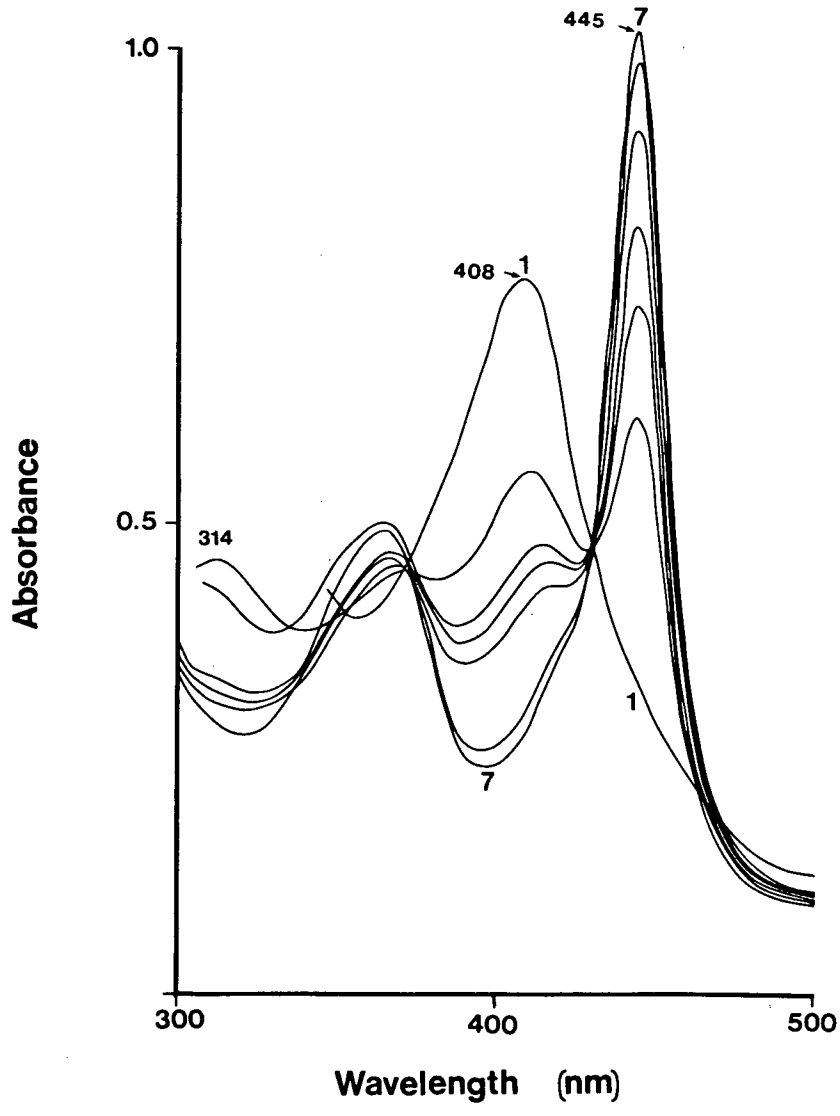


Figure IV.43 Spectral changes observed for Equilibrium Run 5 by CO addition to the ferrous, substrate-bound cytochrome P450cam in the presence of a small excess of dithionite reducing agent.

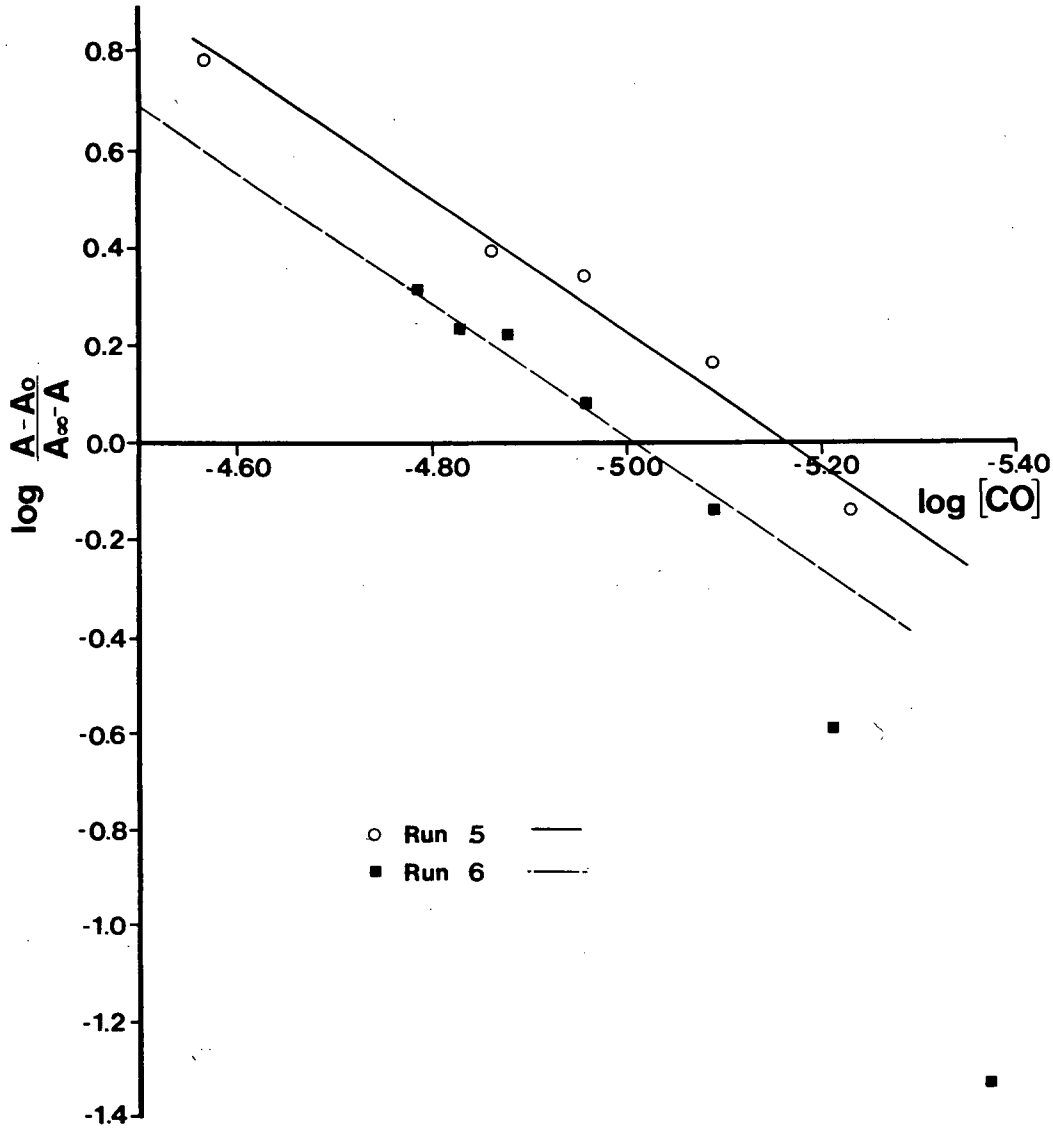


Figure IV.44 Plots of log $\frac{A-Ao}{A_\infty-A}$ *vs.* log[CO] for Equilibrium Runs 5 and 6 for spectral changes in the presence of a small excess of dithionite.

slight excess of dithionite" the apparent effects of the reducing agent observed in the present work may not have been manifested in their study. The effects of excess dithionite such as those described above are of major interest since dithionite is used extensively for hemoprotein reductions and is generally felt not to interfere with hemoprotein reactivity. Whether the observed reactivity of the P450cam enzymes in the presence of excess dithionite is unique to these hemoproteins awaits further study; measuring the Kco value in the presence of NADH as the reducing agent or following the total disappearance of the 314nm dithionite peak would be of immediate interest.

Assuming then that the Kco value determined above represented the equilibrium constant for the reaction of CO with the ferrous state of native substrate-bound cytochrome P450cam, the CO-dissociation rate constant, k_{off}, was calculated at $1.8s^{-1}$ ± 15% at 20°C which is in excellent agreement with the measured values of $1.7s^{-1}$ at 24°C[10] and $2.8s^{-1}$ at 20°C.

CHAPTER V

GENERAL CONCLUSIONS AND SOME RECOMMENDATIONS FOR FUTURE WORK

V General Conclusions and Some Recommendations for Future Work

The work in this thesis describes a reliable method for the isolation and purification of cytochrome P450cam from bacterial cells of *Pseudomonas putida*, strain PpG 786, a general procedure for the heme removal and replacement in the native enzyme, and a complete system for both kinetic and equilibrium studies of the reaction of CO with the ferrous state of native and reconstituted P450cam enzymes.

Bacteria, maintained on minimal agar containing camphor as the carbon and energy source, were propagated *via* a four-stage growth sequence. L-broth starter cultures, two sets of 500 mL shake-flasks, and the 14L fermentor cultures, allowed for the most rapid production of the bacteria at the expense of camphor and liquid medium. Several experiments at the shake-flask stage indicated that the bacteria must be maintained in the presence of camphor in order to avoid long lag times in the growth sequence, due possibly to the loss of the "CAM-plasmid" specific for camphor metabolism.

Isolation and purification of native P450cam from ≃400 of bacterial cell paste provided good yields of the enzyme in purity high enough for the kinetic and equilibrium experiments. The isolation procedure invoked production of a cell-free protein solution followed by separation of the cytochrome and related monooxygenase components by DE-52 anion-exchange chromatography; purification of the protein components was performed by Sephadex G-100 chromatography. The anion-exchange

chromatography was sufficient for the isolation of contaminant-free cytochrome P450cam and putidaredoxin but the flavoprotein, putidaredoxin reductase, contained an apparent substrate-free cytochrome P450cam impurity which could not readily be removed; isolation of contaminant-free putidaredoxin reductase will require modification of the present procedure possibly in accordance with the method of Gunsalus and Wagner.[37] Purified putidaredoxin and putidaredoxin reductase were not required in the present work; however, future studies should employ an enzyme activity assay for the native and, more importantly, the reconstituted P450cam derivatives which require these proteins.[37] Spectral data obtained for putidaredoxin and the substrate-free and substrate-bound states of cytochrome P450 cam were comparable with the literature valves.

The reconstitution procedure described in this work was used to reconstitute the native enzyme with protohemin chloride. The resultant reconstituted enzyme showed spectral characteristics identical to those of the native cytochrome, except for a small shoulder in the absorption spectrum at 417nm indicative of a substrate-free P450cam impurity. No attempts were made to remove the impurity since it did not appear to affect the kinetic experiments. Although this method was used successfully for reconstitution with protohemin chloride, the recently published method of Wagner *et al.*[149] gives higher yields and is apparently better suited for handling the P450cam system. Clearly, reconstitution of native cytochrome P450cam with meso-, deutero-,

diacetyldeutero and dibromodeuterohemins is of major importance for future studies.

Kinetic studies on the reaction of CO with the ferrous state of substrate-bound native and protohemin-reconstituted cytochrome P450cam showed that the reaction could be described by the reaction shown below,

$$\text{Fe(II)P450cam} + \text{CO} \underset{k_{off}}{\overset{k_{on}}{\rightleftharpoons}} \text{Fe(II) P450cam-CO}, \quad K_{CO} = \frac{k_{on}}{k_{off}}$$

where the forward reaction for the binding of CO to the ferrous enzyme was a second-order process, and the reverse reaction for dissociation of CO from the ligand-bound adduct was a first-order process. All kinetic experiments were performed successfully by the flash photolysis method on the apparatus described in Section III 5, except for the apparent limited sweep-time range (>2.0 msec/div) of the oscilloscope for the analog converter-derived linear rate plots. Reactions were run at fixed protein concentrations ($\simeq 1.0 \times 10^{-5}$M) in the presence of a large excess of the CO ligand and monitored at the Soret maxima of the CO-free complex or the CO-bound adduct. All absorbance *vs.* time plots indicated approximately 30% photodecomposition of the CO-bound species and showed a pseudo first-order dependence on hemoprotein concentration. Second-order rate constants, k_{on}, for the myoglobin-CO system, which was used to test and develop the flash unit, were determined as $4.1 \times 10^{5} M^{-1} S^{-1} \pm 10\%$ at 20°C, in excellent agreement with the literature values. The corresponding k_{on} value for the substrate-bound native P450cam of $6.8 \times 10^{4} M^{-1} S^{-1} \pm 20\%$

at 20°C was in good agreement with the literature, while the previously unreported k_{on} valve for the substrate-bound proto-hemin-reconstituted enzyme of $6.4X10^{4}M^{-1}S^{-1}$ ± 10% at 20°C was in good agreement with that of the native enzyme. The k_{off} valves of 69 S^{-1} ± 30%, 12 S^{-1} ± 20% and 8.7S^{-1} ± 20% for the myoglobin, and the native and reconstituted P450cam systems, respectively, were also obtained from the kinetic experiments but were felt to be high due to enhancement of the CO-dissociation reaction by the monitoring light beam of the flash unit. Comparison of the myoglobin system with the P450cam systems showed about a 6-fold enhancement of the "on" and "off" rate constants for the myoglobin system which is thought to reflect the presence of substrate, camphor, and thiolate axial ligation in the P450cam systems. Analysis of the reaction of CO with cytochrome P450cam reconstituted with meso-, deutero-, diacetyldeutero-, and dibromodeuterohemin, using the flash photolysis techniques described in the present work, would be of interest as would temperature studies for the determination of activation parameters.

The equilibrium studies of CO-binding to native cytochrome P450cam were used for the calculation of the k_{off} values since those obtained from the kinetic experiments were considered unreliable. A Kco of $1.3X10^{5}M^{-1}$ ± 15% at 20°C gave a calculated k_{off} value of 1.8 S^{-1} ± 15% at 20°C both the equilibrium and rate constant being in good agreement with literature values for the substrate-bound enzyme. Equilibrium

CO-binding was apparently affected by the dithionite reducing agent and several semi-quantitative experiments showed that at low dithionite concentration more reliable equilibrium constants were obtained; the Kco value reported above from the present work was obtained at lower dithionite concentration. Although further experimentation is required on this system these results are of interest because of the ubiquitous use of dithionite as a hemoprotein reductant. These results indicate that dithionites (or its decomposition or oxidation products) may in fact interact with the reduced hemoprotein but whether cytochrome P450cam is unique in this characteristic is unknown. Clearly, any future work on the CO-binding equilibrium for bacterial cytochrome P450cam must invoke a detailed assessment of these findings plus extension to the study of the reconstituted derivatives for the Kco determinations, as well as the corresponding thermodynamic parameters for CO-binding.

REFERENCES

1) Cooper, D. W., Rosenthal, O., Snyder, R., and Wilner, C., eds., "Cytochromes P450 and b_5. Structure, Function, and Interaction", Plenum, New York, (1974).

2) Cooper, D. W., and Salhanick, H. A., eds., "Multienzyme Systems in Endocrinology: Progress in Purification and Methods of Investigation", New York Acad. Sci., New York, (1973).

3) Estabrook, R. W., Gillette, J. R., and Leibman, K. C., eds., "Microsomes and Drug Oxidations", Williams and Wilkins, Baltimore, Maryland, (1972).

4). King, T. E., Mason, H. S., and Morrison, M., eds., "Oxidases and Related Redox Systems", Univ. Park Press, Baltimore, Maryland, (1973).

5) Boyd, G. S., and Smellie, R. M. S., eds., "Biological Hydroxylation Mechanisms", Biochem. Soc . Symp. No.34, Academic Press, New York, (1972).

6) Dolphin, D., ed., "The Porphyrins", Vol.VII, Academic Press, New York, (1979).

7) Sheldon, R. A., and Kochi, J. K., eds., "Metal-Catalysed Oxidations of Organic Compounds", Academic Press, New York, (1981).

8) James, B. R., in "The Porphyrins", Vol.V, (Dolphin, D, ed.), Academic Press, New York, (1979), p.205.

9) James, B. R., Adv. Chem. Series, 191, 254 (1980).

10) Dolphin, D., James, B. R., and Welborn, C. H., J. Mol. Catal. 7, 201 (1980).

11) Klingenberg, M., Arch. Biochem. Biophys. 75, 376 (1958).

12) Williams, G. R., unpublished results, (1954) quoted in Ref. 11.

13) Omura, T., and Sato, R., J. Biol. Chem. 239, 2370 (1964).

14) Omura, T., and Sato, R., J. Biol. Chem. 239, 2379 (1964).

15a) Hayano, M., and Dorfman, R. I., Arch. Biochem. Biophys. 36, 237 (1952).

b) Conney, A. H., Brown, R. R., Miller, J. A., and Miller, E. C., Cancer Res. 17, 628 (1957).

c) Brodie, B. B., Gillette, J. R. and LaDu, B. N., Annu. Rev. Biochem. 27, 427 (1958).

16) Mason, H. S., Adv. Enzymol. Relat. Areas Mol. Biol. 19, 79 (1957).

17) Hayaishi, O., ed., "Oxygenases", Academic Press, New York, (1962), p.1.

17a) Massart and Vercauteren, quoted in Ref. 17.

18) Ryan, K. J., and Engel, L. L., J. Biol. Chem. 225, 103 (1957).

19) Warburg, O., "Heavy Metal Prosthetic Groups and Enzyme Action", Chapters XII and XIII, Oxford Univ., Clarendon Press, (1949).

20) Estabrook, R. W., Cooper, D. Y., and Rosenthal, O., Biochem. Z. 338, 741 (1963).

21a) Cooper, D. Y., Levin, S., Narasimhulu, S., Rosenthal, O., and Estabrook, R. W., Science 147, 400 (1965).

b) Gillette, J. R., Advan. Pharmacol. 4, 219 (1966).

c) Cushman, D. W., Tsai, R. L., and Gunsalus, I. C., Biochem. Biophys. Res. Commun. 26, 577 (1967).

22) Narasimhulu, S., Cooper, D. Y., and Rosenthal, O., Life Sci. 4, 2102 (1965).

23) Schenkman, J. B., Remmer, H., and Estabrook, R. W., Mol. Pharmacol. 3, 113 (1967).

24) Remmer, H., and Merker, H. J., Ann. N.Y. Acad. Sci. 123, 79 (1965).

25) Conney, A. H., Pharmacol. Rev. 19, 317 (1967).

26) Welton, A. F., O'Neal, F. O., Chaney, L. C., and Aust, St. D., J. Biol. Chem. 250, 5631 (1975).

27) Ullrich, V., Frommer, U., and Weber, P., Hoppe-Seyler's Z. Physiol. Chem. 354, 514 (1973).

28) Imai, Y., and Sato, R., Eur. J. Biochem. 1, 419 (1967).

29) Katagiri, B. N. Ganguli, B. N., and Gunsalus, I. C., J. Biol. Chem. 243, 3543 (1968).

30) Gunsalus, I. C., Meeks, J. R., Lipscomb, J. D., DeBrunner, P., and Munck, E., in "Molecular Mechanisms of Oxygen Activation", (Hayaishi, O., ed), Academic Press, New York, (1974), p.559.

31) Gunsalus, I. C., Hoppe-Seyler's Z. Physiol. Chem. 349, 1610 (1968).

32) Ishimura, Y., Ullrich, V., and Peterson, J. A., Biochem. Biophys. Res. Commun. 42, 140 (1971).

33a) Griffin, B. W., Peterson, J. A., and Estabrook, R. W., in "The Porphyrins", Vol.VII, (Dolphin, D., ed), Academic Press, New York, (1979), p.333.

b) Peterson, J. A., Arch. Biochem. Biophys. 144, 678 (1971).

c) Peterson, J. A., and Griffin, B. W., Arch. Biochem. Biophys. 151, 427 (1972).

d) Peterson, J. A., Ishimura, Y., and Griffin, B. W., Arch. Biochem. Biophys. 149, 197 (1972).

34) Estabrook, R. W., Hildebrandt, A. G., Remmer, H., Schenkman, J. B., Rosenthal, O., and Cooper, D. Y., Colloq. Ges. Biol. Chem. 19, 142 (1968).

35) Cushman, D. W., Tsai, R. L., and Gunsalus, I. C., Biochem. Biophys. Res. Commun. 26, 577 (1967).

36) Yu, C. A., Gunsalus, I. C., Katagiri, M., Shurara, K., and Takemori, S., J. Biol. Chem. 249, 94 (1974).

37) Gunsalus, I. C., and Wagner, G. C., Methods Enzymol. 52, 166 (1978).

38) Wagner, G. C., and Gunsalus, I. C., in "The Biological Chemistry of Iron", (Dunford, H. B., Dolphin, D., Raymond, K. N., and Seiker, L., eds.), D. Reidl Publishing Co., Boston, (1982), p.405.

39) Autor, A. P., Kaschnitz, R. M., Heidema, J. K., and Coon, M. J., Mol. Pharmacol., 9, 39 (1973).

40) Ryan, D., Thomas, P. E., Korzeniowski, D., and Levin, W., J. Biol. Chem. 254, 1365 (1979).

41) Groves, J. T., Haushatter, R. C., Nakamura, M., Nemo, T. E., and Evans, B. J., J. Am. Chem. Soc. 103, 2884 (1981).

42) Dolphin, D., in "Biological Chemistry of Iron", (Dunford, H. B., Dolphin, D., Raymond, K. N., and Seiker, L., eds.), D. Reidl Publishing Co., Boston, (1981), p.283.

43) Coon, M. J., Conney, A. H., Estabrook, R. W., Gelbain, H. V., Gillette, J. R., and O'Brien, P. J., eds., "Microsomes, Drug Oxidations, and Chemical Carcinogenesis", Academic Press, New York, (1980).

44) Keevil, T., and Mason, H. S., Methods Enzymol. 52, 3 (1978).

45) Lu, A. Y. H., Kuntzman, R., and Conney, A. H., in "Frontiers of Gastrointestinal Research", Vol.2, (Vander Reis, L., Karger, S., Basel, A. G., eds.), (1976), p.1.

46) Cooper, D. Y., Schleyer, H., Estabrook, R. W., and Rosenthol, O., in "Progress in Endocrinology", (Gaul, C., ed.), Mouton, The Netherlands, (1969), p.784.

47) Hamberg, H., Sameulsson, B., Bjorkem, I., and Danielsson, H., in "Molecular Mechanisms of Oxygen Activation", (Hayaishi, O., ed.), Academic Press, New York, (1974), p.29.

48) Wada, F., Shibala, M., Masarobo, G., and Sakamoto, Y., Biochem. Biophys, Acta 162, 518 (1968).

49) Orrenius, S., and Ernster, L., in "Molecular Mechanisms of Oxygen Activation", (Hayaishi, O., ed.), Academic Press, New York, (1974), p.229.

50) Testa, B., and Jenner, P., "Drug Metabolism", Marcel Dekker, Inc., New York, (1976).

51) Hutson, D. H., in "Foreign Compound Metabolism in Mammals", Vol.4, The Chemical Society, London, (1977), p.260.

52) Goldenberg, H., Fishman, V., Biochem. Biophys. Res. Commun. 14, 404 (1964).

53a) Estabrook, R. W., Baron, J., Franklin, M., Mason, I., Waterman, M., and Peterson, J., in "Molecular Basis of Electron Transport", (Shultz, J., and Cameron, B. F., eds.), Academic Press, New York, (1972), p.197.

b) Coon, M. J., Stobel, H. W., Heidema, J. K., Kaschnitz, R. M., Autor, A. P., and Ballau, D. P., in "Molecular Basis of Electron Transport", (Shultz, J., and Cameron, B. F., eds.), Academic Press, New York, (1972), p.231.

54) Ortiz de Montellano, P. R., Yost, G. S., Mico, B. A., Dinizo, S. E., Correia, M. A., and Kambara, H., Arch. Biochem. Biophys. 197, 524 (1979).

55) Watanabe, Y., Iyanagi, T., and Oae, S., Tetrahedron Lett., 3685 (1980).

56) Ray, J. W., Biochem. Pharmacol. 16, 99 (1967).

57) Conrad, H. E., Dubus, R., Namtiredt, M. J., and Gunsalus, I. C., J. Biol. Chem. 240, 495 (1965).

58) Cardini, G., and Jurtshuk, P., J. Biol. Chem. 245, 2789 (1970).

59) Russel, D. W., J. Biol. Chem. 246, 3870 (1971).

60) Appleby, C. A., Biochem. Biophys. Acta 147, 399 (1967).

61) Lindenmayer, A., and Smith, L., Biochem. Biophys. Acta 93, 445 (1964).

62) Ichikawa, Y., and Yamano, T., Arch. Biochem. Biophys. 121, 742 (1967).

63) Estabrook, R. W., Franklin, M. R., Cohen, B., Shigematzu, A., and Hildebrandt, A. G., Metabolism 20, 187 (1971).

64) Strobel, H. W., Lu, A. Y. H., Heidema, J., and Coon, M. J., J. Biol. Chem. 245, 4851 (1970).

65) Haugen, D. A., VanderHoevan, T. A., and Coon, M. J., J. Biol. Chem. 250, 3567 (1975).

66) Ullrich, V., in "Microsomes and Drug Oxidations", (Ullrich, V., Roots, I., Hildebrandt, A., Estabrook, R. W., and Conney, A. H., eds.), Pergamon Press, New York, (1976), p.192.

67) Park, D. V., in "Enzyme Induction", (Parke, D. V., ed.), Plenum Press, New York, (1975), p.208.

68) Nubert, D. W., in "Symposia Medica Hoecht 14", (Estabrook, R. W., and Lindenlaub, E., eds.), (1979), p.419.

69) Cammer, W., and Estabrook, R. W., Arch. Biochem. Biophys. 122, 735 (1967).

70) Estabrook, R. W., Baron, J., Peterson, J. A., and Ishimira, Y., Biochem. Soc. Symp., Edinburgh, (1971).

71) Bumpus, J. A., Obidoa, O., and Dus, K. M., in "Microsomes, Drug Oxidations and Chemical Carcinogenesis", (Coon, M. J., Conney, A. H., Estabrook, R. W., Gelboin, H. V., Gillette, J. R., and O'Brien, P. J., eds.), Academic Press, New York, (1980), p.203.

72) Jenna, D. M., Yagi, H., Thakker, D. R., Lehr, R. E., Wood, A. W., Levin, W., and Conney, A. H., in "Microsomes, Drug Oxidations and Chemical Carcinogenesis", (Coon, M. J., Conney, A. H., Estabrook, R. W., Gelboin, H. V., Gillette, J. R., and O'Brien, P. J., eds.), Academic Press,New York, (1980), p.1041.

73) Ortiz de Montellano, P. R., and Kunze, K. L., J. Biol. Chem. 255, 5578 (1980).

74) Heidelberger, C., Ann. Rev. Biochem. 44, 79 (1975).

75) McDonagh, A. F., Paspisil, R., and Meyer, U. A., Biochem. Soc. Trans. 4, 297 (1976).

76) Ortiz de Montellano, P. R., Kunze, K. L., Beilan, H. S., and Wheeler, C., Biochemistry 21, 1331 (1982).

77) Ortiz de Montellano, P. R., and Kunze, K. L., J. Am. Chem. Soc. 102, 7373 (1980).

78) Kunze, K. L., and Ortizde Montellano, P. R., J. Am. Chem. Soc. 103, 4225 (1981).

79) Jun-Ichiro, S., and Dolphin, D., private communication.

80) Ortiz de Montellano, P. R., Beilan, H. S., Kunze, K. L., and Mico, B. A., J. Biol. Chem. 256, 4395 (1981).

81) Gunsalus, I. C., and Sligar, S. G., Adv. Enzymol. 47, 1 (1978).

82) Gunsalus, I. C., Wagner, G. C., and Debrunner, P. G., in "Microsomes, Drug Oxidations, and Chemical Carcinogenesis", (Coon, M. J., Conney, A. H., Estabrook, R. W., Gelboin, H. V., Gillette, J. R., and O'Brien, P. J., eds.), Academic Press, New York, (1980), p.233.

83) Enzyme Nomenclature, Elsevier Publishing Co., Amsterdam, (1965), p.19.

84) Hanui, M., Tanaka, M., Yasunobu, K. T., and Gunsalus, I. C., J. Biol. Chem. 257, 12657 (1982).

85) Hanui, M., Armes, L. G., and Yasunobu, K. T., J. Biol. Chem. 257, 12664 (1982).

86) Wagner, G. C., Perez, M., Toscano, W. A., and Gunsalus, I. C., J. Biol. Chem. 256, 6262 (1981).

87) Dus, K., Katagiri, M., Yu, C. A., Erbes, D. L., and Gunsalus, I. C., Biochem. Biophys. Res. Commun. 40, 1423 (1970).

88) Hanui, M., Tanaka, M., Yasunabu, K. T., and Gunsalus, I. C., in "Microsomes, Drug Oxidations and Chemical Carcinogenesis", (Coon, M. J., Conney, A. H., Estabrook, R. W., Gelboin, H. V., Gillette, J. R., and O'Brien, P. J., eds.), Academic Press, New York, (1980), p.85.

89) Haugen, D. A., Armes, L. G., Yasunoba, K. T., and Coon, M. J., Biochem. Biophys. Res. Commun. 77, 967 (1977).

90) Wagner, G. C., private communication.

91) Miyake, Y., Galor, J. L., and Mason, H. S., J. Biol. Chem. 243, 5788 (1968).

92) Jefcoate, C. R. E., and Gaylor, J. L., Biochemistry, 8, 3464 (1969).

93) Blumberg, W. E., and Peisch, J., in "Probes of Structure and Function of Macrocycles and Membranes", (Chance, B., Yanetoni, T., and Mildvan, A. E., eds.) Vol.II, Academic Press, New York, (1971), p.215.

94a) Chang, C. K., and Dolphin, D., J. Am. Chem. Soc. 97, 5948 (1975).

b) Chang, C. K., and Dolphin, D., J. Am. Chem. Soc. 98, 1607 (1976).

c) Chang, C. K., and Dolphin, D., Proc. Natl. Acad. Sci. U.S.A. 73, 3338 (1976).

95) Collman, J. P., and Sorell, T. N., J. Am. Chem. Soc. 97, 4133 (1975).

96) Stern, J. O., and Peisch, J., J. Biol. Chem. 249, 7495 (1974).

97) Hanson, L. K., Eaton, W. A., Sligar, S. G., Gunsalus, I. C., Gouterman, M., and Connel, C. R., J. Am. Chem. Soc. 98, 2672 (1976).

98) Ruf, H. H., and Wende, P., J. Am. Chem. Soc. 99, 5499 (1977).

99) Dolphin, D., James, B. R., and Welborn, H. C., Biochem. Biophys. Res. Commun. 88, 415 (1979).

100) Gunsalus, I. C., Meeks, J. R., and Lipscomb, J. D., Ann. N. Y. Acad. Sci. 212, 107 (1973).

101) Chiang, R., Makino, R., Spomer, W. E., and Hager, L. P., Biochemistry 14, 4166-4171 (1975).

102) Morris, D. R., and Haber, L. P., J. Biol. Chem. 241, 1763 (1966).

103) Hollenburg, P. F., and Hager, L. P., J. Biol. Chem. 248, 2630 (1973).

104) Williams, R. J. P., Moore, G. R., and Wright, P. E., in "Biological Aspects of Inorganic Chemistry", (Addison, A. W., Cullen, W. R., Dolphin, D., and James, B. R., eds.) John Wiley and Sons, Toronto, (1977), p.369.

105) Peterson, J. A., in "Microsomes Drug Oxidations and Chemical Carcinogenesis", (Coon, M. J., Conney, A. H., Estabrook, R. W., Gelboin, H. V., Gillette, J. R., and O'Brien, P. J., eds.), Academic Press, New York, (1980), p.455.

106) Dolphin, D., and James, B. R., Adv. Chem. Series. 211, 99 (1983).

107) Griffin, B. W., Peterson, J. A., Werringloer, J., and Estabrook, R. W., Ann, N. Y. Acad. Sci. 244, 107 (1975).

108) Murray, R. I., Gunsalus, I. C., and Dus, K. M., J. Biol. Chem. 257, 12517 (1982).

109) Antonini, E., and Brunori, M., in "Hemoglobin and Myoglobin in their Reactions with Ligands", (Newberger, A., and Tatum,E. L., eds.), North-Holland Publishing Company, Amsterdam, (1971).

110) Nordblom, G. D., and Coon, M. J., Arch. Biochem. Biophys. 180, 343 (1977).

111) Coon, M. J., and White, R. E., in "Metal Ion Activation of Dioxygen", (Spiro, T. G., ed.), Wiley Interscience, New York (1980) p.73.

112) Estabrook, R. W., and Werringloer, J., in "Microsomes and Drug Oxidations", (Ullrich, V., Roots, I., Hildebrandt, A., Estabrook, R. W., and Conney, A. H., eds.), Pergamon Press, Oxford, New York (1977), p.748.

113) McCandlish, E., Miksztal, A. R., Nappa, M., Sprenger, A. Q., Valentine, J. S., Stong, J. D., and Spiro, T. G., J. Am. Chem. Soc. 102, 4268 (1980).

114) Welborn, C. H., Dolphin, D., and James, B. R., J. Am. Chem. Soc. 103, 2869 (1981).

115) Sligar, S. G., Kennedy, K. A., and Pearson, D. C., Proc. Natl. Acad. Sci. U.S.A. 77, 1240 (1980).

116) Collman, J. P., Marrocco, M., Denisevich, P., Koval, C., and Anson, F. G., J. Electroanal. Chem. Interfacial Electrochem. 101, 117 (1979).

117) Lichtenberger, F., Nastainczyk, W., and Ullrich, V., Biochem. Biophys. Res. Commun. 70, 939 (1976).

118a) Groves, J. T., in "Metal Ion Activation of Dioxygen", (Spiro, G. T., ed.), Wiley Interscience, New York, (1980), p.125.

b) Groves, J. T., Nemo, T. E., and Myers, R. S., J. Am. Chem. Soc. 101, 1032 (1979).

119) Leung, T., Dolphin, D., and James, B. R., unpublished results.

120) Hewson, W. D., and Hager, L. P., in "The Porphyrins", (Dolphin, D., ed.) Vol.VII, Academic Press, New York, (1979), p.295.

121) Hager, L. P., Doubek, D. L., Silverstein, R. M., Hargis, J. H., and Martin, J. C., J. Am. Chem. Soc. 94, 4364 (1972).

122) Roberts, J. E., Hoffman, B. M., Rutter, R., and Hager, L. P., J. Am. Chem. Soc. 103, 7654 (1981).

123) March, J., ed., in "Advanced Organic Chemistry", McGraw-Hill Book Co., New York, (1968), p.158.

124) Groves, J. T., and Kruper, W. J., Jr., J. Am. Chem. Soc. 101, 7613 (1979).

125) Ullrich, V., Ahr, H. J., Castle, L., Kuthan, H., Nastainczyk, W., and Ruff, H. H., in "Biological Chemistry of Iron", (Dunford, H. B., Dolphin, D., Raymond, K. N., and Sieker, L., eds.), D. Reidl Publishing Co., Boston, (1982), p.413.

126) Browett, W. R., and Stillian, M. J., Inorg. Chem. Acta 49, 69 (1981).

127) Kadlubar, F. F., Morton, K. C., and Ziegler, D. M., Biochem. Biophys. Res. Commun. 54, 1255 (1974).

128) Augusto, O., Beilan, H. S., and Ortiz de Montellano, P. R., J. Biol. Chem. 257, 11288 (1982).

129) Dolphin, D., Addison, A. W., Cairns, M., DiNello, R. K., Farrell, N. P., James, B. R., Paulson, D. R., and Welborn, C., Int. J. Quantum Chem. XVI, 311 (1979).

130) Wilson, D. F., and Erecinska, M., in "The Porphyrins", Vol.XII, (Dolphin, D., ed.), Academic Press, New York, (1979), p.2.

131) Haldane, J., and Smith, J. L., J. Physiol. 20, 497 (1896).

132) Gibson, Q. H., J. Physiol. 134, 112 (1956).

133a) Dolphin, D., James, B. R., and Welborn, C. H., in "Microsome Drug Oxidations, and Chemical Carcinogenesis", (Coon, M. J., Conney, A. H., Estabrook, R. W., Gelboin, H. W., Gillette, J. R., and O'Brien, P. J., eds.), Academic Press, New York (1980) p.187.

b) Debey, P., Hui Bon Hoa, G., and Douzou, P., FEBS Lett., 32, 227 (1973).

c) Debey, P., Balny, C., and Douzou, P., FEBS Lett. 35, 86 (1973).

d) Gray, R. D., J. Biol. Chem. 253, 4364 (1978).

e) Bonfils, C., Saldana, J. L., Debey, P., Maurel, P., Balney, C., and Douzou, P., Biochimie 61, 681 (1979).

f) Rosen, P., and Steir, A., Biochem. Biophys. Res. Commun. 51, 603 (1973).

g) Debey, P., and Douzou, P., FEBS Lett. 39, 271 (1974).

h) Omura, R., Sato, R., Cooper, D. Y., Rosenthal, O., and Estabrook, R. W., Fed. Proc. 24, 1181 (1965).

134) Porter, G., Techniques in Organic Chemistry 8, 1055 (1963).

135) Traylor, T. G., and Traylor, P. S., Ann. Rev. Biophys. Bioeng. 11, 105 (1982).

136a) Dinello, R. K., and Chang, C. K., in "The Porphyrins", Vol.I, (Dolphin, D., ed.), Academic Press, New York, (1978), p.289.

b) Caughey, W. S., Alben, J. O., Fujimoto, W. Y., and York, J. L., J. Org. Chem. 31, 2631 (1966).

c) Caughey, W. S., Fujimoto, W. J., and Johnson, B. P., Biochemistry 5, 3830 (1966).

137a) Fuhrhop, J. H., and Smith, K. M., in "Porphyrins and Metalloporphyrins", (Smith, K. M., ed.), Elsevier Scientific Publishing Co., New York, (1975), p.804.

b) Fuhrhop, J. H., and Smith, K. M., in "Porphyrins and Metallophorphyrins", (Smith, K. M., ed.), Elsevier Scientific Publishing Co., New York, (1975), p.837.

138) Paul, K. G., Theorell, H., and Akeson, A., Acta. Chem. Scand. 7, 1284, (1953).

139) Adler, A. D., Longo, F. R., Kampas, F., and Kim, J., J. Inorg. Nucl. Chem. 32, 2443 (1970).

140) Corwin, A. H., and Erdman, J. G., J. Am. Chem. Soc. 68, 2473 (1946).

141) Fischer, H., and Zeile, K., Justus Liebigs Ann. Chem. 468, 98 (1929).

142) Fieser, L. F., and Fieser, M., "Reagents for Organic Synthesis", John Wiley and Sons Ltd., New York, (1967), p.967.

143) Seybert, D. W., Moffat, K., Gibson, Q. H., and Chang, C. K., J. Biol. Chem. 252, 4225 (1977).

144) Bradshaw, W. H., Conrad, H. E., Corey, E. J., Gunsalus, I. C., and Lednicer, D., J. Am. Chem. Soc. 81, 5507 (1959).

145) Lennox, E. S., Virology, 1, 190 (1955).

146) Shriver, D. F., "The Manipulations of Air Sensitive Compounds", McGraw Hill, New York, N.Y., (1969).

147) Strittmatter, P., J. Biol. Chem. 235, 2492 (1960).

148) Yu, C. A., and Gunsalus, I. C., J. Biol. Chem. 249, 107 (1974).

149) Wagner, G. C., Perez, M., Toscano, W. A., and Gunsalus, I. C., J. Biol. Chem. 256, 6262 (1981).

150) Muller-Eberhard, U., Liem, H. H., Yu, C. A., and Gunsalus, I. C., Biochem. Biophys. Res. Comm. 35, 229 (1969).

151) Breslow, E., J. Biol. Chem. 239, 486 (1964).

152) Chang, C. K., Ph.D. Thesis, University of California, San Diego, 1973.

153) Chang, C. K., Applied Spectroscopy 30, 364 (1976).

154) Carraher, R., and Chartier, C., "Electronic Flash Photography", Litton Educational Publishing, Inc., New York, U.S.A., (1980), p.32.

155) Weast, R. C., ed. "CRC, Handbook of Chemistry and Physics", 50th Edition, The Chemical Rubber Co., Cleveland, Ohio, (1970), p.D138.

156) Hasinoff, B. B., Biochemistry. 13, 3111 (1974).

157) Edgerton, H. E., ed., "Electronic Flash, Strobe", MIT Press, Massachusettes, U.S.A., (1979), p.55.

158) Conrad, H. E., Dubus, R., and Gunsalus, I. C., Biochem. Biophys. Res. Comm. 6, 293 (1961).

159) Hedegaard, J., and Gunsalus, I. C., J. Biol. Chem. 240, 4038 (1965).

160) Davis, B. D., Dulbecco, R., Eisen, H. N., Ginsberg, H. S., and Wood, W. B., eds. "Microbiology", Harper and Row Publishers, New York, (1967), p.76.

161) Stanier, R. Y., Palleroni, N. J., and Doudoroff, M., J. Gen. Microbiol. 45, 159 (1966).

162) Rheinwald, J. C., Chakrabarty, A. M., and Gunsalus, I. C., Proc. Natl. Acad. Sci. 70, 885 (1973).

163) Novick, R. P., Scientific American, Vol.243, No.6, (December 1980), p.102.

164) Yu, C. A., and Gunsalus, I. C., J. Biol. Chem. 249, 102 (1974).

165) Wagner, G. C., Perez, M., Toscano, W. A., and Gunsalus, I. C., J. Biol. Chem. 256, 6262 (1981).

166) Welborn, H. C., private communication.

167) Frost, A. A., and Pearson, R. G., eds. "Kinetics and Mechanisms", 2nd Edition, Wiley, New York, (1961), p.186.

168) Computer programme to be published by D. Thackery, M.Sc. Thesis, U.B.C., (1983).

169) Cotton, F. A., and Wilkinson, G., "Advanced Inorganic Chemistry", Interscience Publishers, New York, (1972), p.451.

APPENDIX

APPENDIX I

FLASH PHOTOLYSIS UNIT OPERATING INSTRUCTIONS

Flash Photolysis Unit Operating Instructions

A) Turn-on Procedures:

a) Turn on the Oscilloscope (20 min. to warm up)

b) Turn on the High Voltage (HV) supply for the PMT. (Make sure the voltage adjustment knob is fully counterclockwise because fuse is sensitive to high voltage surge).

c) Turn on the Low Voltage (LV) supply for monochromatic light source. Close the slit control located at the right of the monochromator. Turn on lamp *via* switch at the back of the lamp compartment.

d) Turn on the Analog Rate Converter. Set output at transmittance (T) and balance at calibrate (Cal).

e) Turn on Trigger Control.

f) Turn on voltage supply for flashgun (make sure flashgun is switched off).

B) Calibration of Oscilloscope:

a) On the dual trace vertical amplifier (Tektronix 5A18N) depress display on and set mode and trigger switch to Channel 2 (Ch2). The Ch2 amplifier should light up. Now select input coupling to DC, ground (gnd) the inputs and set amplitude to 0.1 V/div.

On the time base amplifier (Tektronix 5B10N) set time base at 2msec/div, source on line, coupling at DC, slope at positive, t, and the trigger level at a bit positive above neutral.

Use position knob on the Ch2 vertical amplifier to zero-in the baseline. The baseline is usually zeroed on the second line from the bottom on the scope grid. The central 6x8 portion of the gird provides the most accurate calibration. (When zeroing the baseline, the focus and intensity controls of the D11 storage unit should be used to give a properly illuminated line and remember that high intensities focussed on a small area will destroy the screen).

b) Turn the amplitude switch all the way down to 2mV/div. The baseline often tends to deviate from zero. Use the Ch2 position control to bring the line back to zero. Switch the amplitude to 0.1V/div. and check the baseline. If it deviates from zero again readjust with position control. The baseline should be adjusted to zero during the experiment each time the amplitude setting is changed and should be checked regularly throughout an experiment.

c) Release the gnd button on the vertical amplifier; the baseline should remain at zero. If line disappears from screen, carefully repeat the above procedure. At this point the signal is coming directly from the PMT.

d) Calibration of the vertical amplifier, time base amplifier, and the CRT can easily be performed by consulting the instruction manual for the Tektronix R5103N Oscilloscope.

C) Calibration of Spectrophotometer:

a) Select the desired wavelength for the monitoring beam by dialing the wavelength control knob at the left of the Beckman monochromator. Check the filter selector plate at the exit slit of the monochromator; make sure it is pushed all the way in (no filter).

b) It is essential to properly align the monitoring beam to give maximum intensity and perfect collimation at the PMT. Open the exit slit of the monochromator fully (2.0mm), remove the cell extension, and place a piece of white paper in the cell holder to intercept the beam (see Figure III.15). The rectangular outline of the beam should appear on the paper. The monitoring beam can be aligned with the three screws at the rear of the lamp compartment. An intense rectangle of light should be seen throughout the visible region (400-700nm). Alignment at the PMT can be checked by removing the detector and inserting the strip of paper in the light beam (see Figure III.15). The same intense rectangle should be observed. Adjustment of the collimating tube may be needed to achieve the proper alignment. Once this is completed, close the slit and replace cell extention.

c) Set the vertical amplifier of the scope to 0.2V/div, zero the baseline and release the gnd. Turn the slit width control of the Beckman monochromator until it gives 1V (5 vertical divisions) on the screen. Check the slit width dial of the monochromator; if it is not in the range of between 0.25-0.4mm, use the voltage adjustment of HV power supply to bring it into this region. The HV reading should be ≈480V. The slit width should never be greater than 0.5mm. If these parameters cannot be met the lamp may need replacement. The output screw of the LV. supply can be used for minor adjustments.

d) The above calibration is easily checked by switching the output of the Analog Converter from T to A; the voltage on the screen should read zero. If the deviation from zero is larger than 20mV, switch back to T, double check to see if the scope reads 1V, and switch back to A. If the deviation still exists, it gives a sign that the first log amplifier circuit of the Analog converter may need calibration. This procedure calibrates the spectrophotometer such that at 100% transmittance (T) the absorbance (A) equals zero. The calibration should be done in the electrical shop of the Chemistry Department, U.B.C. The calibration should be checked

regularly throughout the experiment.

D) Calibration of the Flashgun Pulse:

a) Select the proper broad bandpass filter (see Section III.5.3.1), place in front of the flashgun (see Figure III.15), and set up the scope as follows; vertical amplifier on 5V/div (maximum setting); time base amplifier on lmsec/div, source at external (Ext), slope at +, single sweep pushed in (the ready light should be on); Analog converter on T; and D11 storage unit on storage with enhancement of both channels pushed in. The intensity control should be turned clockwise until the beam spot is located. The spot should appear at the baseline. Press erase to clear the screen.

b) Close the slit on the monochromator, make sure the exit filter are removed (i.e. no filters), pull the light pipe from the flashgun sensor area and set the H.V. supply for the PMT at 450-500V.

c) Turn On the flashgun. The capacitor will be fully charged when the indicator light comes on. This will take about 15 seconds.

d) Push the Scope button on the Trigger Control. A baseline at zero volts should appear.

Quality of the line can be adjusted using the intensity and focus controls. Push Reset; the Ready light should come on. Now press Main on the Trigger Control; both the flashgun and scope should fire simultaneously. A square wave signal of amplitude ≈15V should decay exponentially to the baseline in ≈8msec. The duration of the flash can be shortened by positioning the free end of the fibre optics tube next to the flashgun sensor (see Figure III.15). The same square trace should be obtained in ≈200μsec.

e) Reset oscilloscope, change vertical amplitude to 20mV/div and sweep time to 0.1 msec/div. Place 3.0 O.D. neutral density filter in the U-shaped pocket holder (see Figure III.15) and obtain a trace. The flash trace should fall back to the baseline in 150-250 μsec and should show fine structure characteristics of the light pulse. Fine-tuning of the light pipe position can be made now. Remove the neutral density filter and replace with a suitable narrow bandpass interference filter (see Section III.5.3.1). Obtain a trace. In the ideal case no flashing light should reach the PMT, however, the closer the transmission band widths of the complementary filters, the more light is leaked to the PMT. The trace will probably show identical characteristics to that obtained with the neutral

density filter in place. Once the flash duration is properly adjusted, erase the scope and set back to continuous scan (Section B).

E) Rate Measurement:

a) With the reference cell in the sample holder, calibrate spectrophotometer (Section C). The scope should read zero with the Analog Converter at A and balance at Cal. Now put the sample cell into the cell holder. The reading should change to a voltage corresponding exactly to the O.D. units of absorbance measured on the Cary spectrophotometer. Use balance control to bring the trace to zero.

b) Switch the vertical amplitude to 0.1V/div or 50mV/div. If the line deviates from zero readjust with the position control. Change the mode of the scope to stored single scan with external triggering (Section D). Select a sweep time (e.g. 5msec/div) and trigger the scope to register a baseline on the stored screen. Adjust the focus and intensity controls to give a clean line of sharp contrast. With baseline obtained, reset the scope, and fire Main on the Trigger control. The scope should show an exponential decay curve.

c) Select the optimum voltage amplitude, position and time base settings to afford the most appealing

exponential decay display. Record all parameters and take a picture. Do not erase until you have a well-developed photograph.

d) To convert the exponential decay curve into a linear rate plot first the trace selector located on the Analog Converter must be positioned to the correct direction (up for increasing decays and down for decreasing decays).

e) The converter internally supplies a reference voltage A_∞ of +0.4V which can be internally adjusted with the trimmer pot labelled R_7 (Figure III.18). To measure this voltage close the slit to give the zero baseline and switch the output to $A-A_\infty$. The reading on the scope should be either -0.4V (if the trace selector is at decreasing decays) or +0.4V (at increasing decays). In order to normalize the data this reference voltage must be subtracted from each absorbance value on the exponential decay curve.

f) To do this, recalibrate the unit as in Section A. With the Analog converter at A the continuous trace should be at zero baseline. Now, using the course and fine balance controls add or subtract 0.4V from this baseline trace. Switch the output to $A-A_\infty$, the beam should fall back to the zero baseline. The signal is now normalized. Change the amplitude setting to 0.1V/div, use the position control to fine tune

the baseline, switch output of the Analog Converter to k, select a time base setting which is about 2x or 5x faster than the setting used to obtain the exponential trace, reset the scope, fire the scope trigger to obtain a baseline, reset the scope, fire the scope trigger to obtain a baseline, reset the scope, and then fire the Main trigger to obtain a linear trace. The slope in volts/S, is the rate constant in S^{-1} of the exponential decay process under study.

g) If part of the linear trace is dislocated on the screen move this up or down to any arbitrary co-ordinates by adjusting the intercept control. All the three position controls of the Analog Converter (i.e. Coarse, Fine Balance and Intercept) are arranged such that turning clockwise moves their corresponding traces down on the screen. The intercept of this rate plot on the scope equals In A_O-A_∞ only when the intercept control is completely turned clockwise.

h) When the upper part of the linear trace appears noisy or badly smeared, it indicates that a faster sweep rate is needed. Switching to the next increment on the time base setting usually improves the appearance of this rate plot. Record all parameters and take picture. Do not erase trace until a well developed photograph is obtained.

F) Shutdown Procedures:

a) Turn off the flashgun and power supply.

b) Turn off Trigger control.

c) Return the output to T, balance to Cal., turn of the Analog Rate Converter.

d) Switch off the lamp and turn off Low Voltage power supply.

e) Turn off the High Voltage PMT supply.

f) Switch the scope to the non-storage mode. Turn off the oscilloscope.

G) Trouble Shooting:

a) Noise level too high:

Always bear in mind that the higher light intensity the PMT receives, the higher the cathode voltage (less negative high voltage) it requires to maintain the output level, and less noise and dark current will result. However, this light intensity is limited by the monochromator slit, thus, S/N level will trade off with the spectrophotometer's resolution. Whenever abnormally high noise levels show up, always remove the sample cuvette, switch the Analog Converter output to T, Balance at Cal., perform the routine calibrations as listed in Section C.

Then check:

1) The light system: exit filters in O position? PMT properly aligned? Cell extention or anything blocking the light path? Slit width too narrow?

2) The electronic system: try to ground every individual part; check connection between PMT and HV supply and the Analog Converter. HV too high?

b) Too much flash light leaked into the PMT detector: Check the filter system. The only way to reduce the sensitivity of the PMT detector toward the flash light is to reduce HV supply and increase the intensity of the monitoring beam (with less resolution).

c) Trigger Control malfunction:

1) It only triggers the scope sweep but not the flash unit:

a) Check the flashgun to see if it is properly charged.

b) Check the trigger connection of the flash-gun.

c) Have flashgun circuitry checked out, particularly thyrister component.

2) If it does not trigger the flashgun nor the scope.

a) Check button switches.

b) Check the trigger level on the scope, adjust it more +ve (more sensitive).

3) It only triggers the flash unit but not the scope.

a) Check the trigger level of the scope; increase sensitivity, if necessary.

d) Malfunction of the Analog Converter:

a) Consult construction description[152,153] and circuit diagram, (Figure III.18), recalibrate it if needed.

b) In emergency, the whole analog converter circuit can be dispensed by connecting the PMT anode output directly to the scope according to the following diagram. This circuit changes the display to %T units.

APPENDIX II

DERIVATION OF THE RATE LAW FOR THE INTERACTION OF CARBON MONOXIDE WITH SIMPLE HEMOPROTEINS

Derivation of the Rate Law for the Interaction of Carbon Monoxide with Simple Hemoproteins

For the reaction of hemoproteins containing a single heme unit such as myoglobin and cytochrome P450cam the reaction with carbon monoxide can be represented by reaction scheme (1),

$$Fe(II) + CO \underset{k_{off}}{\overset{k_{on}}{\rightleftharpoons}} Fe(II)\text{-}CO, \qquad (1)$$

where Fe(II) is the hemoprotein, Fe(II)-CO is the hemoprotein-CO adduct, k_{on} is the association velocity constant and k_{off} is the dissociation velocity constant. Hence the equilibrium constant, Kco, is given by (2),

$$Kco = \frac{k_{on}}{k_{off}} = \frac{[Fe(II)\text{-}CO]_e}{[Fe(II)]_e[CO]_e}, \qquad (2)$$

where the subscript e represents equilibrium concentrations of each component.

The rate of the process indicated by scheme (1) shown above is

$$-\frac{d[Fe(II)]}{dt} = \frac{d[Fe(II)\text{-}CO]}{dt} = k_{on}[Fe(II)][CO] - k_{off}[Fe(II)\text{-}CO] \qquad (3)$$

Since reaction scheme (1) was carried out under conditions of large excess of CO in comparison with Fe(II) (i.e. pseudo first-order in [Fe(II)]),the product $k_{on}[CO] = k'$ is constant and (3) becomes

$$-\frac{d[Fe(II)]}{dt} = \frac{d[Fe(II)\text{-}CO]}{dt} = k'[Fe(II)] - k_{off}[Fe(II)\text{-}CO] \qquad (4)$$

An integrated form of (4) can be obtained by rewriting the equation in terms of product formation in reaction scheme (1) (i.e. in terms of [Fe(II)-CO]) knowing that

$$[Fe(II)]_o = [Fe(II)\text{-}CO] + [Fe(II)]$$

where $[Fe(II)]_o$ is the total hemoprotein concentration at time zero, [Fe(II)-CO] is the concentration CO-bound sites in the hemoprotein at time $\underline{t}$, and [Fe(II)] is the concentration of free sites at time $\underline{t}$. Rearranging the above equation to give (5)

$$[Fe(II)] = [Fe(II)]_o - [Fe(II)\text{-}CO] \qquad (5)$$

and substituting (5) into (4), equation (6) can be obtained, which gives the rate of the process shown in reaction scheme (1) in terms of product formation

$$\frac{d[Fe(II)\text{-}CO]}{dt} = k'[Fe(II)]_o - (k' + k_{off})\,[Fe(II)\text{-}CO] \qquad (6)$$

Equation (6) can now be integrated using standard integral (7)

$$\int \frac{dx}{a + bx} = \frac{1}{b} \ln (a + bx) + c \qquad (7)$$

where $a = k'\,[Fe(II)]_o$

$b = -(k' + k_{off})$

$x = [Fe(II)\text{-}CO]$

Collecting terms and assigning the experimental limits of integration, (6) can be rewritten in terms of (7) to give (8)

$$\int_{[Fe(II)]_o}^{[Fe(II)\text{-}CO]} \frac{d\,[Fe(II)\text{-}CO]}{k'[Fe(II)]_o - (k' + k_{off})[Fe(II)\text{-}CO]} = \int_o^t dt \qquad (8)$$

Integration and evaluation of (8) gives (9), the integrated form of rate equation (6)

$$\ln \frac{k'[Fe(II)]_o - (k' + k_{off})[Fe(II)\text{-}CO]}{k'[Fe(II)]_o - (k' + k_{off})[Fe(II)]_o} = (k' + k_{off})t \quad (9)$$

The above equation can be simplified by introducing equilibrium concentrations by allowing rate equation (4) to equal 0. For this case by setting $\frac{d[Fe(II)\text{-}CO]}{dt} = 0$

$$k'[Fe(II)]_e = k_{off}[Fe\text{-}CO]_e = k'([Fe(II)]_o - [Fe(II)\text{-}CO]_e) \quad (10)$$

Where the subscript e refers to equilibrium concentrations, then

$$[Fe(II)]_o = [Fe(II)\text{-}CO]_e \frac{k_{off} + k'}{k'} \quad (11)$$

and (9) can then be written

$$\ln \frac{[Fe(II)]_o - [Fe(II)\text{-}CO]_e}{[Fe(II)\text{-}CO] - [Fe(II)\text{-}CO]_e} = (k' + k_{off})t \quad (12)$$

where $[Fe(II)]_o$, $[Fe(II)\text{-}CO]_e$ and $[Fe(II)\text{-}CO]$ are, respectively, the concentration of CO-bound hemoprotein sites at time zero, at equilibrium and at time, t. The result of equation (12) is that the approach to equilibrium is a first-order process with the observed rate constant, k_{obs}, the sum of the pseudo first-order rate constant for the forward and the first-order rate constant for the reverse reactions of reaction scheme (1). Since

$$k_{obs} = (k' + k_{off}) \quad \text{and} \quad k' = k_{on}[CO]$$

plots of k_{obs} *vs.* [CO] give a straight line with slope, k_{on} and intercept, k_{off}.

Since the flash photolysis experiments involved spectrophotometric analysis of the reaction mixtures, equation (12) can be rewritten in terms of absorbances using Beer's Law (13) along with expressions equating the total absorbance of the reaction solution with the concentration of absorbing species at time zero (14), at equilibrium (15) and at time, $\underline{t}$ (16).

$$A = \varepsilon bc \tag{13}$$

$$[Fe(II)]_o = \frac{A_o}{\varepsilon_{Fe(II)}} \tag{14}$$

$$A_e = \varepsilon_{Fe(II)}[Fe(II)]_e + \varepsilon_{Fe(II)-CO}[Fe(II)-CO]_e \tag{15}$$

$$A = \varepsilon_{Fe(II)}[Fe(II)] + \varepsilon_{Fe(II)-CO}[Fe(II)-CO] \tag{16}$$

Solving for the concentration of each species in equations (11) in terms of absorbances denoted in expressions (14), (15) and (16) gives equation (17)

$$\ln \frac{A_o - A_e}{A - A_e} = k_{obs}t \tag{17}$$

where A is the absorbance of the Fe(II)-CO adduct at time $\underline{t}$

A_e is the absorbance of the Fe(II)-CO adduct at equilibrium

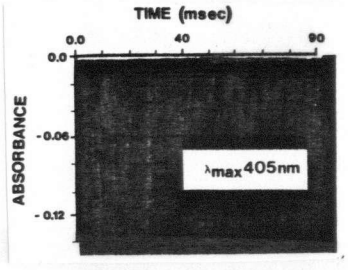
A_o is the absorbance of the Fe(II)-CO adduct at the start of the reaction and k_{obs} is the observed rate constant.

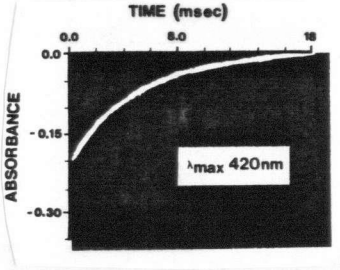
Derivation of equation (17) in terms of the 5-coordinate unbound hemoprotein would result in the same expression differing only in the sign of the slope of the k_{obs} *vs.* [CO] graph.

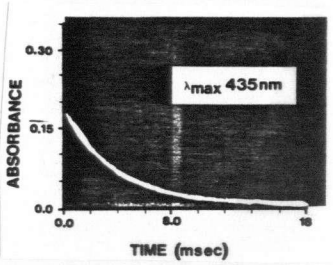
APPENDIX III

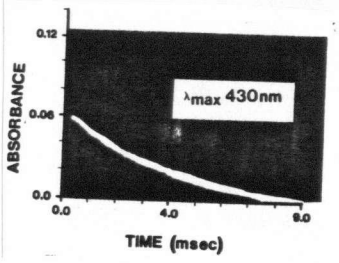
RAW DATA FOR THE SPECTRUM OF THE KINETIC INTERMEDIATE PRODUCED BY THE PHOTODECOMPOSITION OF THE CARBON MONOXIDE COMPLEXES OF MYOGLOBIN AND CYTOCHROME P450cam

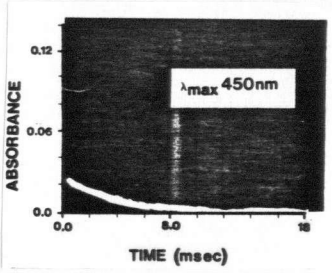
Appendix IIIa Raw data for the kinetic intermediate of the Mb-CO system.

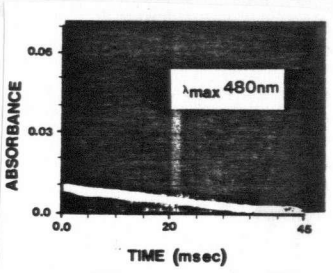




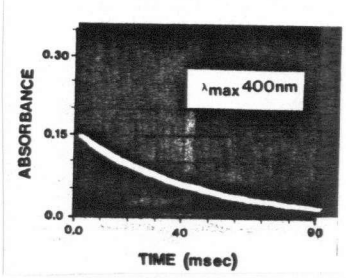


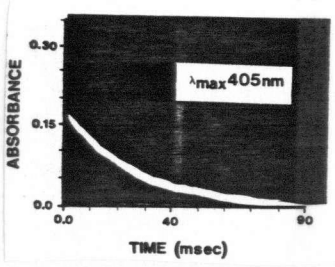


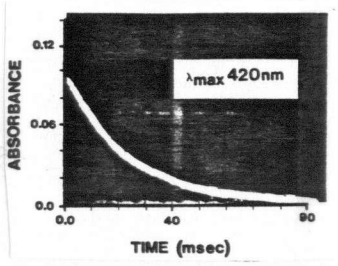


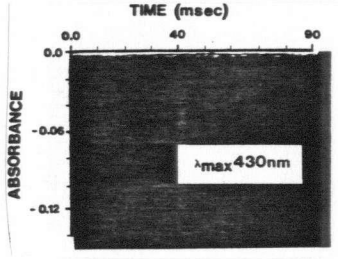


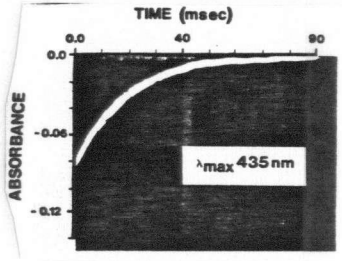
Appendix IIIb Raw data for the kinetic Intermediate of the P450cam-CO system.

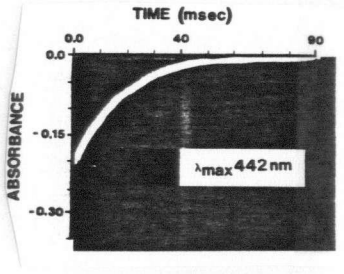


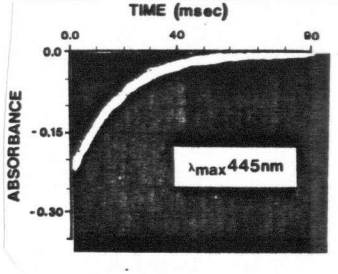


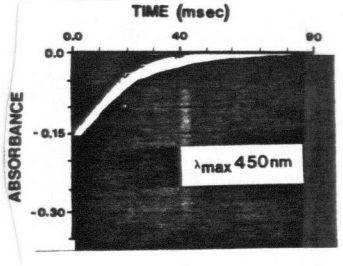


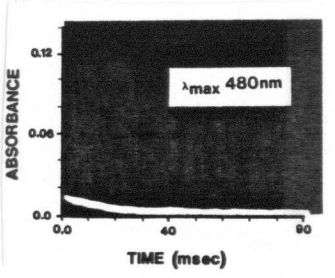












APPENDIX IV

RAW DATA FOR THE FLASH PHOTOLYSIS KINETIC STUDIES OF THE Mb-CO, AND NATIVE AND PROTOHEMIN-RECONSTITUTED P450cam-CO SYSTEMS

Appendix IVa Raw data for kinetic Run 2 for the Mb-CO system.

Absorbance Data for Hemoproteins

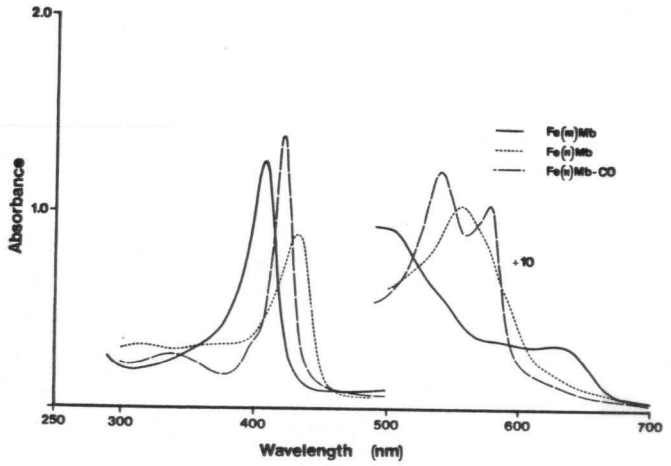
Sample Description: Myoglobin

Experiment Description: Kinetic Run 2 for the Myoglobin-CO system

[Hemoprotein]: 6.43×10^{-6} M

Absorbance Data

Hemoprotein Sepcies	λ_{max} (nm)	Absorbance	Calculated mM	Literature[10,9] mM
Oxidised	630	2.2×10^{-2}	3.4	3.9
	505	6.8×10^{-2}	11	10.2
	408	1.2	185	188
Reduced	555	8.7×10^{-2}	14	13.8
	432	8.4×10^{-1}	131	121
Reduced-CO	577	9.0×10^{-2}	14	13.9
	540	1.0×10^{-1}	16	15.4
	422	1.33	207	207
	340	2.0×10^{-1}	31	



FLASH PHOTOLYSIS EXPERIMENTS

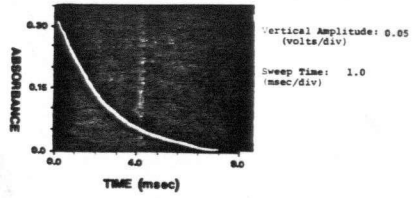
Sample Description: Myoglobin -CO complex

Temperature: 20 ± 0.2°C

Monitoring Wavelength: 432nm

Data Table

Run	Plot Form	Cary O.D.	Flash Unit Volt.	P_T (mm Hg)	P_{H_2O} (mm Hg)	P_{CO} (mm Hg)	$[CO] \times 10^4$ (M/L)	Half Life (msec)
2.1	Exp. Decay	0.48	0.50	758	17.5	741	10.1	1.5



Vertical Amplitude: 0.05 (volts/div)

Sweep Time: 1.0 (msec/div)

Half Life Data

Half Life #	Vertical Drop (volts)	Horizontal Sweep (msec)
0	0.300	0
1	0.150	1.8 (1.8)
2	0.075	2.1 (1.3)
3	0.038	3.7 (1.6)
4	0.019	5.1 (1.4)

$t_{\frac{1}{2}}$ = 1.5msec

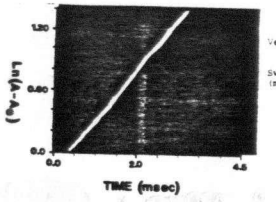
FLASH PHOTOLYSIS EXPERIMENTS

Sample Description: Myoglobin-CO complex

Temperature: 20 ± 0.2°C

Data Table

Run	Plot Form	Cary O.D.	Flash Unit Volt.	P_T (mm Hg)	P_{H_2O} (mm Hg)	P_{CO} (mm Hg)	$[CO] \times 10^4$ (M/L)	k_{obs} ($msec^{-1}$)
2.1	Rate Plot	0.48	0.50	758	17.5	741	10.1	5.1×10^{-1}



Vertical Amplitude: 0.2 (volts/div)

Sweep Time: 0.5 (msec/div)

Slope (mean)		Slope (max)		Slope (min)	
X (msec)	Y (volts)	X (msec)	Y (volts)	X (msec)	Y (volts)
0.5	0.06	0.5	0.04	0.5	0.10
1.0	0.32	1.0	0.32	1.0	0.34
1.5	0.57	1.5	0.57	1.5	0.57
2.0	0.84	2.0	0.85	2.0	0.83
2.5	1.09	2.5	1.12	2.5	1.07

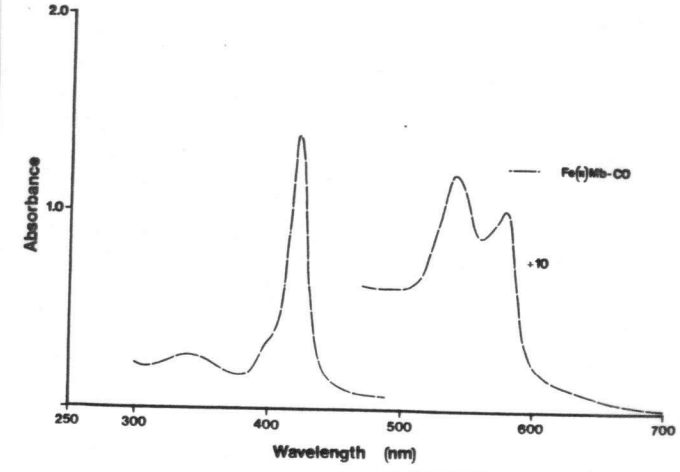
Least Squares Analysis

m: 5.1×10^{-1} $msec^{-1}$

y-intercept: -1.9×10^{-1}

δy: 1.8×10^{-2}

δm: 6.4×10^{-3} $msec^{-1}$



FLASH PHOTOLYSIS EXPERIMENTS

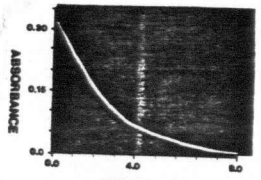
Sample Description: Myoglobin -CO complex

Temperature: 20 ± 0.2°C

Monitoring Wavelength: 432nm

Data Table

Run	Plot Form	Cary O.D.	Flash Unit Volt.	P_T (mm Hg)	P_{H_2O} (mm Hg)	P_{CO} (mm Hg)	[CO]x10^4 (m/L)	Half Life (msec)
2.2	Exp. Decay	0.48	0.50	648	17.5	631	8.58	1.6



Vertical Amplitude: 0.05 (volts/div)

Sweep Time: 1.0 (msec/div)

Half Life Data

Half Life θ	Vertical Drop (volts)	Horizontal Sweep (msec)
0	0.325	0
1	0.163	1.9 (1.9)
2	0.081	3.5 (1.6)
3	0.041	5.3 (1.8)
4	0.020	6.7 (1.4)

$t_{\frac{1}{2}}$ = 1.6 msec

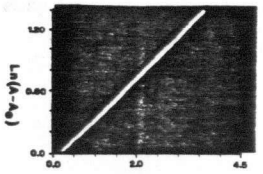
FLASH PHOTOLYSIS EXPERIMENTS

Sample Description: Myoglobin-CO complex

Temperature: 20±0.2°C

Data Table

Run	Plot Form	Cary O.D.	Flash Unit Volt.	P_T (mm Hg)	P_{H_2O} (mm Hg)	P_{CO} (mm Hg)	[CO]x10^4 (m/L)	k_{obs} (msec^{-1})
2.2	Rate Plot	0.48	0.50	648	17.5	631	8.58	4.0x10^{-1}



Vertical Amplitude: 0.2 (volts/div)

Sweep Time: 0.5 (msec/div)

Slope (mean) X (msec)	Slope (mean) Y (volts)	Slope (max) X (msec)	Slope (max) Y (volts)	Slope (min) X (msec)	Slope (min) Y (volts)
0.5	0.13	0.5	0.10	0.5	0.15
1.0	0.33	1.0	0.30	1.0	0.33
1.5	0.53	1.5	0.52	1.5	0.53
2.0	0.73	2.0	0.73	2.0	0.73
2.5	0.94	2.5	0.94	2.5	0.92
3.0	1.13	3.0	1.14	3.0	1.12

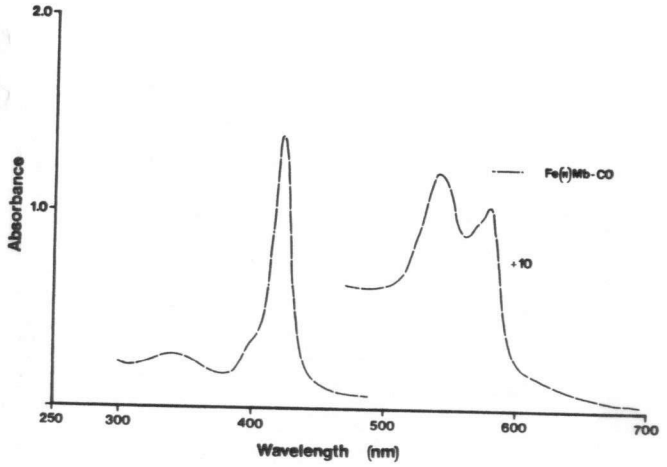
Least Squares Analysis

m: 4.0x10^{-1}msec^{-1}

y-intercept: -7.8x10^{-2}

δy:1.3x10^{-2}

δm:3.5x10^{-3}msec^{-1}



FLASH PHOTOLYSIS EXPERIMENTS

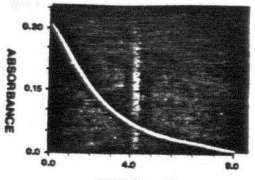
Sample Description: Myoglobin-CO complex

Temperature: 20±0.2°C

Monitoring Wavelength: 432nm

Data Table

Run	Plot Form	Cary O.D.	Flash Unit Volt.	P_T (mm Hg)	P_{H_2O} (mm Hg)	P_{CO} (mm Hg)	[CO]x10^4 (m/L)	Half Life (msec)
2.3	Exp. Decay	0.48	0.50	547	17.5	530	7.21	1.8



Vertical Amplitude: 0.05 (volts/div)

Sweep Time: 1.0 (msec/div)

Half Life Data

Half Life θ	Vertical Drop (volts)	Horizontal Sweep (msec)
0	0.300	0
1	0.150	2.1 (2.1)
2	0.075	3.9 (1.8)
3	0.038	5.3 (1.4)
4	0.019	7.2 (1.9)

$t_{\frac{1}{2}}$ = 1.8 msec

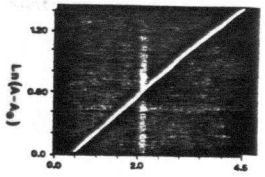
FLASH PHOTOLYSIS EXPERIMENTS

Sample Description: Myoglobin-CO complex

Temperature: 20 ± 0.2°C

Data Table

Run	Plot Form	Cary O.D.	Flash Unit Volt.	P_T (mm Hg)	P_{H_2O} (mm Hg)	P_{CO} (mm Hg)	[CO]x10^4 (m/L)	k_{obs} (msec^{-1})
2.3	Rate Plot	0.48	0.50	547	17.5	530	7.21	3.6x10^{-1}



Vertical Amplitude: 0.2 (volts/div)

Sweep Time: 0.5 (msec/div)

Slope (mean) X (msec)	Slope (mean) Y (volts)	Slope (max) X (msec)	Slope (max) Y (volts)	Slope (min) X (msec)	Slope (min) Y (volts)
0.5	0.03	0.5	0.03	0.5	0.05
1.0	0.21	1.0	0.21	1.0	0.23
1.5	0.38	1.5	0.38	1.5	0.38
2.0	0.57	2.0	0.58	2.0	0.57
2.5	0.75	2.5	0.78	2.5	0.75
3.0	0.92	3.0	0.95	3.0	0.91
3.5	1.10	3.5	1.14	3.5	1.08

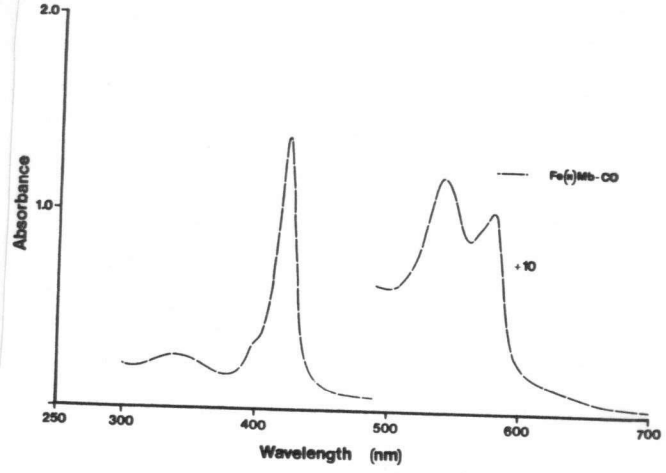
Least Squares Analysis

m:3.6x10^{-1}msec^{-1}

y-intercept: -1.4x10^{-1}

δy: 1.6x10^{-2}

δm:3.5x10^{-3}msec^{-1}



FLASH PHOTOLYSIS EXPERIMENTS

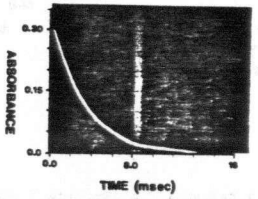
Sample Description: Myoglobin-CO complex

Temperature: 20 ±0.2°C

Monitoring Wavelength: 432nm

Data Table

Run	Plot Form	Cary O.D.	Flash Unit Volt.	P_T (mm Hg)	P_{H_2O} (mm Hg)	P_{CO} (mm Hg)	[CO]x10^4 (m/L)	Half Life (msec)
2.4	Exp. Decay	0.48	0.50	448	17.5	431	5.86	2.1



Vertical Amplitude: 0.05 (volts/div)

Sweep Time: 2.0 (msec/div)

Half Life Data

Half Life #	Vertical Drop (volts)	Horizontal Sweep (msec)
0	0.300	0
1	0.150	2.4 (2.4)
2	0.075	4.5 (2.1)
3	0.038	6.7 (2.2)
4	0.019	8.4 (1.7)

$t_{\frac{1}{2}}$ = 2.1 msec

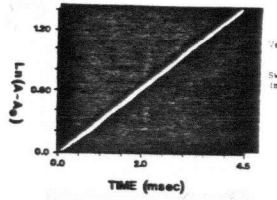
FLASH PHOTOLYSIS EXPERIMENTS

Sample Description: Myoglobin-CO complex

Temperature: 20 ±0.2°C

Data Table

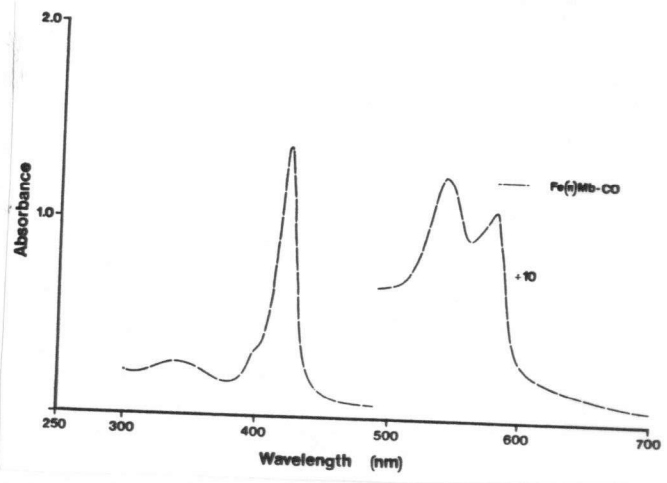
Run	Plot Form	Cary O.D.	Flash Unit Volt.	P_T (mm Hg)	P_{H_2O} (mm Hg)	P_{CO} (mm Hg)	[CO]x10^4 (m/L)	k_{obs} (msec^{-1})
2.4	Rate Plot	0.48	0.50	448	17.5	431	5.86	3.3x10^{-1}



Vertical Amplitude: 0.2 (volts/div)

Sweep Time: 0.5 (msec/div)

Slope (mean)		Slope (max)		Slope (min)		Least Squares Analysis
X (msec)	Y (volts)	X (msec)	Y (volts)	X (msec)	Y (volts)	
0.5	0.14	0.5	0.12	0.5	0.15	m:3.3x10^{-1}msec^{-1}
1.0	0.30	1.0	0.28	1.0	0.30	y-intercept: -3.4x10^{-2}
1.5	0.46	1.5	0.46	1.5	0.46	δy: 1.3x10^{-2}
2.0	0.62	2.0	0.62	2.0	0.62	δm:2.9x10^{-3}msec^{-1}
2.5	0.79	2.5	0.79	2.5	0.78	
3.0	0.98	3.0	0.98	3.0	0.94	
3.5	1.12	3.5	1.14	3.5	1.10	



FLASH PHOTOLYSIS EXPERIMENTS

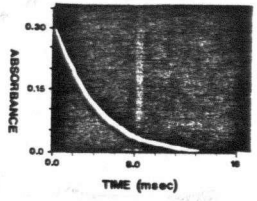
Sample Description: Myoglobin-CO complex

Temperature: 20±0.2°C

Monitoring Wavelength: 432nm

Data Table

Run	Plot Form	Cary O.D.	Flash Unit Volt.	P_T (mm Hg)	P_{H_2O} (mm Hg)	P_{CO} (mm Hg)	[CO]x10^4 (m/L)	Half Life (msec)
2.5	Exp. Decay	0.48	0.50	350	17.5	333	4.53	2.6



Vertical Amplitude: 0.05 (volts/div)

Sweep Time: 2.0 (msec/div)

Half Life Data

Half Life #	Vertical Drop (volts)	Horizontal Sweep (msec)
0	0.300	0
1	0.150	2.9 (2.9)
2	0.075	5.4 (2.5)
3	0.038	7.8 (2.4)
4	0.019	10.4 (2.6)

$t_{\frac{1}{2}}$ = 2.6msec

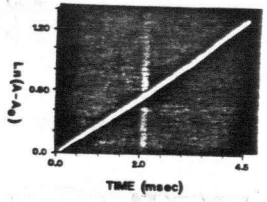
FLASH PHOTOLYSIS EXPERIMENTS

Sample Description: Myoglobin-CO complex

Temperature: 20±0.2°C

Data Table

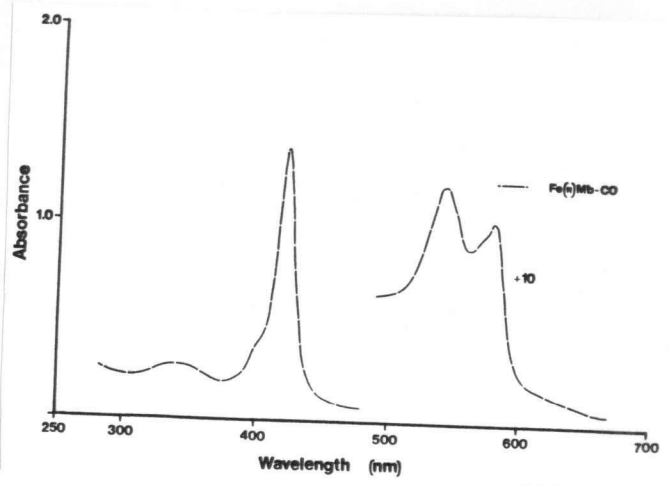
Run	Plot Form	Cary O.D.	Flash Unit Volt.	P_T (mm Hg)	P_{H_2O} (mm Hg)	P_{CO} (mm Hg)	[CO]x10^4 (m/L)	k_{obs} (msec^{-1})
2.5	Rate Plot	0.48	0.50	350	17.5	333	4.53	2.9x10^{-1}



Vertical Amplitude: 0.2 (volts/div)

Sweep Time: 0.5 (msec/div)

Slope (mean)		Slope (max)		Slope (min)		Least Squares Analysis
X (msec)	Y (volts)	X (msec)	Y (volts)	X (msec)	Y (volts)	
0.5	0.11	0.5	0.11	0.5	0.14	m:2.9x10^{-1}msec^{-1}
1.0	0.23	1.0	0.23	1.0	0.28	y-intercept: -3.1x10^{-2}
1.5	0.40	1.5	0.42	1.5	0.42	
2.0	0.54	2.0	0.56	2.0	0.54	δy: 2.1x10^{-3}
2.5	0.69	2.5	0.72	2.5	0.69	δm:3.8x10^{-3}msec^{-1}
3.0	0.84	3.0	0.87	3.0	0.82	
3.5	0.98	3.5	1.01	3.5	0.96	
4.0	1.13	4.0	1.17	4.0	1.09	



FLASH PHOTOLYSIS EXPERIMENTS

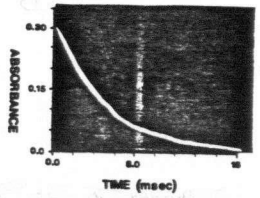
Sample Description: Myoglobin-CO complex

Temperature: 20±0.2°C

Monitoring Wavelength: 432nm

Data Table

Run	Plot Form	Cary O.D.	Flash Unit Volt.	P_T (mm Hg)	P_{H_2O} (mm Hg)	P_{CO} (mm Hg)	$[CO]\times10^4$ (m/L)	Half Life (msec)
2.6	Exp. Decay	0.48	0.50	253	17.5	236	3.21	3.7



Vertical Amplitude: 0.05 (volts/div)

Sweep Time: 2.0 (msec/div)

Half Life Data

Half Life #	Vertical Drop (volts)	Horisontal Sweep (msec)
0	0.300	0
1	0.150	3.8 (3.8)
2	0.075	7.0 (3.2)
3	0.038	10.8 (3.8)
4	0.019	14.9 (4.1)

$t_{\frac{1}{2}}$ = 3.7 msec

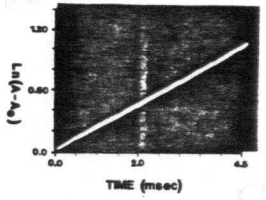
FLASH PHOTOLYSIS EXPERIMENTS

Sample Description: Myoglobin-CO complex

Temperature: 20±0.2°C

Data Table

Run	Plot Form	Cary O.D.	Flash Unit Volt.	P_T (mm Hg)	P_{H_2O} (mm Hg)	P_{CO} (mm Hg)	$[CO]\times10^4$ (m/L)	k_{obs} ($msec^{-1}$)
2.6	Rate Plot	0.48	0.50	253	17.5	236	3.21	2.2×10^{-1}



Vertical Amplitude: 0.2 (volts/div)

Sweep Time: 0.5 (msec/div)

Slope (mean) X (msec)	Slope (mean) Y (volts)	Slope (max) X (msec)	Slope (max) Y (volts)	Slope (min) X (msec)	Slope (min) Y (volts)
0.5	0.13	0.5	0.11	0.5	0.16
1.0	0.25	1.0	0.23	1.0	0.26
1.5	0.36	1.5	0.34	1.5	0.37
2.0	0.47	2.0	0.46	2.0	0.47
2.5	0.58	2.5	0.58	2.5	0.58
3.0	0.70	3.0	0.70	3.0	0.69
3.5	0.80	3.5	0.82	3.5	0.78
4.0	0.92	4.0	0.93	4.0	0.90

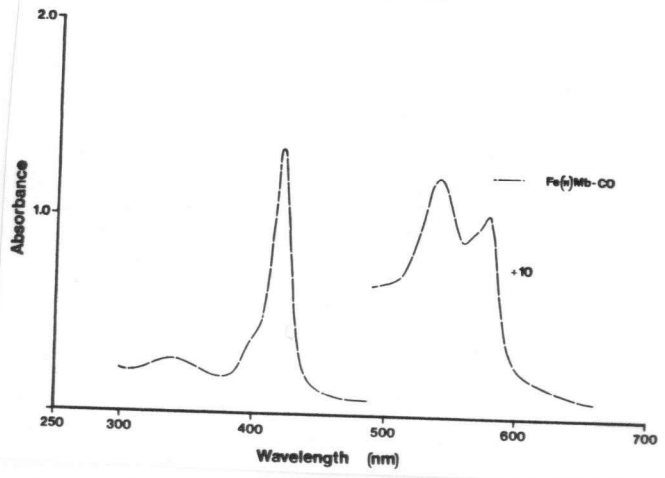
Least Squares Analysis

m: $2.2\times10^{-1}msec^{-1}$

y-intercept: 2.2×10^{-2}

δy: 1.3×10^{-2}

δm: $2.3\times10^{-3}msec^{-1}$



FLASH PHOTOLYSIS EXPERIMENTS

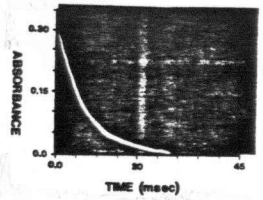
Sample Description: Myoglobin-CO complex

Temperature: 20±0.2°C

Monitoring Wavelength: 432nm

Data Table

Run	Plot Form	Cary O.D.	Flash Unit Volt.	P_T (mm Hg)	P_{H_2O} (mm Hg)	P_{CO} (mm Hg)	$[CO]\times10^4$ (m/L)	Half Life (msec)
2.7	Exp. Decay	0.48	0.50	214	17.5	197	2.68	4.5



Vertical Amplitude: 0.05 (volts/div)

Sweep Time: 5.0 (msec/div)

Half Life Data

Half Life #	Vertical Drop (volts)	Horisontal Sweep (msec)
0	0.300	0
1	0.150	4.6 (4.6)
2	0.075	9.0 (4.4)
3	0.038	13.3 (4.3)
4	0.019	18.0 (4.7)

$t_{\frac{1}{2}}$ = 4.5 msec

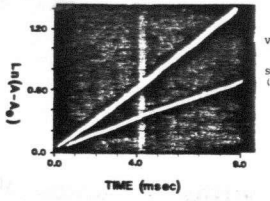
FLASH PHOTOLYSIS EXPERIMENTS

Sample Description: Myoglobin-CO complex

Temperature: 20±0.2°C

Data Table

Run	Plot Form	Cary O.D.	Flash Unit Volt.	P_T (mm Hg)	P_{H_2O} (mm Hg)	P_{CO} (mm Hg)	$[CO]\times10^4$ (m/L)	k_{obs} ($msec^{-1}$)
2.7	Rate Plot	0.48	0.50	214	17.5	197	2.68	1.6×10^{-1}



Vertical Amplitude: 0.2 (volts/div)

Sweep Time: Top: 1.0 (msec/div)
Bottom: 0.5

Slope (mean) X (msec)	Slope (mean) Y (volts)	Slope (max) X (msec)	Slope (max) Y (volts)	Slope (min) X (msec)	Slope (min) Y (volts)
1.0	0.17	1.0	0.16	1.0	0.19
2.0	0.33	2.0	0.32	2.0	0.34
3.0	0.49	3.0	0.49	3.0	0.49
4.0	0.64	4.0	0.64	4.0	0.64
5.0	0.79	5.0	0.80	5.0	0.79
6.0	0.95	6.0	0.96	6.0	0.94

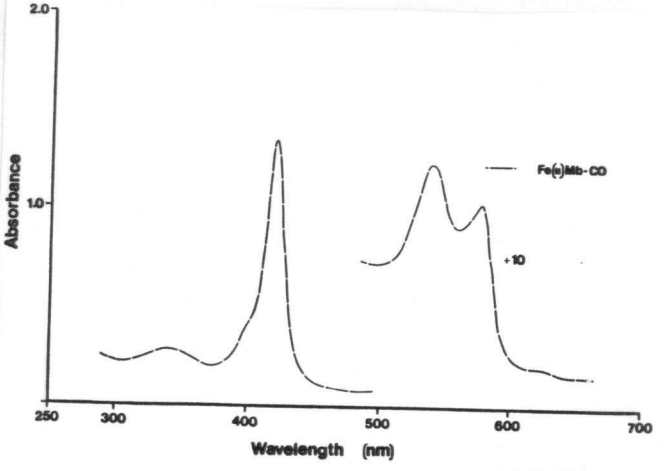
Least Squares Analysis

m: $1.6\times10^{-1}msec^{-1}$

y-intercept: 2.0×10^{-2}

δy: 8.0×10^{-3}

δm: $1.1\times10^{-3}, sec^{-1}$



Appendix IVb Raw data for kinetic Run 3 for the native P450cam-CO system.

Absorbance Data for Hemoprotein

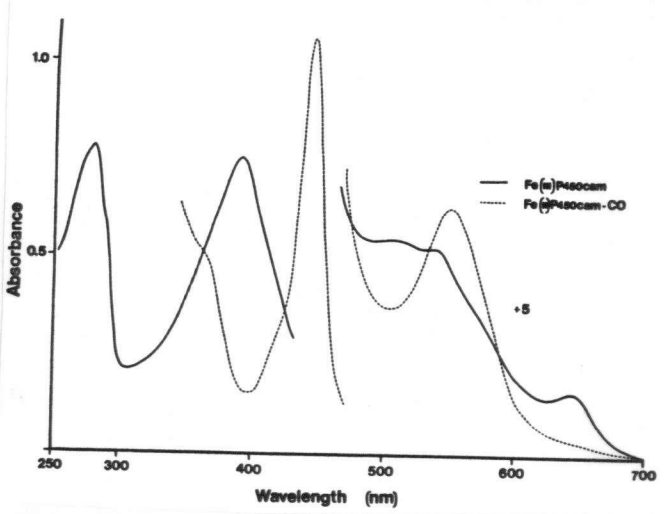
Sample Description: Native substrate-bound Cytochrome P450cam

Experiment Description: Kinetic Run 3 for the native substrate-bound P450cam-CO system

[Hemoprotein]: 8.75×10^{-6} M

Absorbance Data

Hemoprotein Species	λ_{max} (nm)	Absorbance	Calculated εmM	Literature[37] εmM
Oxidized (FeIII)	643	3.3×10^{-2}	3.8	5.4
	510	1.0×10^{-1}	11.5	11.2
	540	1.1×10^{-1}	12.0	13.0
	391	7.4×10^{-1}	85.0	102
Reduced-CO	550	1.2×10^{-1}	14.0	14.0
	445	1.05	120	120



FLASH PHOTOLYSIS EXPERIMENTS

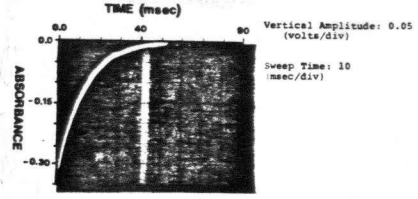
Sample Description: Native P450cam-CO complex

Temperature: 20 ±0.2°C

Monitoring Wavelength: 442nm

Data Table

Run	Plot Form	Cary O.D.	Flash Unit Volt.	P_T (mm Hg)	P_{H_2O} (mm Hg)	P_{CO} (mm Hg)	[CO]x10^4 (M/L)	Half Life (msec)
3.1	Exp. Decay	0.968	0.970	750	17.5	733	9.96	8.5



Vertical Amplitude: 0.05 (volts/div)

Sweep Time: 10 (msec/div)

Half Life Data

Half Life θ	Vertical Drop (volts)	Horizontal Sweep (msec)
0	0.3	0
1	0.15	9 (9)
2	0.075	18 (9)
3	0.038	25 (7)
4	0.019	34 (9)

$t_{\frac{1}{2}}$ = 8.5 msec

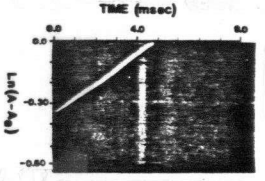
FLASH PHOTOLYSIS EXPERIMENTS

Sample Description: Native P450cam-CO complex

Temperature: 20±0.2°C

Data Table

Run	Plot Form	Cary O.D.	Flash Unit Volt.	P_T (mm Hg)	P_{H_2O} (mm Hg)	P_{CO} (mm Hg)	[CO]x10^4 (M/L)	k_{obs} (msec^{-1})
3.1	Rate Plot	0.968	0.970	750	17.5	733	9.96	7.1×10^{-2}



Vertical Amplitude: 0.1 (volts/div)

Sweep Time: 1.0 (msec/div)

Slope (mean) X (msec)	Slope (mean) Y (volts)	Slope (max) X (msec)	Slope (max) Y (volts)	Slope (min) X (msec)	Slope (min) Y (volts)
0	-0.345	0	-0.350	0	-0.335
1.0	-0.270	1.0	-0.270	1.0	-0.265
1.5	-0.220	1.5	-0.220	1.5	-0.220
2.0	-0.200	2.0	-0.200	2.0	-0.200
3.0	-0.130	3.0	-0.130	3.0	-0.130
3.5	-0.090	3.5	-0.085	3.5	-0.100
4.0	-0.055	4.0	-0.050	4.0	-0.060
4.5	-0.020	4.5	-0.010	4.5	-0.030

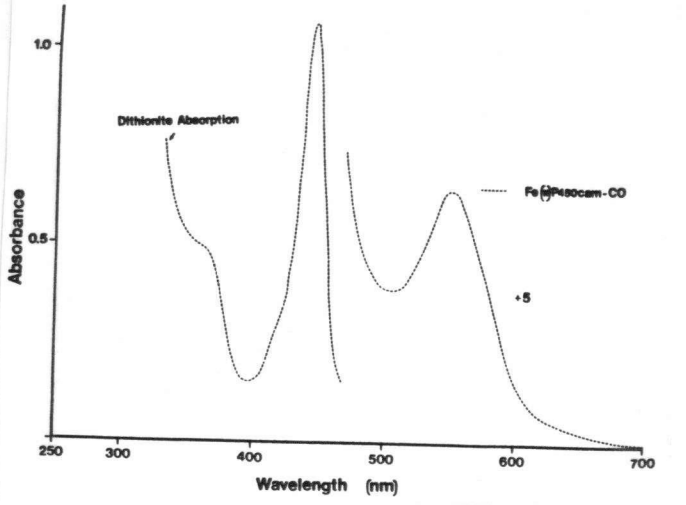
Least Squares Analysis

m:7.1×10^{-2}msec^{-1}

y-intercept: -3.4×10^{-1}

δy: 2.8×10^{-3}

δm:1.2×10^{-3}msec^{-1}



FLASH PHOTOLYSIS EXPERIMENTS

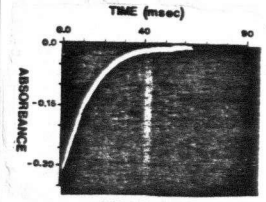
Sample Description: Native P450cam-CO complex

Temperature: 20±0.2°C

Monitoring Wavelength: 442nm

Data Table

Run	Plot Form	Cary O.D.	Flash Unit Volt.	P_T (mm Hg)	P_{H_2O} (mm Hg)	P_{CO} (mm Hg)	[CO]x10^4 (m/L)	Half Life (msec)
3.2	Exp. Decay	0.975	0.980	650	17.5	633	8.60	9.3



Vertical Amplitude: 0.05 (volts/div)

Sweep Time: 10 (msec/div)

Half Life Data

Half Life #	Vertical Drop (volts)	Horizontal Sweep (msec)
0	0.32	0
1	0.16	9 (9)
2	0.08	18 (9)
3	0.04	27 (9)
4	0.02	37 (10)

$t_{\frac{1}{2}}$ = 9.3 msec

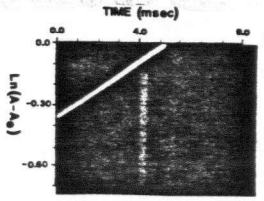
FLASH PHOTOLYSIS EXPERIMENTS

Sample Description: Native P450cam-CO complex

Temperature: 20±0.2°C

Data Table

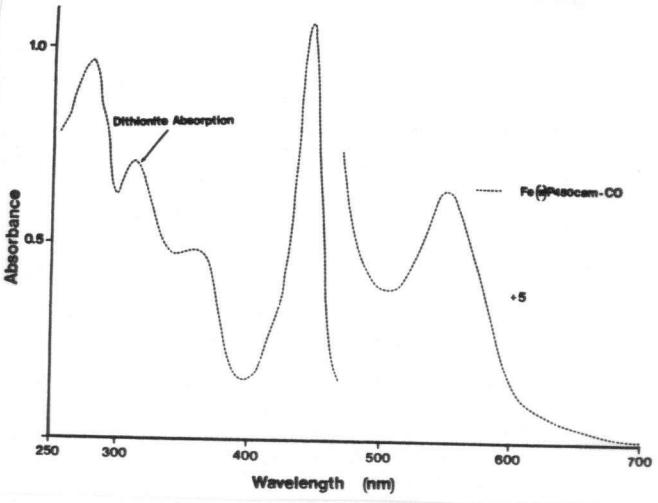
Run	Plot Form	Cary O.D.	Flash Unit Volt.	P_T (mm Hg)	P_{H_2O} (mm Hg)	P_{CO} (mm Hg)	[CO]x10^4 (m/L)	k_{obs} (msec^{-1})
3.2	Rate Plot	0.975	0.980	650	17.5	633	8.60	7.1x10^{-2}



Vertical Amplitude: 0.1 (volts/div)

Sweep Time: 1.0 (msec/div)

Slope (mean)		Slope (max)		Slope (min)		Least Squares Analysis
X (msec)	Y (volts)	X (msec)	Y (volts)	X (msec)	Y (volts)	
0	-0.370	0	-0.370	0	-0.360	m:7.1x10^{-2}msec^{-1}
1.0	-0.295	1.0	-0.295	1.0	-0.295	y-intercept: -3.7x10^{-1}
2.0	-0.230	2.0	-0.230	2.0	-0.230	δy: 1.9x10^{-3}
3.0	-0.155	3.0	-0.150	3.0	-0.160	δm:7.7x10^{-4}msec^{-1}
4.0	-0.085	4.0	-0.075	4.0	-0.090	
5.0	-0.015	5.0	-0.005	5.0	-0.025	



FLASH PHOTOLYSIS EXPERIMENTS

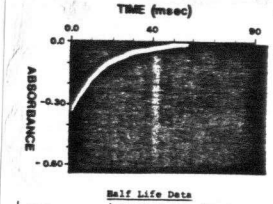
Sample Description: Native P450cam-CO complex

Temperature: 20±0.2°C

Monitoring Wavelength: 442nm

Data Table

Run	Plot Form	Cary O.D.	Flash Unit Volt.	P_T (mm Hg)	P_{H_2O} (mm Hg)	P_{CO} (mm Hg)	[CO]x10^4 (m/L)	Half Life (msec)
3.3	Exp. Decay	0.980	0.970	550	17.5	533	7.24	10



Vertical Amplitude: 0.1 (volts/div)

Sweep Time: 10 (msec/div)

Half Life Data

Half Life #	Vertical Drop (volts)	Horizontal Sweep (msec)
0	-0.340	0
1	-0.170	10 (10)
2	-0.085	20 (10)
3	-0.042	31 (11)
4	-0.021	42 (11)

$t_{\frac{1}{2}}$ = 10 msec

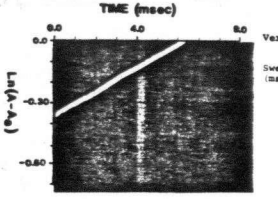
FLASH PHOTOLYSIS EXPERIMENTS

Sample Description: Native P450cam-CO complex

Temperature: 20±0.2°C

Data Table

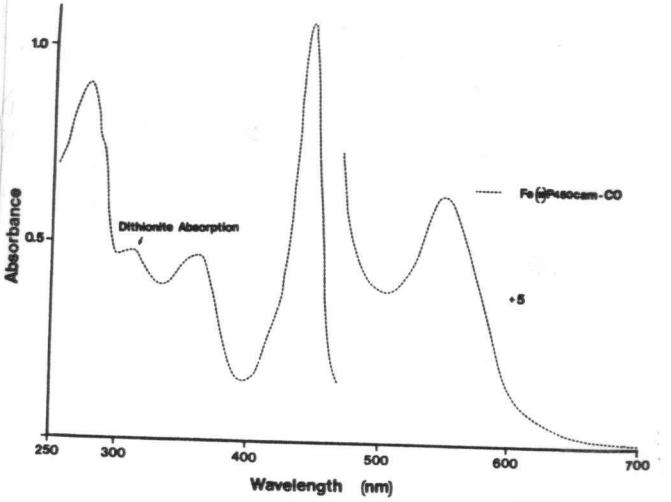
Run	Plot Form	Cary O.D.	Flash Unit Volt.	P_T (mm Hg)	P_{H_2O} (mm Hg)	P_{CO} (mm Hg)	[CO]x10^4 (m/L)	k_{obs} (msec^{-1})
3.3	Rate Plot	0.980	0.980	550	17.5	533	7.24	5.9x10^{-2}



Vertical Amplitude: 0.1 (volts/div)

Sweep Time: 1.0 (msec/div)

Slope (mean)		Slope (max)		Slope (min)		Least Squares Analysis
X (msec)	Y (volts)	X (msec)	Y (volts)	X (msec)	Y (volts)	
0	-0.370	0	-0.370	0	-0.360	m: 5.9x10^{-2}msec^{-1}
1.0	-0.315	1.0	-0.315	1.0	-0.300	y-intercept: -3.7x10^{-1}
2.0	-0.250	2.0	-0.250	2.0	-0.245	δy: 1.5x10^{-3}
3.0	-0.195	3.0	-0.190	3.0	-0.190	δm:4.8x10^{-4}msec^{-1}
4.0	-0.135	4.0	-0.130	4.0	-0.135	
5.0	-0.075	5.0	-0.070	5.0	-0.075	
6.0	-0.020	6.0	-0.010	6.0	-0.020	



FLASH PHOTOLYSIS EXPERIMENTS

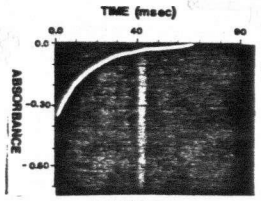
Sample Description: Native P450cam-CO complex

Temperature: 20±0.2°C

Monitoring Wavelength: 442nm

Data Table

Run	Plot Form	Cary O.D.	Flash Unit Volt.	P_T (mm Hg)	P_{H_2O} (mm Hg)	P_{CO} (mm Hg)	[CO]x10^4 (M/L)	Half Life (msec)
3.4	Exp. Decay	0.980	0.980	450	17.5	433	5.88	12



Vertical Amplitude: 0.1 (volts/div)

Sweep Time: 10 (msec/div)

Half Life Data

Half Life #	Vertical Drop (volts)	Horizontal Sweep (msec)
0	-0.350	0
1	-0.175	11 (11)
2	-0.086	23 (12)
3	-0.043	35 (12)
4	-0.022	47 (12)

$t_{\frac{1}{2}}$ = 12 msec

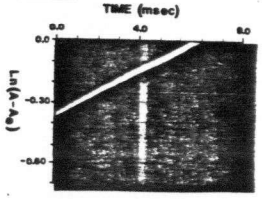
FLASH PHOTOLYSIS EXPERIMENTS

Sample Description: Native P450cam-CO complex

Temperature: 20±0.2°C

Data Table

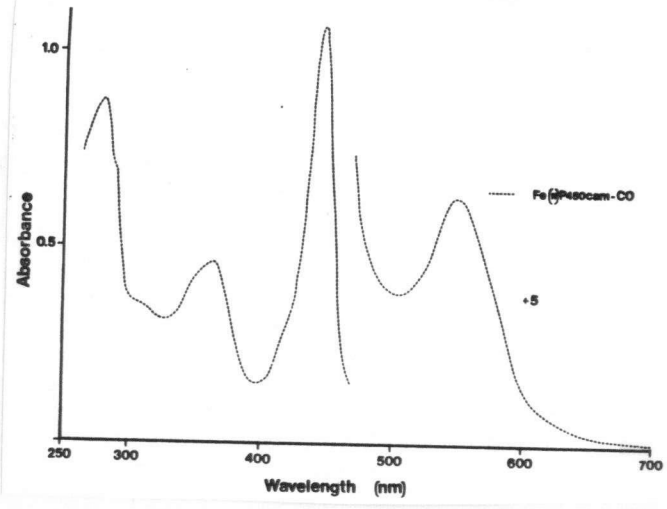
Run	Plot Form	Cary O.D.	Flash Unit Volt.	P_T (mm Hg)	P_{H_2O} (mm Hg)	P_{CO} (mm Hg)	[CO]x10^4 (m/L)	k_{obs} ($msec^{-1}$)
3.4	Rate Plot	0.980	0.970	450	17.5	433	5.88	$5.3x10^{-2}$



Vertical Amplitude: 0.1 (volts/div)

Sweep Time: 1.0 (msec/div)

Slope (mean)		Slope (max)		Slope (min)		Least Squares Analysis
X (msec)	Y (volts)	X (msec)	Y (volts)	X (msec)	Y (volts)	
0	-0.360	0	-0.365	0	-0.355	m: $5.3x10^{-2}msec^{-1}$
1.0	-0.310	1.0	-0.310	1.0	-0.300	y-intercept: $-3.6x10^{-1}$
2.0	-0.250	2.0	-0.250	2.0	-0.250	
3.0	-0.200	3.0	-0.200	3.0	-0.200	δy: $1.7x10^{-3}$
4.0	-0.145	4.0	-0.140	4.0	-0.150	
5.0	-0.090	5.0	-0.085	5.0	-0.100	δm:$5.7x10^{-4}msec^{-1}$
6.0	-0.040	6.0	-0.030	6.0	-0.050	



FLASH PHOTOLYSIS EXPERIMENTS

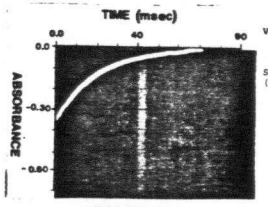
Sample Description: Native P450cam-CO complex

Temperature: 20±0.2°C

Monitoring Wavelength: 442nm

Data Table

Run	Plot Form	Cary O.D.	Flash Unit Volt.	P_T (mm Hg)	P_{H_2O} (mm Hg)	P_{CO} (mm Hg)	[CO]x10^4 (M/L)	Half Life (msec)
3.5	Exp. Decay	0.970	0.970	350	17.5	333	4.52	14



Vertical Amplitude: 0.1 (volts/div)

Sweep Time: 10 (msec/div)

Half Life Data

Half Life #	Vertical Drop (volts)	Horizontal Sweep (msec)
0	-0.340	0
1	-0.170	15 (15)
2	-0.085	29 (14)
3	-0.042	43 (14)
4	-0.021	57 (14)

$t_{\frac{1}{2}}$ = 14 msec

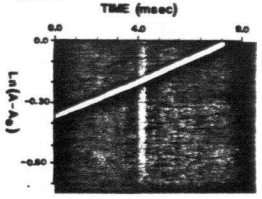
FLASH PHOTOLYSIS EXPERIMENTS

Sample Description: Native P450cam-CO complex

Temperature: 20±0.2°C

Data Table

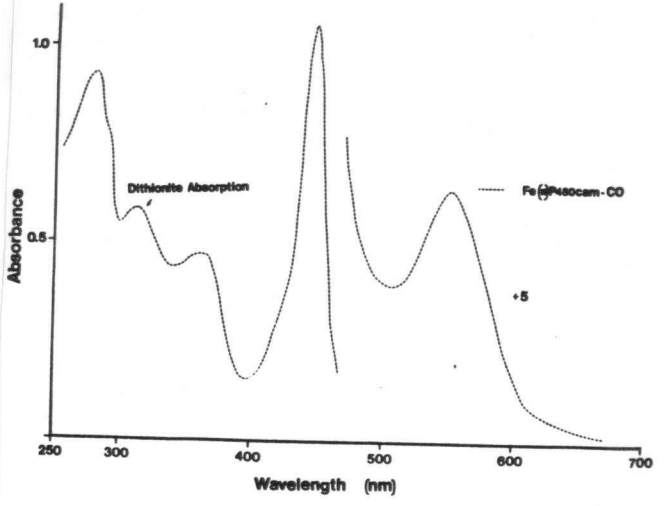
Run	Plot Form	Cary O.D.	Flash Unit Volt.	P_T (mm Hg)	P_{H_2O} (mm Hg)	P_{CO} (mm Hg)	[CO]x10^4 (m/L)	k_{obs} ($msec^{-1}$)
3.5	Rate Plot	0.970	0.970	350	17.5	333	4.52	$4.3x10^{-2}$



Vertical Amplitude: 0.1 (volts/div)

Sweep Time: 1.0 (msec/div)

Slope (mean)		Slope (max)		Slope (min)		Least Squares Analysis
X (msec)	Y (volts)	X (msec)	Y (volts)	X (msec)	Y (volts)	
0	-0.370	0	-0.380	0	-0.360	m:$4.3x10^{-2}msec^{-1}$
1.0	-0.330	1.0	-0.335	1.0	-0.320	y-intercept: $-3.7x10^{-1}$
2.0	-0.285	2.0	-0.285	2.0	-0.280	
3.0	-0.245	3.0	-0.245	3.0	-0.235	δy: $1.8x10^{-3}$
4.0	-0.200	4.0	-0.195	4.0	-0.200	
5.0	-0.160	5.0	-0.150	5.0	-0.160	δm:$5.1x10^{4}msec^{-1}$
6.0	-0.115	6.0	-0.110	6.0	-0.115	
7.0	-0.070	7.0	-0.060	7.0	-0.080	



FLASH PHOTOLYSIS EXPERIMENTS

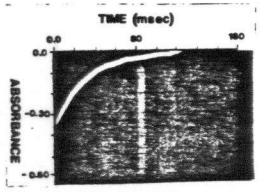
Sample Description: Native P450cam-CO complex

Temperature: 20±0.2°C

Monitoring Wavelength: 442nm

Data Table

Run	Plot Form	Cary O.D.	Flash Unit Volt.	P_T (mm Hg)	P_{H_2O} (mm Hg)	P_{CO} (mm Hg)	[CO]x10^4 (m/L)	Half Life (msec)
3.6	Exp. Decay	0.970	0.980	250	17.5	233	3.16	21



Vertical Amplitude: 0.1 (volts/div)

Sweep Time: 20 (msec/div)

Half Life Data

Half Life #	Vertical Drop (volts)	Horizontal Sweep (msec)
0	-0.340	0
1	-0.170	21 (21)
2	-0.085	43 (22)
3	-0.043	64 (21)
4	-0.021	84 (20)

$t_{\frac{1}{2}}$ = 21 msec

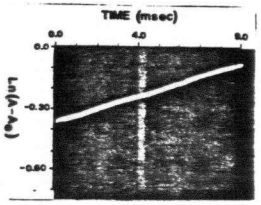
FLASH PHOTOLYSIS EXPERIMENTS

Sample Description: Native P450cam-CO complex

Temperature: 20±0.2°C

Data Table

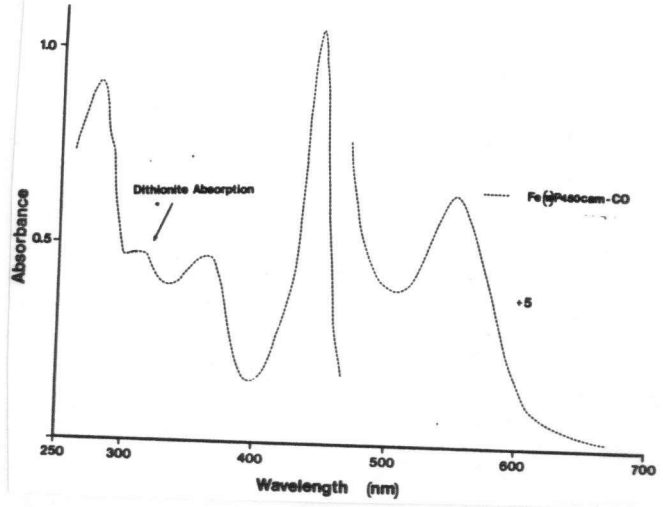
Run	Plot Form	Cary O.D.	Flash Unit Volt.	P_T (mm Hg)	P_{H_2O} (mm Hg)	P_{CO} (mm Hg)	[CO]x10^4 (m/L)	k_{obs} (msec^{-1})
3.6	Rate Plot	0.970	0.970	250	17.5	233	3.16	3.1x10^{-2}



Vertical Amplitude: 0.1 (volts/div)

Sweep Time: 1.0 (msec/div)

Slope (mean)		Slope (max)		Slope (min)		Least Squares Analysis
X (msec)	Y (volts)	X (msec)	Y (volts)	X (msec)	Y (volts)	
0	-0.365	0	-0.380	0	-0.355	m: 3.1x10^{-2}msec^{-1}
1.0	-0.335	1.0	-0.340	1.0	-0.330	y-intercept: -3.7x10^{-1}
2.0	-0.300	2.0	-0.310	2.0	-0.295	δy: 1.8x10^{-3}
3.0	-0.270	3.0	-0.275	3.0	-0.270	δm:5.0x10^{-4}msec^{-1}
4.0	-0.240	4.0	-0.240	4.0	-0.240	
5.0	-0.210	5.0	-0.210	5.0	-0.210	
6.0	-0.175	6.0	-0.175	6.0	-0.185	
7.0	-0.150	7.0	-0.140	7.0	-0.155	



FLASH PHOTOLYSIS EXPERIMENTS

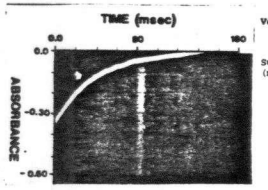
Sample Description: Native P450cam-CO

Temperature: 20±0.2°C

Monitoring Wavelength: 442nm

Data Table

Run	Plot Form	Cary O.D.	Flash Unit Volt.	P_T (mm Hg)	P_{H_2O} (mm Hg)	P_{CO} (mm Hg)	[CO]x10^4 (m/L)	Half Life (msec)
3.7	Exp. Decay	0.967	0.970	200	17.5	183	2.48	27



Vertical Amplitude: 0.1 (volts/div)

Sweep Time: 20 (msec/div)

Half Life Data

Half Life #	Vertical Drop (volts)	Horizontal Sweep (msec)
0	-0.340	0
1	-0.170	28 (28)
2	-0.085	56 (28)
3	-0.043	84 (28)
4	-0.021	110 (26)

$t_{\frac{1}{2}}$ = 27 msec

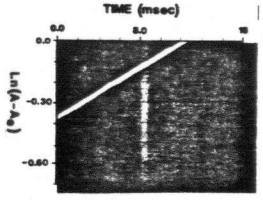
FLASH PHOTOLYSIS EXPERIMENTS

Sample Description: Native P450cam-CO complex

Temperature: 20±0.2°C

Data Table

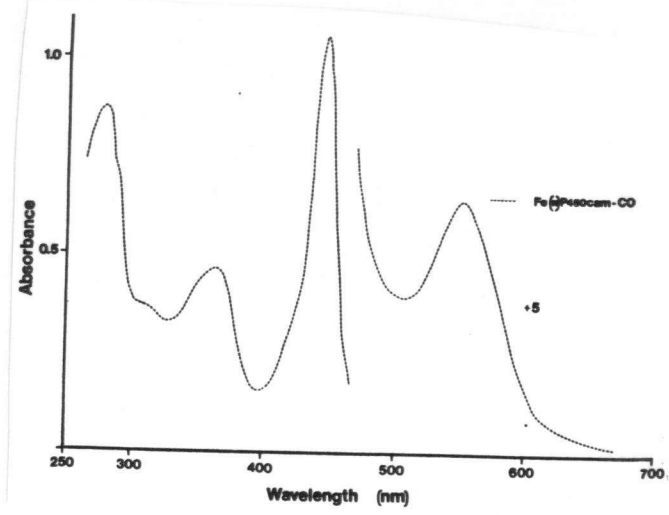
Run	Plot Form	Cary O.D.	Flash Unit Volt.	P_T (mm Hg)	P_{H_2O} (mm Hg)	P_{CO} (mm Hg)	[CO]x10^4 (m/L)	k_{obs} (msec^{-1})
3.7	Rate Plot	0.967	0.970	200	17.5	183	2.48	3.0x10^{-2}



Vertical Amplitude: 0.1 (volts/div)

Sweep Time: 2.0 (msec/div)

Slope (mean)		Slope (max)		Slope (min)		Least Squares Analysis
X (msec)	Y (volts)	X (msec)	Y (volts)	X (msec)	Y (volts)	
0	-0.370	0	-0.390	0	-0.370	m:3.0x10^{-2}msec^{-1}
2.0	-0.320	2.0	-0.320	2.0	-0.310	y-intercept: -3.8x10^{-1}
4.0	-0.255	4.0	-0.255	4.0	-0.250	δy: 2.1x10^{-3}
6.0	-0.195	6.0	-0.195	6.0	-0.195	δm:3.5x10^{-4}msec^{-1}
8.0	-0.130	8.0	-0.130	8.0	-0.130	
10	-0.070	10	-0.075	10	-0.065	
12	-0.015	12	0.0	12	-0.025	



Appendix IVc Raw data for kinetic Run 2 for the protohemin-reconstituted P450cam-CO system.

Absorbance Data for Hemoproteins

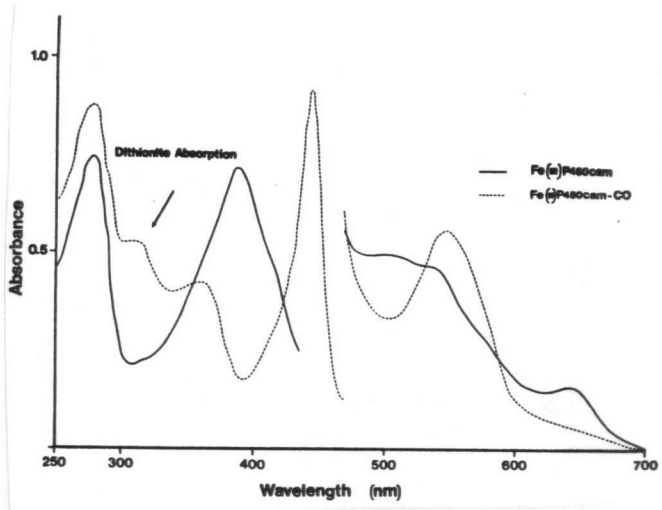
Sample Description: Protohemin-reconstituted, substrate-bound cytochrome P450cam

Experiment Description: Kinetic Run 2 for the protohemin-reconstituted, substrate-bound P450cam -CO system .

[Hemoprotein] : 7.44×10^{-6} M

Absorbance Data

Hemoprotein Species	λ_{max} (nm)	Absorbance	Calculated εmM	Literature[10] εmM
Oxidized	643	3.1×10^{-2}	4.2	5.4
	540	9.0×10^{-2}	12	11.2
	510	9.4×10^{-2}	13	13.0
	390	7.0×10^{-1}	94	10.2
Reduced-CO	545	1.1×10^{-1}	15	14.0
	445	8.9×10^{-1}	120	12.0
	365	3.9×10^{-1}	53	60.8



FLASH PHOTOLYSIS EXPERIMENTS

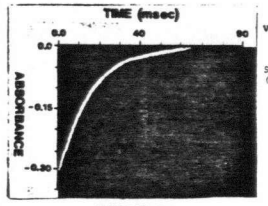
Sample Description: Protohemin-reconstituted P450cam-CO complex

Temperature: 20±0.2°C

Monitoring Wavelength: 442nm

Data Table

Run	Plot Form	Cary O.D.	Flash Unit Volt.	P_T (mm Hg)	P_{H_2O} (mm Hg)	P_{CO} (mm Hg)	$[CO] \times 10^4$ (m/L)	Half Life (msec)
2.1	Exp. Decay	0.807	0.810	750	17.5	733	9.96	10.5



Vertical Amplitude: 0.05 (volts/div)

Sweep Time: 10 (msec/div)

Half Life Data

Half Life #	Vertical Drop (volts)	Horizontal Sweep (msec)
0	0.300	0
1	0.150	11 (11)
2	0.075	22 (11)
3	0.038	32 (10.0)
4	0.019	42 (10.0)

$t_{\frac{1}{2}}$ = 10.5msec

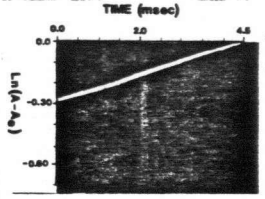
FLASH PHOTOLYSIS EXPERIMENTS

Sample Description: Protohemin-reconstituted P450cam-CO complex

Temperature: 20±0.2°C

Data Table

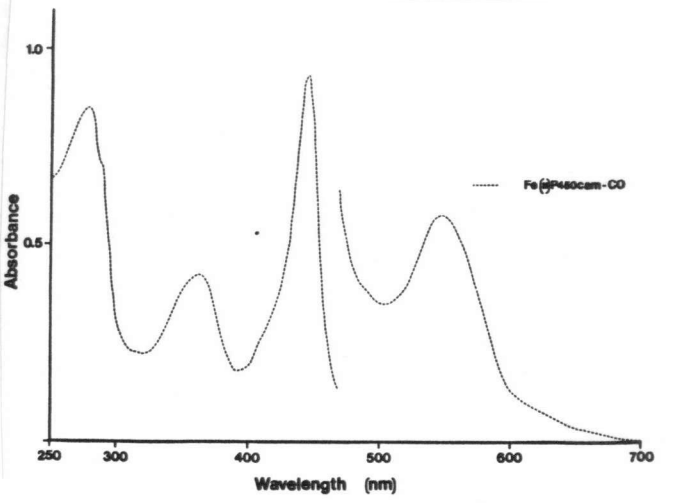
Run	Plot Form	Cary O.D.	Flash Unit Volt.	P_T (mm Hg)	P_{H_2O} (mm Hg)	P_{CO} (mm Hg)	$[CO] \times 10^4$ (m/L)	k_{obs} ($msec^{-1}$)
2.1	Rate Plot	0.807	0.810	750	17.5	733	9.96	6.6×10^{-2}



Vertical Amplitude: 0.1 (volts/div)

Sweep Time: 0.5 (msec/div)

Slope (mean)		Slope (max)		Slope (min)		Least Squares Analysis
X (msec)	Y (volts)	X (msec)	Y (volts)	X (msec)	Y (volts)	
0	-0.295	0	-0.305	0	-0.270	m:6.6×10^{-2} $msec^{-1}$
0.5	-0.260	0.5	-0.270	0.5	-0.250	y-intercept:
1.0	-0.230	1.0	-0.230	1.0	-0.215	-2.9×10^{-1}
1.5	-0.200	1.5	-0.200	1.5	-0.190	Δy: 2.2×10^{-3}
2.0	-0.165	2.0	-0.165	2.0	-0.155	Δm:1.1×10^{-3} $msec^{-1}$
2.5	-0.130	2.5	-0.130	2.5	-0.130	
3.0	-0.100	3.0	-0.090	3.0	-0.095	
3.5	-0.060	3.5	-0.055	3.5	-0.060	
4.0	-0.030	4.0	-0.020	4.0	-0.030	



FLASH PHOTOLYSIS EXPERIMENTS

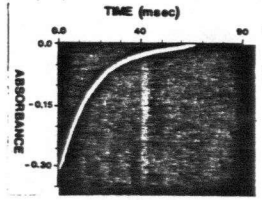
Sample Description: Protohemin-reconstituted P450cam-CO complex

Temperature: 20±0.2°C

Monitoring Wavelength: 442nm

Data Table

Run	Plot Form	Cary O.D.	Flash Unit Volt.	P_T (mm Hg)	P_{H_2O} (mm Hg)	P_{CO} (mm Hg)	$[CO]\times10^4$ (m/L)	Half Life (msec)
2.2	Exp. Decay	0.833	0.840	650	17.5	633	8.60	11



Vertical Amplitude: 0.05 (volts/div)

Sweep Time: 10 (msec/div)

Half Life Data

Half Life #	Vertical Drop (volts)	Horizontal Sweep (msec)
0	0.300	0
1	0.150	11.5 (12)
2	0.075	22 (11)
3	0.038	32 (10)
4	0.019	43 (11)

$t_{\frac{1}{2}}$ = 11msec

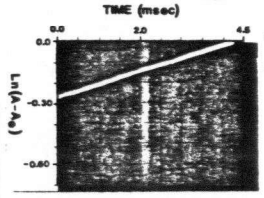
FLASH PHOTOLYSIS EXPERIMENTS

Sample Description: Protohemin-reconstituted P450cam-CO complex

Temperature: 20±0.2°C

Data Table

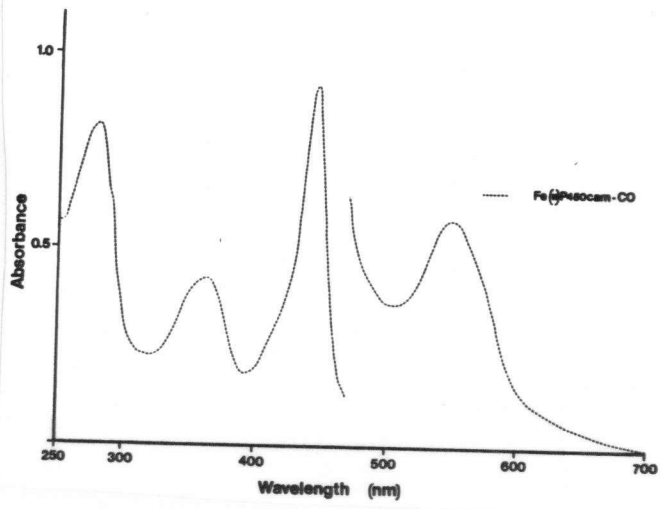
Run	Plot Form	Cary O.D.	Flash Unit Volt.	P_T (mm Hg)	P_{H_2O} (mm Hg)	P_{CO} (mm Hg)	$[CO]\times10^4$ (m/L)	k_{obs} ($msec^{-1}$)
2.2	Rate Plot	0.833	0.840	650	17.5	633	8.60	6.1×10^{-2}



Vertical Amplitude: 0.1 (volts/div)

Sweep Time: 0.5 (msec/div)

Slope (mean)		Slope (max)		Slope (min)		Least Squares Analysis
X (msec)	Y (volts)	X (msec)	Y (volts)	X (msec)	Y (volts)	
0	-0.270	0	-0.270	0	-0.255	m: 6.1×10^{-2} $msec^{-1}$
0.5	-0.240	0.5	-0.240	0.5	-0.230	y-intercept:
1.0	-0.210	1.0	-0.210	1.0	-0.200	-2.7×10^{-1}
1.5	-0.175	1.5	-0.175	1.5	-0.175	δy: 1.7×10^{-3}
2.0	-0.150	2.0	-0.150	2.0	-0.150	δm: 8.7×10^{-3} $msec^{-1}$
2.5	-0.115	2.5	-0.100	2.5	-0.115	
3.0	-0.085	3.0	-0.075	3.0	-0.085	
3.5	-0.055	3.5	-0.050	3.5	-0.060	
4.0	-0.020	4.0	-0.015	4.0	-0.030	



FLASH PHOTOLYSIS EXPERIMENTS

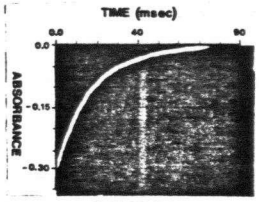
Sample Description: Protohemin-reconstituted P450cam-CO complex

Temperature: 20±0.2°C

Monitoring Wavelength: 442nm

Data Table

Run	Plot Form	Cary O.D.	Flash Unit Volt.	P_T (mm Hg)	P_{H_2O} (mm Hg)	P_{CO} (mm Hg)	$[CO]\times10^4$ (m/L)	Half Life (msec)
2.3	Exp. Decay	0.824	0.820	550	17.5	533	7.24	13



Vertical Amplitude: 0.05 (volts/div)

Sweep Time: 10 (msec/div)

Half Life Data

Half Life #	Vertical Drop (volts)	Horizontal Sweep (msec)
0	0.300	0
1	0.150	11.5 (12)
2	0.075	23 (11)
3	0.038	36 (13)
4	0.019	50 (14)

$t_{\frac{1}{2}}$ = 13msec

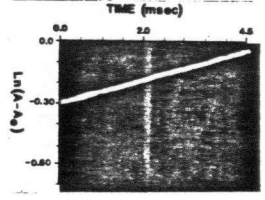
FLASH PHOTOLYSIS EXPERIMENTS

Sample Description: Protohemin-reconstituted P450cam-CO complex

Temperature: 20±0.2°C

Data Table

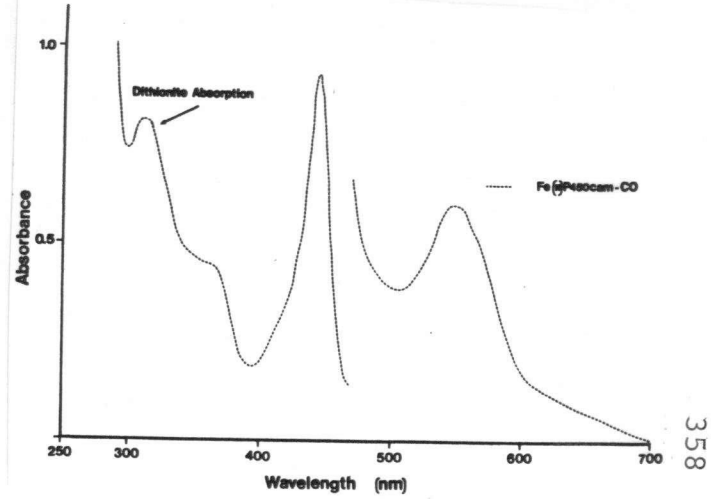
Run	Plot Form	Cary O.D.	Flash Unit Volt.	P_T (mm Hg)	P_{H_2O} (mm Hg)	P_{CO} (mm Hg)	$[CO]\times10^4$ (m/L)	k_{obs} ($msec^{-1}$)
2.3	Rate Plot	0.824	0.820	550	17.5	533	7.24	5.3×10^{-2}



Vertical Amplitude: 0.1 (volts/div)

Sweep Time: 0.5 (msec/div)

Slope (mean)		Slope (max)		Slope (min)		Least Squares Analysis
X (msec)	Y (volts)	X (msec)	Y (volts)	X (msec)	Y (volts)	
0	-0.300	0	-0.305	0	-0.280	m: 5.3×10^{-2} $msec^{-1}$
0.5	-0.265	0.5	-0.270	0.5	-0.260	y-intercept:
1.0	-0.240	1.0	-0.245	1.0	-0.240	-2.9×10^{-1}
1.5	-0.210	1.5	-0.210	1.5	-0.210	δy: 1.9×10^{-3}
2.0	-0.190	2.0	-0.190	2.0	-0.190	δm: 9.7×10^{-4} $msec^{-1}$
2.5	-0.160	2.5	-0.155	2.5	-0.165	
3.0	-0.130	3.0	-0.130	3.0	-0.140	
3.5	-0.080	3.5	-0.070	3.5	-0.090	
4.0	-0.080	4.0	-0.070	4.0	-0.090	



FLASH PHOTOLYSIS EXPERIMENTS

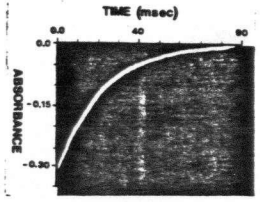
Sample Description: Protohemin-reconstituted P450cam-CO complex

Temperature: 20±0.2°C

Monitoring Wavelength: 442°C

Data Table

Run	Plot Form	Cary O.D.	Flash Unit Volt.	P_T (mm Hg)	P_{H_2O} (mm Hg)	P_{CO} (mm Hg)	[CO]x10^4 (M/L)	Half Life (msec)
2.4	Exp Decay	0.833	0.830	450	17.5	433	5.88	15



Vertical Amplitude: 0.05 (volts/div)

Sweep Time: 10 (msec/div)

Half Life Data

Half Life θ	Vertical Drop (volts)	Horizontal Sweep (msec)
0	0.300	0
1	0.150	17 (17)
2	0.075	32 (15)
3	0.038	45 (13)
4	0.019	58 (13)

$t_{\frac{1}{2}}$ = 15msec

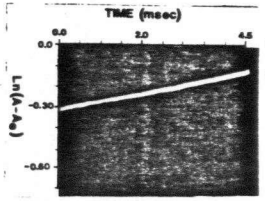
FLASH PHOTOLYSIS EXPERIMENTS

Sample Description: Protohemin-reconstituted P450cam-CO complex

Temperature: 20±0.2°C

Data Table

Run	Plot Form	Cary O.D.	Flash Unit Volt.	P_T (mm Hg)	P_{H_2O} (mm Hg)	P_{CO} (mm Hg)	[CO]x10^4 (M/L)	k_{obs} ($msec^{-1}$)
2.4	Rate Plot	0.833	0.830	450	17.5	433	5.88	4.1x10^{-2}



Vertical Amplitude: 0.1 (volts/div)

Sweep Time: 0.5 (msec/div)

Slope (mean) X (msec)	Slope (mean) Y (volts)	Slope (max) X (msec)	Slope (max) Y (volts)	Slope (min) X (msec)	Slope (min) Y (volts)
0	-0.315	0	-0.325	0	-0.305
0.5	-0.290	0.5	-0.305	0.5	-0.280
1.0	-0.270	1.0	-0.280	1.0	-0.265
1.5	-0.250	1.5	-0.255	1.5	-0.255
2.0	-0.230	2.0	-0.235	2.0	-0.230
2.5	-0.210	2.5	-0.210	2.5	-0.210
3.0	-0.190	3.0	-0.190	3.0	-0.195
3.5	-0.170	3.5	-0.165	3.5	-0.175
4.0	-0.150	4.0	-0.145	4.0	-0.160

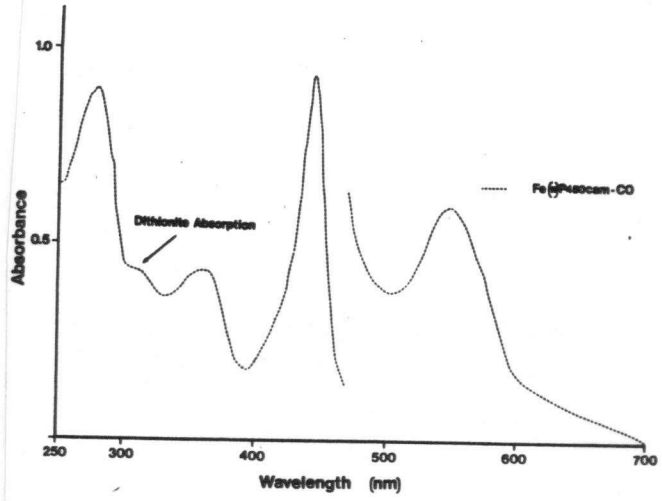
Least Squares Analysis

m:4.1x10^{-2}msec^{-1}

y-intercept: -3.1x10^{-1}

δy: 1.8x10^{-3}

δm:8.9x10^{-4}msec^{-1}



FLASH PHOTOLYSIS EXPERIMENTS

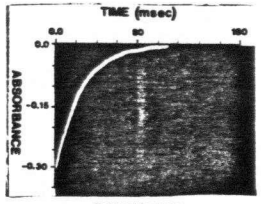
Sample Description: Protohemin-reconstituted P450cam-CO complex

Temperature: 20±0.2°C

Monitoring Wavelength: 442nm

Data Table

Run	Plot Form	Cary O.D.	Flash Unit Volt.	P_T (mm Hg)	P_{H_2O} (mm Hg)	P_{CO} (mm Hg)	[CO]x10^4 (M/L)	Half Life (msec)
2.5	Exp. Decay	0.832	0.820	350	17.5	333	4.52	18



Vertical Amplitude: 0.05 (volts/div)

Sweep Time: 20 (msec/div)

Half Life Data

Half Life θ	Vertical Drop (volts)	Horizontal Sweep (msec)
0	0.300	0
1	0.150	18 (18)
2	0.075	35 (17)
3	0.038	51 (16)
4	0.019	70 (19)

$t_{\frac{1}{2}}$ = 18msec

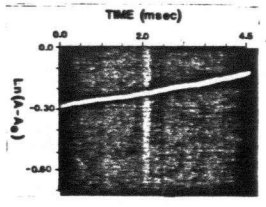
FLASH PHOTOLYSIS EXPERIMENTS

Sample Description: Protohemin-reconstituted P450cam-CO complex

Temperature: 20±0.2°C

Data Table

Run	Plot Form	Cary O.D.	Flash Unit Volt.	P_T (mm Hg)	P_{H_2O} (mm Hg)	P_{CO} (mm Hg)	[CO]x10^4 (M/L)	k_{obs} ($msec^{-1}$)
2.5	Rate Plot	0.838	0.830	350	17.5	333	4.52	3.5x10^{-2}



Vertical Amplitude: 0.1 (volts/div)

Sweep Time: 0.5 (msec/div)

Slope (mean) X (msec)	Slope (mean) Y (volts)	Slope (max) X (msec)	Slope (max) Y (volts)	Slope (min) X (msec)	Slope (min) Y (volts)
0	-0.300	0	-0.300	0	-0.285
0.5	-0.280	0.5	-0.280	0.5	-0.270
1.0	-0.260	1.0	-0.260	1.0	-0.250
1.5	-0.245	1.5	-0.245	1.5	-0.235
2.0	-0.225	2.0	-0.225	2.0	-0.220
2.5	-0.210	2.5	-0.210	2.5	-0.210
3.0	-0.190	3.0	-0.190	3.0	-0.190
3.5	-0.170	3.5	-0.170	3.5	-0.175
4.0	-0.150	4.0	-0.150	4.0	-0.155

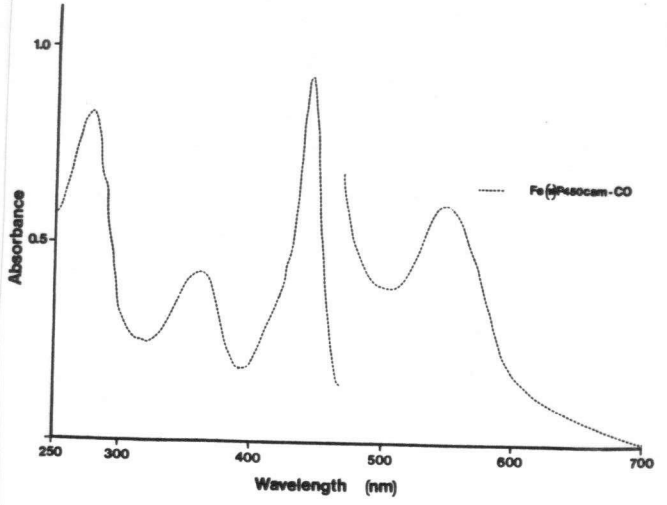
Least Squares Analysis

m: 3.5x10^{-2}msec^{-1}

y-intercept: -2.9x10^{-1}

δy: 1.3x10^{-3}

δm:6.5x10^{-4}msec^{-1}



FLASH PHOTOLYSIS EXPERIMENTS

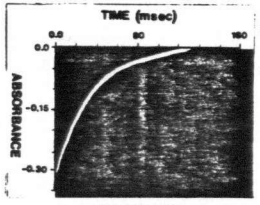
Sample Description: Protohemin-reconstituted P450cam-CO complex

Temperature: 20±0.2°C

Monitoring Wavelength: 442nm

Data Table

Run	Plot Form	Cary O.D.	Flash Unit Volt.	P_T (mm Hg)	P_{H_2O} (mm Hg)	P_{CO} (mm Hg)	[CO]x10^4 (m/L)	Half Life (msec)
2.6	Exp. Decay	0.834	0.830	250	17.5	233	3.16	25



Vertical Amplitude: 0.05 (volts/div)

Sweep Time: 20 (msec/div)

Half Life Data

Half Life #	Vertical Drop (volts)	Horizontal Sweep (msec)
0	0.300	0
1	0.150	25 (25)
2	0.075	49 (24)
3	0.038	74 (25)
4	0.019	98 (24)

$t_{\frac{1}{2}}$ = 25msec

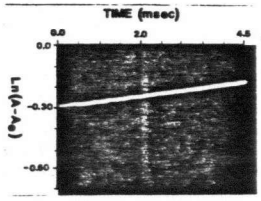
FLASH PHOTOLYSIS EXPERIMENTS

Sample Description: Protohemin-reconstituted P450cam-CO complex

Temperature: 20±0.2°C

Data Table

Run	Plot Form	Cary O.D.	Flash Unit Volt.	P_T (mm Hg)	P_{H_2O} (mm Hg)	P_{CO} (mm Hg)	[CO]x10^4 (m/L)	k_{obs} (msec^{-1})
2.6	Rate Plot	0.832	0.830	250	17.5	233	3.16	2.3x10^{-2}



Vertical Amplitude: 0.1 (volts/div)

Sweep Time: 0.5 (msec/div)

Slope (mean) X (msec)	Slope (mean) Y (volts)	Slope (max) X (msec)	Slope (max) Y (volts)	Slope (min) X (msec)	Slope (min) Y (volts)
0	-0.295	0	-0.300	0	-0.280
0.5	-0.280	0.5	-0.285	0.5	-0.275
1.0	-0.270	1.0	-0.270	1.0	-0.265
1.5	-0.260	1.5	-0.260	1.5	-0.255
2.0	-0.250	2.0	-0.250	2.0	-0.250
2.5	-0.235	2.5	-0.235	2.5	-0.235
3.0	-0.225	3.0	-0.225	3.0	-0.225
3.5	-0.210	3.5	-0.205	3.5	-0.210
4.0	-0.200	4.0	-0.195	4.0	-0.205

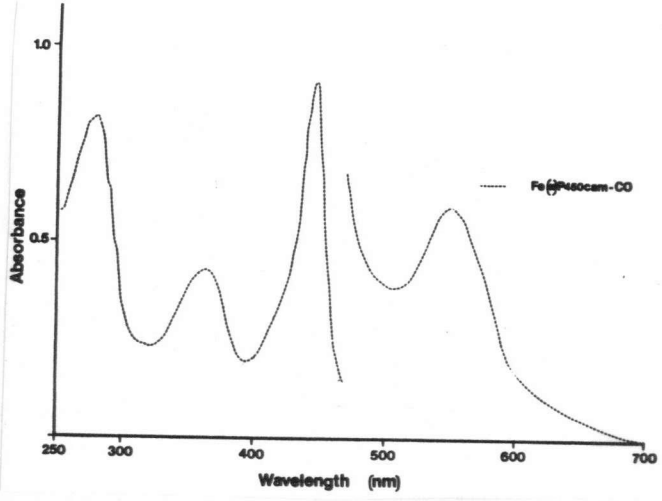
Least Squares Analysis

m: 2.3x10^{-2}msec^{-1}

y-intercept: 2.9x10^{-1}

δy: 1.3x10^{-3}

δm: 6.4x10^{-4}msec^{-1}



FLASH PHOTOLYSIS EXPERIMENTS

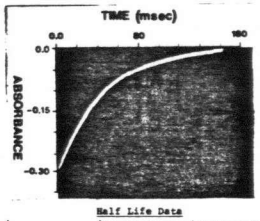
Sample Description: Protohemin-reconstituted P450cam-CO complex

Temperature: 20±0.2°C

Monitoring Wavelength: 442nm

Data Table

Run	Plot Form	Cary O.D.	Flash Unit Volt.	P_T (mm Hg)	P_{H_2O} (mm Hg)	P_{CO} (mm Hg)	[CO]x10^4 (m/L)	Half Life (msec)
2.7	Exp. Decay	0.822	0.820	200	17.5	183	2.48	30



Vertical Amplitude: 0.05 (volts/div)

Sweep Time: 20 (msec/div)

Half Life Data

Half Life #	Vertical Drop (volts)	Horizontal Sweep (msec)
0	0.300	0
1	0.150	30 (30)
2	0.075	60 (30)
3	0.038	91 (31)
4	0.019	120 (29)

$t_{\frac{1}{2}}$ = 30msec

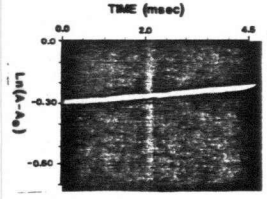
FLASH PHOTOLYSIS EXPERIMENTS

Sample Description: Protohemin-reconstituted P450cam-CO complex

Temperature: 20±0.2°C

Data Table

Run	Plot Form	Cary O.D.	Flash Unit Volt.	P_T (mm Hg)	P_{H_2O} (mm Hg)	P_{CO} (mm Hg)	[CO]x10^4 (m/L)	k_{obs} (msec^{-1})
2.7	Rate Plot	0.822	0.820	200	17.5	183	2.48	1.4x10^{-2}



Vertical Amplitude: 0.1 (volts/div)

Sweep Time: 0.5 (msec/div)

Slope (mean) X (msec)	Slope (mean) Y (volts)	Slope (max) X (msec)	Slope (max) Y (volts)	Slope (min) X (msec)	Slope (min) Y (volts)
0	-0.290	0	-0.295	0	-0.285
0.5	-0.280	0.5	-0.285	0.5	-0.275
1.0	-0.275	1.0	-0.275	1.0	-0.270
1.5	-0.265	1.5	-0.265	1.5	-0.265
2.0	-0.260	2.0	-0.260	2.0	-0.260
2.5	-0.255	2.5	-0.255	2.5	-0.255
3.0	-0.245	3.0	-0.240	3.0	-0.250
3.5	-0.240	3.5	-0.230	3.5	-0.245
4.0	-0.235	4.0	-0.220	4.0	-0.240

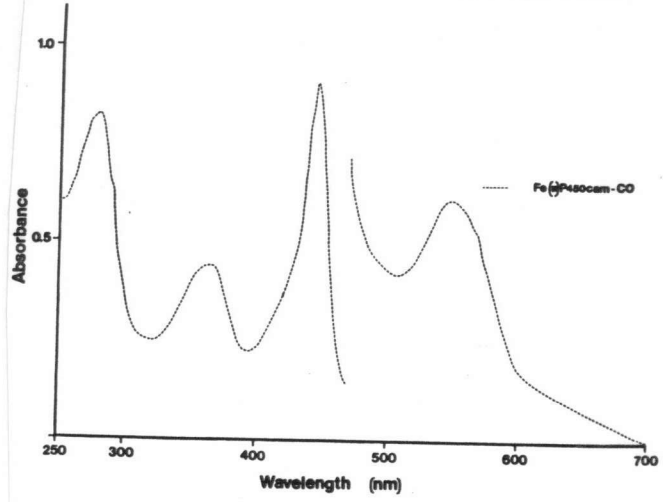
Least Squares Analysis

m: 1.4x10^{-2}msec^{-1}

y-intercept: -2.9x10^{-1}

δy: 1.4x10^{-3}

δm: 6.9x10^{-3}msec^{-1}



APPENDIX V

RAW DATA FOR THE SPECTROPHOTOMETRIC DETERMINATION OF THE EQUILIBRIUM CONSTANT FOR THE REACTION OF CO WITH THE FERROUS SUBSTRATE-BOUND STATE OF NATIVE CYTOCHROME P450cam

Appendix Va

Raw data for Equilibrium Run 1

Equilibrium Data

Sample Description: Native P450cam-CO Complex

Temperature: 20±0.2°C

Vapour Pressure of H_2O:

Theoretical[155]	Experimental
228 mm oil	200 mm oil
17.5 mm Hg	15.4 mm Hg

Data Table

Species #	Wanted Pco mm Hg(oil)	P_{Total} (mm oil)	Pco (mm oil)	A445nm	A408nm
1	0	200	0	0.222	0.588
2	3.0 (39.0)	239	39.0	0.222	0.582
3	4.0 (52.0)	256	56.0	0.323	0.523
4	6.0 (78.0)	280	80.0	0.410	0.449
5	8.0 (104)	307	107	0.503	0.390
6	10 (130)	335	135	0.592	0.337
7	12 (156)	359	159	0.636	0.295
8	14 (182)	387	187	0.673	0.281
9	20 (260)	466	266	0.732	0.246
10	45 (585)	797	597	0.810	0.177
11	760			0.889	0.134

Data Analysis

Wavelength Maxima : 445nm

Absorbance of Pure Species: A_o = 0.222

A_∞ = 0.889

Data Table

Pco (mm Hg)	[CO]x10^6 (M)	Log [CO]	A-Ao	A$_\infty$-A	$\frac{A-Ao}{A_\infty-A}$	log $\frac{A-Ao}{A_\infty-A}$
3.01	4.09	-5.39	-	-	-	-
4.33	5.89	-5.23	0.101	0.566	0.178	-0.749
6.18	8.41	-5.08	0.188	0.479	0.392	-0.406
8.27	11.3	-4.95	0.281	0.386	0.728	-0.138
10.4	14.2	-4.85	0.370	0.297	1.25	0.095
12.3	16.7	-4.78	0.414	0.253	1.64	0.214
14.5	19.7	-4.71	0.451	0.216	2.09	0.320
20.6	28.0	-4.55	0.510	0.517	3.25	0.512
46.2	62.8	-4.20	0.588	0.079	7.44	0.872

Raw data for Equilibrium Run 2

Equilibrium Data

Sample Description: Native P450cam-CO Complex

Temperature: 20±0.2°C

Vapour Pressure of H_2O:

Theoretical[155]	Experimental
228 mm oil	240 mm oil
17.5 mm Hg	18.6 mm Hg

Data Table

Species #	Wanted Pco mm Hg(oil)	P_{Total} (mm oil)	Pco (mm oil)	A445nm	A408nm
1	0	240		0.245	0.613
2	3.0 (39.0)	280	40.0	0.286	0.572
3	4.0 (52)	297	57.0	0.358	0.526
4	6.0 (78)	320	80.0	0.457	0.442
5	8.0 (104)	349	109	0.575	0.383
6	10.0 (130)	375	135	0.644	0.337
7	12.0 (156)	402	162	0.685	0.295
8	14.0 (182)	419	179	0.712	0.280
9	20.0 (260)	500	260	0.755	0.254
10	760		= 1 atm	0.911	0.141

Data Analysis

Wavelength Maxima : 445nm

Absorbance of Pure Species: A_o = 0.245

A_∞ = 0.911

Data Table

Pco (mm Hg)	[CO]x10^6 (M)	Log [CO]	A-Ao	A$_\infty$-A	$\frac{A-Ao}{A_\infty-A}$	log $\frac{A-Ao}{A_\infty-A}$
3.09	4.20	-5.38	0.041	0.625	6.56×10^{-2}	-1.18
4.41	5.99	-5.22	0.113	0.553	2.04×10^{-1}	6.90×10^{-1}
6.18	8.41	-5.08	0.212	0.454	4.67×10^{-1}	-3.31×10^{-1}
8.43	11.5	-4.94	0.330	0.336	9.82×10^{-1}	-7.83×10^{-3}
10.4	14.2	-4.85	0.399	0.267	1.49	1.75×10^{-1}
12.5	17.0	-4.77	0.440	0.226	1.95	2.89×10^{-1}
13.8	18.8	-4.73	0.467	0.199	2.35	3.71×10^{-1}
20.1	27.3	-4.56	0.510	0.156	3.27	5.14×10^{-1}

Raw data for Equilibrium Run 4

Equilibrium Data

Sample Description: Native P450cam-CO Complex

Temperature: 20±0.2°C

Vapour Pressure of H_2O:

Theoretical[155]	Experimental
228 mm oil	229 mm oil
17.5 mm Hg	17.7 mm Hg

Data Table

Species #	Wanted Pco mm Hg(oil)	P_{Total} (mm oil)	Pco (mm oil)	A445nm	A408nm
1	0	229		0.234	0.587
2	3.00 (39)	276	46.5	0.304	0.545
3	4.00 (52)	282	52.5	0.356	0.505
4	6.00 (78)	309	80.0	0.462	0.424
5	8.00 (104)	335	106	0.572	0.359
6	10.0 (130)	362	133	0.626	0.320
7	12.0 (156)	387	158	0.658	0.292
8	14.0 (182)	414	185	0.685	0.277
9	20.0 (260)	490	261	0.733	0.242
10	760			0.876	0.141

Data Analysis

Wavelength Maxima : 445nm

Absorbance of Pure Species: A_o = 0.234

A_∞ = 0.876

Data Table

Pco (mm Hg)	[CO]x10^6 (M)	Log [CO]	A-Ao	A$_\infty$-A	$\frac{A-Ao}{A_\infty-A}$	log $\frac{A-Ao}{A_\infty-A}$
3.59	4.89	-5.31	0.070	0.572	0.122	-0.912
4.06	5.52	-5.26	0.122	0.520	0.235	-0.630
6.19	8.41	-5.08	0.228	0.414	0.551	-0.259
8.19	11.1	-4.95	0.338	0.304	1.11	0.046
10.3	14.0	-4.85	0.392	0.250	1.57	0.195
12.2	16.6	-4.78	0.424	0.218	1.95	0.289
14.3	19.4	-4.71	0.451	0.191	2.36	0.373
20.2	27.4	-4.56	0.499	0.143	3.49	0.543

Appendix Vb

Raw data for Equilibrium Run 5

Equilibrium Data

Sample Description: Native P450cam-CO Complex

Temperature: 20±0.2°C

Vapour Pressure of H_2O:	Theoretical[155]	Experimental
	228 mm oil	244 mm oil
	17.5 mm Hg	18.9 mm Hg

Data Table

Species #	Wanted Pco mm Hg(oil)	P_{Total} (mm oil)	Pco (mm oil)	A445nm	A408nm
1	0	244	0	0.306	0.743
2	2.00 (26)	272	28.0	0.319	0.735
3	4.00 (52)	300	56.0	0.593	0.538
4	6.00 (78)	322	78.0	0.713	0.453
5	8.00 (104)	348	104	0.776	0.423
6	10.0 (130)	374	130	0.793	0.392
7	20.0 (259)	504	260	0.897	0.329
8	35.0 (453)	699	455	0.966	0.277
9	47.0 (608)	848	604	0.992	0.257

Data Analysis

Wavelength Maxima : 445nm

Absorbance of Pure Species: A_O = 0.306

A_∞ = 0.992

Data Table

Pco (mm Hg)	$[CO]\times10^6$ (M)	Log [CO]	A-Ao	A_∞-A	$\frac{A-Ao}{A_\infty-A}$	log $\frac{A-Ao}{A_\infty-A}$
2.17	2.94	-5.53	0.013	0.673	1.93×10^{-2}	-1.71
4.33	5.89	-5.23	0.287	0.399	7.19×10^{-1}	-0.143
6.03	8.20	-5.09	0.407	0.279	1.46	0.164
8.04	10.9	-4.96	0.470	0.216	2.18	0.339
10.1	13.7	-4.86	0.487	0.199	2.45	0.389
20.1	27.3	-4.56	0.591	0.095	6.22	0.794
35.2	47.8	-4.32	0.660	0.026	25.4	1.40
46.7	63.5	-4.20	0.686	0.00	0	1.0

Raw data for Equilibrium Run 6

Equilibrium Data

Sample Description: Native P450cam-CO Complex

Temperature: 20±0.2°C

Vapour Pressure of H_2O:	Theoretical[155]	Experimental
	227 mm oil	229 mm oil
	17.5 mm Hg	18.2 mm Hg

Data Table

Species #	Wanted Pco mm Hg(oil)	P_{Total} (mm oil)	Pco (mm oil)	A445nm	A408nm
1	0	235	0	0.259	0.653
2	3.00 (39)	276	41.0	0.289	0.629
3	4.00 (52)	288	59.0	0.396	0.558
4	6.00 (78)	305	76.5	0.541	0.465
5	8.00(104)	334	105	0.626	0.399
6	10.0(130)	354	125	0.678	0.392
7	12.0(156)	370	141	0.683	0.372
8	14.0 (182)	411	182	0.736	0.345
9	760			0.932	0.207

Data Analysis

Wavelength Maxima : 445nm

Absorbance of Pure Species: A_O = 0.259

A_∞ = 0.932

Data Table

Pco (mm Hg)	$[CO]\times10^6$ (M)	Log [CO]	A-Ao	A_∞-A	$\frac{A-Ao}{A_\infty-A}$	log $\frac{A-Ao}{A_\infty-A}$
3.17	4.31	-5.37	0.030	0.643	4.67×10^{-2}	-1.33
4.56	6.20	-5.21	0.137	0.536	0.256	-0.592
5.91	8.04	-5.09	0.282	0.391	0.721	-0.142
8.11	11.0	-4.96	0.367	0.306	1.20	7.89×10^{-2}
9.66	13.1	-4.88	0.419	0.254	1.65	0.217
10.9	14.8	-4.83	0.424	0.429	1.70	0.231
1.41	19.2	-4.72	0.477	0.196	2.43	0.386